N-Phosphinoamidinate Nickel Complexes

by

Casper Marcus Guzner Macaulay

Submitted in partial fulfilment of the requirements
for the degree of Doctor of Philosophy

at

Dalhousie University
Halifax, Nova Scotia
November 2019

DEDICATION

From
VT
LiCl
B_2Pin_2
0.001g
Praxair
Rubber Bands
$Me_2PhSiNHdipp$
Rotavap Extractions

To
Family
Friends

TABLE OF CONTENTS

LIST OF TABLES

LIST OF FIGURES

LIST OF SCHEMES

ABSTRACT

Society demands cheaper and more abundant metal catalysts to accomplish the tasks previously performed by precious metal catalysts. In turn, chemists have developed ancillary ligands designed to harness the power of first-row metals, such as Mn, Fe, Co, and Ni. In Chapter 1, these design principles are rationalized and summarized, and applied to a variety of important ligand classes. One such class includes *N*-phosphinoamidinate (PN) ligands. (PN) complexes of first-row metals have been applied as precatalysts for hydrosilative carbonyl reductions (in the case of Fe) and terminally selective alkene isomerization/hydroboration (I-H; in the case of Co). Given a recent surge of advances in homogeneous catalysis using Ni, I began my thesis research with synthetic attempts towards (PN) complexes of Ni. Over the course of my research, I developed a family of related complexes. Ultimately, I was able to harness these complexes to generate the reactive, transient, three-coordinate Ni hydride **(PN)NiH**, which unlocked three thesis chapters. In Chapter 2, I describe a mechanistic study of alkene I-H via isostructural (PN) Mn, Fe, Co, and Ni precatalysts. The Ni precatalyst performed poorly, and isolable Ni hydride complexes proved unsuitable for the reaction, but the diamagnetism of the Ni complexes afforded *in situ* monitoring of catalytic intermediates to help determine the origin of terminal selectivity. Chapter 3 contains an analogous study of hydrosilative amide reduction, wherein **(PN)NiH** instead proved remarkably competent to reduce challenging substrates via optimization of reaction conditions. Iterative optimization of the precatalyst proved the utility of **(PN)Ni(O*t*Bu)**, itself a rare example of a three-coordinate nickel alkoxo complex. Chapter 4 reports the spectroscopic and X-ray characterization of a unique compound conceived by **(PN)NiH** inserting benzene. It also includes unusual β- or γ- agostic **(PN)Ni(alkyl)** complexes synthesized in attempts to access **(PN)NiH** in a controlled fashion via β-hydride elimination.

LIST OF ABBREVIATIONS USED

1a = 1-octene
1b = *cis*-4-octene
1c = *trans*-4-octene
2a = *n*-octylBPin
2b = internal hydroboration products
2c = internal alkenes
2d = *n*-octane
3a = *N*,*N*-dibenzylbenzamide
3b = *N*,*N*-diisopropylbenzamide
4a = tribenzylamine
4a' = dibenzylamine
4b = *N*-benzyl-*N*,*N*-diisopropylamine
5 = **{(PN)Ni}$_2$(μ^2-η^3:η^3-C_6H_8)**
5$_d$ = **{(PN)Ni}$_2$(μ^2-η^3:η^3-C_6D_8)**
Ad = 1-adamantyl
Anal. Calcd. = analysis calculated
app = apparent
Ar = aryl
arom = aromatic
BHA = Buchwald-Hartwig amination
BHE = β-hydride elimination
BINAP = 2,2'-Bis(diphenylphosphino)-1,1'-binaphthyl
σ-BM = σ- bond metathesis
Bn = benzyl
br = broad
Bu = butyl
CCD = charge-coupled device
C_6D_6 = benzene-d_6
C_6D_{12} = cyclohexane-d_{12}
$CDCl_3$ = chloroform-d_1
C_6H_6 = benzene
$C_6H_8^{2-}$ = cyclohexadienyl dianion
C_6H_{12} = cyclohexane
COD = *cis*,*cis*-1,5-cyclooctadiene
COSY = homonuclear correlation spectroscopy
Cp = cyclopentadienyl
Cy = cyclohexyl
d = doublet
DBPin = pinacolborane-d_1
DEPT = distortionless enhancement of polarisation transfer
DFT = density functional theory
DIPAMP = ethane-1,2-diylbis[(2-methoxyphenyl)phenylphosphane]
dipp = 2,6-diisopropylphenyl
DMAP = 4-dimethylaminopyridine
dme = dimethoxyethane
dmp = 2,6-dimethylphenyl
dppe = bis(diphosphino)ethane
dtbpe = bis(di-*tert*-butylphosphinoethane)
dtbpm = bis(di-*tert*-butylphosphanyl)methane)
E = main group element
e- = electron
ee = enantiomeric excess
equiv = equivalent(s)
Et = ethyl
Et_2O = diethyl ether
GC = gas chromatography
h = hour
HBPin = pinacolborane
Hex = hexyl
HMBC = heteronuclear multiple bond correlation spectroscopy
HMQC = heteronuclear multiple quantum correlation spectroscopy
HNacNac = β-diketimine
HPLC-MS = high-pressure liquid chromatography-mass spectrometry
HPN = *N*-phosphinoamidine
HSQC = heteronuclear single-quantum correlation spectroscopy
Hz = Hertz
I-H = isomerization/hydroboration
***i*Pr** = *iso*-propyl
$^nJ_{XX'}$ = *n* bond coupling constant between atom X and atom X`
KC_8 = potassium graphite
L = two-electron neutral donor ligand
L_n = *n* generic ligands

L-DOPA = L-3,4-dihydroxyphenylalanine
m = multiplet
M = generic transition metal or mol/L
MAC = methyl-2-acetamidoacrylate
Me = methyl
Mes = mesityl
MHz = megahertz
min = minutes
NacNac = β-diketiminate
Ni_2H_2 = **$[(PN)NiH]_2$**
$Ni_2{}^nH_2$ = **$[(PN)Ni^nH]_2$**, *n* = 0, 1, 2
Ni_2Cl_2 = $[(PN)NiCl]_2$
NHC = *N*-heterocyclic carbene
NMR = nuclear magnetic resonance spectroscopy
Np = neopentyl
OA = oxidative addition
OAc = acetate group
Ph = phenyl
(PN) = *N*-phosphinoamidinate
ppm = parts per million
pr = propyl
PTFE = polytetrafluoroethylene
pyr = pyridine
R = alkyl or hydride group
RE = reductive elimination
s = singlet
SHOP = Shell olefin polymerization
***t*Bu** = *tert*-butyl
THF = tetrahydrofuran
TOF = turnover frequency
TON = turnover number
TMEDA = tetramethylethylenediamine
tol = toluene
UDEFT = uniform driven equilibrium Fourier transform
X = one-electron anionic donor ligand
XRD = X-ray diffraction
δ = chemical shift
η = indicator of hapticity
κ = indicator of denticity

ACKNOWLEDGEMENTS

The scientific document that follows represents many years from many people. My supervisors, Dr. Mark Stradiotto and Dr. Laura Turculet provided those years with steady leadership despite myriad challenges from many sources, including hurricanes, emergencies, and myself. They continue to be instrumental in my personal growth, education, and future. I could not have asked for more dedicated supervisors.

Co-workers: Dr. Fabien Lindeperg, Jillian Clark, Dr. Luke Murphy, Helia Hollenhorst, Dylan Hale, Dr. Takahiko Ogawa, Dr. Christopher Lavoie, and Joseph Tassone were all present throughout key stages of my degree. They helped teach me techniques related to safe handling of chemicals, equipment maintenance, EndNote, Word, TopSpin, writing, responsibility, productivity, mental health, and empathy.

Past group members: Dr. Colin Kelly, Marshall Hoey, Dr. Preston MacQueen, Dr. Nic Rotta-Loria and Alex Gatien all played important roles during my graduate experience.

From Dalhousie: Committee members Dr. Jean Burnell (former), Dr. Alex Speed, and Dr. Fran Cozens all helped guide my research, and taught me for some amount of time at Dalhousie. Dr. Mike Lumsden was a constant source of expertise and help. Dr. Ulrike Werner-Zwanziger helped me in a time of need. Xiao Feng, Ryan MacKinnon, and Mike Boutillier represent an incredibly dedicated technical team. Thanks to CGSS for fun and funding, and thanks to the softball team for the memories and my limited shoulder mobility.

From Queen's: Thank you to Dr. Cathleen Crudden for agreeing to be my external examiner. I hope this document and my defence were relatively pleasant for you.

To thank collaborators: the team at CPChem funded the research. Dr. Robert MacDonald, Dr. Michael J. Ferguson, and Dr. Yuqiao Zhou from the University of Alberta were essential to the X-ray characterization of the complexes found in this document, and the Ess Group from BYU performed DFT calculations.

Dr. Gregory Welch gave me a chance to be a chemist when I certainly would not have given myself one, and I will always be thankful for that. Dr. Arthur Hendsbee was a true mentor, and I wish him the best.

My parents, brothers, sister-in-law, and cousins were all helpful in unique ways.

Dr. Melissa McGonnell and Joanne Mills helped me overcome various difficulties with writing a relatively large document.

Red Circus was exactly the type of team I needed to help add structure to my life during my studies, and Hucktales has been a source of lasting friendships.

Jordin, I love you, and I swear I'm coming to bed soon.

CHAPTER 1: INTRODUCTION

1.1 The Importance of Organotransition Metal Chemistry

Homogeneous catalysis featuring ligand-supported transition metal complexes has revolutionized modern society. Pharmaceuticals, plastics, and functional materials that underpin our standard of living are enabled by carbon-carbon and carbon-heteroatom bond-forming reactions catalyzed by such complexes. To recognize the significance of such chemistry in recent years, Nobel prizes were awarded in 2001, 2005, and 2010 for advances in asymmetric catalysis,[1] olefin metathesis,[2] and palladium-catalyzed cross-coupling reactions.[3] These types of chemistry have associated costs, however, as noble metals such as ruthenium, rhodium, and palladium are utilized prominently therein. Noble metals are expensive, toxic, rare, and associated with terrestrial sources that feature political conflicts. Catalytic systems featuring metals such as iron, cobalt, or nickel that could perform or outperform noble metals related to these types of chemistry are highly sought-after.[4]

1.1.1 Reconsidering the Use of First Row Organotransition Metal Catalysts

The development of cross-coupling chemistry serves as an informative case study regarding the competitiveness, and complementarity, of noble and first row homogeneous catalysts. First row catalysts for cross-coupling were held in high regard during the infancy of the field. Nobel laureate Negishi, in a publication from 1976 describing aryl-alkyl cross-coupling, remarked that the nickel-catalyzed reaction proceeded faster and at lower temperature compared to the analogous palladium-catalyzed reaction.[5] However, a survey conducting in 2011 revealed that 90% of cross-coupling reactions preformed on a scale of >100 mmol were performed by use of palladium.[6] If first row metals are

cheaper, more abundant, and easy to obtain, then why is the field of homogeneous catalysis dominated by noble metals?

To answer in part, base metal chemistry has some associated practical drawbacks that hinder the development of such catalytic systems. First row metal complexes often exhibit paramagnetism, which impedes Nuclear Magnetic Resonance (NMR) characterization of a given precatalyst coordination compound. This makes it difficult to ascertain purity or solution connectivity of a given species. Furthermore, advanced mechanistic studies of reactions of the paramagnetic complex by use of NMR methods, such as deuterium labelling, or measurement of reaction rates via integration of diagnostic NMR peaks, are similarly restricted. Whereas single crystal X-ray diffraction (XRD) data can describe solid state connectivity, the relationship of the chosen crystal to the bulk sample can always be questioned, even when reliable elemental analysis data are available.

First row complexes are known to participate in one-electron chemistry, which can lead to the generation of radical species, and unexpected product distributions in catalytic applications. For example, while palladium favours 0, +2, and +4 oxidation states, catalytic nickel species possessing 0, +1, +2, +3, and even +4 oxidation states have been demonstrated.[7] Reaction mechanisms that involve single electron transfer can be complicated and irregular, and set a high barrier to entry for understanding fundamental patterns.

Moreover, traditional computational methods that model proposed mechanisms involving single electron transfer can be difficult to optimize.[8] In contrast, noble metals typically perform two-electron chemistry involving diamagnetic species, which in

combination with superior NMR characterizability, has allowed for greater understanding of their associated catalytic mechanisms. Such mechanistic insights are crucial to the iteration of catalyst design; as such, noble metal catalysis has benefitted from an enormous amount of iteration in comparison to base metal catalysis. Notwithstanding these issues, the divergent properties of first row metals, relative to the noble metals, provide unique opportunities for the development of new substrate transformations. Indeed, several important advances in base metal catalysis, outlined in subsequent sections, have been demonstrated in recent years, driven in part by advances in ancillary ligand design.

1.2 Principles in Ligand Design

To provide context for these advances, it is necessary to first explain some terminology associated with ligand classification. Ligands are a class of molecules that bond to transition metals to form complexes. The size, shape, and electronic properties of the binding ligands in turn influence the electronic and geometric properties of the metal center, and thus, influence their reactivity. While there are many types of ligands, they can be subdivided by donor type, hapticity, and denticity, among other categories. Two-electron donor ligands (L-donors), such as phosphines, carbon monoxide, and alkenes, form dative bonds with transition metals, whereas one-electron donor ligands (X-ligands), such as halides, alkyls, and amides, form covalent bonds. At a molecular orbital level, these interactions may be along the interatomic bond axis (σ-donation) or orthogonal to the bond axis (π-donation). The metal may also "backdonate" to a donor ligand, depending on the energy and symmetry of the orbitals involved in bonding. In the context of reactivity, ligands can be divided further divided into 'ancillary' and 'reactive'

ligands. Ancillary ligands do not typically participate directly in substrate transformations; rather, they offer a stabilizing framework for the metal. Reactive ligands are altered in some way or lost during a reaction. However, this distinction has become less useful, as examples of cooperative chemistry between otherwise 'ancillary' ligands and the complexed metal have been exploited,[9] such as in transfer hydrogenations.[10]

Ligands may bind as a contiguous set of donor atoms, whereby each atom involved in bonding increases the hapticity (denoted by η^n, where n is number of contiguous atoms) of the ligand by one. For instance, in Figure 1-1, the η^3-allyl ligand binds with a metal M over three contiguous atoms, in contrast to the η^1-propenyl ligand or the η^2-propene. The allyl-metal bonding involves three delocalized electrons from the allyl fragment, making the allyl ligand an LX donor.

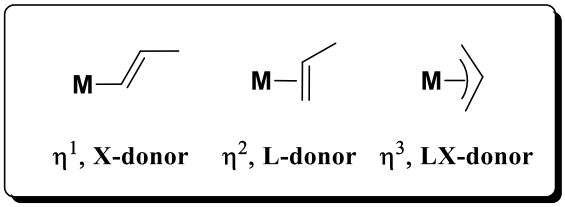

Figure 1-1. Some ligand bonding motifs depicting changes in hapticity (η).

1.2.1 Mono- and Polydentate Ligands

The denticity of a ligand describes the number n of non-contiguous bonding points between the ligand and the metal center, as denoted by κ^n. For example, bis(diphenylphosphino)ethane (dppe) typically chelates to a metal center at each of the two phosphine groups, and would be a κ^2 ligand as represented in Figure 1-2. Chelating ligands, or ligands with denticity of two or greater, are featured prominently in catalytic systems because of their ability to stabilize reactive metal species. If one donor of a chelating ligand of denticity κ^2 were to labilize from a metal in some solvent, rendering

the ligand κ^1, the anchoring effect of its partner donor would increase the rate of donor rebinding relative to if the labilized donor had no restrictions on movement. This property is known as the chelate effect.[11] As expressed in Figure 1-2, loss of a non-chelating donor could rapidly lead to reaction with solvent and possibly further undesired reactivity, or unwanted polynuclear oligomerization and deactivation.

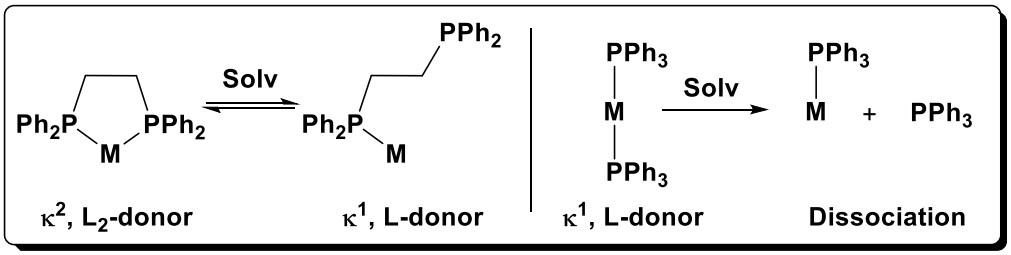

Figure 1-2. Representation of the chelate effect.

1.2.2 Monodentate Phosphine Ligands

Ligands of the type κ^1 are known as monodentate ligands. Notwithstanding the potential benefits of bidentate ligation, monodentate phosphine ligands are ubiquitous in catalysis. With respect to their electronic properties, they can act as both as σ-donors and π-acceptors. While previously subject to some debate, it is now considered that the π-symmetrical σ* orbital on the phosphine is responsible for accepting π-backdonation from the bound metal, as opposed to d orbitals.[12] The donor ability of phosphines can be carefully tuned. Alkyl substituents on the phosphine, such as *t*Bu groups, increase the donor ability via inductive effects. Aryl phosphines are comparatively less strongly donating, on account of mesomeric effects that reduce electron density at phosphorus. Phosphines that feature bonds to more electronegative groups are poorer σ-donors and stronger π-acceptors (e.g. phosphites). The tunability of these properties is important, as electron density at the metal center of a complex is directly related to its ability to

perform fundamental reactions. For example, the higher the electron density of the metal, the more likely it is to undergo oxidative addition processes.

Steric effects of substituents on the phosphine have been extensively tabulated. Tolman introduced the concept of a "cone angle," which is defined as the solid angle formed with the metal at the vertex and the hydrogen atoms at the perimeter of the cone.[13] A higher cone angle results from relatively higher steric repulsion amongst the substituents. For example, PMe_3 has a lower cone angle (118°) than PPh_3 (145°). Relatedly, although a Ph unit has a greater number of carbons than a *t*Bu group, P*t*Bu_3 has a larger cone angle (182°) on account of the planarity of Ph. This means that a P*t*Bu_3 group would be taking up more of the coordination sphere of a metal it was bonded to, which in turn restricts steric access to the metal. It is important to be able to tune the sterics of ligands, because processes such as reductive elimination become more favorable as the ligands become bulkier.

A prominent example of an organometallic complex that features monodentate phosphine ligation is Wilkinson's catalyst, $(PPh_3)_3RhCl$.[14] Wilkinson's catalyst facilitates oxidative addition of molecular hydrogen, which allows for the hydrogenation of various unsaturated species, such as alkenes. This was the first homogeneous catalyst that rivaled the reaction rates of typically less selective heterogeneous catalysts, and the report was noted to be inspirational to Nobel laureate William S. Knowles' efforts towards asymmetric catalysis.[1] Tetrakis(triphenylphosphine)palladium(0) is another example of a revolutionary monodentate phosphine-based precatalyst. This precatalyst readily facilitates palladium(0) – palladium(II) catalytic cycles, and has been broadly applied in cross-coupling reactions, including Stille,[15] Suzuki,[16] and Heck reactions.[17]

1.2.3 Monodentate N-Heterocyclic Carbene Ligands

N-Heterocyclic carbenes[18] (NHCs) are a series of highly sterically demanding monodentate ligands. Two examples of unsaturated (IPr) and saturated (SIPr) NHCs are shown in Figure 1-3. Despite the implied electron-deficient nature of carbenes, NHCs act as strong σ-donors on account of stabilizing π-donation from the lone pair on the adjacent nitrogens to the carbene.[19]

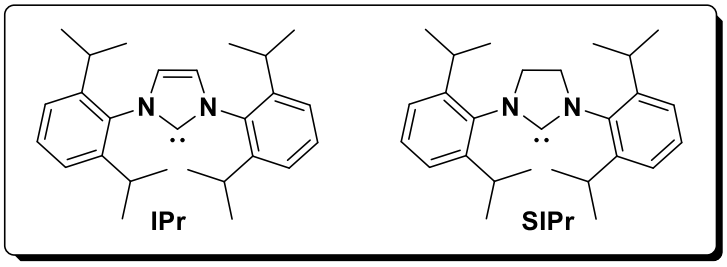

Figure 1-3. Examples of N-heterocyclic carbenes.

NHC ancillary ligands were successfully applied in the manifold of olefin metathesis.[20] Olefin metathesis enables polymerizations and ring-closing reactions that have widespread applications in the assembly of pharmaceuticals,[21] and enable the construction of intricate molecular structures such as catenanes and knots.[22] The 2nd generation Grubbs catalyst is stabilized by NHC ligation, and is shown in Figure 1-4.[23]

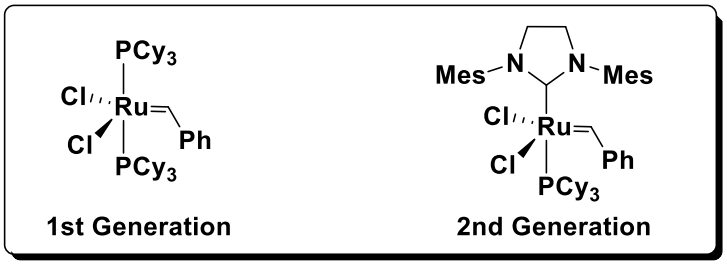

Figure 1-4. 1st and 2nd generation Grubbs' catalysts.

1.2.4 Bisphosphine Ligands

Bisphosphine (P_2) ligands have excelled as ligands in innumerable catalytic reactions. The earliest catalysts for asymmetric synthesis with reasonable enantiomeric excesses were rhodium species featuring P_2 ligands. In particular, the synthesis of L-DOPA, an agent used for treating Parkinson's disease, exploited the chiral-at-phosphine DIPAMP shown in Figure 1-5.[24] Alternatively, Kagan demonstrated that chiral backbones could impart such asymmetry on substrates.[25] Arguably the most famous ligand for use in homogeneous late-metal catalysis, BINAP, exploits this insight by using the axial chirality of the binaphthyl fragment as its source of asymmetry. The two enantiomers of BINAP are shown in Figure 1-5.

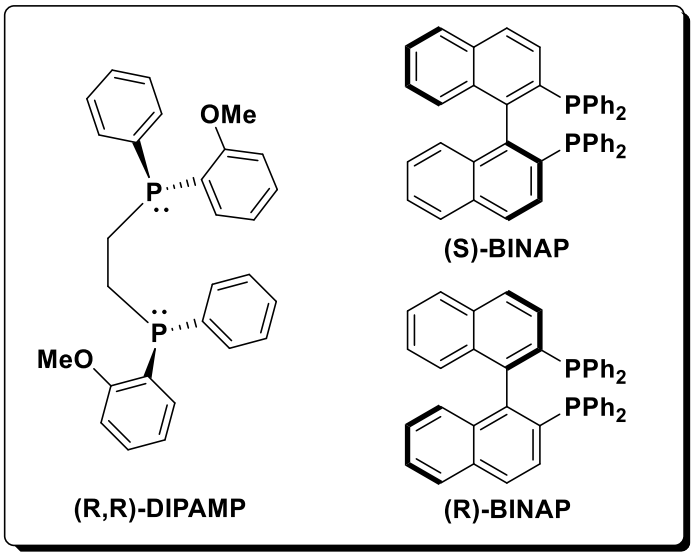

Figure 1-5. (R,R)-DIPAMP and the two enantiomers of BINAP.

BINAP enables metal-catalyzed asymmetric hydrogenations of ketones and olefins with exceptionally high turnover frequencies (TOFs) and turnover numbers (TONs).[26] Beyond asymmetric catalysis, racemic BINAP also has been shown to support

active catalysts for palladium-catalyzed C-N cross-coupling reactions (i.e., Buchwald-Hartwig amination, BHA),[27] among others.

These ligands have inspired considerable research into the development of new phosphines, of which a selection will be mentioned here. DuPhos ligands are a series of P_2 variants developed by DuPont used in asymmetric catalysis, such as asymmetric hydrogenations, aminations, and amidations.[28] XantPhos is a wide bite-angle P_2 that has been applied in hydroformylation chemistry, BHA, and the α-arylation of ketones.[29] PAd-DalPhos is a relatively electron-poor and sterically hindered P_2 with a much lower bite angle that eliminates the need for palladium in a variety of C-N cross-coupling reactions having been designed specifically for compatibility with nickel.[30] These ligands are displayed in Figure 1-6.

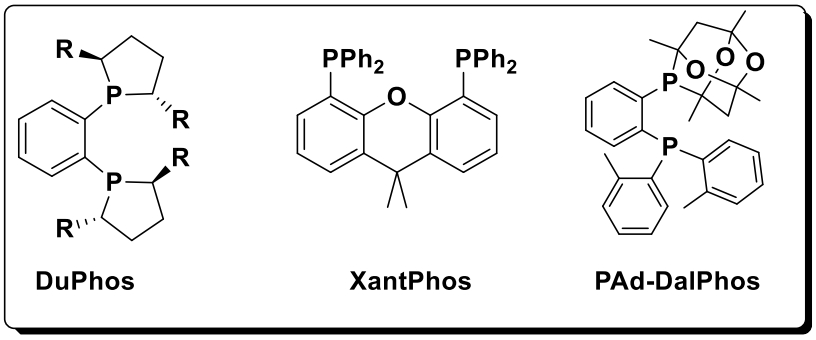

Figure 1-6. A selection of modern P_2 ligands.

1.2.5 Monoanionic Bidentate Ligands

In comparison to a neutral L_2 bidentate ligand, a monoanionic LX bidentate ligand binds more strongly to the metal, on account of the additional covalent bonding character and electrostatic interactions. Monoanionic ligands also allow for the stabilization of higher oxidation state metals without the need for many additional stabilizing ligands or a non-coordinating counterion. β-diketiminates (colloquially known

as NacNac) are a set of monoanionic ligands that have a storied history of supporting reactive metals in stoichiometric and catalytic chemistry since their initial synthesis in the 1960s.[31] In particular, NacNac complexes have been broadly applied in olefin polymerization.[32] The NacNac architecture is derivative of a β-diketimine (HNacNac) precursor structure that acts as a neutral L_2 donor, but it has a relatively acidic proton that can be removed with base to furnish the β-diketiminate, as illustrated in Scheme 1-1 (one tautomer of the HNacNac shown).

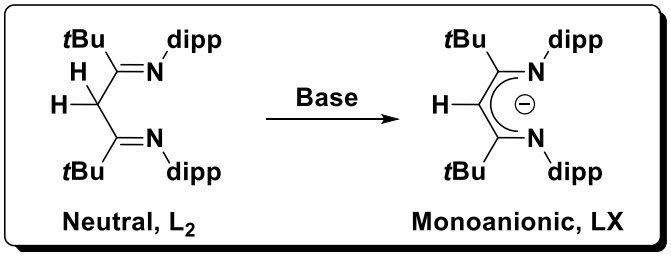

Scheme 1-1. Deprotonation of neutral β-diketimine to form a β-diketiminate (NacNac).

1.2.6 Mixed Donor Bidentate Ligands

Mixed donor ligands include two or more different donor atoms and have divergent properties from P_2 for a few reasons: Firstly, the type of basicity (hard or soft) of a ligand contributes to the affinity of that ligand to a metal. For example, hard donors, such as nitrogen, bind strongly to electron deficient early group transition metals, whereas soft donors, such as phosphorus, bind preferentially to electron rich late metals.[33] In theory, a bidentate ligand that included a hard and a soft donor should be able to stabilize both hard and soft Lewis acids.

In catalytic cycles, the oxidation state of the metal center may change, meaning that a ligand that can stabilize multiple oxidation states should theoretically increase its ability to maintain catalytic integrity. A mismatched donor, such as a hard nitrogen donor

binding to a soft late metal, such as palladium(0), may reversibly labilize; this property is known as hemilability. Hemilability of a donor can allow for the accommodation of a substrate that otherwise may have been sterically or electronically denied access, but also allow for ligand rebinding and stabilization of the metal following the ejection of the modified substrate.[34] Secondly, many catalytic processes involve both oxidative addition and reductive elimination, and generally, the types of characteristics that support oxidative addition (high electron density at metal, low steric bulk) are in opposition to those that support reductive elimination (low electron density at metal, high steric bulk). It should be noted that excessively lowering the steric bulk of the ligand may result in oligomerization of the complex, and loss of coordinative unsaturation that facilitates oxidative addition. If one of the addition or elimination steps is much slower than the other, it can hamper the ability of a catalytic cycle to turn over. Phosphine ligands are primarily σ-donating in character but can be π-accepting depending on the substituents of the phosphine, which slightly reduces the electron density on the metal center and makes the metal center more amenable to reductive elimination processes. Nitrogen, on the other hand, only has σ-donor character as a ligand. Accordingly, replacing one phosphine with a nitrogen has been hypothesized to influence the metal to prefer oxidative additions, notwithstanding the comparable dominance of P_2 ligands to neutral bisamine ligands in this regard.[35] Additionally, phosphines are more strongly *trans*-labilizing than nitrogen, meaning a transition state involving a PN-metal complex and a substrate should arrange in a predictable fashion, which could improve the selectivity of a reaction. A PN ligand that takes advantage of the electronic benefits of PN ligation, in combination with a bulky steric profile, is Mor-DalPhos. Palladium complexes of Mor-DalPhos catalyze a broad

scope of cross-couplings, most notably BHAs. The donor nitrogen can be modified in donor strength by changing its hybridization. Phosphinooxazoline (PHOX) ligands are a set of PN ligands that feature a cyclic sp^2 nitrogen that utilizes these differences in donor properties in regio- and enantioselective allylic alkylations.[35] The nitrogen has been shown to be hemilabile.[36] The structures of Mor-DalPhos and PHOX are detailed in Figure 1-7.

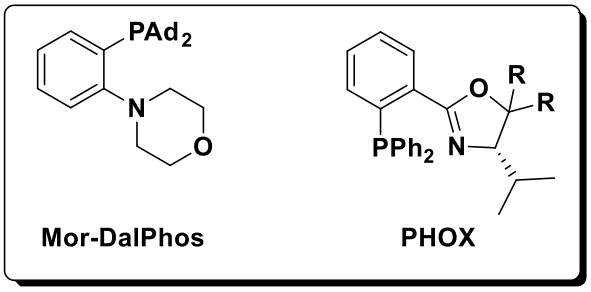

Figure 1-7. Structures of bidentate PN ligand families Mor-DalPhos and PHOX.

1.2.7 Mixed Donor Monoanionic Bidentate Ligands

LX bidentate ligands with a mixed donor pair are heavily utilized as catalysts for olefin chemistry. In particular, the Shell Higher Olefin Process (SHOP) for making polymers and oligomers of olefins helps supply the global demand for plastics and linear α-olefins (LAOs).[37] Linear α-olefins are used as lubricants, detergents, and feedstocks for higher order synthetic goals. The dominant catalytic systems for SHOP involve a nickel(II) complex supported by an LX donor PO bidentate ligand, which electronically enforces a square planar geometry at nickel, despite the large growing carbon chain that one might expect to sterically demand a tetrahedral environment.[37] Metal-alkyl intermediates that include additional stabilization via agostic interactions have also been shown to be involved in such chemistry. [38] Progress in SHOP chemistry was made with NO ligands, which may show higher TONs and TOFs compared to previous

technology.[39] Some ligands used in supporting active SHOP catalysts are shown in Figure 1-8.

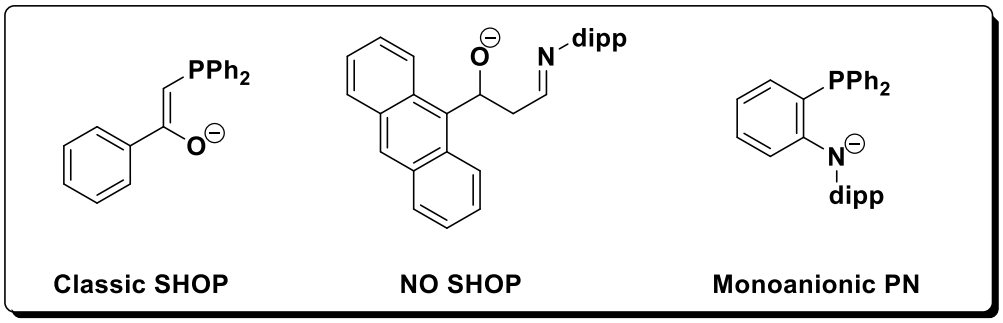

Figure 1-8. PO, NO, and PN ligands.

Ni(II) complexes supported by monoanionic PN ligands[40] (Figure 1-8) have been applied in Kumada cross couplings,[41] and were found to suppress undesired β-hydride elimination (BHE) processes. They have also been applied in carbonyl hydrosilation,[42] through a proposed transient hydride intermediate. Chapters 2 – 4 feature further exploration of this design framework.

1.2.8 Typical and Atypical Ligand-Metal Coordination Geometries

Among late-group transition metal complexes, the 18 and 16 e- "rules" tend to direct the coordination of ligands. An 18 e- complex is typically bonded to six ligands in an octahedral geometry, where the central metal atom or ion has a d^6 electron configuration. A 16 e- complex is typically bonded to four ligands in a tetrahedral or square planar geometry, where the central metal atom or ion has a d^8 electron configuration. Representative complexes are shown in Figure 1-9.

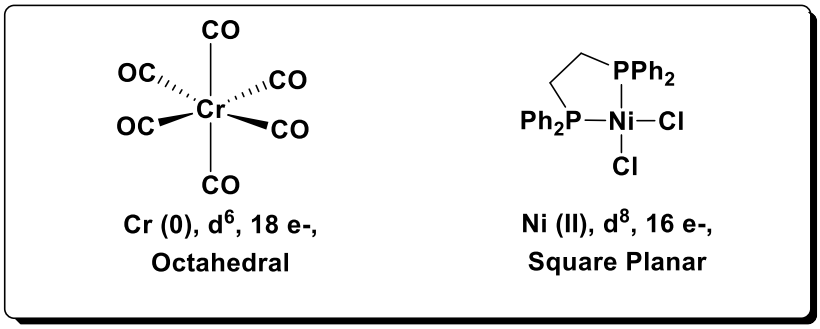

Figure 1-9. Representative 18 and 16 e- complexes.

While these are the most common geometric and electronic arrangements, important exceptions have been reported in the literature. Of particular interest are coordinatively (fewer than 4 ligands) and electronically unsaturated (fewer than 16 e-) complexes. Metal centers with such properties have been found in the active sites of various enzymes, such as nitrogenases, which perform biologically crucial, and energetically challenging, nitrogen fixation.[43] This has encouraged research into the development of synthetic mimics of such active sites that feature unsaturated metal complexes.

1.3 Low-coordinate Complexes

1.3.1 Ligand Design for Low-coordinate Complexes

The desirable reactivity of low-coordinate complexes, in turn, causes practical problems related to their synthesis and isolation. Consider, for example, a hypothetical 14 e-, three-coordinate nickel(II) hydride complex supported by a monoanionic, bidentate mixed donor LX ligand as shown in Scheme 1-2.

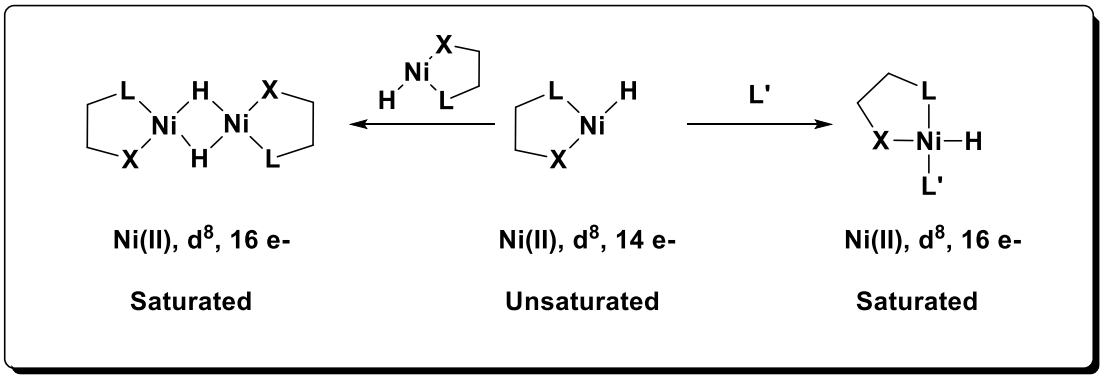

Scheme 1-2. Challenges associated with isolating low-coordinate complexes.

Two potential routes to saturation involve reaction with other ligands or solvent, or dimerization. While dimers or oligomers may be less reactive on account of their saturation, they also bear markedly different physical properties, such as molecular weight and polarity, compared to their monomer counterparts. This can lead to reaction design problems related to differences in solubility between the monomer and the dimer. Fortunately, compound oligomerization can be managed by appropriate ligand design.

Prominent strategies to stabilize low-coordinate metal centers involve increasing the steric bulk of the surrounding ligands, exploiting the chelate effect, and utilizing covalent bonding between the chelating ligand and the metal center. A hypothetical appropriately bulky ligand allows for chelation of nickel, but inhibits dimerization via steric repulsion, as shown in Scheme 1-3.

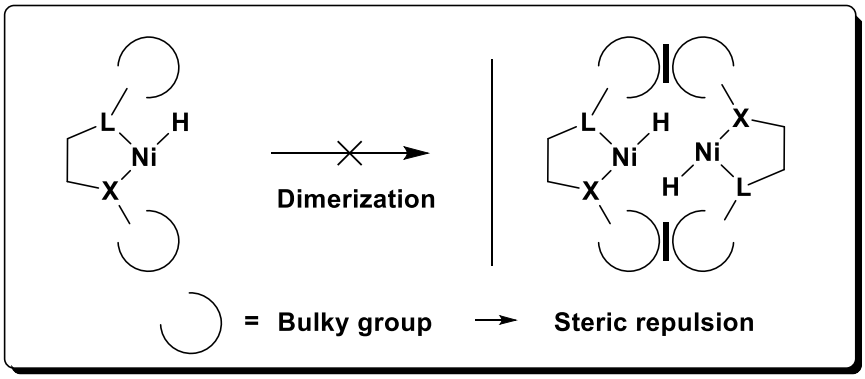

Scheme 1-3. Steric inhibition of dimerization.

However, excessive steric bulk can inhibit ligand metalation, as illustrated in Scheme 1-4.

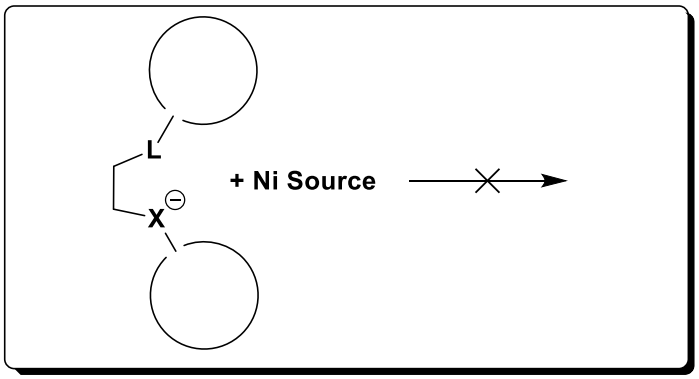

Scheme 1-4. Steric inhibition of metalation.

One pertinent class of successful ligands for stabilizing unsaturated metal complexes that observe these principles are, homobidentate, monoanionic NacNac ligands that feature bulky *t*Bu and dipp (2,6-diisopropylphenyl) substituents. Some examples, including the first reported three-coordinate methyl complex of a transition metal, are shown in Figure 1-10.[44]

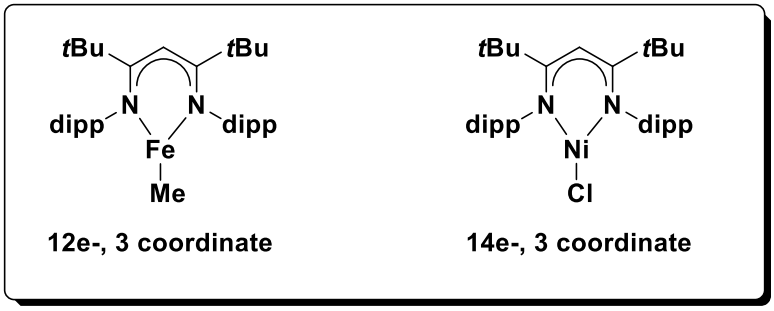

Figure 1-10. Some low-coordinate complexes stabilized by NacNac ligation.

These complexes have shown unusual reactivity. Reduction of the three-coordinate (NacNac)nickel(II) bromide analogue enabled the binding of dinitrogen by nickel, of which there had been few previous reports. Specifically, reduction of the complex with potassium graphite (KC_8) allowed for binding of dinitrogen and the formal reduction of the dinitrogen triple bond, as described in Scheme 1-5.[45]

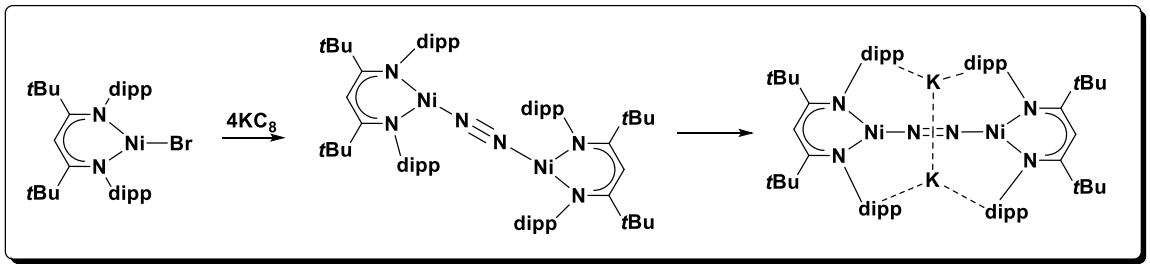

Scheme 1-5. Reduction of dinitrogen by a NacNac nickel(II) complex and KC_8.

1.3.2 Case Study: Low-coordinate Nickel Complexes

As mentioned in Scheme 1-3, alterations to either chelating or non-chelating ligands can have a dramatic impact on the coordination geometry of the complex. Mononuclear anionic ligands such as halides and hydrides, on account of their ionic radii[46] have minimal steric profile compared to multinuclear ligands, such as substituted amides. Changing the *t*Bu groups on the NacNac ligand depicted in Figure 1-10 to methyl groups results in the corresponding nickel(II) complex being dimeric and four-coordinate at nickel, as opposed to the monomeric, three-coordinate complex shown. However, the

salt metathesis of that (NacNac)nickel(II) chloride dimer with a bulky amide salt, as represented in Scheme 1-6, generates a three-coordinate complex.[47]

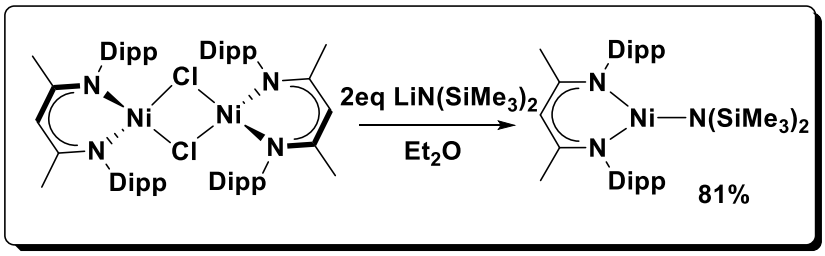

Scheme 1-6. Synthesis of a three-coordinate NacNac nickel(II) amido complex.

1.3.3. Transient Low-coordinate Complexes

The preferred coordination number for a given ancillary ligand-metal complex may depend on the nature of the attached reactive ligand(s). This phenomenon has implications for catalytic reaction design. For example, migratory insertion reactions into metal hydride bonds are important steps in catalytic reactions, such as olefin chain-walking and polymerization.[48] The complexes introduced in Scheme 1-3 and Scheme 1-4 offer a framework for describing these implications. While the "stable" three-coordinate hydride complex (of which only one isolated example has been reported for a transition metal complex, itself a dimer assembled via ancillary ligand coordination to bridging K^+ ions rather than bridging via the hydrides)[49] featuring the bulky ligand might be resistant to dimerization, it would also likely bind olefin more slowly for steric reasons. For this reason, one might choose the less bulky ligand, and generate the otherwise non-isolable, transient mononuclear nickel hydride *in situ* in a mixture of reactants via activation of a precatalyst. In a catalytic mixture, the large excess of substrate would inhibit dimerization of this otherwise highly reactive compound for both kinetic and thermodynamic reasons. Firstly, the rate of dimerization would plausibly be second order with respect to the mononuclear nickel hydride, and the presence of excess substrate would rapidly capture

any mononuclear hydride, minimizing its concentration, and thus the rate of dimerization. Secondly, any dimer that did form could plausibly react in equilibrium with substrate in a manner such that one half of the dimer would be displaced, and Le Châtelier's principle may favor such a reaction based on the excess of substrate. These arguments are summarized in Scheme 1-7. However, highly stable dimers may not react with even large excesses of substrate.

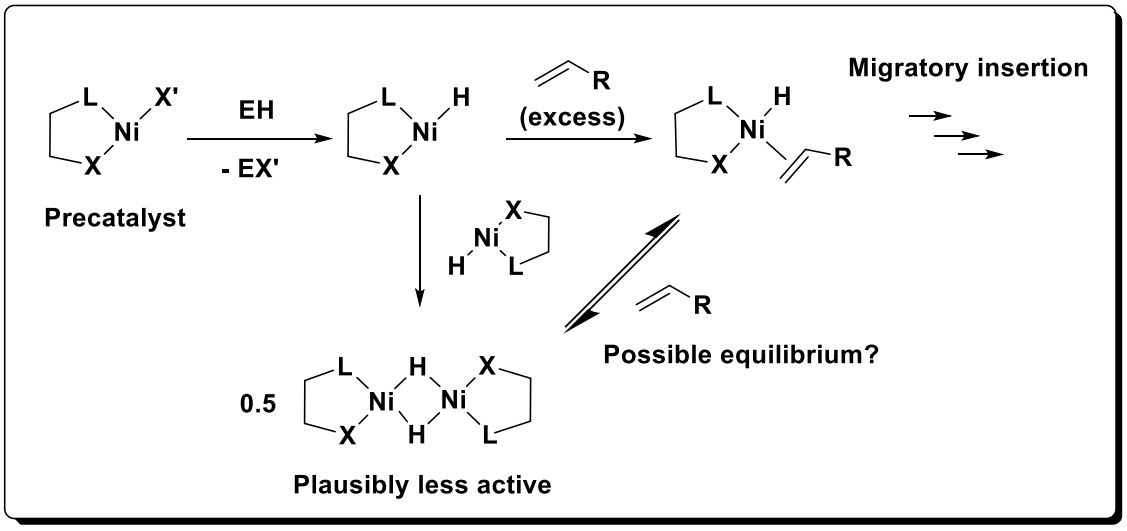

Scheme 1-7. Hypothetical reactivity of a transient nickel hydride.

However, in a traditional batch reaction, as the reactants are consumed, the catalyst will begin to dimerize and deactivate for the opposite reasons. Additionally, by-products of precatalyst activation could plausibly complicate the reaction. Finally, precatalysts themselves must be carefully designed such that they are convenient to handle. The side product of precatalyst activation, for instance EX′ in Scheme 1-7, might interfere with the desired reactivity. Ideally, the X′ leaving group is chosen such that it is small enough to allow exposure of the metal to the activator (EH in Scheme 1-7) for rapid activation, but large enough to inhibit dimerization and saturation of the metal. Even if those factors are satisfied, the electronics of X′ should be tuned such that the M-X′ bond

is not especially strong nor weak, to minimize the needed reactivity of the activator and maximize ease of storage and handling of the precatalyst. Léonard and Chirik reported that while an isolable dimeric diimine nickel(I) hydride complex was shown to catalyze alkene hydrogenation, superior performance was found via activation of a nickel precatalyst with the same ligand system.[50]

Another strategy for precatalyst design, employed in SHOP precatalysts, typically involves a mononuclear, 16 e- precatalyst featuring a bidentate, mixed donor monoanionic ligand, as well as a monodentate L donor. The monodentate ligand can de-coordinate in the presence of olefin to open up an active site for olefin binding, and subsequent insertion into a Ni-X′ bond.[51] Following an arbitrary number of olefin insertions, BHE, and olefin substitution, an on-cycle active species is generated. This process is summarized in Scheme 1-8.

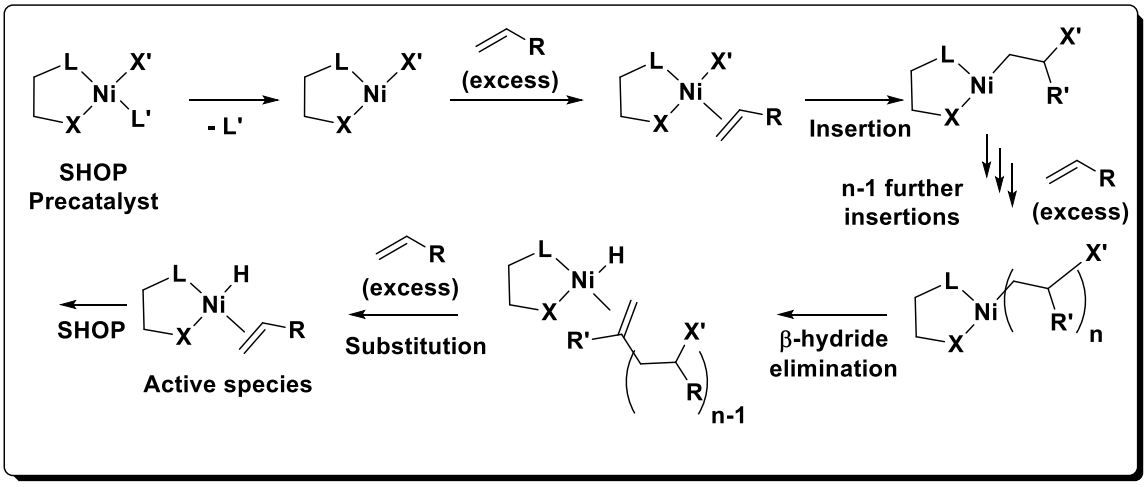

Scheme 1-8. Activation of a typical SHOP precatalyst.

In contrast, one could eschew the precatalyst route, and choose a ligand such that the metal hydride complex is isolable. For nickel hydrides specifically, this requires coordination numbers greater than three. Accordingly, one common ancillary ligand

archetype to stabilize such complexes are tridentate ligands, colloquially known as 'pincer' ligands. As an aside, some definitions of pincer ligands[52] require rigidity or enforced meridional geometry, although this distinction is less useful considering unexpected deviations from meridionality,[53] rigidity,[54] or even reversible cleavage of the ligand,[55] within systems that occasionally support 'traditional' pincer geometries.[56] In other cases, the hemilability of one of the donor ligands facilitates substrate binding.[57] Nevertheless, nickel hydride pincer complexes have been successfully as catalysts for a number of transformations, such as CO_2 hydroboration.[54,58] With these considerations in mind, I will describe some specific advances in base metal catalysis.

1.4 Case Studies in Contemporary Base Metal Catalysis

1.4.1 Cobalt: A Replacement for Noble Metals in Asymmetric Hydrogenation

While pioneering work in the field of asymmetric hydrogenations was performed by Knowles using rhodium catalysts, dramatic improvements in cobalt-based asymmetric hydrogenation have been demonstrated in recent years. Inspired by the successes of cobalt(II) alkyl pincer complexes in some representative reactions,[59] the Chirik group, in combination with researchers at Merck, delved into the high throughput screening of ligand-cobalt systems for utility in asymmetric hydrogenations. To find a suitable system, combinations of 192 bidentate phosphine ligands and cobalt alkyl precursors were screened in the asymmetric hydrogenation of the ubiquitous methyl 2-acetamidoacrylate (MAC).[60] In particular, DuPhos-type ligands, shown in Figure 1-6, enabled conversions and enantiomeric excesses (*ee*) >90% without the need for noble metals. Even the hindered alkene *trans*-methylstilbene, previously only accessible for asymmetric hydrogenation by iridium catalysts,[61] was successfully hydrogenated in high conversion

and *ee* with cobalt and certain bulky bisphosphines. This chemistry has been extended more recently to the hydrogenation of enamides.[62]

1.4.2 Iron: A Replacement for Ruthenium in Transfer Hydrogenation

Transfer hydrogenation involves the transfer of an equivalent of dihydrogen from a non-gaseous hydrogen source, such as an alcohol, across an unsaturated bond. This is an appealing chemical process, as the handling of gaseous dihydrogen presents practical and safety challenges. Noyori developed a revolutionary catalytic system featuring a chiral diphosphine/diamine tetradentate ruthenium complex for the asymmetric transfer hydrogenation of aryl ketones.[63] The Morris group applied this ligand framework to iron, with optimized alterations over several publications,[10a-c,64] and recently demonstrated that iron can effectively transfer hydrogenate imines and ketones with high yields and enantioselectivity.[10d] Noyori's ruthenium catalyst and Morris' iron catalyst from his 2013 publication in *Science* are pictured in Figure 1-11.

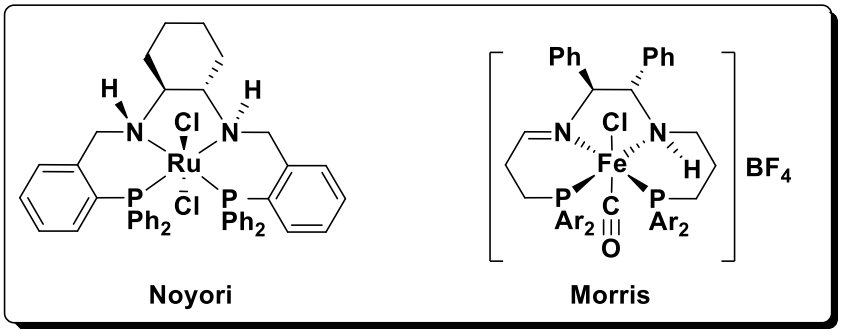

Figure 1-11. Ruthenium and iron transfer hydrogenation catalysts.

1.4.3 Nickel: A Replacement for Palladium in C-N Cross-coupling

C-N cross-coupling reactions are crucial in efficiently furnishing the nitrogenous functional groups included in many pharmaceuticals. Palladium complexes supported by bulky and electron-rich ancillary ligands, such as P_2 or NHCs, emerged as the state-of-

the-art in such catalysis. These reactions are challenging because the catalyst not only must enable the oxidative addition of the aryl-pseudohalide substrate and the reductive elimination of the aminated product, but also discourage the monoarylated product from re-entering the catalytic cycle. Independent initial reports by Stradiotto[65] and Hartwig[66] described the unprecedented nickel-catalyzed monoarylation of ammonia using JosiPhos type systems. However, in their reports, other well-established bulky and electron-rich phosphine ligands that perform well with palladium, such as Mor-DalPhos, proved unsuitable in analogous nickel chemistry. Recent findings from the Stradiotto group describe an active nickel catalyst supported by PAd-DalPhos (Figure 1-6), a bulky P_2 that is more electron deficient than ligands associated with palladium.[30a] This nickel catalyst is efficient for a broad scope of challenging ammonia and amine monoarylations, including the first reports of (hetero)aryl mesylate aminations. Recent advances in ligand design specific for nickel-catalyzed C-N cross-coupling reactions were summarized in a review by Lavoie and Stradiotto.[30b]

1.5 N-Phosphinoamidine/amidinate Ligands

The examples presented above demonstrate that carefully chosen ligands can impart "nobility" on base metals with respect to catalysis. In the quest to develop new low-coordinate base metal complexes for use in establishing new stoichiometric and catalytic chemistry, the Stradiotto and Turculet groups, in collaboration with Chevron-Phillips Chemical (CPChem), initiated an investigation of PN bidentate donor ligands. Investigations quickly identified the ability of these ligands to be readily converted between monoanionic and neutral forms. Despite the aforementioned catalytic capability of monoanionic ligands and neutral PN ligands separately, the combination of these

motifs had remained poorly explored. Derived from the amidinate framework,[67] the chosen ligand backbone is highly modular, owing to the alterability of substituents of the aniline, benzonitrile, and phosphine used in its synthesis, as outlined in Scheme 1-4.

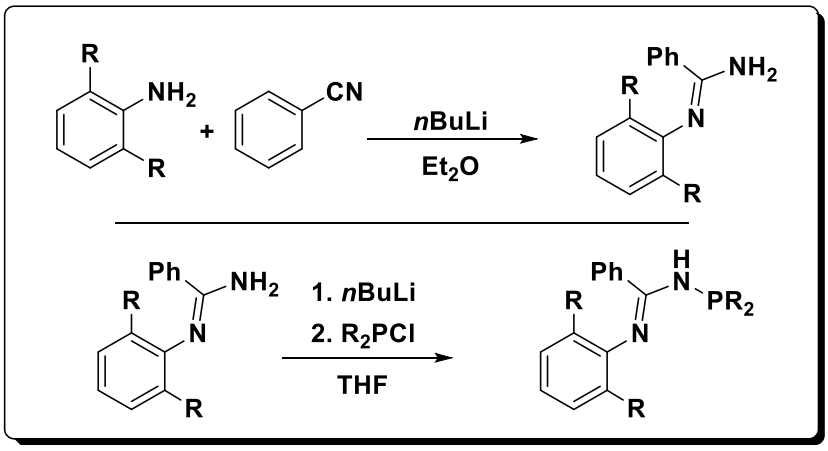

Scheme 1-9. Modular synthesis of HPN ligand.

Similar to NacNac, the monoanionic *N*-phosphinoamidinate (PN) ligand can be generated by treatment of the protonated HPN with base, shown in Scheme 1-10. The successes of NacNac as a stabilizing ancillary ligand for low-coordinate complexes inspired confidence that PN complexes with appropriately sized substituents could perform analogously, with differences in reactivity stemming from the five-membered chelate of a PN complex and the mixed-donor nature.

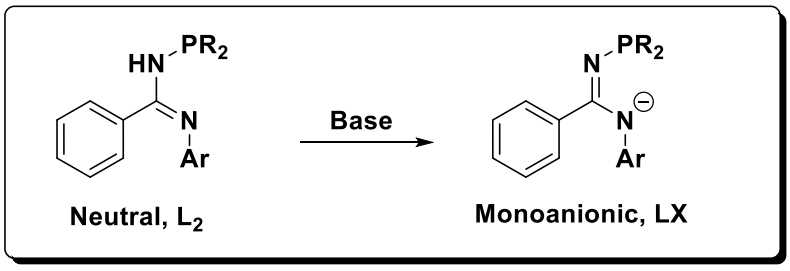

Scheme 1-10. Conversion of neutral HPN to anionic PN via treatment with base.

Building on an initial report from CPChem of selective olefin tri- and tetramerization using HPN chromium complexes,[68] monoanionic PN complexes of iron,[69]

cobalt,[70] ruthenium,[71] and platinum[72] were synthesized and applied in stoichiometric and catalytic reactions. In particular, a three-coordinate, formally 12e- (PN)iron complex was shown to be a precatalyst for the efficient hydrosilylation of ketones,[69] while a three-coordinate, formally 13e- (PN)cobalt complex was shown to be a precatalyst for the remarkable terminal isomerization/hydroboration (I-H) of alkenes.[70] In the case of platinum, PN ligation allowed for the isolation of a rare neutral, three coordinate platinum(II) amido species.[72] The (PN)chromium,[68] iron,[69] cobalt,[70] and platinum[72] complexes are shown in Figure 1-12. Notably, analogous (PN)nickel complexes had not yet been reported at the outset of this research. Motivations for developing such complexes stemmed from the broad utility of nickel in homogeneous catalysis.

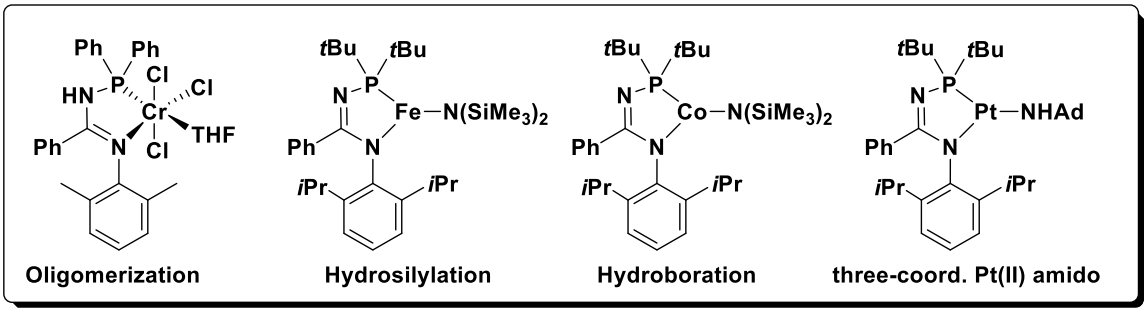

Figure 1-12. (H)PN complexes of Cr, Fe, Co, Pt, and their utility.

1.6 Further Applications of Nickel in Homogeneous Catalysis

Nickel retains the cheap cost of base metals, while maintaining the same electron-rich d-orbital configuration as its more celebrated partners in group 10, palladium and platinum. Accordingly, homogeneous nickel catalysts have been applied in a wide variety of different reactions.[4d] Previously mentioned examples include (PO) and (NO)nickel complexes that are used in SHOP chemistry (Figure 1-8), and (P_2)Ni complexes that enable challenging C-N cross couplings (Section 1.4.3). Nickel-catalyzed cross-coupling reactions that once showed great promise[5] have been further developed, and now include

challenging sp^3-sp^3 cross couplings[73] that rival and even surpass analogous palladium systems.[74] Tridentate (L_2X)nickel pincer complexes assist the selective hydrosilylation of olefins with tolerance for carbonyl groups,[75] as well as the selective reduction of carbon dioxide.[54,76] The complexes responsible for those reactions are shown in Figure 1-13.

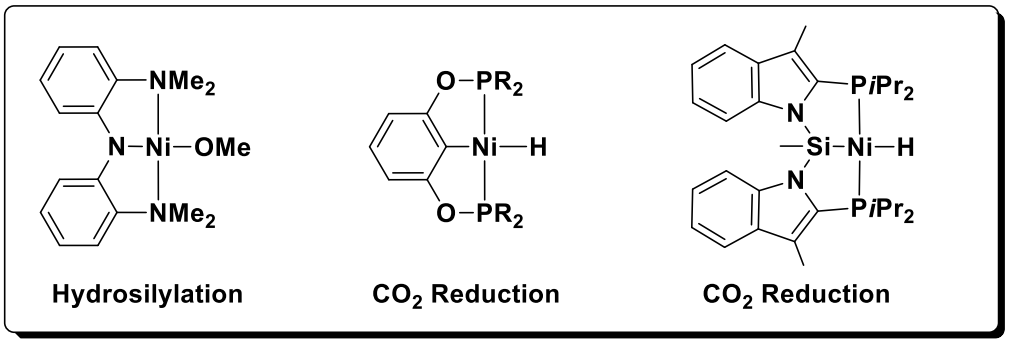

Figure 1-13. Nickel pincer complexes used in hydrosilylation and CO_2 reduction.

1.7 Thesis Goals

In this context, I will describe my strategy towards developing (PN)nickel chemistry. Firstly, synthetic routes towards low-coordinate nickel complexes were devised, to determine if analogous complexes to the (PN)iron, cobalt, and platinum complexes were achievable. Initial forays into (PN)Ni chemistry focused on simple nickel halides that could act as precursors for further reactions. Targets included nickel(II) complexes of the type **(HPN)Ni(X)$_2$** or **[(PN)Ni(X)]$_2$**, as represented in Figure 1-14.

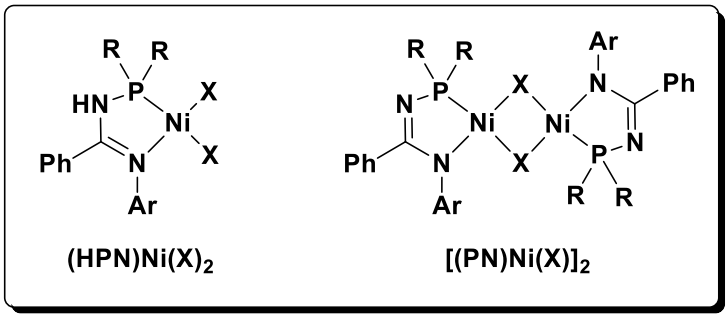

Figure 1-14. Initial synthetic targets.

X-ray diffraction experiments were occasionally necessary to determine the connectivity of these complexes. For this reason, P*t*Bu$_2$ and Ndipp were chosen as the substituents on the PN backbone (this specific analogue will be abbreviated as **(HPN)** and **(PN)** for the neutral and anionic forms, respectively), as these had proven to afford crystalline ligands and complexes in previous studies.[69-72] With these precursors in hand, attempts to generate low-coordinate complexes were undertaken, as outlined in subsequent sections. Treatment of such precursors with MNR$_n$, MOR, or MR reagents produced various low-coordinate complexes of the type (PN)Ni(NR$_n$), (PN)Ni(OR), or (PN)Ni(R), which were interrogated for new stoichiometric chemistry, or applied as precatalysts. In Chapter 2, three-coordinate **(PN)M** complexes (M = Mn, Fe, Co, Ni) were compared with in the context of alkene isomerization-hydroboration. The **(PN)NiN(SiMe$_3$)$_2$** precatalyst (abbreviated as **(PN)Ni**) was associated with complex reactivity, inspiring a mechanistic study to determine the nature of catalytic intermediates. In Chapter 3, iterations of three-coordinate **(PN)NiX** complexes were analogously compared in hydrosilative amide reductions, and **(PN)Ni(O*t*Bu)** was found to enable ambient temperature reductions of challenging substrates. In Chapter 4, the coordination chemistry of **(PN)Ni-** hydride and alkyl complexes were explored, and the

insertion of benzene into a Ni-H bond is described, along with the synthesis of β- and γ-agostic alkyl complexes.

CHAPTER 2: ALKENE ISOMERIZATION–HYDROBORATION CATALYZED BY FIRST-ROW TRANSITION-METAL (MN, FE, CO, AND NI) *N*-PHOSPHINOAMIDINATE COMPLEXES: ORIGIN OF REACTIVITY AND SELECTIVITY

2.1 Introduction

Alkene hydroboration offers an attractive route to alkylboron compounds,[77] which in turn can be employed as synthons in diversity of useful organic transformations, including Suzuki-Miyaura[16,78] cross-couplings. Although alkene hydroboration can in some cases proceed in the absence of a catalyst, reactions conducted in the presence of an appropriate catalyst can enable the use of otherwise unreactive B-H reagents, and/or can afford complementary selectivity versus uncatalyzed transformations.[79] Transition metal catalysts are appealing in this regard, as well-established metal-catalyzed transformations such as alkene isomerization[80] can in principle be paired with hydroboration, leading to selective borylation at a position that is remote from the initial position of the C=C double bond. The challenge in developing such isomerization-hydroboration (I-H) reactions leading to remote functionalization[81] is that the catalyst must enable facile alkene isomerization, while also maintaining high borylation selectivity (i.e., internal versus terminal hydroboration).[82] Such challenging transformations leading to terminal borylation selectivity had for some time been limited to examples involving zirconium, rhodium, or iridium catalysis in combination with pinacolborane (HBPin).[83] (P_2)rhodium and iridium precatalysts functioned with loadings of <5% at ambient temperature, whereas $HZrCp_2Cl$ was required higher loadings (50 mol%). A transition from precious to first-row metals in this chemistry is useful for the reasons outlined in Section 1.1.1

(e.g., cost and abundance). However, as highlighted therein, mechanistic investigations into first-row catalytic reactions are relatively underdeveloped due to the properties of first-row metals (e.g., paramagnetism and single electron chemistry). In 2013, Obligacion and Chirik[84] disclosed the use of (bis(imino)pyridine)CoMe precatalysts (Figure 2-1) to effect alkene I-H with HBPin under mild conditions. On the basis of experimental mechanistic data including isotopic labeling studies, Co-H species were invoked as key catalytic intermediates.[84] The Dalhousie/CPChem research team contemporaneously observed that (PN)metal(amido) precatalysts of the type **(PN)M** (M = Co, Fe; Scheme 2-2) were effective in promoting I-H reactions of alkenes with HBPin, including terminally selective transformations of octenes **1a-c** into the 1-octylboronate product **2a**.[70,85]

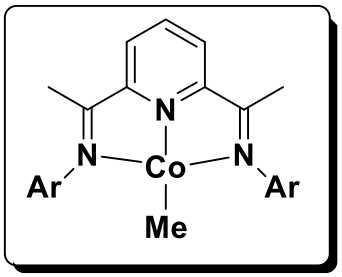

Figure 2-1. (Bis(imino)pyridine)CoMe precatalysts for alkene I-H.

A summary of proposed organometallic steps to facilitate alkene I-H via a general (L_n)MH catalyst is shown in Scheme 2-1. (L_n)MH is generated *in situ* via metathesis of some (L_n)MX precatalyst with HBPin. Coordination of an internal alkene, followed by insertion of the alkene into the hydride bond generates a secondary alkyl species, (L_n)M(*sec*-alkyl). Rather than undergoing metathesis with HBPin to furnish an internal borylation product and regenerate (L_n)MH, instead, the complex undergoes BHE, and re-insertion to generate a terminal alkyl species, (L_n)M(*n*-alkyl). This complex then reacts

with HBPin in either a stepwise (presumably OA/RE) or concerted (σ-bond metathesis) process to produce the terminal hydroboration product and regenerate $(L_n)MH$.

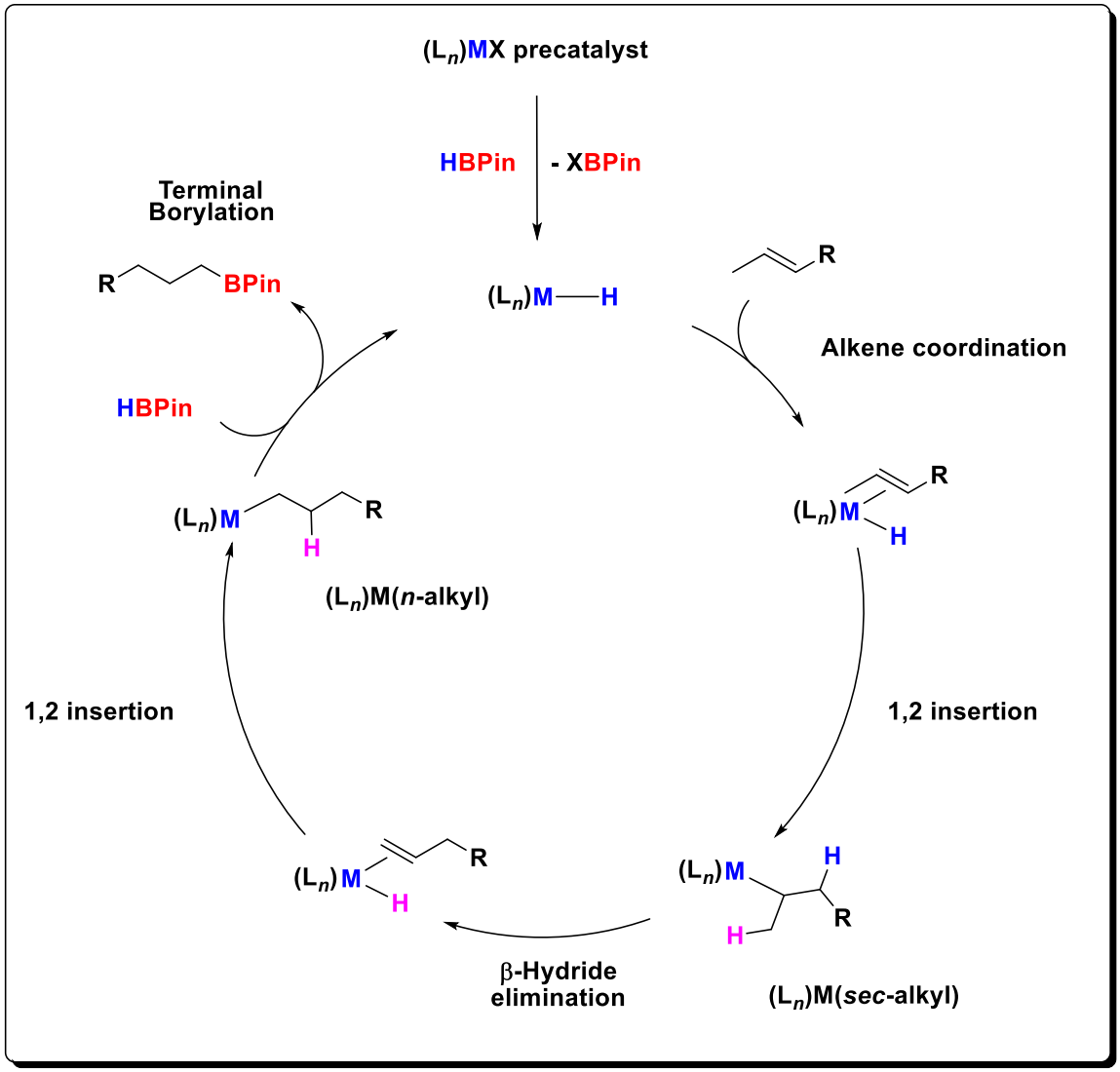

Scheme 2-1. Proposed mechanism for alkene I-H via some $(L_n)MX$ precatalyst.

The Dalhousie/CPChem team subsequently established that **(PN)Co** and **(PN)Fe** can be employed in related transformations involving a collection of terminal, geminal, and internal alkenes, whereby the extent and locale of the terminal selectivity achieved is influenced by the choice of metal precatalyst, as well as the B-H reagent employed (e.g., HBPin versus 1,3,2-diazaborolane).[86,87] Inspired by these differences in reactivity, the

contemporaneous discovery of **(PN)Mn** as an efficient precatalyst for hydrosilative carbonyl reduction,[88] and our curiosity with respect to potential unique reactivity for **(PN)Ni**, I joined this team in a comparative study. Specifically, we sought to compare **(PN)M** precatalysts (M = Mn, Fe, Co, Ni) featuring systematically incremented d-electron populations (d^5-d^8) in catalytic alkene I-H. Upon discovering stark differences in reactivity, we turned to further experimental and computational methods to rationalize these differences and understand the operative mechanism. A summary of the previous work (a) and the work described in this chapter (b) is included in Scheme 2-2.

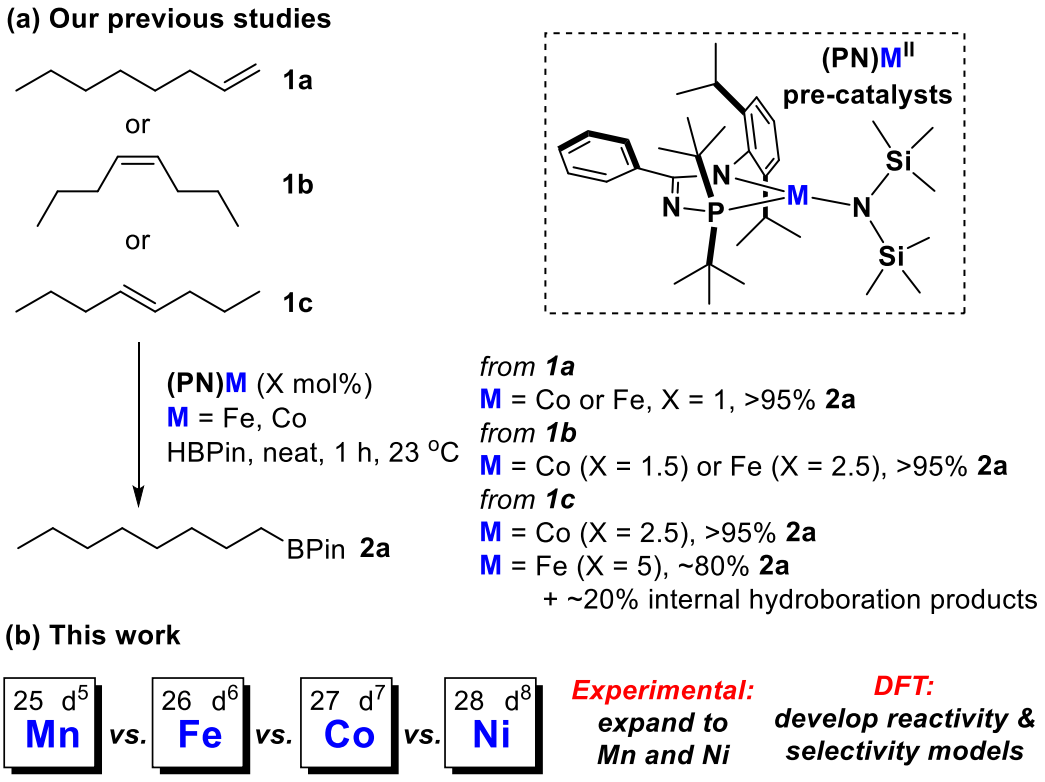

Scheme 2-2. (a) Previous study of octene I-H with HBPin catalyzed by (PN)Fe and Co Complexes; (b) combined experimental and DFT survey of octene I-H employing $(PN)M^{II}$ precatalysts (M = Mn, Fe, Co, Ni).

2.2 Results and Discussion

2.2.1 Contributions

Co-authors contributed greatly to this section of the thesis. Takahiko Ogawa performed I-H and 'isomerization-only' experiments with **(PN)M** (M = Mn, Fe, Co) complexes, and made the crucial observation of n-octane formation in initial reactions involving **(PN)Ni** that produced complex mixtures. The team at Brigham Young University (Samantha J. Gustafson, Jack T. Fuller, Doo-Hyun Kwon, and Daniel H. Ess) was responsible for the computational work. Crystallography was performed by Drs. Michael Ferguson and Robert McDonald at the University of Alberta. Dr. Michael D. Lumsden (Dalhousie) helped with NMR data modelling of the isolated nickel hydride complexes, and their propensity for deuterium incorporation. Otherwise, all work presented in this chapter was carried out by the author. This work has been published. [89]

2.2.2 Synthesis and Characterization of (PN)Ni

Whereas the syntheses of **(PN)M** (M= Mn[88], Fe[69], and Co[69]) were previously accessed via treatment of **(HPN)** with their respective $M(N(SiMe_3)_2)_2$ salts, **(PN)Ni** required an alternative synthetic route on account of the transient stability of $Ni(N(SiMe_3)_2)_2$.[90] As suggested in Figure 1-14, **$((PN)NiCl)_2$** was targeted as a precursor, and it was accessible[91] via treatment of $NiCl_2$dme with the pro-ligand **(HPN)** followed by base, as outlined in Scheme 2-3.

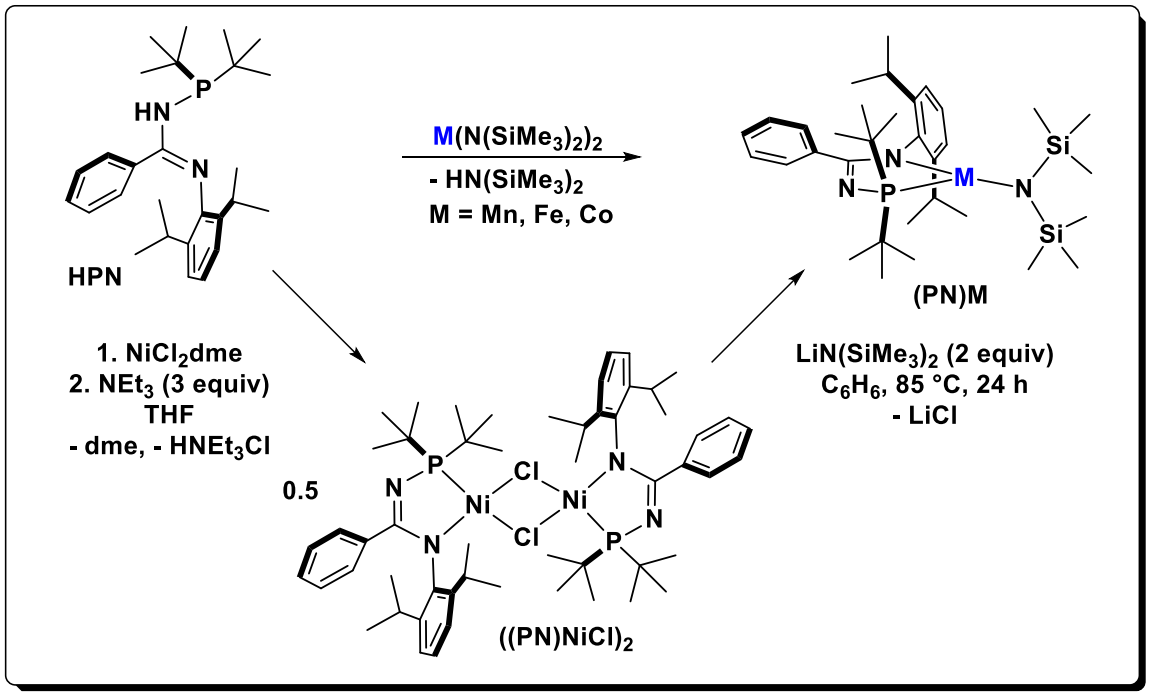

Scheme 2-3. Synthesis of (PN)M complexes, as well as the precursor ((PN)NiCl)$_2$.

Upon workup, (**(PN)NiCl)$_2$ (**henceforth, **Ni$_2$Cl$_2$)** was found to be a diamagnetic compound (see Figure S2-1) displaying sharp NMR resonances consistent with a C_2 symmetric structure, shown in Figure 2-4. Each nickel(II) center is arranged in an approximately square planar geometry. The *trans*-directing nature of the phosphine donor group is evident in the notably longer Ni-Cl' bond length of 2.2919(5) Å compared to the Ni-Cl bond length of 2.1942(5) Å. Notably, an analogous homobidentate complex ((NacNac)NiCl)$_2$ is tetrahedral about each Ni(II) center, inducing paramagnetism, with longer Ni-Cl distances of 2.324(1) and 2.349(1).[47] Apparently, replacement of a nitrogen donor with a stronger-field phosphine donor sufficiently increases the d-orbital splitting of the d^8 nickel center to favor an electronic configuration consistent with square planar geometry, despite the steric effects of the ligand.

Treatment of **Ni$_2$Cl$_2$** with LiN(SiMe$_3$)$_2$ in benzene at elevated temperature (Scheme 2-3) upon workup afforded the target complex **(PN)Ni** in near quantitative

yield. Unlike the analogous paramagnetic Mn, Fe, and Co species, **(PN)Ni** is a diamagnetic complex that exhibits sharp multinuclear resonances consistent with a C_S symmetric structure (see Figure 2-2 and Figure 2-3).

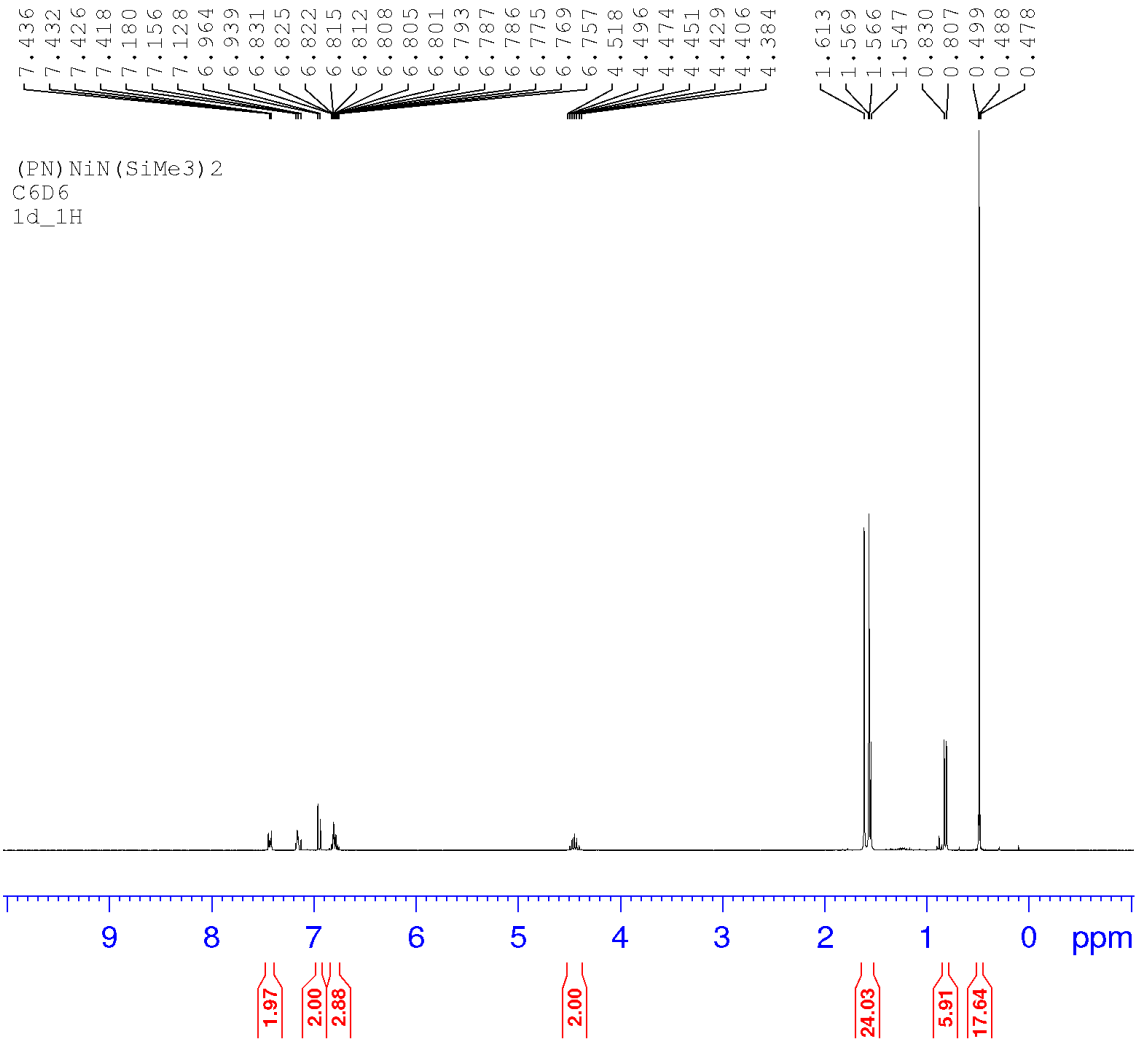

Figure 2-2. ^{1}H NMR spectrum of (PN)Ni (benzene-d_6, 300 MHz). One CH_{arom} is coincident with the residual solvent peak.

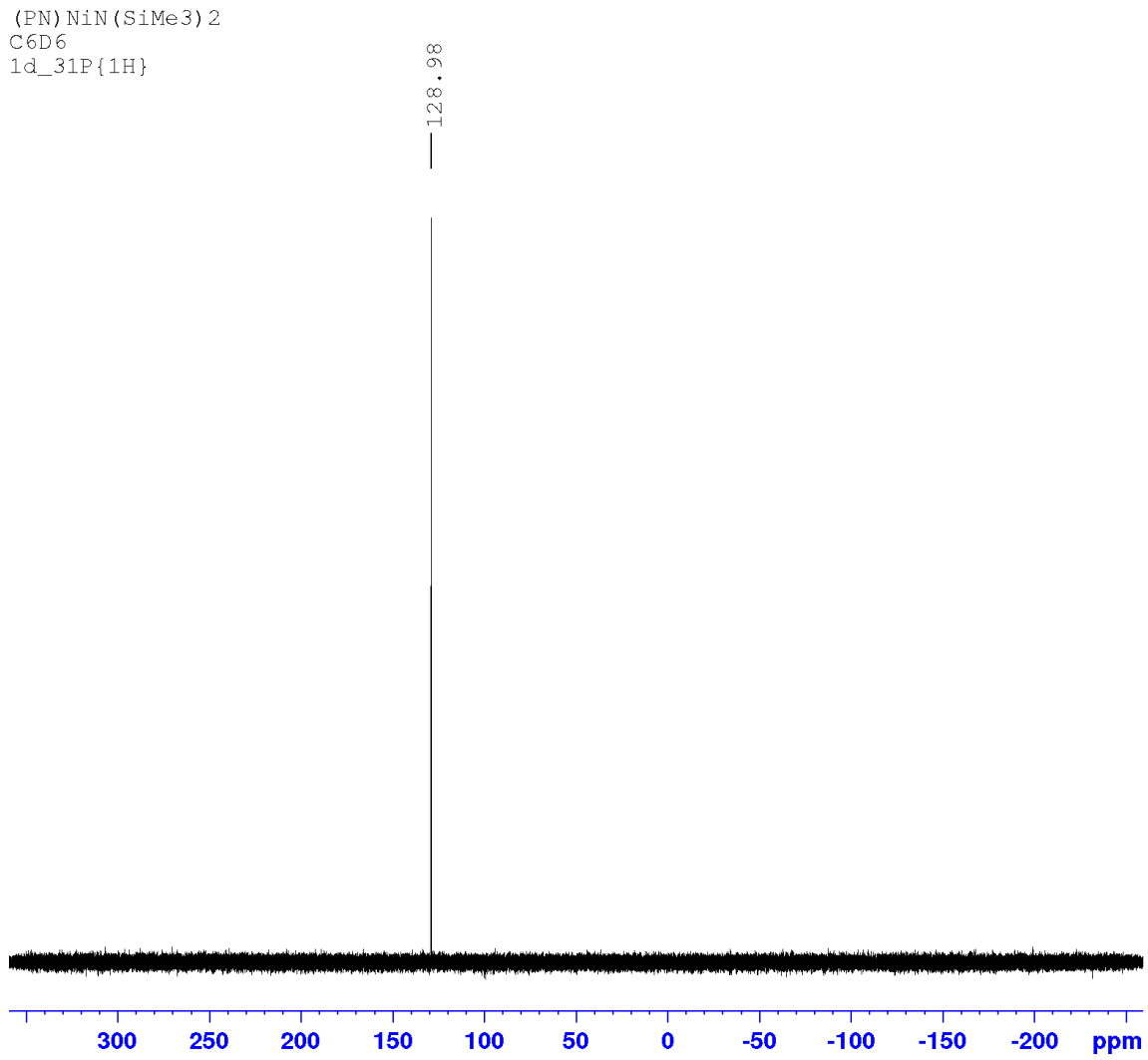

Figure 2-3. $^{31}P\{^{1}H\}$ NMR spectrum of (PN)Ni (benzene-d_6, 121.5 MHz).

The mononuclear, three-coordinate, distorted trigonal-planar structure of **(PN)Ni** was confirmed on the basis of X-ray diffraction analysis (Figure 2-4) and mirrors the connectivity observed within the previously characterized **(PN)M** analogues. In keeping with periodic trends, the M-P and M-N interatomic distances in the **(PN)M** series systematically decrease on going from Mn (e.g., Mn-P 2.5319(4) and 2.5045(4) Å, within two crystallographically independent molecules; Fe-P 2.4434(6) Å; Co-P 2.3873(7) Å) to Ni (Ni-P 2.1564(9) Å). A similar structural trend has been observed in an analogous set

of three-coordinate (NacNac)MN(SiMe$_3$)$_2$ complexes, where the Ni member of the series (Ni-N(SiMe$_3$)$_2$ 1.873(2) Å; *cf* 1.849(2) Å in **(PN)Ni**), is paramagnetic.[47]

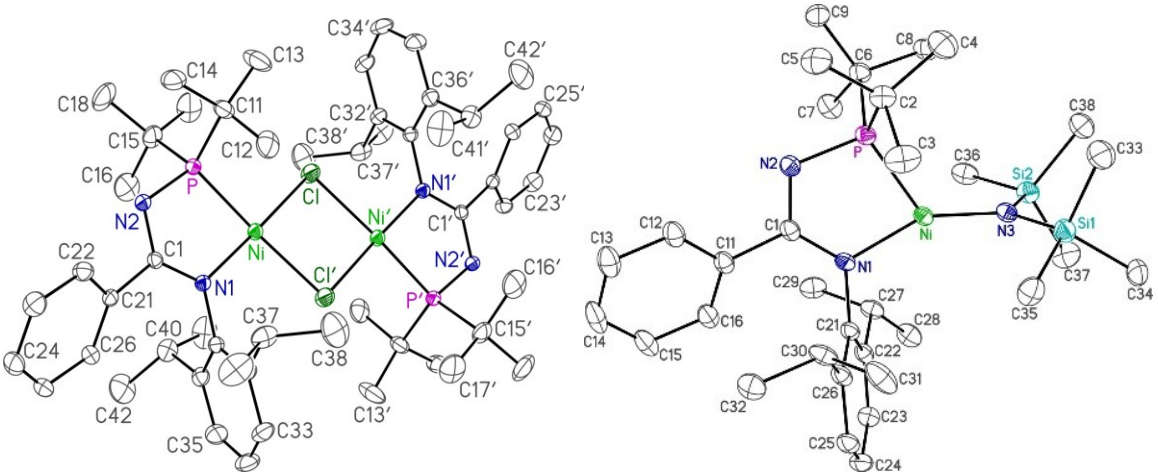

Figure 2-4. Crystallographically determined structures of Ni$_2$Cl$_2$ (left) and (PN)Ni (right). Selected interatomic distances (Å) and angles (°) for (PN)Ni: Ni-P 2.1564(9), Ni-N(1) 1.898(2), Ni-N(3) 1.849(2), P-Ni-N(1) 81.90(7), P-Ni-N(3) 126.31(8), N(1)-Ni-N(3) 151.77(10).

2.2.3 Comparative Screening of (PN)M Precatalysts

2.2.3.1 I-H of 1a with (PN)M Precatalysts

With a series of structurally analogous **(PN)M** precatalysts now synthetically accessible, attention was directed to comparing their catalytic performance in the I-H of octenes with HBPin, beginning with **1a**, where terminal selectivity can be achieved in the absence of accompanying alkene isomerization (Scheme 2-4). For consistency, 3 mol% **(PN)M** was employed in all the experiments reported herein. In keeping with previous preliminary experimentation,[70] **(PN)Fe** and **(PN)Co** proved to be highly active and selective for terminal hydroboration, affording quantitative conversion to **2a** under mild conditions (23 °C, 1 h) on the basis of NMR and GC-MS data. Conversely, despite the utility of **(PN)Mn** in the hydrosilative reduction of carbonyl compounds,[88] negligible conversion of **1a** occurred when using in **(PN)Mn** place of **(PN)Fe** or **(PN)Co** at room

temperature; even under more forcing conditions (65 °C, 18 h), poor conversion (< 50%) and product selectivity was achieved using **(PN)Mn**. Similar poor conversion of **1a** was achieved when using **(PN)Ni** at room temperature. However, in using **(PN)Ni** at elevated temperature (65 °C, 18 h), full conversion of **1a** was achieved, with *n*-octane (**2d**) and **2a** being the major products of the reaction, along with several uncharacterized higher retention time/molecular weight species (collectively **2e**). The formation of *n*-octane in this transformation was rather surprising, in terms of the stark difference in reactivity behavior relative to the other **(PN)M** precatalysts, and given that appreciable dehydrogenative borylation products[92] were not detected in any of the catalytic transformations reported herein. Whereas the higher retention time/molecular weight products (**2e**) in such reactions involving **(PN)Ni** may arise from dihydrogen-evolving processes, it is possible to rationalize the dihydrogen needed to account for the observed formation of *n*-octane as being derived exclusively from HBPin. Indeed, *n*-octane is not observed as a reaction product in transformations conducted under 'isomerization-only' conditions employing a catalytic, rather than stoichiometric, quantity of HBPin, as discussed in the context of Scheme 2-7.

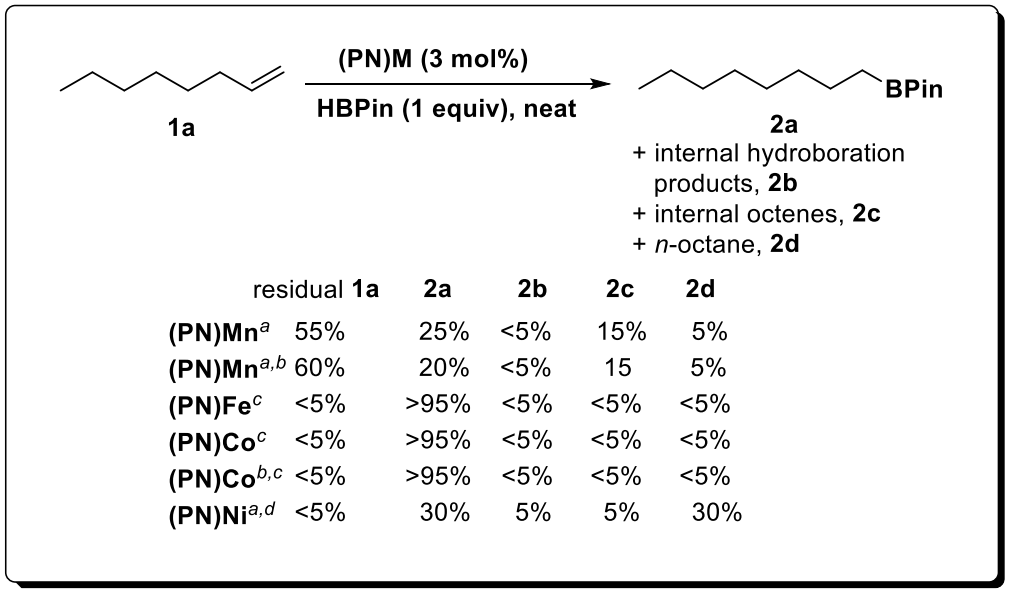

	residual **1a**	**2a**	**2b**	**2c**	**2d**
(PN)Mn[a]	55%	25%	<5%	15%	5%
(PN)Mn[a,b]	60%	20%	<5%	15	5%
(PN)Fe[c]	<5%	>95%	<5%	<5%	<5%
(PN)Co[c]	<5%	>95%	<5%	<5%	<5%
(PN)Co[b,c]	<5%	>95%	<5%	<5%	<5%
(PN)Ni[a,d]	<5%	30%	5%	5%	30%

Scheme 2-4. I-H of 1a with HBPin using (PN)M (M = Mn, Fe, Co, Ni). Unless stated, estimated conversion and product identification based on calibrated ^{1}H and $^{13}C\{^{1}H\}$ NMR data. [a] 65 ˚C, 18 h (negligible conversion of **1a** observed at 23 ˚C, 1 h). [b] Estimated conversion of **1a** and product proportions of the basis of calibrated GC data. [c] 23 ˚C, 1 h. [d] Relative proportion of **1a** and **2a-d**, including small but detectable amounts diborylation products, and substantial quantities (~30%) of higher retention time/molecular weight species (collectively **2e**; i.e., greater than **2a**), confirmed on the basis of calibrated GC-MS data.

While NMR spectroscopic analysis of the product mixtures in such transformations revealed the presence of only small amounts of B_2Pin_2, support for the hypothesis that primarily the hydride in HBPin provides reducing equivalents leading to *n*-octane was derived from analogous I-H experiments conducted using DBPin with **(PN)Ni** (65 °C, 18 h), where substantial deuterium incorporation in the aliphatic region of the generated products was confirmed on the basis of ^{2}H NMR data (Figure 2-5, Figure S2-26).

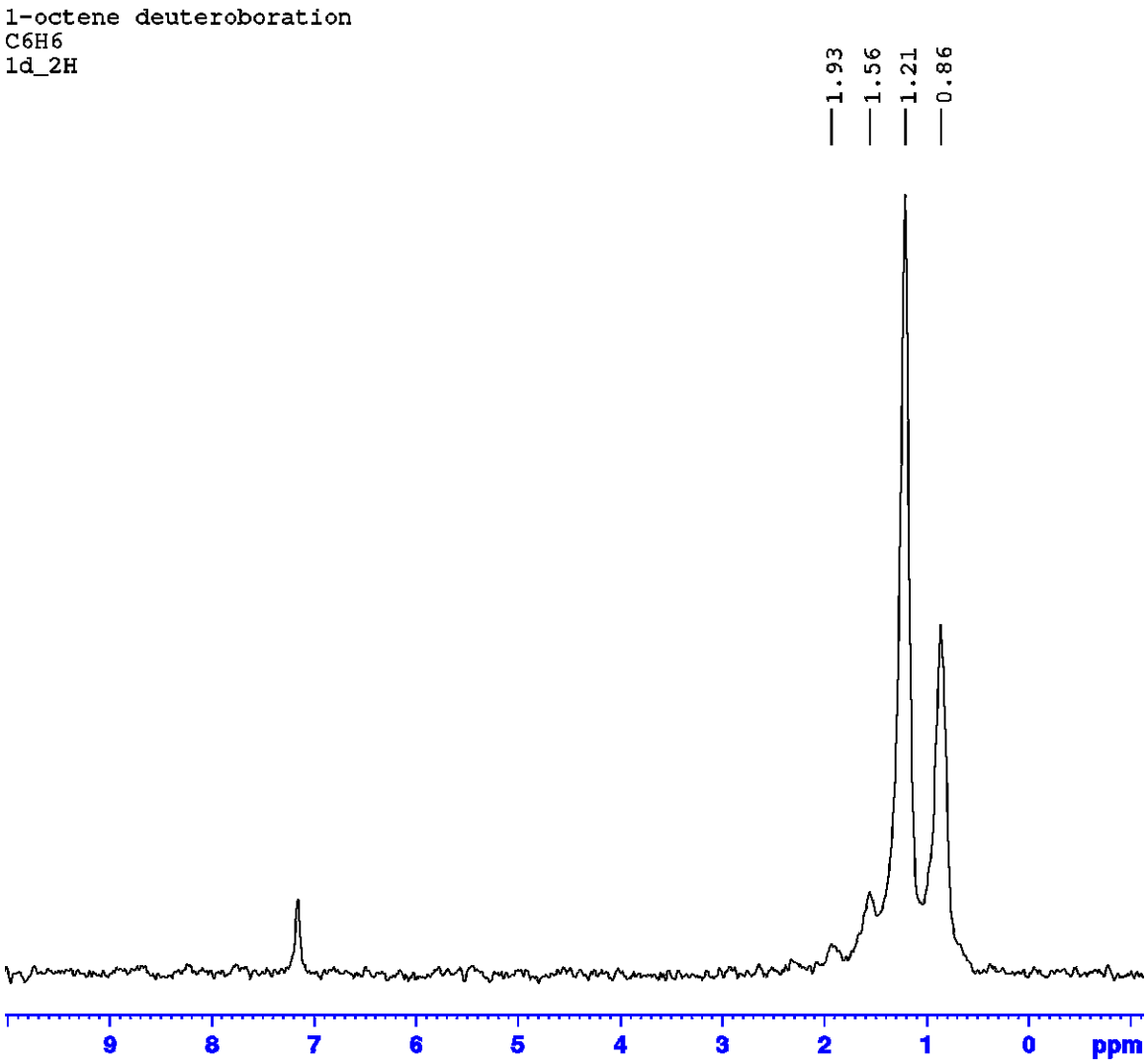

Figure 2-5. ^{2}H NMR spectrum of the C_6H_6 portion of the reaction of 1-octene with DBPin catalyzed by (PN)Ni(N(SiMe$_3$)$_2$).

2.2.3.2 I-H of 1b and 1c with (PN)M Precatalysts

Similar reactivity trends were observed in the I-H of **1b** with HBPin using **(PN)M** precatalysts (Scheme 2-5). **(PN)Fe** and **(PN)Co** once again provided clean conversion of **1b** to **2a** at room temperature (23 °C, 1 h), while **(PN)Mn** and **(PN)Ni** proved inactive under these mild conditions. Whereas negligible conversion was also achieved when using **(PN)Mn** at elevated temperature (65 °C, 18 h), under these conditions **(PN)Ni** generated a product mixture like that obtained in related transformations involving **1a**.

The **(PN)M** precatalyst series performed analogously in the I-H of **1c** (Scheme 2-6), with the exception that an erosion in selectivity for the terminal hydroboration product (**2a**) was noted when using **(PN)Fe**, in keeping with our preliminary observations.[70] In examining the effect of dilution on the I-H of **1a-c** with HBPin by use of **(PN)Ni** (65 °C, 18 h), the presence of added cyclohexane (0-500 μL) was found to have negligible impact on the observed **2a**:**2d**:**2e** ratio.

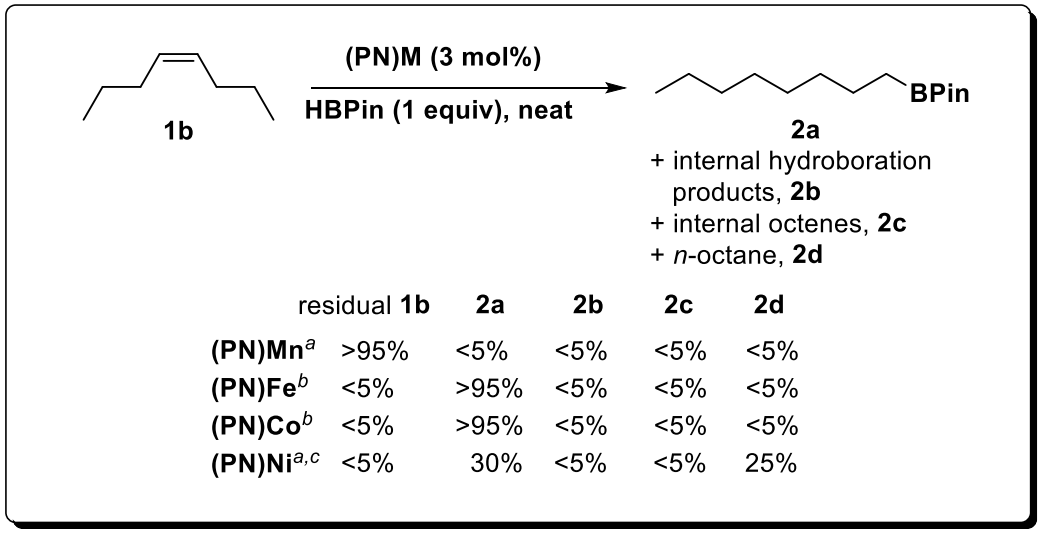

	residual **1b**	**2a**	**2b**	**2c**	**2d**
(PN)Mn[a]	>95%	<5%	<5%	<5%	<5%
(PN)Fe[b]	<5%	>95%	<5%	<5%	<5%
(PN)Co[b]	<5%	>95%	<5%	<5%	<5%
(PN)Ni[a,c]	<5%	30%	<5%	<5%	25%

Scheme 2-5. I-H of 1b with HBPin using (PN)M (M = Mn, Fe, Co, Ni). Unless stated, estimated conversion and product identification based on calibrated ^{1}H and $^{13}C\{^{1}H\}$ NMR data. [a] 65 ˚C, 18 h (negligible conversion observed at 23 ˚C, 1 h). [b] 23 ˚C, 1 h. [c] Estimated conversion and product proportions based on calibrated GC data; substantial quantities (~30%) of higher retention time/molecular weight species (collectively **2e**; i.e., greater than **2a**) observed.

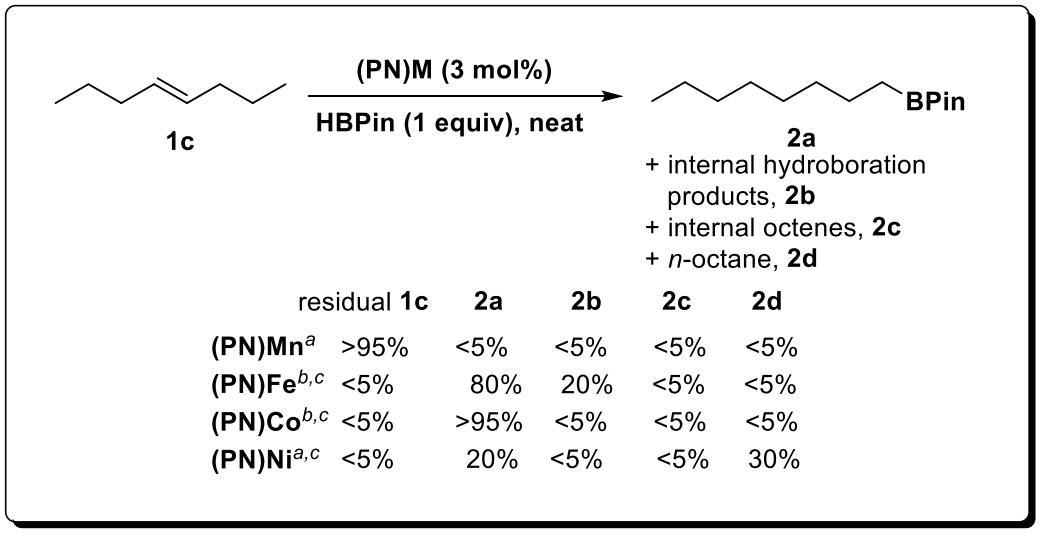

Scheme 2-6. I-H of 1c with HBPin using (PN)M (M = Mn, Fe, Co, Ni). Unless stated, estimated conversion and product identification based on calibrated ^{1}H and ^{13}C{^{1}H} NMR data. [a] 65 ˚C, 18 h (negligible conversion of **1c** observed at 23 ˚C, 1 h). [b] 23 ˚C, 1 h. [c] Estimated conversion and product proportions of the basis of calibrated GC data, with speciation confirmed on the basis of calibrated ^{1}H and ^{13}C{^{1}H} NMR data; for **(PN)Ni** substantial quantities (~30%) of higher retention time/molecular weight species (collectively **2e**; i.e., greater than **2a**) observed.

2.2.3.3 Isomerization of 1a or 1c Using Catalytic (PN)M/HBPin Mixtures

Terminal selectivity in the I-H of internal alkenes requires, among other things, that the catalyst promote facile alkene isomerization steps. To assess the ability of **(PN)M** precatalysts in this regard, I-H experiments analogous to those described above involving either **1a** or **1c** were conducted, with the exception of employing catalytic (5 mol%), rather than stoichiometric, quantities of HBPin (Scheme 2-7). Whereas the lack of activity observed for **(PN)Mn** at 23 ˚C or 65 ˚C was not surprising given the poor performance of this precatalyst in, for example, I-H of **1a** (Scheme 2-4) the similarly poor performance of **(PN)Fe** under analogous conditions contrasts the efficiency of this Fe precatalyst in the I-H of **1a** or **1c** with HBPin (*e.g.* Scheme 2-4). The **(PN)Co** precatalyst proved to be competent for the isomerization of **1a**, with the extent of conversion and observed distribution of octene isomers varying on the basis of the temperature employed

(23 ˚C, 1 h: exclusively 2-octenes; 65 ˚C, 1 h: 2-octenes (45%), 3-octenes (15%), 4-octenes (10%)). However, as was observed with **(PN)Fe**, the lack of conversion of **1c** when using **(PN)Co** under 'isomerization-only' conditions (5 mol% HBPin, 65 ˚C, 18 h; Scheme 2-7) is apparently inconsistent with the efficient and terminally selective I-H of **1c**. In contrast to the other precatalysts, **(PN)Ni** proved unique in its ability to promote the isomerization of both **1a** and **1c**, whereby the observed distribution of octene isomers varied with the reaction time and temperature employed. Under all conditions surveyed, no *n*-octane was detected in the product mixtures, consistent with the view that the net hydrogenation of octenes to afford *n*-octane under I-H conditions using **(PN)Ni** (*vide supra*) involves HBPin as a reactant.

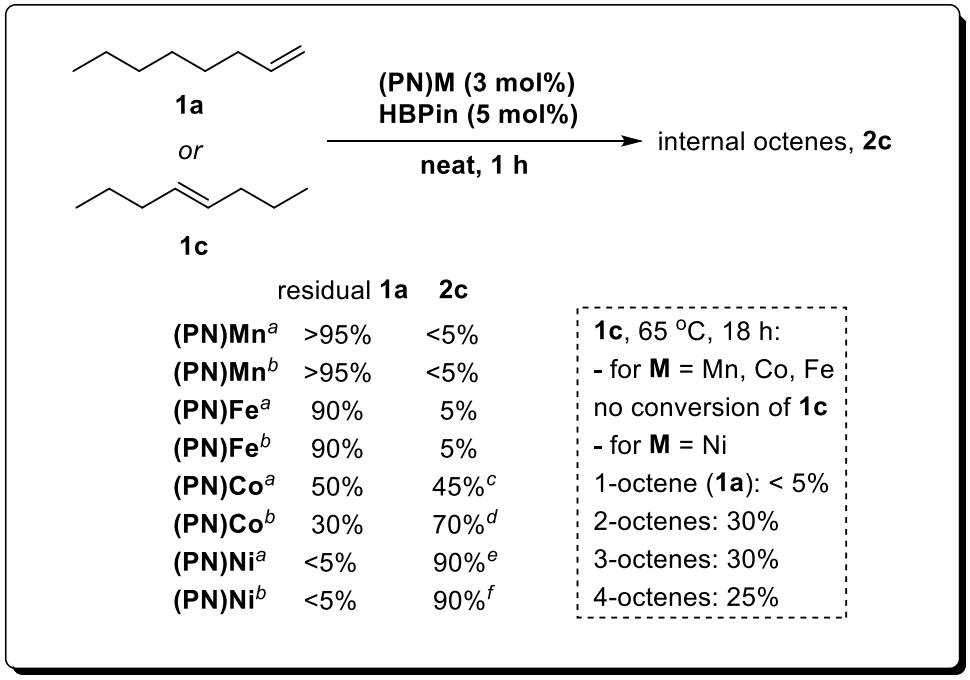

Scheme 2-7. Isomerization of 1a or 1c in the presence of (PN)M (M = Mn, Fe, Co, Ni; 3 mol%)/HBPin (5 mol%) mixtures. Estimated conversion and product identification based on calibrated ^{1}H and ^{13}C{^{1}H} NMR data; no *n*-octane observed throughout. [a] 23 ˚C. [b] 65 ˚C. [c] exclusively 2-octenes. [d] 2-octenes (45%), 3-octenes (15%), 4-octenes (10%). [e] 2-octenes (90%), 3-octenes (10%). [f] 2-octenes (45%), 3-octenes (30%), 4-octenes (15%).

The differing catalytic performance of each of **(PN)Fe** and **(PN)Co** under I-H conditions versus 'isomerization-only' conditions warrants further commentary. The successful terminally selective I-H of **1c** with HBPin to give **2a** by use of **(PN)Fe** or **(PN)Co**, which proceeds under mild conditions (23 ˚C, 1 h; Scheme 2-6), would appear to require that the facile isomerization of **1c** as outlined above. However, no isomerization of **1c** was detected upon activation of **(PN)Fe** or **(PN)Co** with a catalytic quantity of HBPin, even under more forcing conditions (65 ˚C, 18 h; Scheme 2-7). These seemingly contradictory results suggest that the borane reagent may play a more complex role in enabling I-H chemistry than simply serving as the terminal reductant.

2.2.3.4 Investigations of Precatalyst Activation by HBPin

While the paramagnetic nature of **(PN)Fe** and **(PN)Co** obfuscates the nature of metal-containing reactive intermediates, ^{11}B NMR analysis yielded information about the dual role of HBPin as both a precatalyst activator and a borylating agent (as postulated in Scheme 2-1). While it was hypothesized that **(PN)Co** would react vigorously with HBPin on account of its catalytic activity described *vide supra*, reaction of **(PN)Co** with HBPin (1 equiv) in C_6H_{12} (500 μL, 23 °C) did not proceed immediately to completion (Scheme 2-8, Figure 2-6; ^{31}P{^{1}H} NMR consistent with paramagnetic species). Progress of the reaction was monitored by the conversion of the ^{11}B signal attributed to HBPin (sharp doublet) to an upshifted broad singlet associated with the proposed $(SiMe_3)_2$NBPin by-product. An analogous reaction in the presence of excess **1a** (33 equiv, i.e. 'isomerization only conditions') appeared to immediately produce a downshifted broad singlet associated with the hydroboration product **2a** nearly quantitatively (Scheme 2-8, Figure 2-6). One might consider that **(PN)Co** was acting as an I-H catalyst rather than a

precatalyst as discussed further in Section 2.4.1. However, a more likely hypothesis is that **(PN)CoH** is initially generated in minute quantities via metathesis of **(PN)Co** with HBPin, and **(PN)CoH** rapidly catalyzes the alkylation of HBPin with **1a** precluding further metathesis with the ultimately unreacted **(PN)Co**, as shown in Figure 2-6.

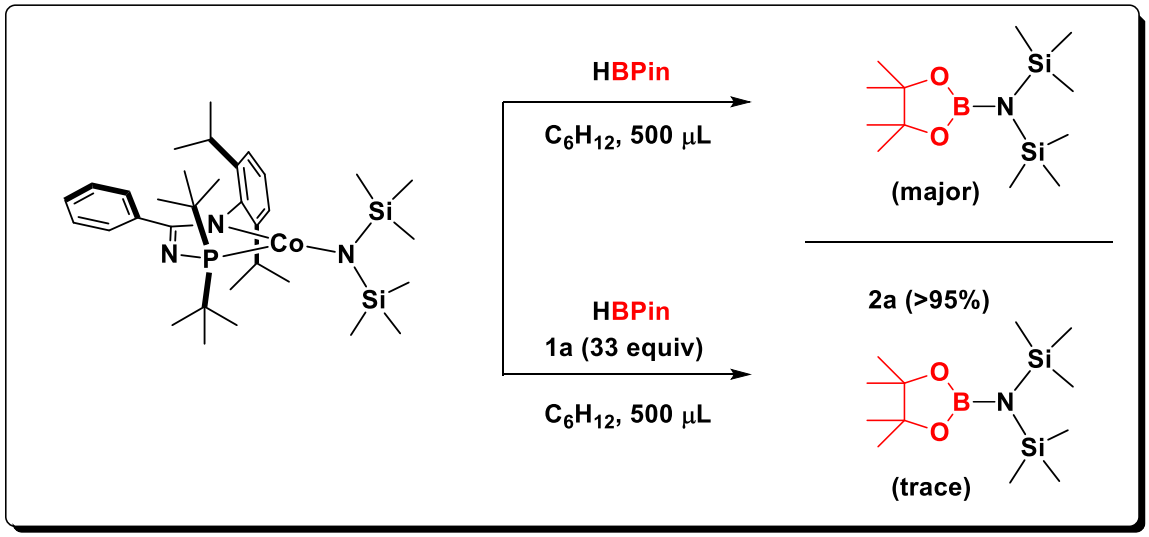

Scheme 2-8. Reactivity of (PN)Co with HBPin in C_6H_{12} (500 µL, 23 °C) in presence or absence of 33 equiv of 1a.

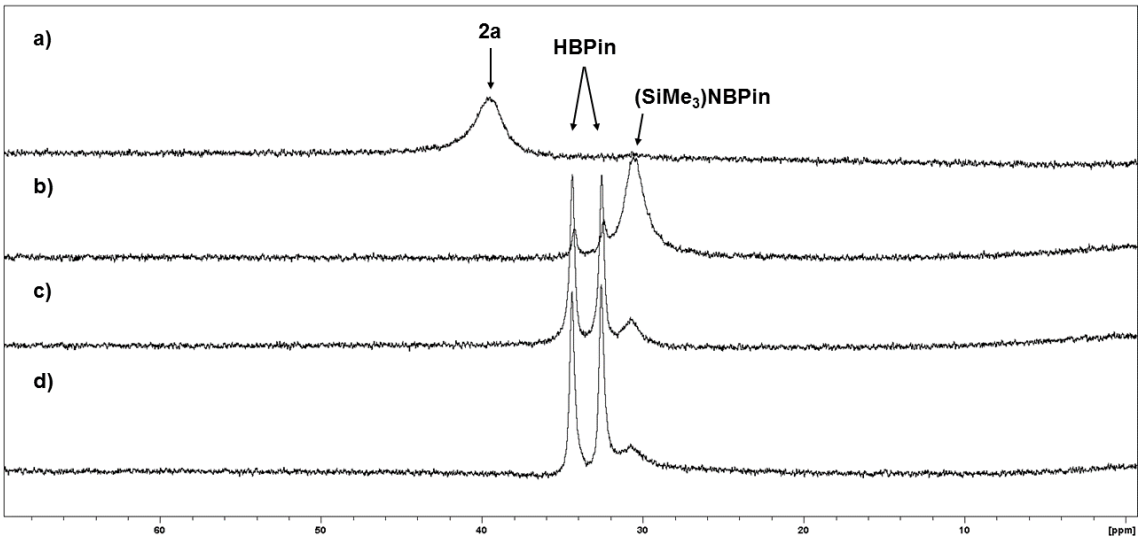

Figure 2-6. ^{11}B NMR (C_6H_{12}, 96.3 MHz, unlocked) spectra of (PN)Co with HBPin in C_6H_{12} (500 µL, 23 °C) in a) presence of 33 equiv of 1a; b-d) absence of 1a. a) 20 min, b) 14 h, c), 40 min, d) 20 min.

These data suggest possible models of reactivity. Most prominently, the rate of precatalyst activation may be much slower than that of I-H, and the effective loading of the active catalytic species may be much lower than the initial loading of the precatalyst. If true, these data imply a compounding effect, where over the course of an I-H reaction, as the concentration of activator is rapidly lowered, the rate of activation is also lowered. Although other aspects of this project were pursued preferentially, future work could include comparing the I-H activity of **(PN)M** precatalyst mixtures under standard conditions (i.e., where HBPin is added last, see experimental) versus those where instead **(PN)M** was allowed to incubate with HBPin until complete consumption of **(PN)M** prior to the addition of the octene.

These data may reconcile the contradiction concerning the relative activity of **(PN)Fe** and **(PN)Co** towards alkene I-H versus alkene isomerization. Transient **(L$_n$)MH** complexes may plausibly bind HBPin reversibly to form pinacolborohydride species of the type **(PN)MH$_2$BPin**.[93] Whereupon **HBPin** is rapidly consumed under 'isomerization only' via I-H processes as indicated in Scheme 2-8, perhaps **(PN)MH** (in absence of HBPin binding) or **(PN)M(alkyl)** (in absence of HBPin as a metathesis partner) species decompose and cannot facilitate further alkene isomerization. However, considering the paramagnetism of **(PN)MX** complexes (M = Mn, Co, Fe), NMR analysis was deemed unlikely to offer data to support or contradict such hypotheses. As such, despite the poor selectivity of **(PN)Ni** as a precatalyst for alkene I-H, analysis of diamagnetic **(PN)NiX** was undertaken to gain further mechanistic insights into **(PN)M-**catalyzed I-H processes.

2.2.4 Synthetic Investigations of Catalytically Relevant (PN)NiH Derivatives

Given the diamagnetic nature of **(PN)Ni**, the reactivity of **(PN)Ni** was explored as a representative of the **(PN)M** series under conditions relevant to catalysis. Nickel hydride[52] species derived from **(PN)M** precatalysts represent putative catalytic intermediates; accordingly, attention was turned to the synthesis of such complexes. Exposure of **Ni_2Cl_2** to $NaEt_3BH$ in THF at room temperature upon workup afforded the dinuclear complex **$((PN)NiH)_2$** (henceforth referred to as **Ni_2H_2**) in 67% isolated yield (Figure 2-7), with connectivity confirmed on the basis of single-crystal X-ray diffraction analysis. The C_2-symmetric solid state structure of **Ni_2H_2** is similar to that observed in **Ni_2Cl_2** and other Group 10 *N*-phosphinoamidinate complexes.[91]

Previously reported $((NacNac)NiH)_2$ complexes disclosed by Limberg and co-workers[94] feature tetrahedral coordination about Ni, are paramagnetic, and in solution are prone to loss of dihydrogen either upon thermal activation (25-80 ˚C, depending on the ancillary ligand substitution) or upon treatment with L-donors such as 4-dimethylaminopyridine (DMAP). In contrast, NMR experiments reveal **Ni_2H_2** to be a diamagnetic complex exhibiting modestly distorted square planar geometry, which is stable to prolonged heating (minimally 90 ˚C for 72 h) on the basis of solution NMR data, and which reacts with DMAP or pyridine to afford adducts of the type **(PN)NiH(L)** (L = DMAP or pyridine; *vide infra*).

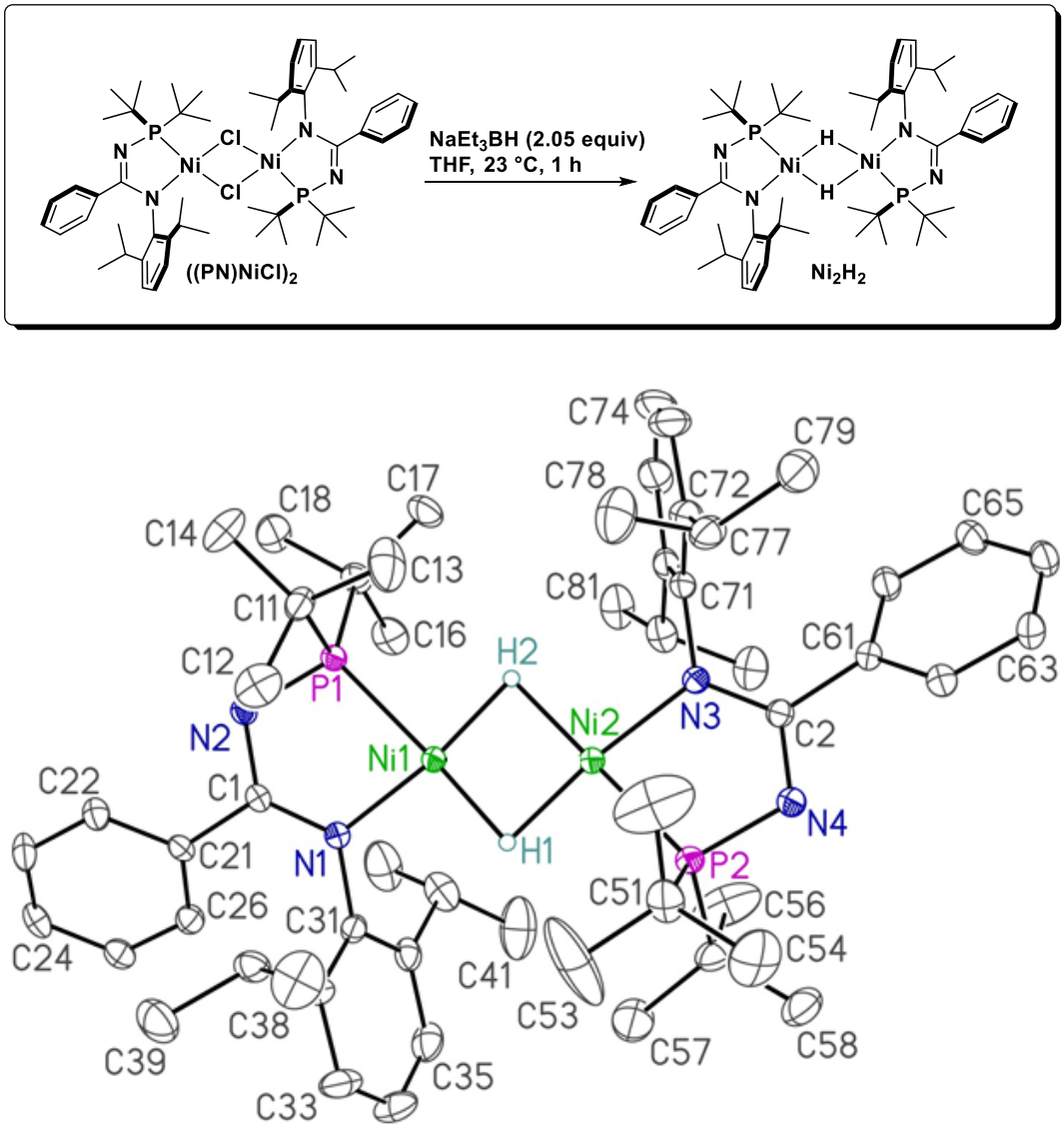

Figure 2-7. Synthesis and crystallographically determined structure of Ni_2H_2. Selected interatomic distances (Å) and angles (°) for **Ni_2H_2**: Ni(1)-P(1) 2.1276(8), Ni(1)-N(1) 1.910(3), Ni(2)-P(2) 2.1311(9), Ni(2)-N(3) 1.915(3), Ni···Ni 2.4069(5), P(1)-Ni(1)-N(1) 82.76(8), P(2)-Ni(2)-N(3) 82.77(8).

Solution NMR data (300 K, benzene-d_6) are consistent with the presence of only one isomeric form of **Ni_2H_2**, likely corresponding to the solid state structure. One $^{31}P\{^1H\}$ NMR resonance (122.3 ppm, Figure S2-8) is observed, and one sharp, symmetrical pattern centred at -27.8 ppm corresponding to the (Ni-*H*)$_2$ core is present in the ^1H NMR spectrum (Figure S2-7), in addition to the other expected ^1H and $^{13}C\{^1H\}$

NMR resonances arising from the symmetry-equivalent PN ligands in **Ni_2H_2**. One singlet resonance centered at -27.9 ppm (300 K, toluene-d_8) is observed in the hydride region of the corresponding $^1H\{^{31}P\}$ NMR spectrum. These data are consistent with the scenario whereby coupling to phosphorus renders the chemically equivalent Ni-H groups in C_2-symmetric **Ni_2H_2** magnetically non-equivalent. In this regard, the hydride region of the ^1H NMR spectrum was modelled successfully as an AA'XX' spin system (J_{HH}' = 11.9 Hz, J_{HP} = -46.1 Hz, J_{HP}' = 35.4 Hz; Figure 2-8).

#	Nucleus Name	n	Shift (ppm)	Width (Hz)	J (Hz) 1	2
1	1H	1	-27.9	3.00	0.00	0.00
			-shift	-	-	-
2	1H	1	-27.9	3.00	11.88	0.00
			-shift	-	JHH	-
3	31P	1	0.0	1.00	-46.11	35.41
			-	-	J13	J14
4	31P	1	0.0	1.00	35.41	-46.11
			-	-	J14	J13

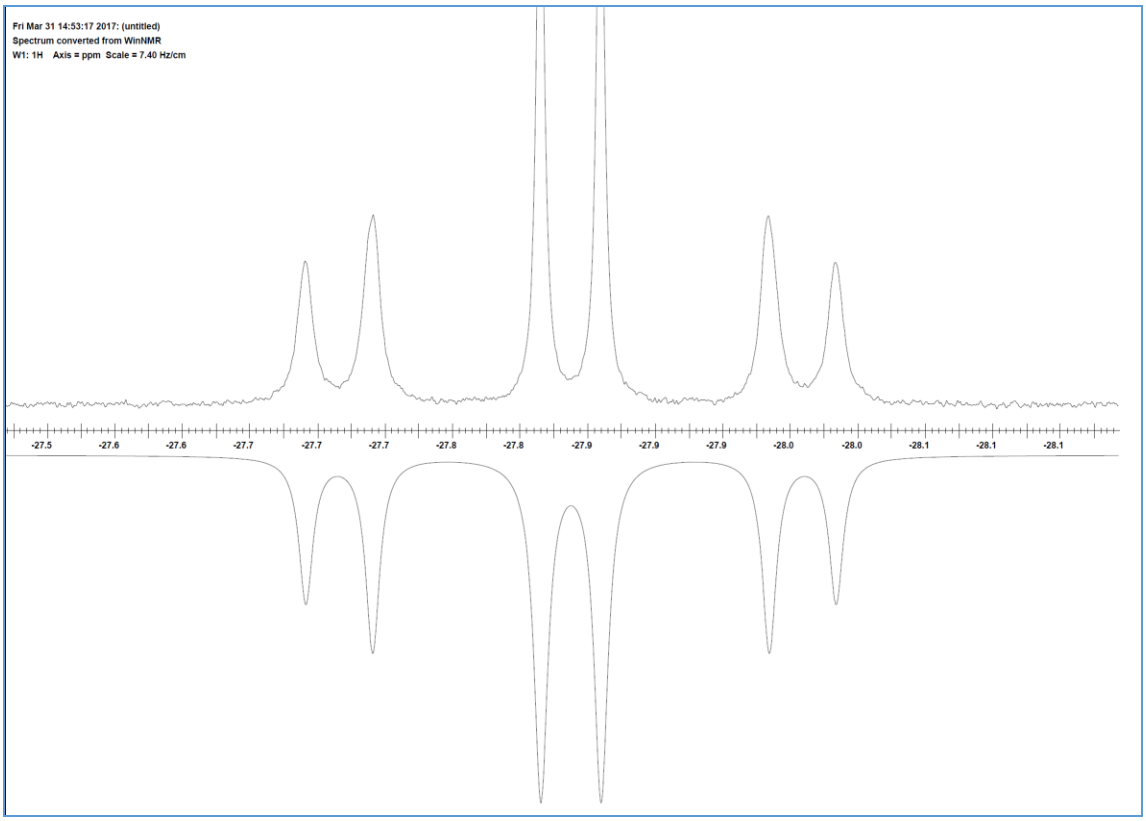

Figure 2-8. Experimental (top) and simulated (bottom) features of the hydride region of the ^{1}H NMR spectrum of Ni_2H_2.

Variable-temperature ^{1}H NMR analysis (300-363 K, toluene-d_8;) of **Ni_2H_2** reveals reversible line broadening in the hydride region at elevated temperature; however, the emergence of new hydride signals was not observed. Similarly, $^{31}P\{^{1}H\}$ NMR data collected over the same temperature range reveals only modest line-broadening and temperature-dependent chemical shift variation, in the absence of new resonances (Figure 2-10). It is plausible that these temperature-dependent NMR lineshape changes may arise

from a monomer-dimer equilibrium involving the unobserved monomer **(PN)NiH**. However, the operation of alternative dynamic processes, including those involving reversible scission of one, but not both, of the Ni-H linkages in **Ni_2H_2** cannot be ruled out.

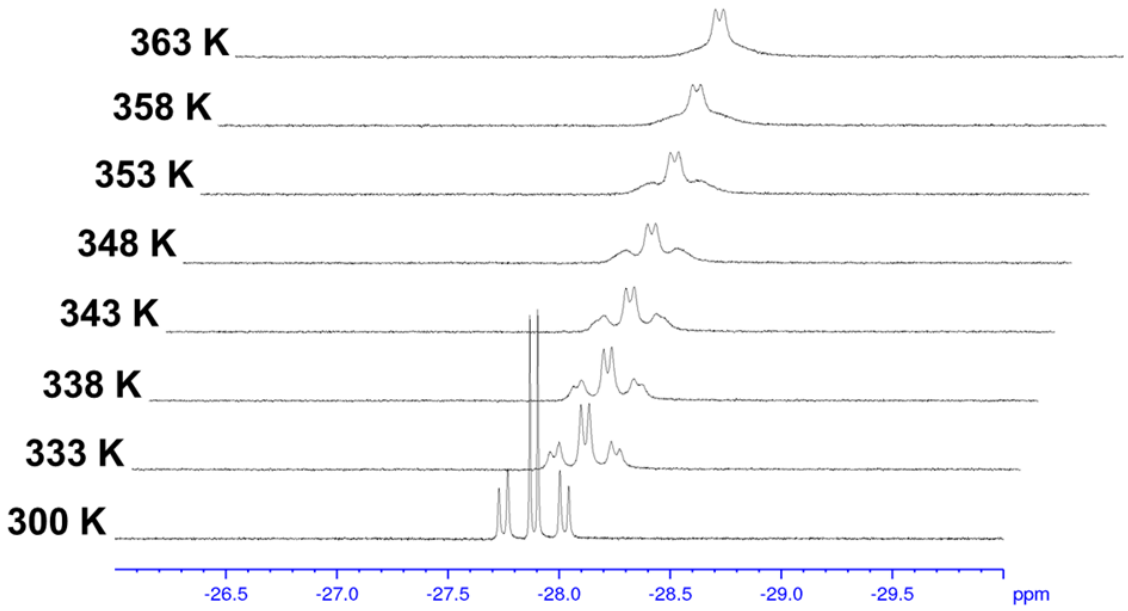

Figure 2-9. Temperature-dependent lineshape changes in the hydride region of the ^{1}H NMR spectrum of Ni_2H_2 (10 mg in 0.75 mL toluene-d_8, 300 MHz).

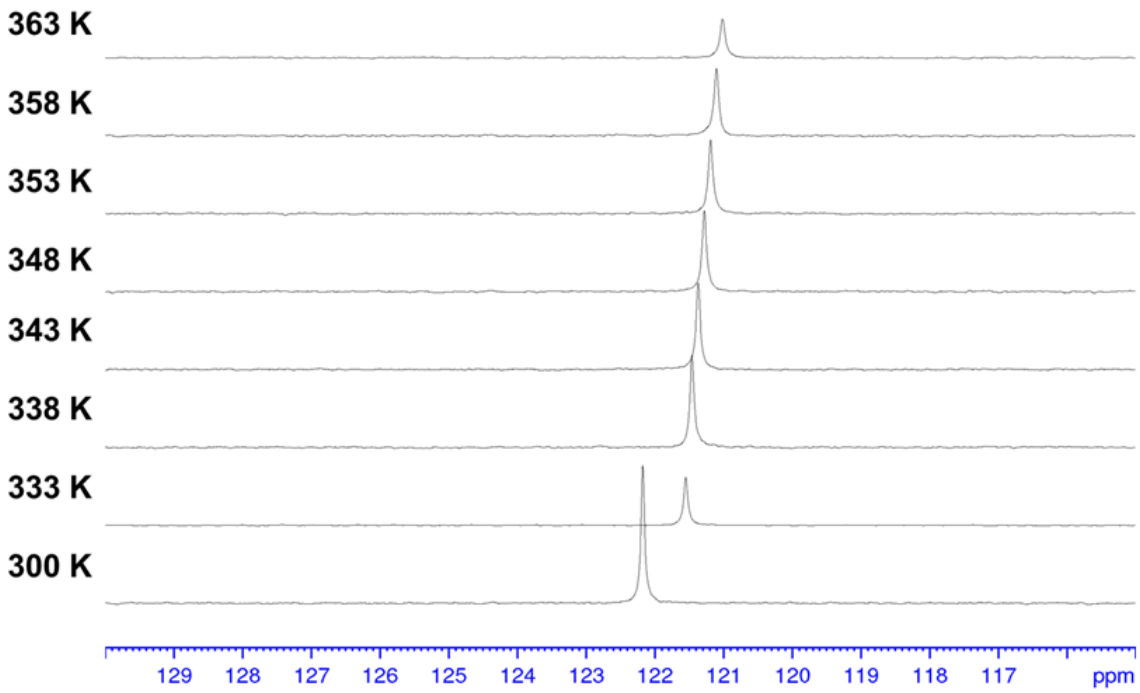

Figure 2-10. Temperature-dependent lineshape changes in the $^{31}P\{^{1}H\}$ NMR spectrum of Ni_2H_2 (10 mg in 0.75 mL toluene-d_8, 121.5 MHz).

Exposure of **Ni_2H_2** to excess DBPin (5 equiv per Ni, 110 ˚C, 72 h, toluene-d_8) resulted in substantial hydridic H/D scrambling to form **$Ni_2{}^nH_2$** isotopologues, as evidenced by: lineshape changes noted in the Ni-H region of the ^{1}H NMR spectrum (Figure S2-11) as well as more complex features in the $^{31}P\{^{1}H\}$ NMR spectrum (Figure S2-10); the appearance of a broad resonance centered at -27.8 ppm in the ^{2}H NMR spectrum; and the emergence of a resonance characteristic of HBPin in the ^{11}B NMR spectrum. Encouraged by this reactivity, the catalytic utility of **Ni_2H_2** in alkene I-H chemistry was examined under our standard conditions (3 mol% Ni, 65 ˚C, 18 h). Surprisingly, the catalytic performance of **Ni_2H_2** diverged significantly from that observed when using **(PN)Ni** as a precatalyst. For each of the octenes examined (**1a-c**), incomplete conversion was observed, and neither the terminal hydroboration product (**2a**)

nor *n*-octane (**2d**) were detected in appreciable amounts; only mixtures of internal octenes (**2c**, 60-75%) were identified as products in these reactions. These observations suggest that dinuclear **Ni$_2$H$_2$** is neither the active catalyst generated when using **(PN)Ni** as a precatalyst, nor is this dimer an effective source of this active catalytic species.

Given the rather robust nature of **Ni$_2$H$_2$**, the ability to break up this dimer upon exposure to nitrogen donor ligands was examined (Figure 2-11). Dissolution of **Ni$_2$H$_2$** in pyridine resulted in the formation of a new phosphorus-containing compound (**(PN)NiH(pyr)**, 131.4 ppm), which in turn was isolated via crystallization as an analytically pure solid in 69% yield. The clean formation of **(PN)NiH(DMAP)** was similarly observed on the basis of ^{31}P{^{1}H} and ^{1}H NMR data upon treatment of **Ni$_2$H$_2$** with excess DMAP (2.4 equiv) in benzene-d_6, where the observation of broadened resonances for free DMAP suggest the operation of an exchange process involving bound and free DMAP. Although minute quantities of crystalline **(PN)NiH(DMAP)** could be obtained from these reactions, the bulk isolation of analytically pure material proved elusive. In contrast to the complex hydride pattern observed in the ^{1}H NMR spectrum for **Ni$_2$H$_2$**, each of **(PN)NiH(pyr)** (-20.2 ppm, $^2J_{HP}$ = 104 Hz) and **(PN)NiH(DMAP)** (-20.9, $^2J_{PH}$ = 107 Hz) feature a simple phosphorus-coupled doublet resonance. Single-crystal X-ray diffraction data confirmed the identities of these new complexes as mononuclear, distorted square planar adducts, featuring a hydride ligand *trans* to the nitrogen donor of the *N*-phosphinoamidinate chelate. As mentioned earlier in the text, the clean formation of the Ni(II) complex **(PN)NiH(DMAP)** in this context contrasts the reactivity of previously reported paramagnetic ((NacNac)NiH)$_2$ species,[94] which undergo reduction to Ni(I) upon treatment with L-donors such as DMAP.

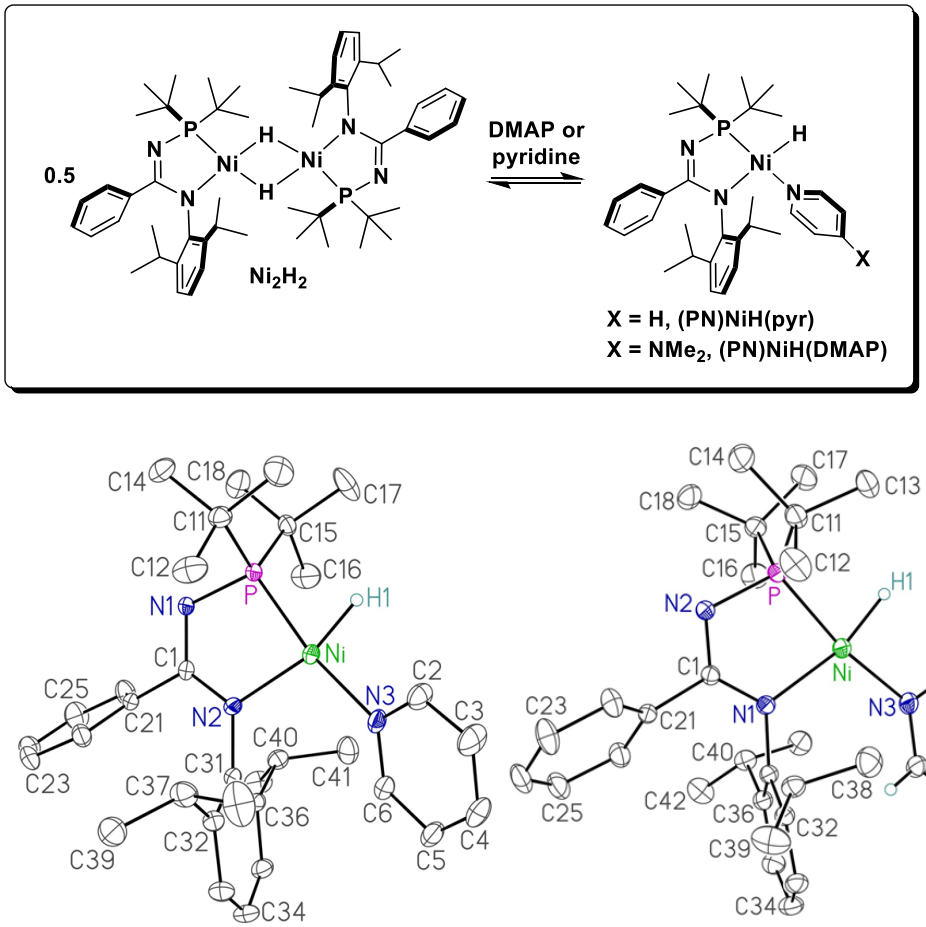

Figure 2-11. Synthesis and crystallographically determined structures of (PN)NiH(pyr) and (PN)NiH(DMAP). Selected interatomic distances (Å) for **(PN)NiH(pyr)**: Ni-P 2.0872(4), Ni-N(2) 1.9691(11), Ni-N(3) 1.9782(11). Selected interatomic distances (Å) for **(PN)NiH(DMAP)**: Ni-P 2.0969(5), Ni-N(1) 1.9796(13), Ni-N(3) 1.9888(14).

Upon dissolution of isolated **(PN)NiH(pyr)** in a solvent other than pyridine, an equilibrium is established involving loss of pyridine to afford **Ni_2H_2** (Figure S2-15). For example, NMR spectroscopic analysis of a solution of **(PN)NiH(pyr)** in benzene-d_6 (0.028 M, 300 K) reveals a 10:1 ratio of **(PN)NiH(pyr)** to **Ni_2H_2** 1 h post-mixing; after 67 h the ratio was found to be 2.4:1. On warming the sample (338 K) the equilibrium shifts in favor of the dimer (0.8:1), and on cooling back to 300 K, gradual return to the previously observed equilibrium ratio (2.4:1) was confirmed after 16 h.

With an isolable mononuclear Ni-H species in hand, the reactivity of this complex in alkene I-H chemistry involving **1a-c** with HBPin was examined. The observed catalytic behavior of **(PN)NiH(pyr)** under standard conditions (3 mol% Ni, 65 ˚C, 18 h) was found to be similar to that of **Ni_2H_2**, with incomplete conversion and product mixtures comprised of internal octenes (**2c**, 50-90%), and only small amounts of **2a** or **2d** (< 20%). As was noted for **Ni_2H_2**, the mononuclear pyridine adduct **(PN)NiH(pyr)** is not an effective source of the active catalytic species generated from **(PN)Ni** under I-H conditions.

2.3 Spectroscopic Analysis of Precatalyst Activation and Catalytic Speciation

Additional stoichiometric reactivity studies were conducted to learn more about the nature of the active catalyst formed from **(PN)Ni** (Scheme 2-9). Exposure of this precatalyst to octenes **1a** or **1c** (33 equiv in keeping with catalytic conditions, 23 ˚C, 24 h, C_6D_{12}) resulted in no observable reaction based on ^{31}P NMR data. Similarly, various attempts to react **(PN)Ni** with stoichiometric HBPin failed to generate products. Conversely, ^{31}P NMR data (Figure S2-19) collected on a sample of **(PN)Ni** that had been exposed to HBPin (33 equiv) under similar conditions (23 ˚C, 24 h, C_6D_{12}) revealed two major signals in ~1:2 ratio: 127.4 ppm (**(PN)Ni**) and 140.0 ppm, the latter of which is tentatively assigned to the borohydride complex **(PN)Ni(H_2BPin)**. After a total reaction time of 43 h, the signal at 140.0 ppm represents the major phosphorus-containing species, with some amount of **Ni_2H_2** (121.3 ppm) being detected. At this stage, heating the sample for (65 ˚C, 6 h, Figure S2-20) resulted in the further conversion to **Ni_2H_2** based on ^{31}P NMR data. Continued heating at 65 ˚C resulted in the loss of a ^{31}P NMR signal attributable to **(PN)Ni(H_2BPin**), with **Ni_2H_2** representing the major phosphorus-

containing product in solution. Notably, in no instance did exposure of **Ni_2H_2** to HBPin (33 equiv per Ni, C_6D_{12}), either at room temperature or upon heating, result in conversion to **(PN)Ni(H_2BPin**) based on ^{31}P NMR data, thereby suggesting that the formation of **Ni_2H_2** from this putative borohydride is irreversible. Efforts to more comprehensively characterize *in situ* putative **(PN)Ni(H_2BPin)** proved challenging, given the excess of HBPin employed, and the use of fewer equivalents of HBPin relative to **(PN)Ni** (23 ˚C, C_6D_{12}) afforded directly a mixture of **(PN)Ni(H_2BPin)** and **Ni_2H_2**. Attempts to isolate **(PN)Ni(H_2BPin)** when formed as the major product as outlined above, by way of concentrating the solution *in vacuo*, resulted in the near quantitative conversion to **Ni_2H_2**, and our efforts to crystallize **(PN)Ni(H_2BPin)** directly from the reaction mixture proved unfruitful.

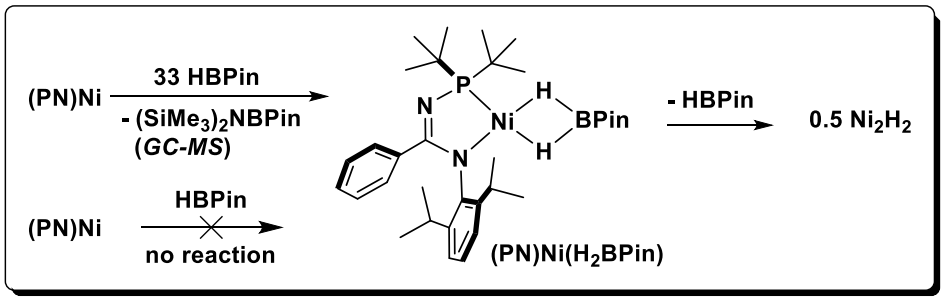

Scheme 2-9. Probing the reactivity of (PN)Ni with HBPin.

The view that exposure of **(PN)Ni** to HBPin affords one or more Ni-H species, and $(SiMe_3)_2$NBPin as a by-product, is supported by the observed formation of putative **(PN)Ni(H_2BPin)** and **Ni_2H_2** (*vide supra*). The unequivocal NMR spectroscopic identification of $(SiMe_3)_2$NBPin as a component of the reaction mixture proved more difficult. To obtain more definitive support for such precatalyst activation steps, an alternative Ni-amido complex was sought for which the B-N product generated upon treatment with HBPin might be more definitively identified using NMR characterization

data. Treatment of **Ni_2Cl_2** with LiNH(2,6-*i*$Pr_2C_6H_3$) (2,6-*i*$Pr_2C_6H_3$ = dipp) at room temperature in THF afforded the diamagnetic complex **(PN)Ni(NHdipp)** in 80% isolated yield, as outlined in Figure 2-12. Single-crystal X-ray diffraction data confirm the mononuclear, three-coordinate, distorted trigonal-planar structure of this complex, which is structurally similar to **(PN)Ni**.

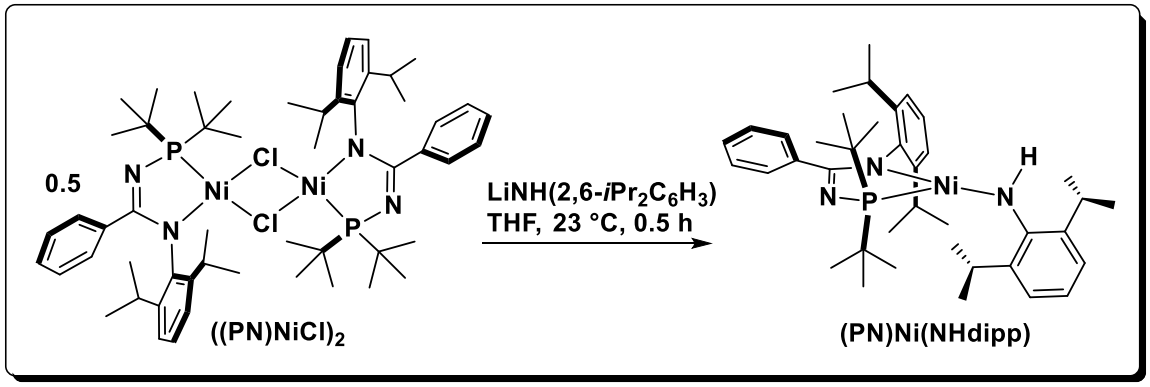

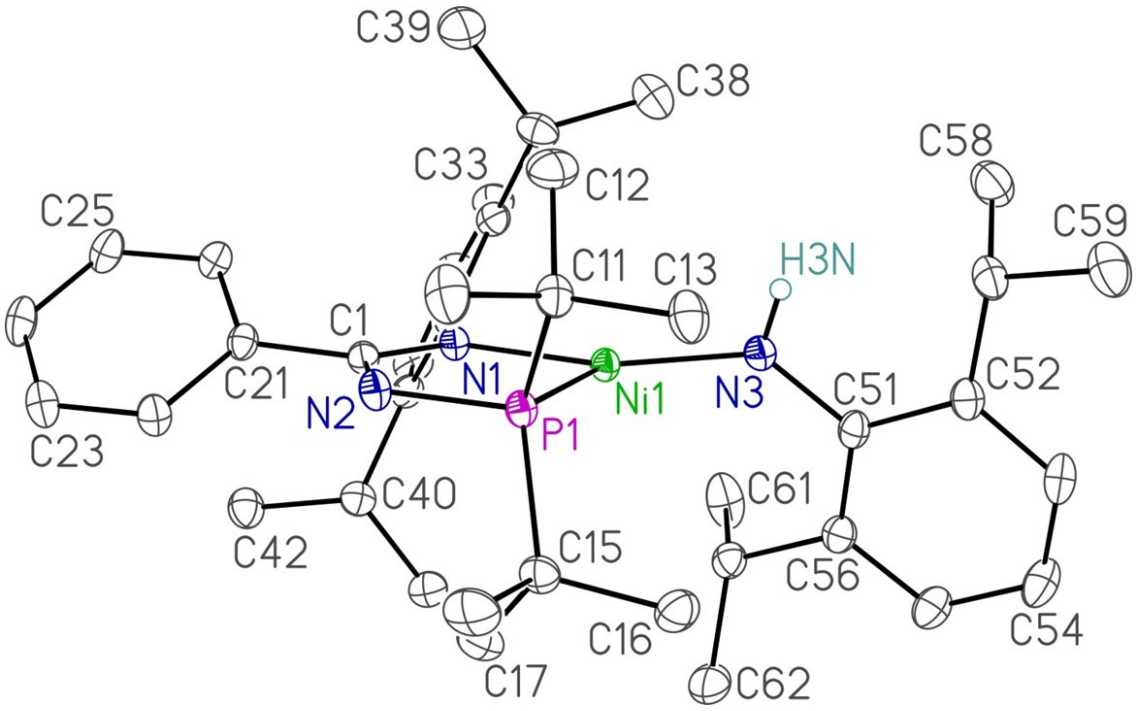

Figure 2-12. Synthesis and crystallographically determined structure of (PN)Ni(NHdipp). Selected interatomic distances (Å) and angles (°) for one of the two crystallographically independent molecules of **(PN)Ni(NHdipp)**: Ni-P 2.1099(5), Ni-N(1) 1.8838(14), Ni-N(3) 1.8013(15), P-Ni-N(1) 83.20(5), P-Ni-N(3) 116.57(6), N(1)-Ni-N(3) 158.84(7), Ni-N(3)-C(51) 136.51(14).

In keeping with our hypothesis surrounding the mode of precatalyst activation, treatment of **(PN)Ni(NHdipp)** with HBPin (1 equiv) in Et_2O (1 h, 23 ˚C), followed by removal of the solvent and dissolution of the reaction mixture in benzene-d_6, revealed the presence of a ~1:2 ratio of **Ni_2H_2** and (dipp)HNBPin (Scheme 2-10), whereby the latter B-N product was unequivocally identified on the basis of NMR spectroscopic data via comparison with literature data.[95] While this metathesis reaction occurs immediately at ambient temperature, it should be noted that a resonance corresponding to **(PN)Ni(H_2BPin)** can be observed over the course of this reaction as **(PN)NiH** is trapped reversibly; premature removal of volatiles may thus leave unreacted **(PN)Ni(NHdipp).**

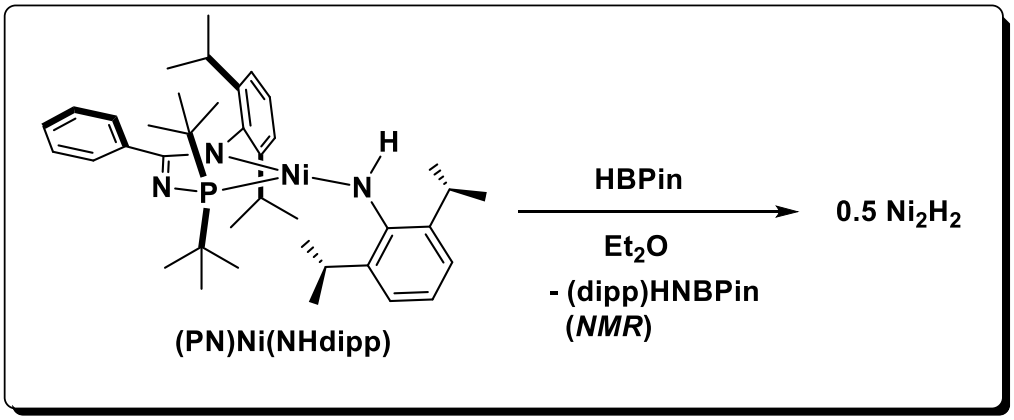

Scheme 2-10. Probing the reactivity of (PN)Ni(NHdipp) with HBPin.

Efforts were then directed toward direct observation of potential intermediates in alkene I-H. **(PN)Ni** was treated with 33 equiv each of **1a** and HBPin under conditions like those employed for catalysis (65 ˚C, 21 h, C_6D_{12}), and reaction progress was monitored by use of ^{31}P NMR methods. The starting precatalyst is consumed, and a cluster of signals centered around 128 ppm represents the major peaks in the ^{31}P NMR spectrum alongside a small amount of **Ni_2H_2**. Plausibly, the cluster arises from isomeric **(PN)Ni(octyl)** species (Figure S2-22). In keeping with the results featured in Scheme 2-4,

NMR spectroscopic analysis of the reaction mixture at this stage confirmed the consumption of **1a** and HBPin, along with the formation of the terminal hydroboration product (**2a**) and *n*-octane (**2d**). In adding a fresh charge of **1a** and HBPin (33 equiv each), the conversion of **1a** and HBPin to **2a** and **2d** once again was observed to proceed on the basis of NMR data over the course of 24 h at 65 ˚C; interestingly, throughout the course of this transformation, no change was observed in the ^{31}P NMR spectrum (Figure S2-23), with putative **(PN)Ni(octyl)** and a small amount of **Ni_2H_2** being observed. These observations are consistent with **(PN)Ni(octyl)** representing the resting state(s) of this catalytic system. Further treatment of this reaction mixture with additional HBPin (33 equiv) after 1 h (Figure S2-24) at 65 ˚C resulted in the re-appearance of the resonance associated with **(PN)Ni(H_2BPin)**, with the signals for **(PN)Ni(octyl)** and **Ni_2H_2** also being present; subsequent addition of **1a** (33 equiv) led to the disappearance of the ^{31}P NMR signal associated with **(PN)Ni(H_2BPin)** after 4 h at 65 ˚C. Unfortunately, efforts to synthesize **(PN)Ni(octyl)** independently via salt metathesis of **Ni_2Cl_2** with octylmagnesium bromide generated complex mixtures of products.

2.3.1 Mechanistic Proposal for (PN)MH-Catalyzed Alkene I-H

When considered collectively, the stoichiometric reactivity studies employing **(PN)Ni** that are presented in this chapter are consistent with the mechanism for octene I-H generalized for **(PN)M** outlined in Scheme 2-11 (with **1c** as a representative substrate, and leading to **2a**). Initial activation of **(PN)M** by HBPin generates a mononuclear hydride **(PN)MH**, which can reversibly bind HBPin to give **(PN)M(H_2BPin)** or dimerize to give **((PN)MH)$_2$**. Then, binding and 1,2-insertion of **1c** by **(PN)MH** to afford **(PN)M(4-octyl)**, and subsequent reversible β-H elimination/1,2-insertion steps, lead to a

distribution of **(PN)M(octyl)** isomers that represent the resting state of the catalyst. In the case of terminally selective transformations, exclusively **(PN)M(1-octyl)** reacts with HBPin to afford **2a** and regenerate **(PN)MH**. A related mechanism has been proposed for the copper-catalyzed asymmetric hydroboration of alkenes.[93]

Building on these empirical observations, DFT computational analysis of this reaction landscape was carried out by a team of collaborators (Ess and co-workers, BYU), with the goal of assessing the validity of this mechanistic picture for the four **(PN)M** precatalysts involved (M = Mn, Fe, Co, Ni), and to gain insights regarding their differing catalytic behavior. Our team was also interested in hoping to understand the complex reactivity of Ni in this regard, including potential mechanisms for observed hydrogenation of alkenes.

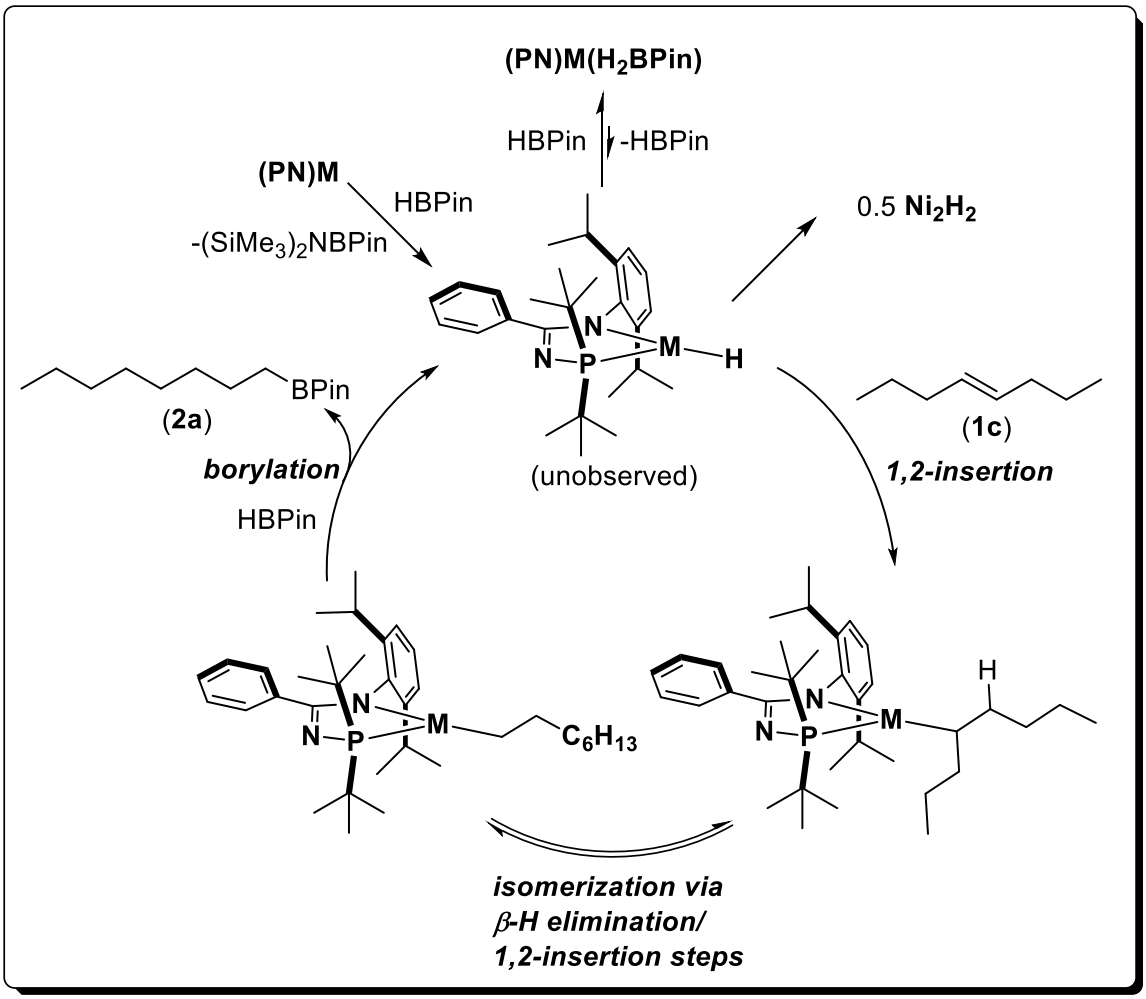

Scheme 2-11. Generalized proposed catalytic cycle for terminally selective alkene I-H involving (PN)M precatalysts.

2.4 Summarized Computational Studies from the Ess Group

2.4.1 Key Computational Findings

To interrogate the proposed mechanism of alkene I-H via **(PN)M** precatalysts (Scheme 2-11), computational investigations using density functional theory (DFT) were conducted. Initial work focused on modelling the structures of the precatalysts in the *n*-octane solvent continuum; the calculated structures were found to closely resemble the solid state structures. In the calculated structures, a singlet electronic state was found for **(PN)Ni**, supporting its experimentally observed diamagnetism.

The calculated modes of precatalyst activation to generate a putative **(PN)MH** intermediate corresponded with experimental observations: 1,2 insertion of 1-octene into the M-(amido) bond was found to be of high energy, consistent with the lack of observed reactivity in this regard, and OA/RE processes that invoke Ni(IV) intermediates were not located. The bond strengths of the M-(amido) bonds were sufficiently large to preclude ionic or radical dissociation of the amido group. Rather, the proposed σ-bond metathesis pathway between HBPin and **(PN)M** to form **(PN)MH** (and $(SiMe_3)_2NBPin$) was favored. The calculated energy barrier for this reaction was found to be highest for **(PN)Ni**, in keeping with the observed sluggish reaction at room temperature, even in the presence of large excesses of HBPin.

Formation of proposed **(PN)M(H_2BPin)** intermediates (Scheme 2-9) was found to be exergonic for Co and Ni; moreover, these species were only slightly higher in energy than the most stable **(PN)M(octyl)** isomers. These data are consistent with the observation of slight conversion from the resonances attributed to **(PN)Ni(octyl)** to those of **(PN)Ni(H_2BPin)** when a catalytic mixture is exposed to excess HBPin.

The ability of **(PN)MH** species to coordinate and insert alkenes was found to be divergent. Coordination of **1c** to **(PN)MH** was found to be endergonic for Mn and Fe, and exergonic for Co and Ni. For Fe, an electronic spin-crossover from a quintet to a triplet state was found to lower the energy for this step. The transition state for the insertion of *trans*-2-, -3-, or -4-octene ligands into the M-H bond was prohibitively endergonic for Mn, modestly endergonic for Fe, and minimally endergonic for Co and Ni (relative to the isomeric **(PN)MH(octene)** species). These data correspond with the

experimentally observed failure of **(PN)Mn** to perform either alkene I-H or isomerization.

The relative energies of the various possible **(PN)M(octyl)** isomers generated via chain-walking steps were probed; collectively, they were found to be lowest in energy among all the on-cycle candidates, supporting the proposal that they behave as resting states in the catalytic cycle (Scheme 2-11). While for Mn and Fe there existed high barriers to octene insertion, among each metal, the various **(PN)M(octyl)** isomers were of similar energy. While this might appear to contradict the observed experimental terminal selectivity for **(PN)Co**, further analysis of the borylation step revealed the origin of selectivity. The borylation step of HBPin and the linear **(PN)M(*n*-octyl)** isomer was compared with a branched **(PN)M(CHR$_2$)** isomer. With HBPin, a σ-bond metathesis pathway to generate octylBPin and regenerate **(PN)MH** was favored. Furthermore, the transition state energies for this step were a), significantly higher for the branched isomer than the linear, and b), for Co and Ni, significantly higher than all transition barriers associated with alkene coordination and chain-walking. For Co and Ni, these data supported a Curtin-Hammett scenario, wherein the origin of terminal selectivity in alkene I-H was dictated by a rate-determining terminal borylation of **(PN)M(*n*-octyl)** with HBPin via σ-bond metathesis.

2.4.2 Limitations and Outlook

Unfortunately, these DFT computational data did not reveal reasons for the unexpected catalytic performance of Ni outlined *vide supra*. While **Ni$_2$H$_2$** was found to be of significantly lower energy than **(PN)NiH**, consistent with experimental results, other findings were less illuminating. Metathesis of either **(PN)NiH** or **(PN)Ni(octyl)**

with HBPin to generate *n*-octane, or reducing equivalents in the form of H_2, as well as **(PN)NiBPin** was found to be unfavorable compared to other competing processes. Furthermore, the higher temperatures required experimentally to facilitate Ni catalysis were not consistent with the computational barriers. Given the apparent inconsistency between the experimental results presented in this chapter and the DFT work of our collaborators, it is plausible that other intermediates or off-cycle processes not captured in the DFT analysis are responsible for these contradictions.

2.4.3 Chapter Summary

In comparing the performance of **(PN)M** (M = Mn, Fe, Co, and Ni) precatalysts in the I-H of octene isomers to form **2a**, divergent reactivity patterns were found. **(PN)Mn** and **(PN)Ni** showed poor performance compared to **(PN)Fe** and **(PN)Co**. Derivative **(PN)MH** intermediates generated upon reaction of **(PN)M** with HBPin appear plausible based on computational data, although this species was not detectable experimentally. Rather, chemistry involving **(PN)NiX** complexes established $\mathbf{Ni_2H_2}$ as a robust off-cycle species, as neither $\mathbf{Ni_2H_2}$ nor the related four-coordinate complexes **(PN)NiH(pyr)** and **(PN)NiH(DMAP)** showed useful performance in I-H chemistry. Experimental and computational data suggest **(PN)Ni(octyl)** isomers generated in equilibrium via BHE processes as being plausible catalytic resting states. $\mathbf{(PN)NiH_2BPin}$ represents a species of similar energy, and the result of **(PN)NiH** generated in the presence of excess HBPin. Borylation selectivity can be understood through a Curtin−Hammett scenario where the barrier for rate-limiting terminal borylation is significantly lower than internal borylation. Computational investigations suggested the importance of spin-crossover events in the proposed catalytic cycle. Unfortunately, the

origin of complex mixtures in the Ni-catalyzed reactions have not been understood. However, inspired by the unexpected propensity of Ni catalysts to reduce unsaturated substrates, I pursued applications that are described in Chapter 3. Directions for further inquiry based on these results are outlined in Chapter 5.

2.5 Experimental

2.5.1 General Experimental Considerations

Unless stated, all experiments were conducted at ambient temperature under nitrogen in an inert-atmosphere glovebox or by using standard Schlenk techniques using oven-dried glassware. Dry, oxygen-free solvents were used unless otherwise indicated. Benzene, toluene, and pentane were deoxygenated and dried by sparging with nitrogen and subsequent passage through a double column solvent purification system packed with alumina and copper-Q5 reactant. Tetrahydrofuran and diethyl ether were purified by distillation under nitrogen from Na/benzophenone. Deuterated solvents and alkene substrates were degassed via three freeze−pump−thaw cycles. All purified/degassed chemicals were stored over 4 Å molecular sieves. Precatalysts **(PN)M** (M = Mn,[88] Fe,[69] Co[69]) and DBPin[96] were also synthesized employing literature procedures. All other reagents were purchased from commercial suppliers and used without further purification. Unless otherwise stated, ^{1}H, ^{13}C, ^{11}B, and ^{31}P NMR characterization data were collected at 300 K on a Bruker AV-500 spectrometer operating at 500.1, 125.7, 160.4, and 202.5 MHz (respectively) with chemical shifts reported in parts per million downfield of $SiMe_4$ for ^{1}H and ^{13}C, $BF_3{\cdot}OEt_2$ for ^{11}B, and 85% H_3PO_4 in D_2O for ^{31}P. ^{1}H and ^{13}C NMR chemical shift assignments are based on data obtained from ^{13}C-DEPTQ135, $^{1}H–^{1}H$ COSY, $^{1}H–^{13}C$ HSQC, and $^{1}H–^{13}C$ HMBC NMR experiments. In

some cases, fewer than expected unique ^{13}C NMR resonances were observed, despite prolonged acquisition times. Splitting patterns are abbreviated as follows: br, broad; app, apparent; s, singlet; d, doublet; t, triplet; m, multiplet, with all coupling constants (J) reported in Hertz (Hz). Mass spectra were obtained using ion trap electrospray ionization (ESI) instruments operating in positive mode. Gas chromatography (GC) data were obtained on an instrument equipped with an SGE BP5 column (30 m, 0.25 mm i.d.). Crystallographic data were obtained at or below 193(2) K on a Bruker D8/APEX II CCD diffractometer equipped with a CCD area detector, employing samples that were mounted in inert oil and transferred to a cold gas stream on the diffractometer. Unit cell parameters were determined and refined on all reflections. Data reduction, correction for Lorentz polarization, and absorption correction were each performed. Structure solution and least-squares refinement on F2 were used throughout. All non-hydrogen atoms were refined with anisotropic displacement parameters. Full crystallographic solution and refinement details are provided in the deposited CIFs online (CCDC 1818286−1818290).[89]

2.5.2 Specific Experimental Considerations

Synthesis of ((PN)NiCl)$_2$

A glass vial containing a magnetic stir bar was charged with $NiCl_2$dme (0.209 g, 0.95 mmol), and subsequently THF (2 mL). Magnetic stirring was initiated, and **HPN** (0.405 g, 0.96 mmol) was added as a solution in THF (6 mL), resulting in the formation of a dark purple solution. After 30 min, the vial contained a bright purple gel. Triethylamine (300 μL, 2.15 mmol) was added to the gel, which reformed as an orange-red solution. After 10 min, the volatile components were removed in vacuo. The remaining residue was triturated with pentane (3 × 3 mL), taken up in benzene (10 mL),

and the mixture was filtered through Celite. The eluent was collected, and the volatile components were removed *in vacuo*. The resulting red residue was triturated with pentane (3 × 3 mL) and dried *in vacuo* to afford analytically pure **Ni_2Cl_2** (0.486 g, 98% yield) as a dark red-purple solid. Anal. Calcd for $C_{54}H_{80}Cl_2N_4Ni_2P_2$: C, 62.64; H, 7.79; N, 5.41. Found: C, 62.53; H, 7.90; N, 5.43. ^{1}H NMR (500.1 MHz, benzene-d_6): δ 7.31 (m, 4 H, H_{arom}), 7.03 (m, 2 H, H_{arom}), 6.91 – 6.89 (overlapping resonances, 4 H, H_{arom}), 6.84 – 6.75 (overlapping resonances, 6 H, H_{arom}), 4.03 (app septet, 4 H, $^3J_{HH}$ = 7 Hz, C*H*Me$_2$), 1.94 (d, 12 H, $^3J_{HH}$ = 7 Hz, CH*Me*$_2$), 1.55 (d, 36 H, $^3J_{PH}$ = 14 Hz, P *tBu*$_2$), 0.98 (d, 12 H, $^3J_{HH}$ = 7 Hz, CH*Me*$_2$). ^{13}C{^{1}H} NMR (125.7 MHz, benzene-d6): δ 177.4 (*C*$_{arom}$, from HMBC), 145.2 (*C*$_{arom}$), 135.2 (d, $^2J_{PC}$ = 22 Hz, PN*C*N), 130.8 (*C*H$_{arom}$), 128.8 (*C*H$_{arom}$), 127.1 (*C*H$_{arom}$), 126.0 (*C*H$_{arom}$), 123.4 (*C*H$_{arom}$), 39.3 (d, $^1J_{PC}$ = 25 Hz, P*C*Me$_3$), 29.1 (*C*HMe$_2$), 28.4 (PC*Me*$_3$), 24.7 (CH*Me*$_2$), 23.5 (CH*Me*$_2$). ^{31}P{^{1}H} NMR (202.5 MHz, benzene-d_6): δ 118.5.

Synthesis of (PN)Ni

In the glovebox, an oven-dried bomb equipped with a stir bar was charged with a dark red solution of **[(PN)NiCl]$_2$** (203.3 mg, 0.196 mmol) in benzene (*ca.* 8 mL). LiN(SiMe$_3$)$_2$ (65.7 mg, 0.392 mmol) was subsequently transferred to the vessel as a solid. The vessel was sealed and taken outside the glovebox, where it was heated in an 85 °C oil bath. After 24 h, the vessel was brought into the glovebox, and solvent was removed *in vacuo*, leaving a dark residue. The residue was triturated with pentane (3 x *ca.* 3 mL), and then brought up in pentane (*ca.* 8 mL) and filtered through Celite. The dark green-yellow eluent was collected in a pre-weighed vial. Removal of solvent *in vacuo* yielded analytically pure **(PN)Ni**. Yield: 246 mg, 98%. Anal. Calcd for: $C_{33}H_{58}N_3NiPSi_2$: C,

61.67; H, 9.10; N, 6.54. Found: C, 61.29; H, 8.93; N, 6.62. ^{1}H NMR (300 MHz, benzene-d_6): δ 7.44 – 7.42 (m, 2 H, H_{arom}), 7.18 – 7.13 (m, 1 H, H_{arom}, overlapping with benzene-d_6), 6.96 – 6.83 (m, 2 H, H_{arom}), 6.83 – 6.76 (overlapping resonances, 3 H, H_{arom}), 4.52 – 4.38 (app septet, 2 H, $^{3}J_{HH}$ = 7 Hz, C*H*Me$_2$), 1.61 – 1.55 (overlapping resonances, 24 H, CH*Me$_2$* and P*tBu$_2$*), 0.83 – 0.81 (d, 6 H, $^{3}J_{HH}$ = 6 Hz, CH*Me$_2$*), 0.48- 0.46 (s, 18 H, N(Si*Me$_3$*)$_2$). ^{13}C{^{1}H} NMR (75.4 MHz, benzene-d_6): δ 176.8 (N*C*N), 146.5 (C_{arom}), 143.2 (C_{arom}), 134.1 (C_{arom}), 132.2 (*C*H$_{arom}$), 130.1 (*C*H$_{arom}$), 128.1 (*C*H$_{arom}$), 127.1 (*C*H$_{arom}$), 125.7 (*C*H$_{arom}$), 38.9 – 38.6 (d, $^{1}J_{CP}$ = 25 Hz, P(*C*Me$_3$)$_2$), 30.0 (*C*HMe$_2$), 29.2 – 29.1 (d, $^{2}J_{CP}$ = 4 Hz, P(C*Me$_3$*)$_2$), 25.2 (CH*Me$_2$*), 24.4 (CH*Me$_2$*), 7.7 (Si*Me$_3$*). ^{31}P{^{1}H} (121.5 MHz, benzene-d_6): δ 128.9. Crystals suitable for X-ray diffraction were grown from a concentrated solution of pentane at -35 °C.

Synthesis of (PN)Ni(NHdipp).

In the glovebox, a glass vial containing a magnetic stir bar was charged with **Ni$_2$Cl$_2$** (0.20 g, 0.19 mmol) and LiNHdipp (0.071 g, 0.39 mmol). THF (*ca*. 10 mL) was added and the resulting mixture stirred at room temperature for 30 minutes. The volatile components of the reaction mixture were subsequently removed *in vacuo*. The remaining residue was triturated with pentane (3 × 3 mL), then taken up in pentane (*ca.* 10 mL) of and filtered through Celite. The filtrate solution was collected, and the volatile components were removed *in vacuo* to afford **(PN)Ni(NHdipp)** (0.20 g, 80% yield) as an analytically pure black solid. Anal. Calcd for $C_{39}H_{58}N_3NiP$: C, 71.13; H, 8.88; N, 6.39. Found: C, 70.88; H, 9.00; N, 6.52. ^{1}H NMR (300 MHz, benzene-d_6): δ 7.53 – 7.49 (m, 2 H, H_{arom}), 7.07 – 6.92 (overlapping resonances, 6 H, H_{arom}), 6.87 – 6.80 (overlapping resonances, 3 H, H_{arom}), 4.92 (sept, 2 H, $^{3}J_{HH}$ = 7 Hz, C*H*Me$_2$), 4.43 (app sept, 2 H,

C*H*Me$_2$), 3.30 (br s, 1 H, N*H*), 1.63 (d, 6 H, $^3J_{HH}$ = 7 Hz, CH*Me*$_2$), 1.46 (d, 18 H, $^3J_{HP}$ = 14 Hz, P*tBu*$_2$), 1.25 (d, 12 H, $^3J_{HH}$ = 7 Hz, CH*Me*$_2$), 0.92 (d, 6 H, $^3J_{HH}$ = 7 Hz, CH*Me*$_2$). ^{13}C{^{1}H} NMR (75.4 MHz, benzene-d_6): δ 174.8 (N*C*N), 150.2 (*C*$_{arom}$), 144.8 (*C*$_{arom}$), 141.9 (*C*$_{arom}$), 138.2 (*C*$_{arom}$), 130.7 (*C*H$_{arom}$), 129.1 (*C*H$_{arom}$), 127.5 (*C*H$_{arom}$), 126.0 (*C*H$_{arom}$), 125.2 (*C*H$_{arom}$), 124.7 (*C*H$_{arom}$), 118.7 (*C*H$_{arom}$), 38.8 (d, $^1J_{CP}$ = 26 Hz, P*C*Me$_3$), 31.0 (*C*HMe$_2$), 29.2 (*C*HMe$_2$), 28.2 (d, $^3J_{CP}$ = 4 Hz, PC*Me$_3$*), 24.6 (CH*Me$_2$*), 23.7 (CH*Me$_2$*), 22.8 (CH*Me$_2$*). ^{31}P{^{1}H} (121.5 MHz, benzene-d_6): δ 135.7. Crystals of **(PN)Ni(NHdipp)** suitable for X-ray diffraction were grown from a concentrated Et$_2$O solution at -35 °C.

Synthesis of Ni$_2$H$_2$.

In the glovebox, **Ni$_2$Cl$_2$** (224 mg, 0.216 mmol) was dissolved in THF (*ca.* 8 mL) in a glass vial equipped with a magnetic stirring bar to form an orange-purple dichroic solution. This solution was stirred for 5 min, and then NaEt$_3$BH (1.0 M in toluene, 443 μL, 0.443 mmol, 2.05 equiv) was added via micropipette to the stirring solution, which turned black, and then dark green over one minute. After 1 h, THF was removed *in vacuo*, the black residue was triturated with pentane (3 x *ca.* 3 mL), extracted into benzene (*ca*. 10 mL), and filtered through Celite. The dark green eluent was concentrated *in vacuo*, triturated with pentane (3x *ca.* 3 mL), and dried *in vacuo* to yield analytically pure **Ni$_2$H$_2$** as a dark green powder. Yield: 140 mg, 67%. Anal. Calcd for C$_{54}$H$_{82}$N$_4$Ni$_2$P$_2$: C, 67.10; H, 8.55; N, 5.80. Found: C, 67.26; H, 9.11; N, 5.62.

^{1}H NMR (500.1 MHz, benzene-d_6): δ 7.43 – 7.41 (m, 4 H, *H*$_{arom}$), 6.96 – 6.93 (m, 2 H, *H*$_{arom}$), 6.86 – 6.85 (overlapping resonances, 10 H, *H*$_{arom}$), 3.79 – 3.70 (app septet, 4 H, C*H*Me$_2$), 1.84 – 1.83 (d, 12 H, ^{3}J$_{HH}$ = 7 Hz, CH*Me$_2$*), 1.38 – 1.35 (d, 36 H, ^{3}J$_{HP}$ = 14 Hz,

P*tBu*$_2$), 0.98 – 0.96 (d, 12 H, $^3J_{HH}$ = 7 Hz, CH*Me*$_2$), -27.74 – -27.93 (m, 2 H, Ni*H*). $^{13}C\{^1H\}$ NMR (125.8 MHz, benzene-d_6): δ 175.1 (C_{arom}), 148.2 (C_{arom}), 143.6 (C_{arom}), 136.0 ($^2J_{PC}$ = 21 Hz, N*C*N), 130.6 (CH$_{arom}$), 128.6 (CH$_{arom}$), 127.1 (CH$_{arom}$), 125.0 (CH$_{arom}$), 124.2 (CH$_{arom}$), 37.7 ($^1J_{PC}$ = 27 Hz, P(CMe$_3$)$_2$), 29.0 (P(C*Me*$_3$)$_2$ and *C*HMe$_2$ overlapping), 25.4 (CH*Me*$_2$), 23.3 (CH*Me*$_2$). $^{31}P\{^1H\}$ NMR (202.5 MHz, benzene-d_6): δ 122.3 (app m due to incomplete decoupling of Ni*H*). A single crystal suitable for X-ray diffraction was grown from the slow evaporation of a concentrated solution of ether.

Synthesis of (PN)NiH(pyr).

In the glovebox, **Ni$_2$H$_2$** (50 mg, 0.052 mmol) was dissolved in pyridine (360 mg, 4.55 mmol) to form a dark green solution that turned dark red-brown over *ca.* 2 min. The solution was concentrated *in vacuo* and cooled at -35 °C, which afforded crystals of **(PN)NiH(pyr)** suitable for single-crystal X-ray diffraction and for which satisfactory elemental analysis data were obtained. Yield: 43 mg, 69%. Anal. Calcd for $C_{32}H_{46}N_3NiP$: C, 68.34; H, 8.24; N, 7.47. Found: C, 68.55; H, 8.39; N, 7.52. Upon contacting non-pyridine solvent, **(PN)NiH(pyr)** dissociates to form an equilibrium mixture of **(PN)NiH(pyr)**, pyridine, and **Ni$_2$H$_2$**. As such, NMR data for **(PN)NiH(pyr)** is inferred from such an equilibrium mixture formed from the dissolution of crystalline **(PN)NiH(pyr)** in benzene-d_6. ^1H NMR (500.1 MHz, benzene-d_6): δ 8.01 – 7.99 (m, 2 H, H_{arom}), 7.80 – 7.78 (m, 2 H, H_{arom}), 6.99 – 6.94 (overlapping resonances, 4 H, H_{arom}), 6.89 – 6.87 (m, 2 H, H_{arom}), 6.56 – 6.53 (m, 1 H, H_{arom}), 6.21 - 6.19 (m, 2 H, H_{arom}), 3.88 – 3.79 (app septet, 2 H, $^3J_{HH}$ = 7 Hz, C*H*Me$_2$), 1.69 (d, 18 H, $^3J_{HP}$ = 13 Hz, P*tBu*$_2$), 1.03 (d, 6 H, $^3J_{HH}$ = 7 Hz, CH*Me*$_2$), 0.97 (d, 6 H, $^3J_{HH}$ = 7 Hz, CH*Me*$_2$), -20.24 (d, 1 H, $^2J_{HP}$ = 104 Hz, Ni*H*). $^{13}C\{^1H\}$ NMR (125.8 MHz, benzene-d_6): δ 175.1 (C_{arom}), 152.2 (CH$_{arom}$),

147.7 (C_{arom}), 143.1 (C_{arom}), 138.3 ($^{2}J_{PC}$ = 33 Hz, N*C*N), 135.6 (CH_{arom}), 131.3 (CH_{arom}), 127.0 (CH_{arom}), 124.0 (CH_{arom}), 123.5 (CH_{arom}), 123.2 (CH_{arom}), 36.1 (d, $^{1}J_{PC}$ = 33 Hz, P(CMe_3)$_2$), 29.2 (d, $^{2}J_{PC}$ = 3 Hz, P(CMe_3)$_2$), 28.5 ($CHMe_2$), 23.9 (CHMe_2), 23.3 (CHMe_2). $^{31}P\{^{1}H\}$ NMR (202.5 MHz, benzene-d_6): δ 131.8 – 131.3 (app m due to incomplete decoupling of Ni*H*).

(PN)NiH(DMAP)

In the glovebox, DMAP (0.005 g, 0.04 mmol) and benzene-d_6 (*ca*. 0.75 mL) were combined in a glass vial. This solution was transferred to another glass vial containing **Ni$_2$H$_2$** (16 mg, 0.017 mmol) via pipet, mixed until the resultant dark green solution was homogeneous, and transferred to an NMR tube. The solution took on a lighter green coloration over the course of ca. 5 h; during this time complete conversion of **Ni$_2$H$_2$** to **(PN)NiH(DMAP)** was monitored by use of $^{31}P\{^{1}H\}$ and ^{1}H NMR methods. Excess DMAP was observable by use of ^{1}H NMR with broadened resonances, presumably due to exchange of free and bound DMAP. Efforts to isolate synthetically useful quantities of analytically pure **(PN)NiH(DMAP)** via crystallization (as was done for **(PN)NiH(pyr)**) were unsuccessful, and loss of DMAP upon workup prevented purification via alternative methods. A minute amount of crystalline material suitable for X-ray diffraction was obtained from a concentrated solution of the complex stored in ether/pentane at −35 °C. ^{1}H NMR (500.1 MHz, benzene-d_6): δ 7.81 – 7.80 (m, 2 H, H_{arom}), 7.72 – 7.70 (m, 2 H, H_{arom}), 7.09 – 6.92 (overlapping resonances, 6 H, H_{arom}), 5.63 -5.62 (m, 2 H, H_{arom}), 4.06 – 4.00 (m, 2 H, C*H*Me$_2$), 1.89 (s, 6 H, NMe_2), 1.76 – 1.73 (d, 18 H, $^{3}J_{PH}$ = 13 Hz, PtBu_2), 1.24 – 1.22 (d, 6 H, $^{3}J_{HH}$ = 7 Hz, CHMe_2), 1.04 – 1.03 (d, 6 H, $^{3}J_{HH}$ = 7 Hz, CHMe_2), -20.75 – -20.97 (d, 1 H, $^{2}J_{PH}$ = 107 Hz, Ni*H*). $^{13}C\{^{1}H\}$ NMR (125.8 MHz, benzene-d_6): δ

174.9 (C_{arom}), 153.4 (C_{arom}), 152.3 (CH_{arom}), 148.4 (C_{arom}), 143.3 (C_{arom}), 139.1 (d, $^{2}J_{PC}$ = 21 Hz, N*C*N), 131.2 (CH_{arom}), 127.8 (CH_{arom}), 127.0 (CH_{arom}), 123.8 (CH_{arom}), 123.5 (CH_{arom}), 105.8 (CH_{arom}), 37.9 (N*Me*$_2$), 36.0 (d, $^{1}J_{PC}$ = 33 Hz, P(*C*Me$_3$)$_2$, 29.3 (d, $^{2}J_{PC}$ = 3 Hz, P(C*Me*$_3$)$_2$), 28.6 (*C*HMe$_2$), 24.2 (CH*Me*$_2$), 23.6 (CH*Me*$_2$). $^{31}P\{^{1}H\}$ NMR (202.5 MHz, benzene-d_6): δ 131.1 – 130.6 (app m due to incomplete decoupling of Ni*H*).

General Procedure for Catalytic Reactions Using HBPin.

In the glovebox, a glass vial was charged with precatalyst **(PN)M** (3 mol %), octene (0.4 mmol), and HBPin (0.4 mmol in the case of I-H, Scheme 2-4, Scheme 2-5, Scheme 2-6; 5 mol % in the case of isomerization, Scheme 2-7). The vial was sealed with a PTFE-lined screw cap featuring a rubber septum, and the cap/vial contact was further sealed externally by wrapping with PTFE tape and electrical tape. The vial was then placed in an aluminum heating block that was set to the desired temperature for the stated amount of time. For analysis by use of GC methods, the reaction vial was then opened to air and extracted with EtOAc (500 μL). Dodecane (50.3 μL, 0.222 mmol) was added to the resultant solution as an internal standard. The solution was filtered through a short silica plug into a glass vial suited for use on a GC autosampler (GC vial). The reaction vial was further extracted with a second portion of EtOAc (500 μL), and the extract was again filtered through the same silica plug and collected into the same GC vial. The vial was sealed with a PTFE screw cap featuring a rubber septum, and its contents were analyzed by use of GC methods. For analysis by use of NMR methods, following the stated reaction time the reaction vial was opened to air and quantitatively extracted with a known amount of a stock solution (20.0 mg/mL) of ferrocene in $CDCl_3$ (0.01−0.03 mmol

ferrocene employed). The vial was further diluted with pure $CDCl_3$ (700−900 μL) and filtered through silica into an NMR tube for subsequent NMR analysis.

Procedure for the Reaction of Octenes with DBPin.

In the glovebox, two glass vials were charged with precatalyst **(PN)Ni** (3 mol %). One vial was charged with 1-octene, while the other was charged with trans-4-octene (in each case, 57.0 μL, 41 mg, 0.36 mmol). DBPin (53.1 μL, 47 mg, 0.36 mmol) was then added to each vial. The vials were sealed with a PTFE-lined screw cap featuring a rubber septum, and the cap/ vial contact was further sealed externally by wrapping with PTFE tape and electrical tape. The vials were then placed in an aluminum heating block set to 65 °C for 18 h. The vials, each containing homogeneous dark-red mixtures, were brought into the glovebox and opened under nitrogen. In each case, the contents of the vial were split via micropipette transfer of a 55 μL aliquot from each sample to a separate glass vial by using a micropipette. For each reaction, one portion was dissolved in C_6H_6 (500 μL), transferred to an NMR tube, and analyzed by use of ^{2}H NMR and ^{11}B NMR methods. The other half was taken out of the glovebox, exposed to air, and dissolved in $CDCl_3$ (*ca*. 500 μL). This latter chloroform fraction was analyzed by use of ^{1}H NMR and $^{13}C\{^{1}H\}$ NMR methods, whereby in the latter case a long relaxation delay was employed to improve quantitation. Notably, components of the mixture were poorly resolved in the spectra obtained, thus complicating assessment of positional deuterium incorporation.

2.6 Supporting Figures

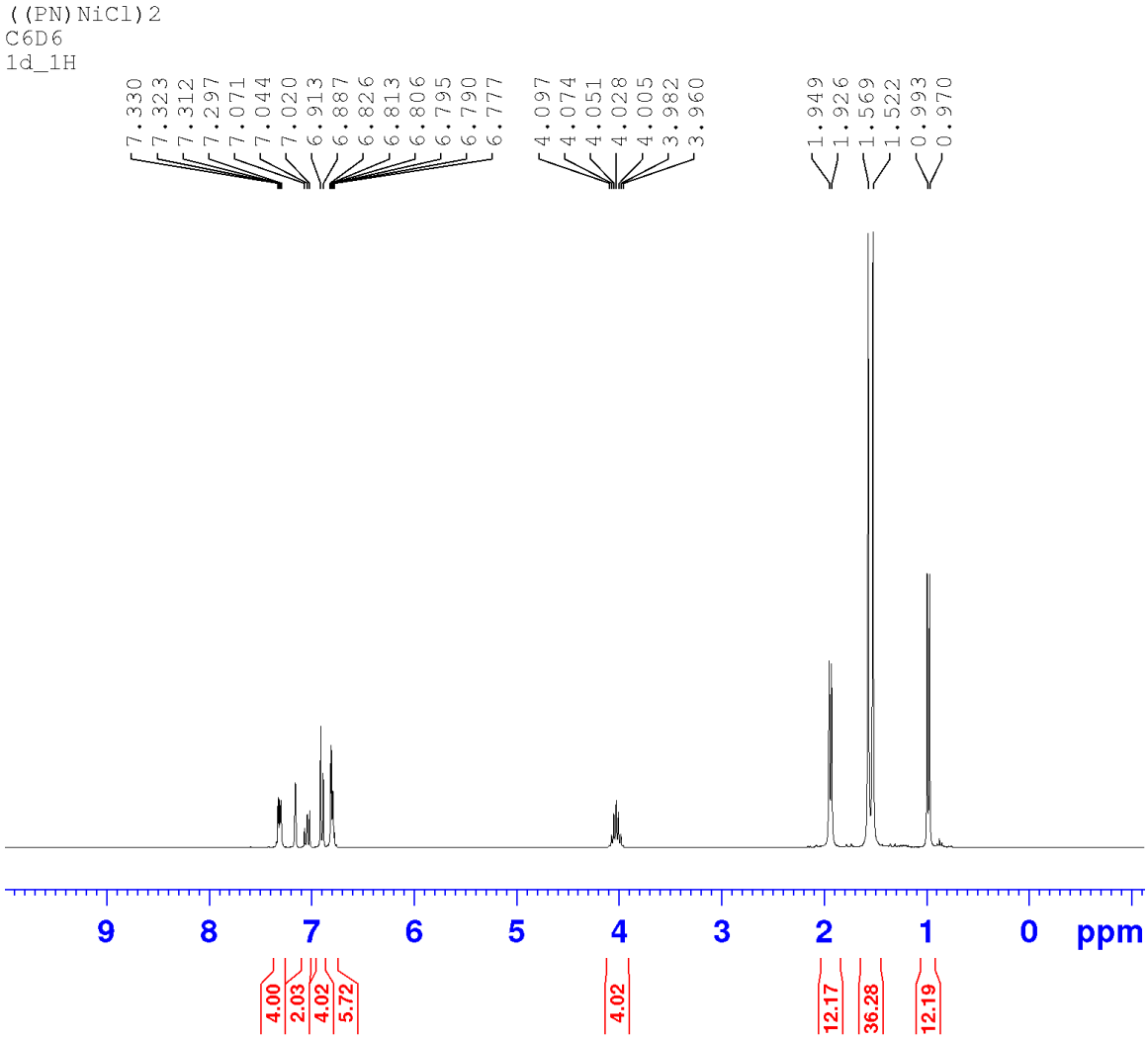

Figure S2-1. ^{1}H NMR spectrum of Ni_2Cl_2 (benzene-d_6, 300 MHz).

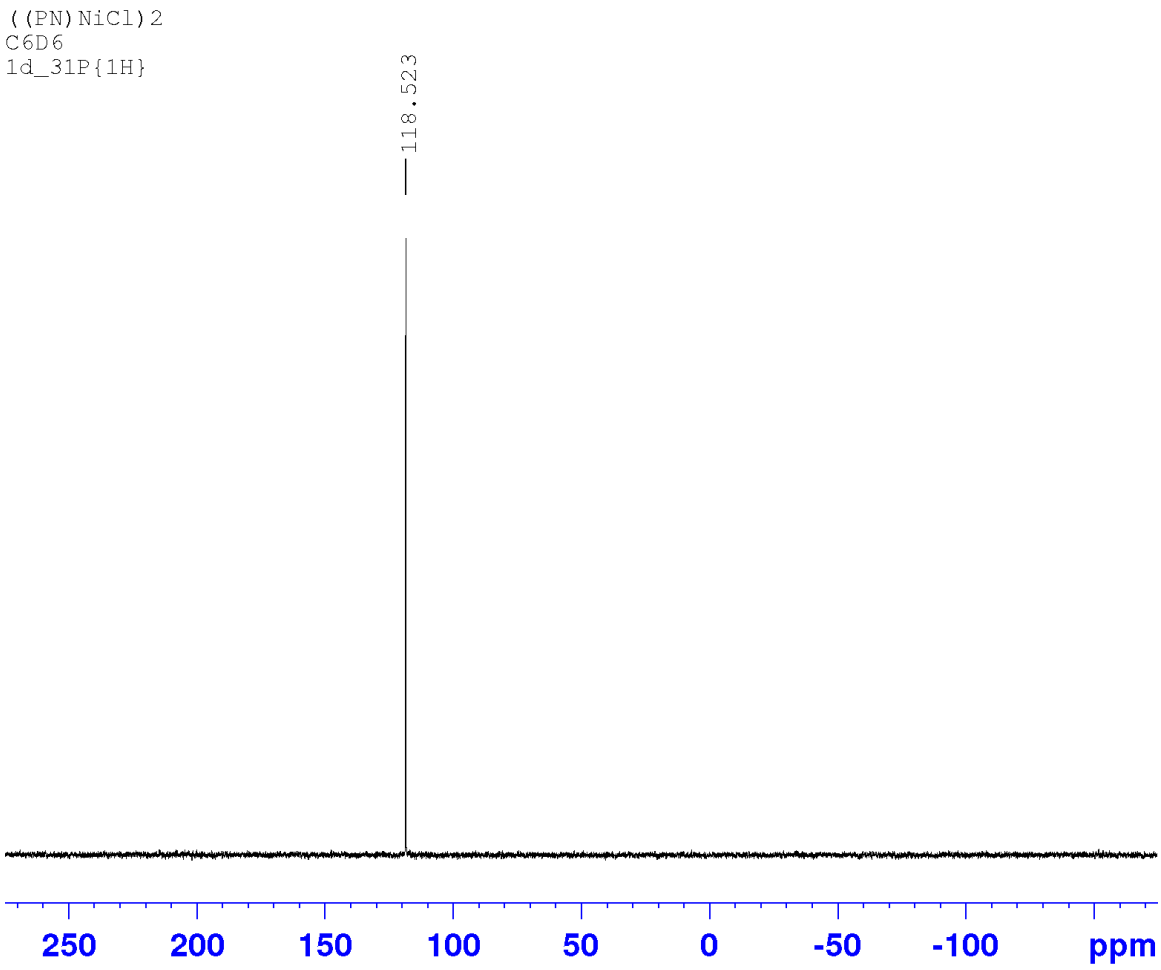

Figure S2-2. $^{31}P\{^{1}H\}$ NMR spectrum of Ni_2Cl_2 (benzene-d_6, 121.5 MHz).

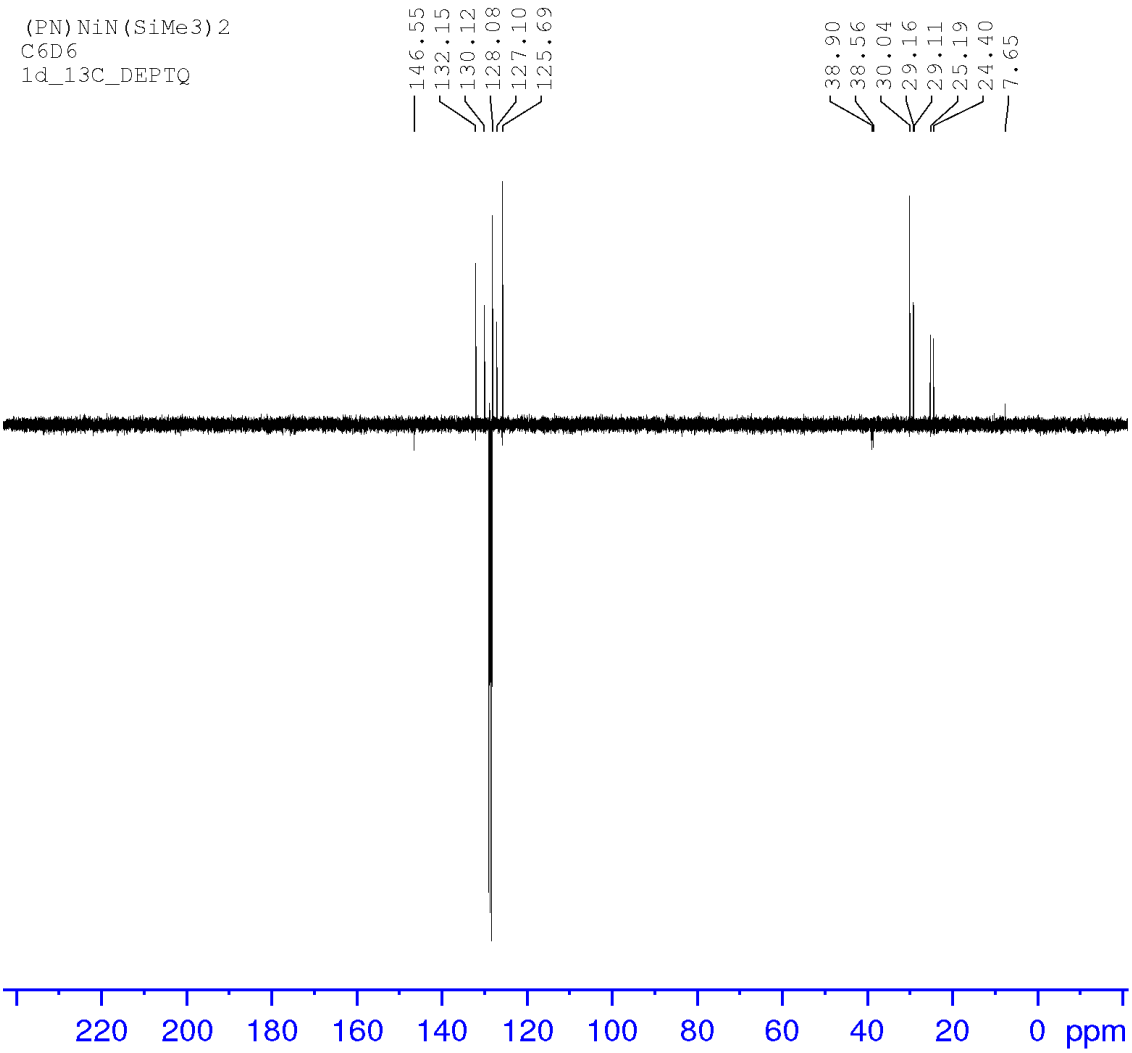

Figure S2-3. ^{13}C-DEPTQ135 NMR spectrum of (PN)Ni (benzene-d_6, 75.4 MHz).

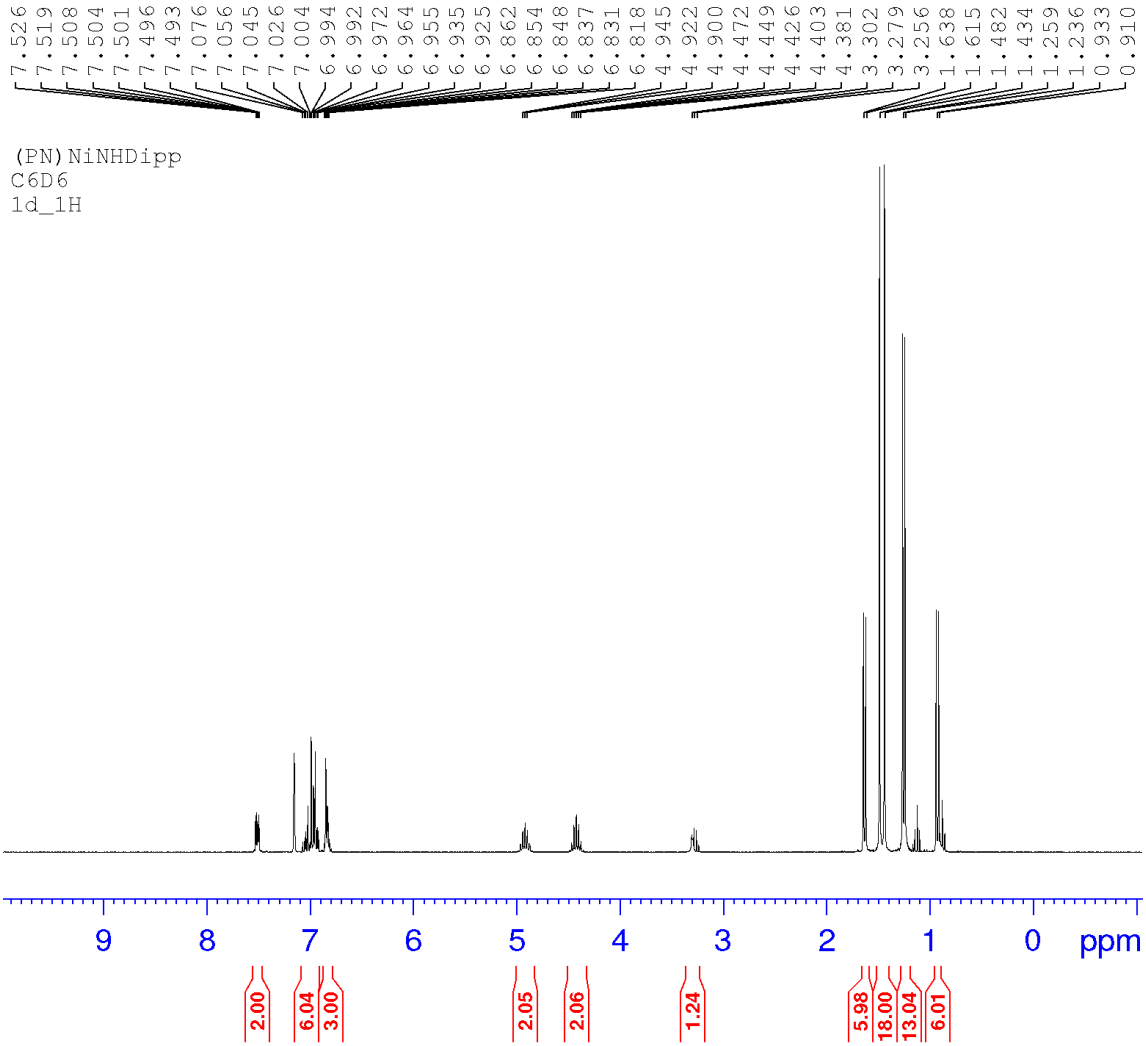

Figure S2-4. ^{1}H NMR spectrum of (PN)Ni(NHdipp) (benzene-*d*$_6$, 300 MHz).

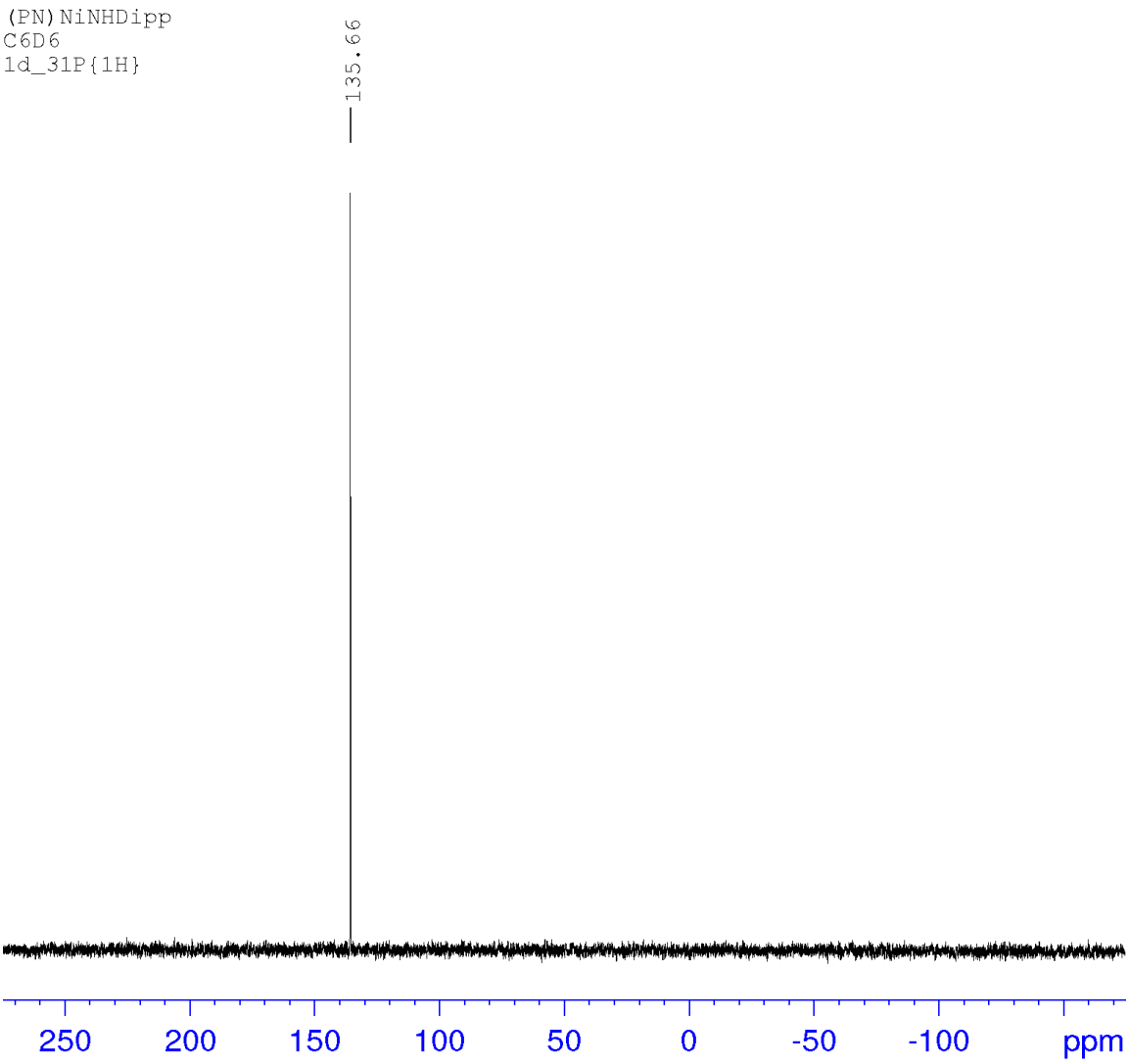

Figure S2-5. $^{31}P\{^{1}H\}$ NMR spectrum of (PN)Ni(NHdipp) (benzene-d_6, 121.5 MHz).

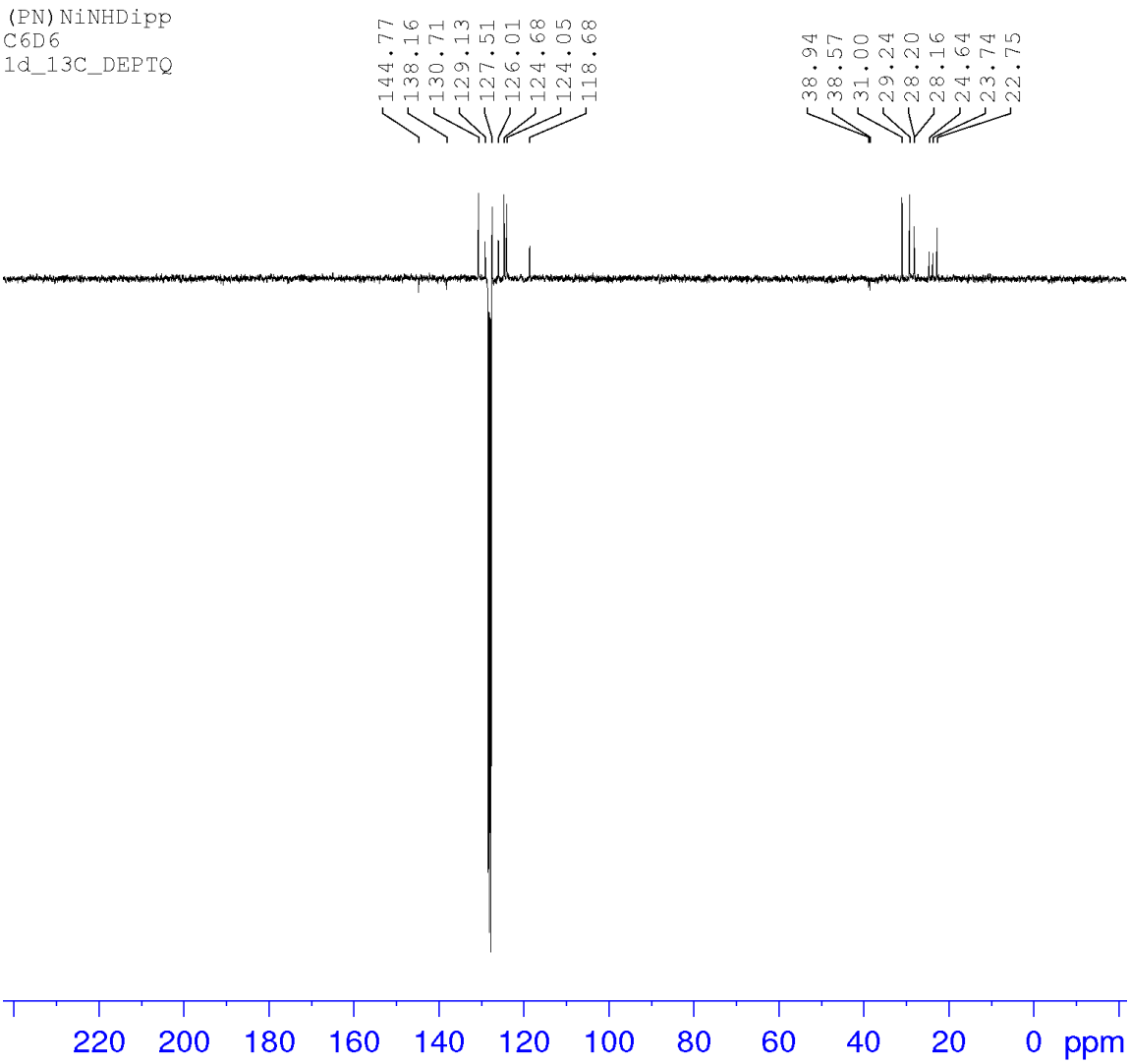

Figure S2-6. ^{13}C-DEPTQ135 NMR spectrum of (PN)Ni(NHdipp) (benzene-d_6, 75.4 MHz).

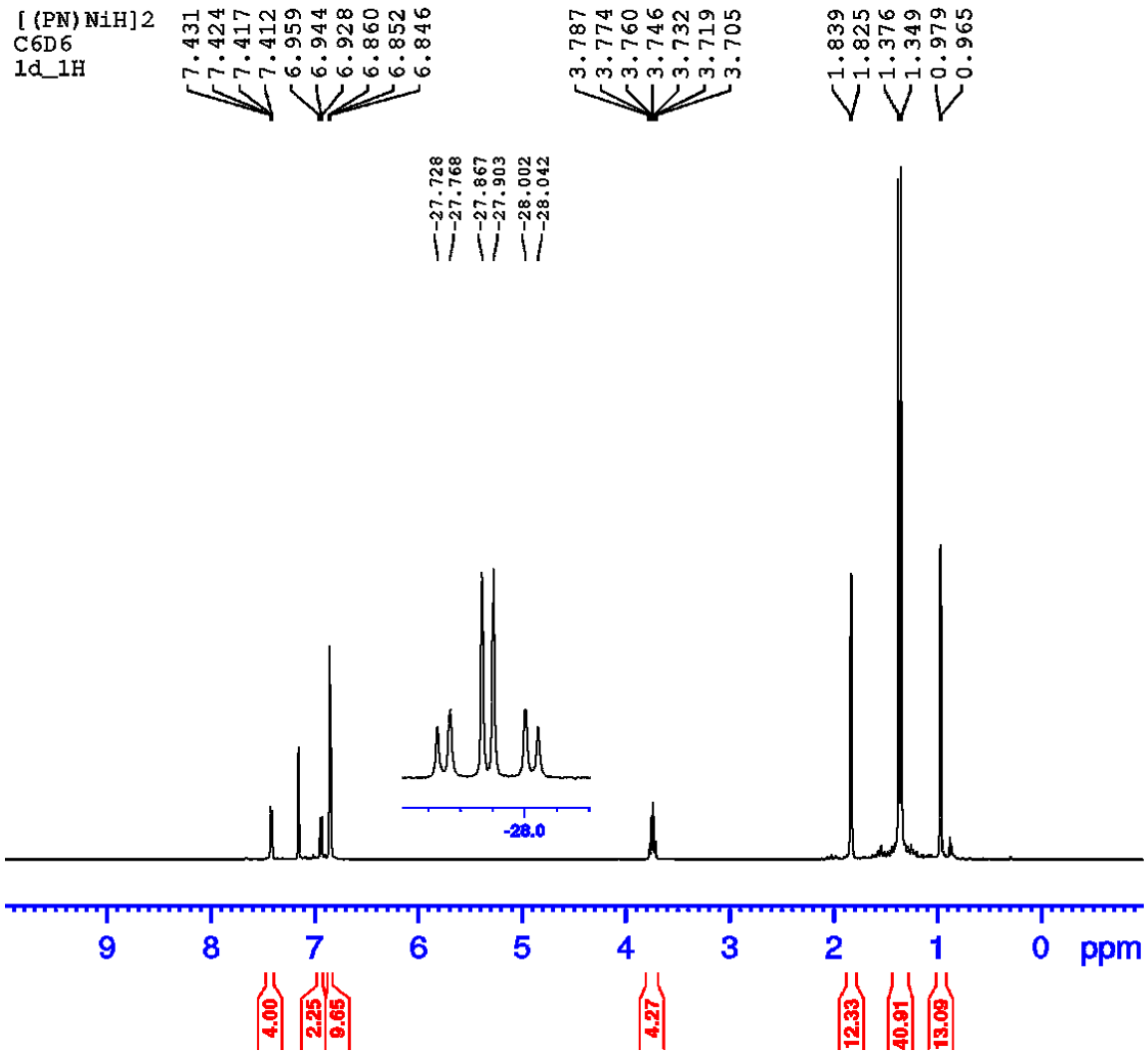

Figure S2-7. ^{1}H NMR spectrum of Ni_2H_2 (benzene-d_6, 500.1 MHz).

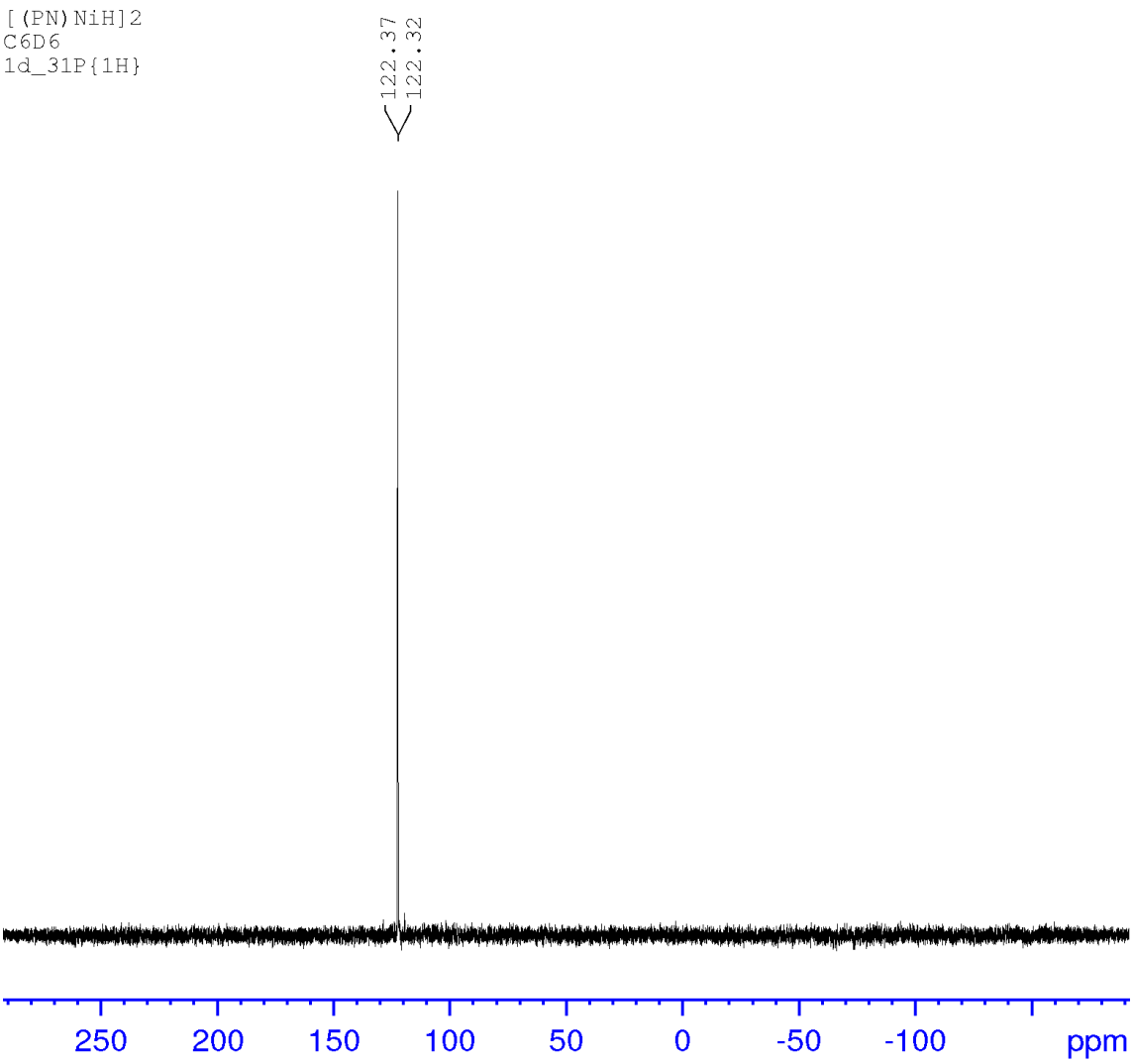

Figure S2-8. $^{31}P\{^{1}H\}$ NMR spectrum of Ni_2H_2 (benzene-d_6, 202.5 MHz); multiplet structure due to inefficient decoupling of the Ni-*H*.

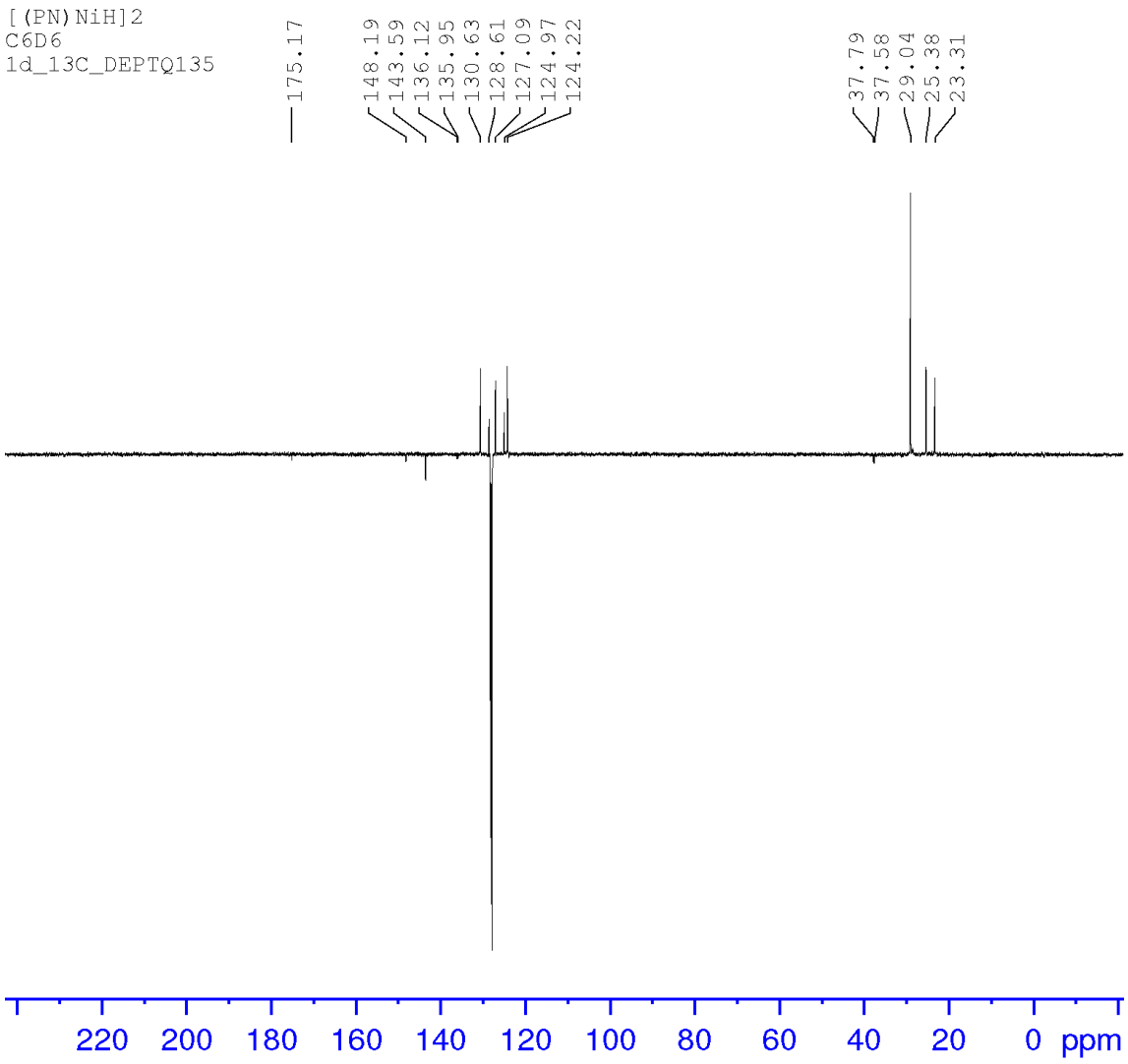

Figure S2-9. ^{13}C-DEPTQ135 NMR spectrum of Ni_2H_2 (benzene-d_6, 125.7 MHz).

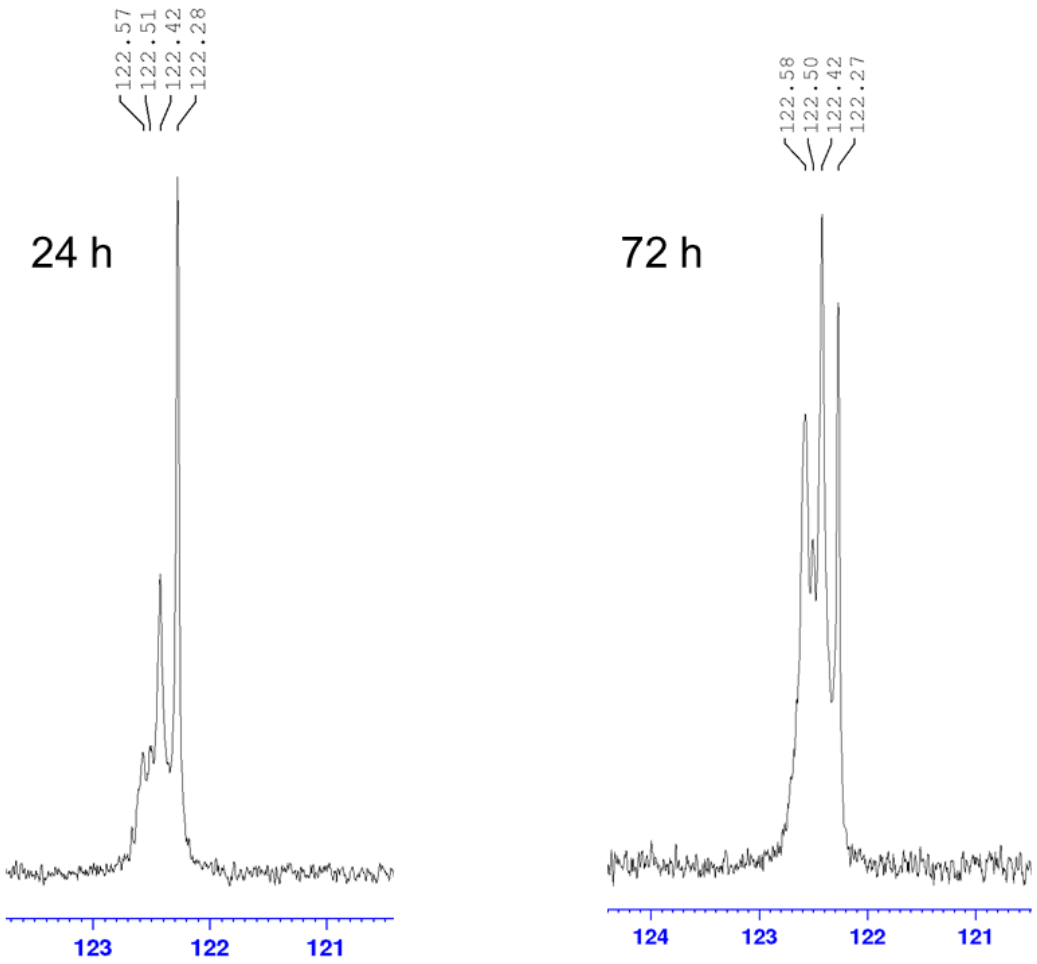

Figure S2-10. $^{31}P\{^{1}H\}$ NMR spectrum acquired after reaction at 110 ˚C between Ni_2H_2 and DBPin (5 equiv per Ni) (toluene-d_8, 121.5 MHz).

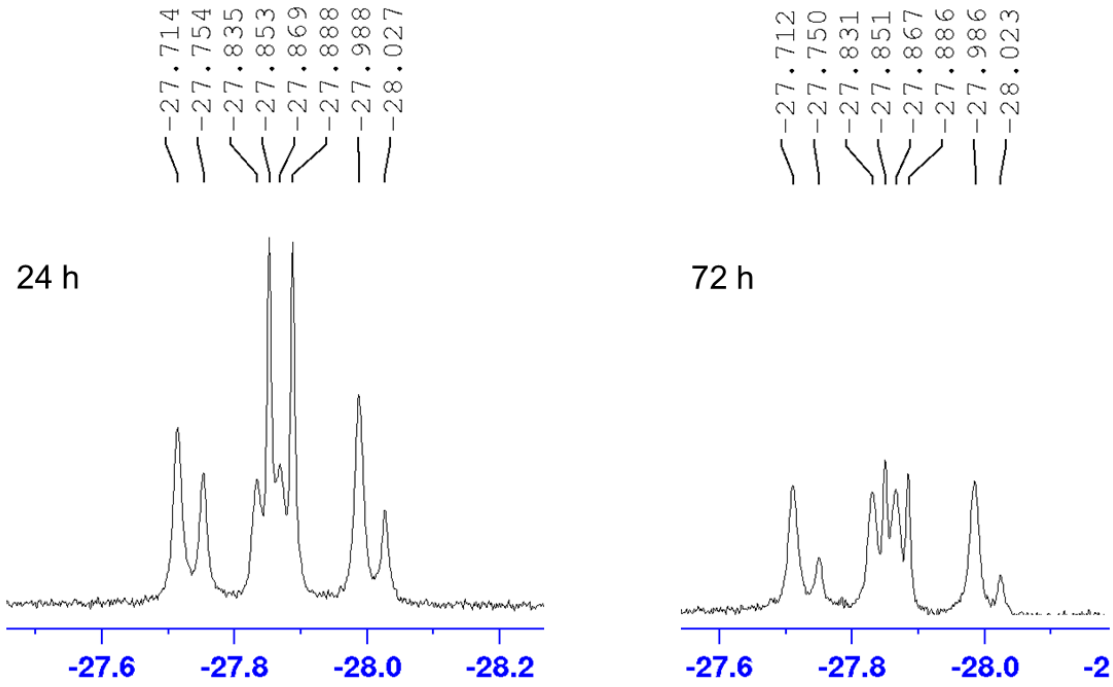

Figure S2-11. ^{1}H NMR spectrum acquired after reaction at 110 ˚C between Ni_2H_2 and DBPin (5 equiv per Ni) (toluene-d_8, 300 MHz).

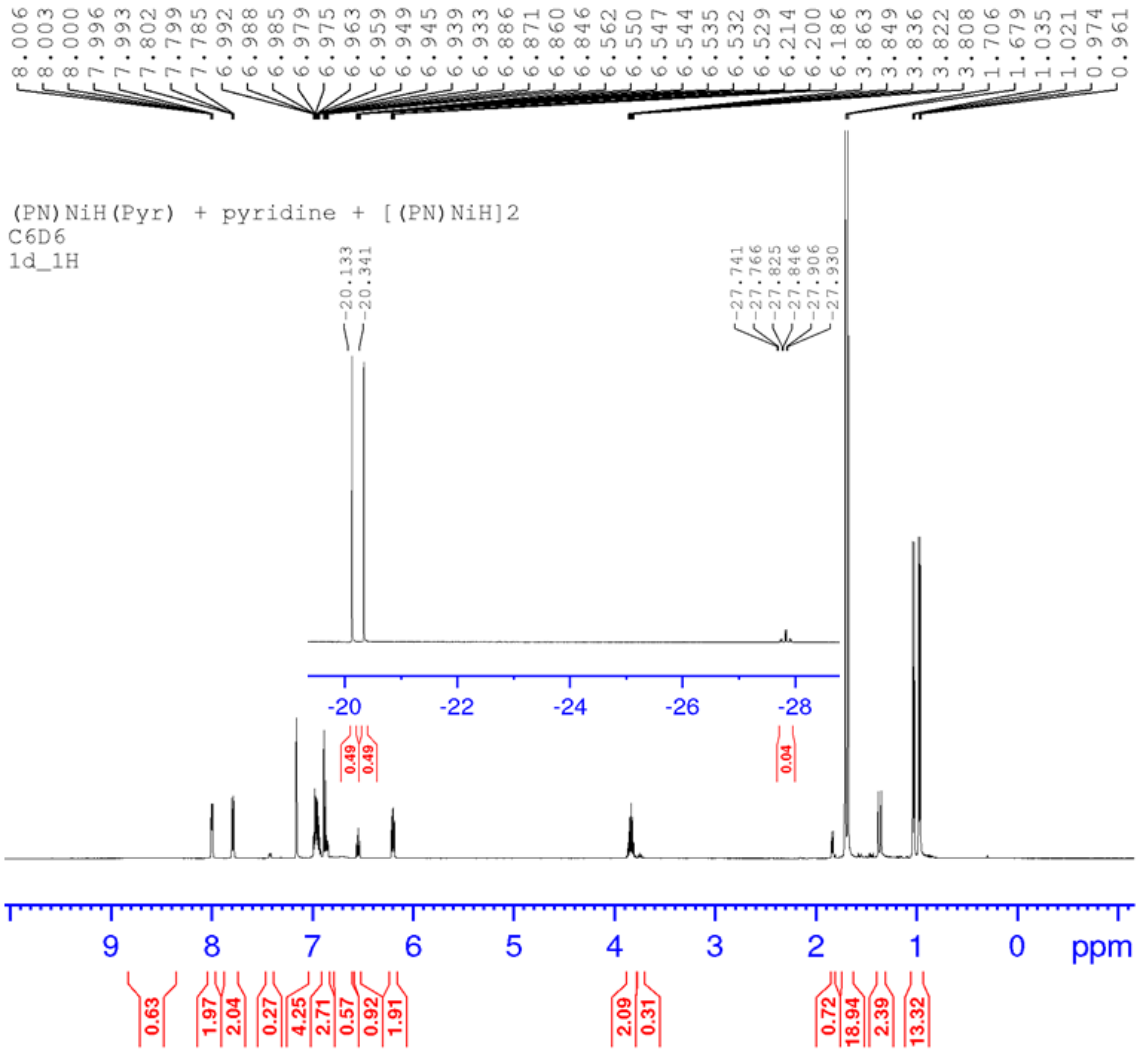

Figure S2-12. ^{1}H NMR spectrum of (PN)NiH(pyr) in equilibrium with Ni_2H_2 (benzene-d_6, 500.1 MHz).

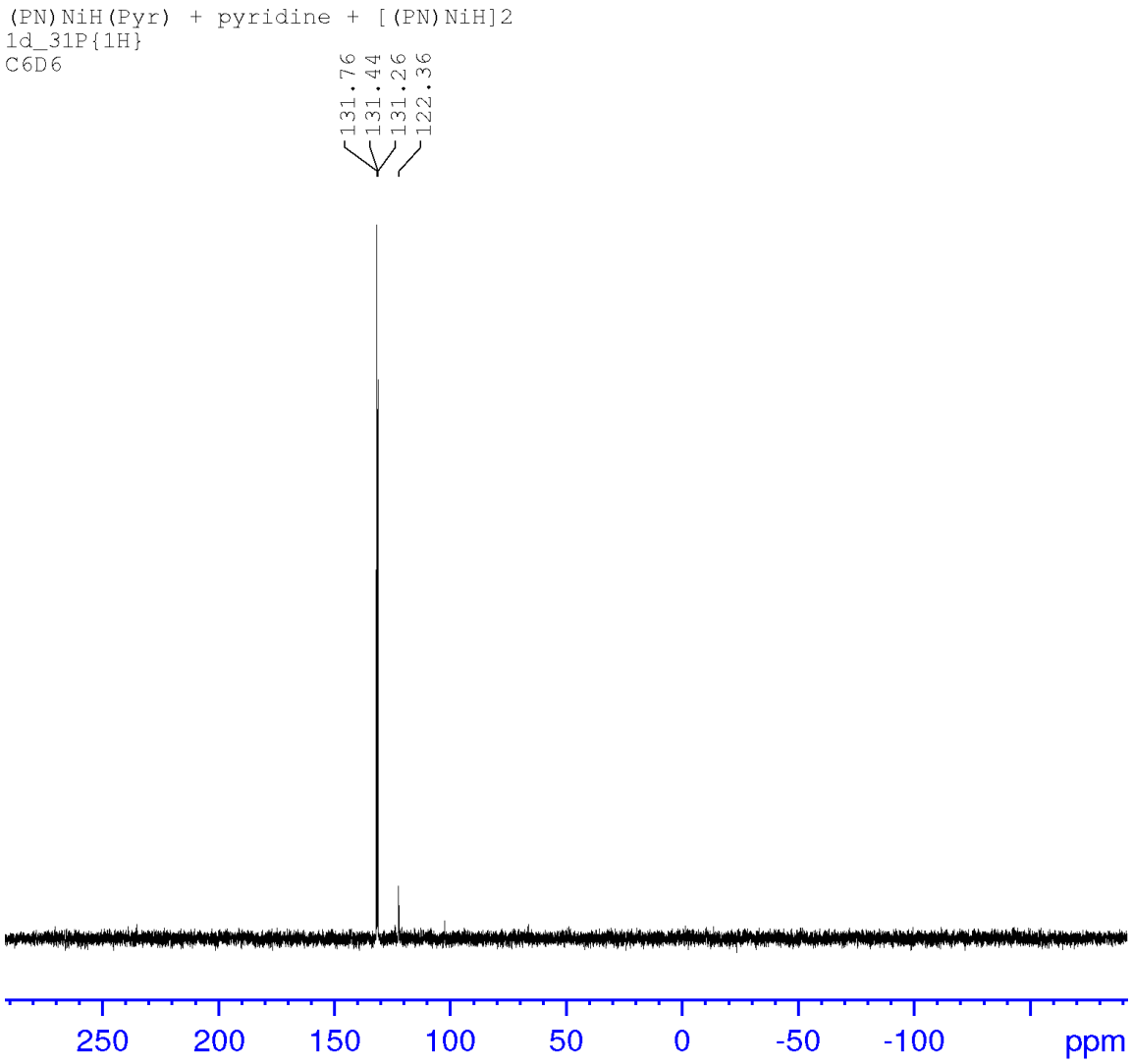

Figure S2-13. $^{31}P\{^{1}H\}$ NMR spectrum of (PN)NiH(pyr) in equilibrium with Ni_2H_2 (benzene-d_6, 202.5 MHz); multiplet structure due to inefficient decoupling of the Ni-*H*.

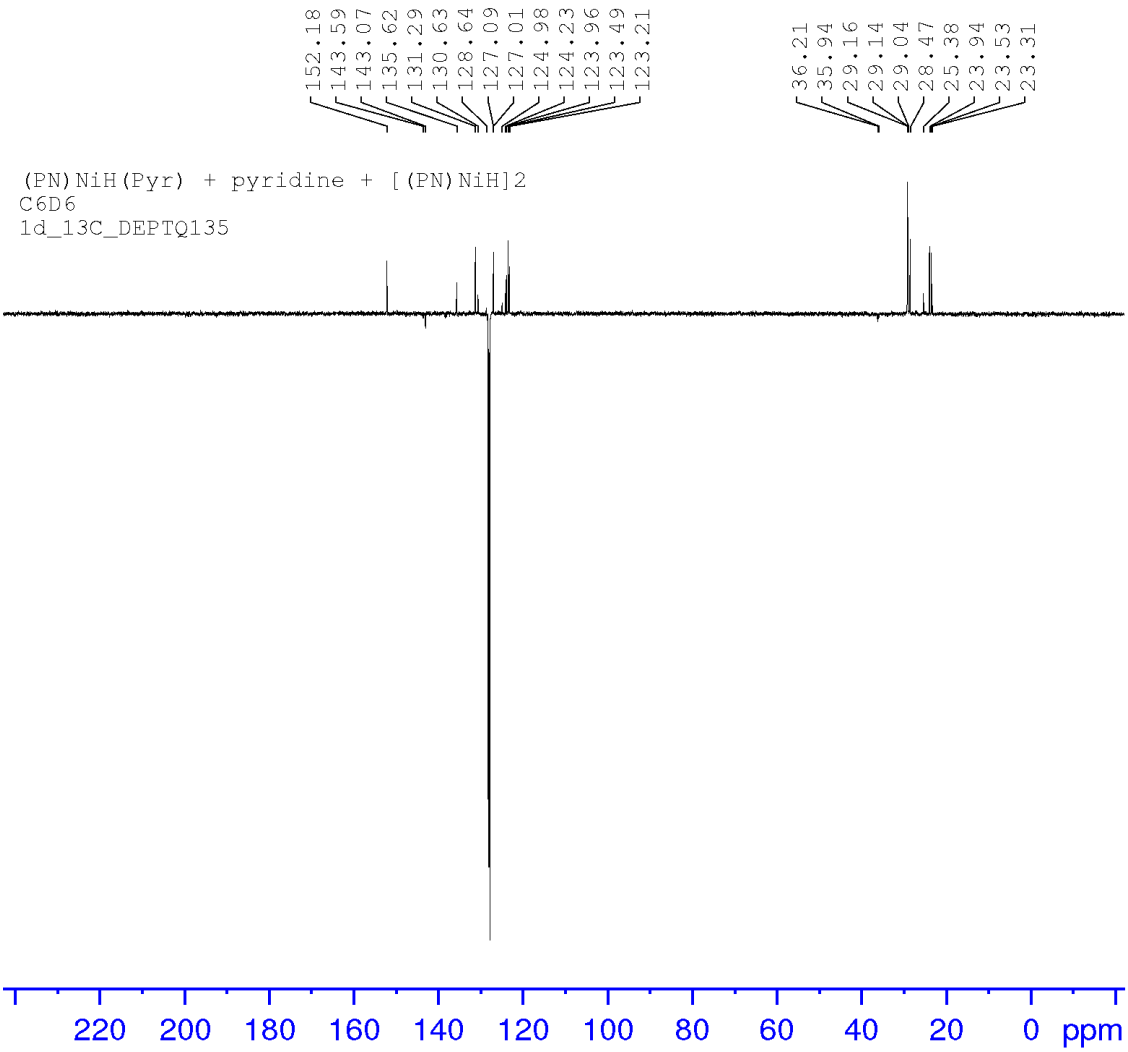

Figure S2-14. ^{13}C-DEPTQ135 NMR spectrum of (PN)NiH(pyr) in equilibrium with Ni_2H_2 (benzene-d_6, 125.7 MHz).

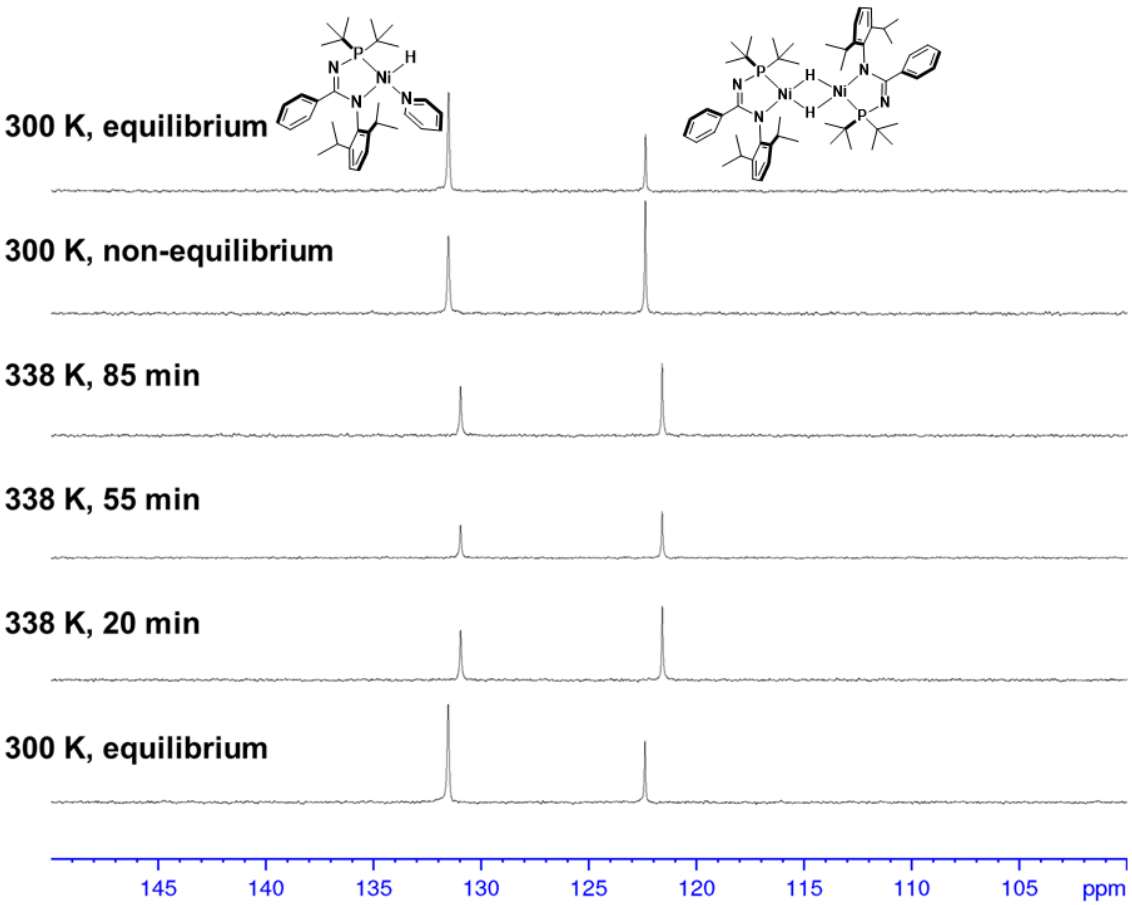

Figure S2-15. Temperature-dependent $^{31}P\{^{1}H\}$ NMR spectra arising from changes in the equilibrium proportions of (PN)NiH(pyr) (12 mg dissolved in 0.75 mL benzene-d_6) and Ni_2H_2 (121.5 MHz).

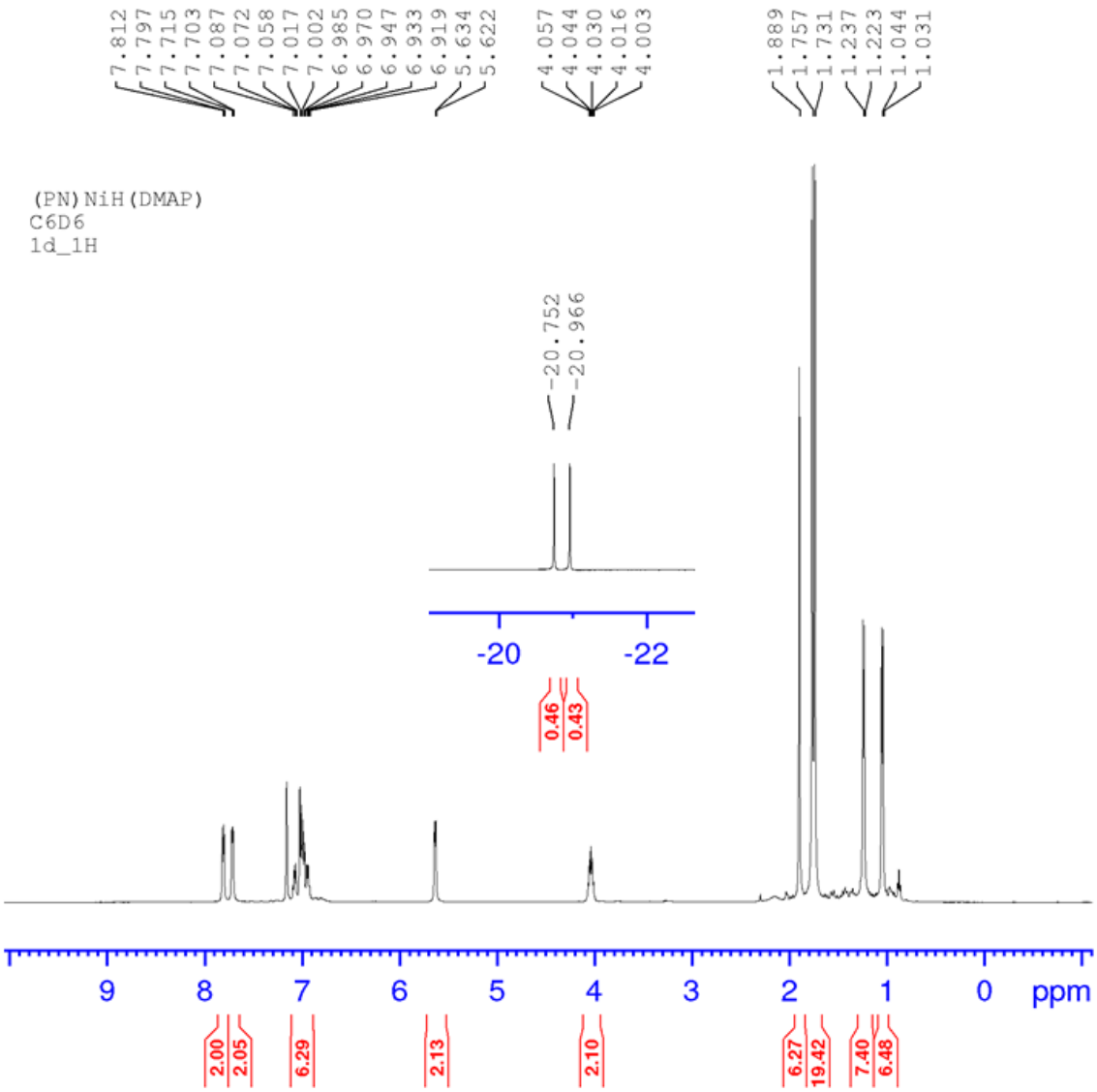

Figure S2-16. ^{1}H NMR spectrum of (PN)NiH(DMAP) (benzene-*d*$_6$, 500.1 MHz).

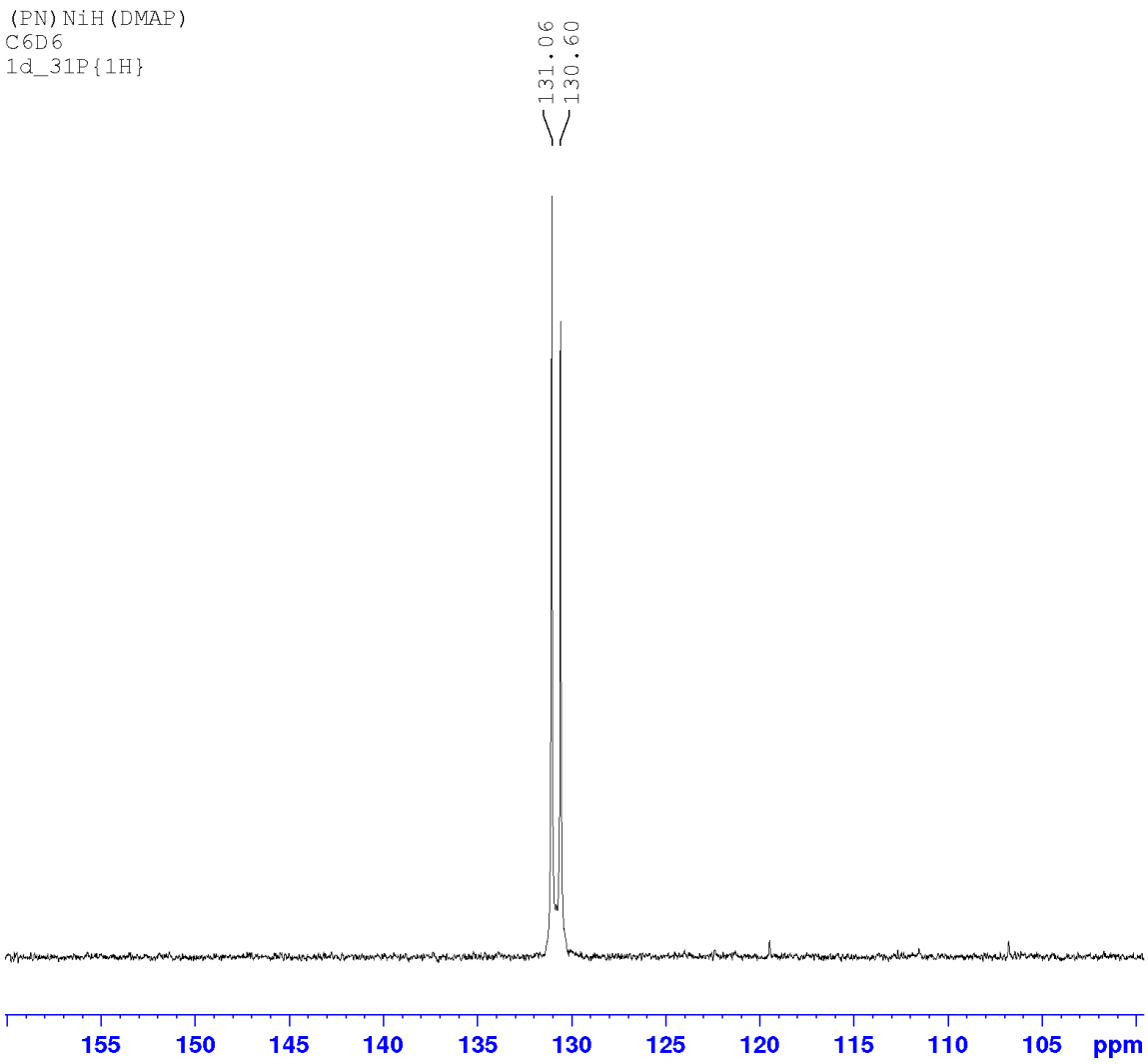

Figure S2-17. $^{31}P\{^{1}H\}$ NMR spectrum of (PN)NiH(DMAP) (benzene-d_6, 202.5 MHz); multiplet structure due to inefficient decoupling of the Ni-*H*.

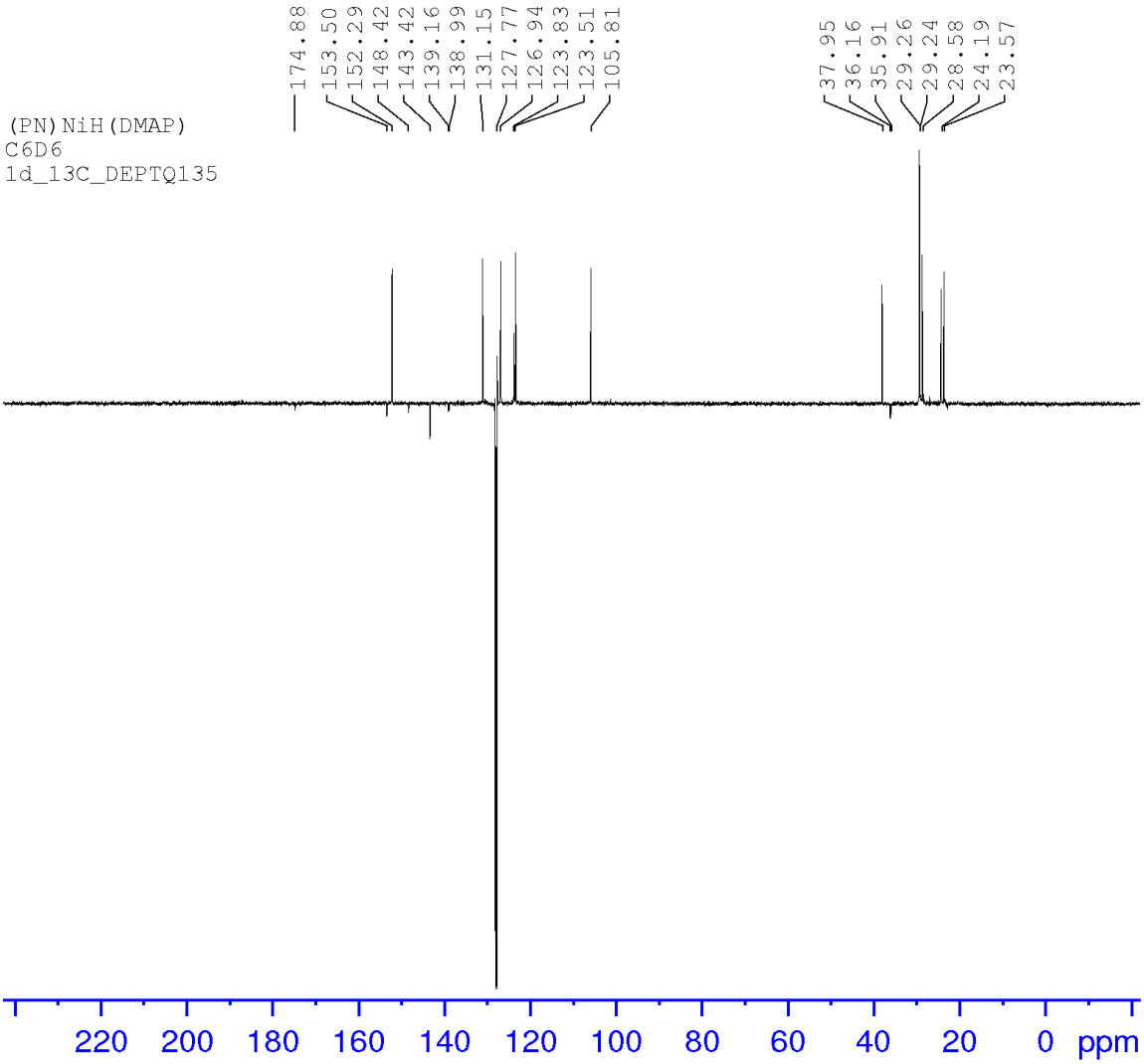

Figure S2-18. ^{13}C-DEPTQ135 NMR spectrum of (PN)NiH(DMAP) (benzene-d_6, 125.7 MHz).

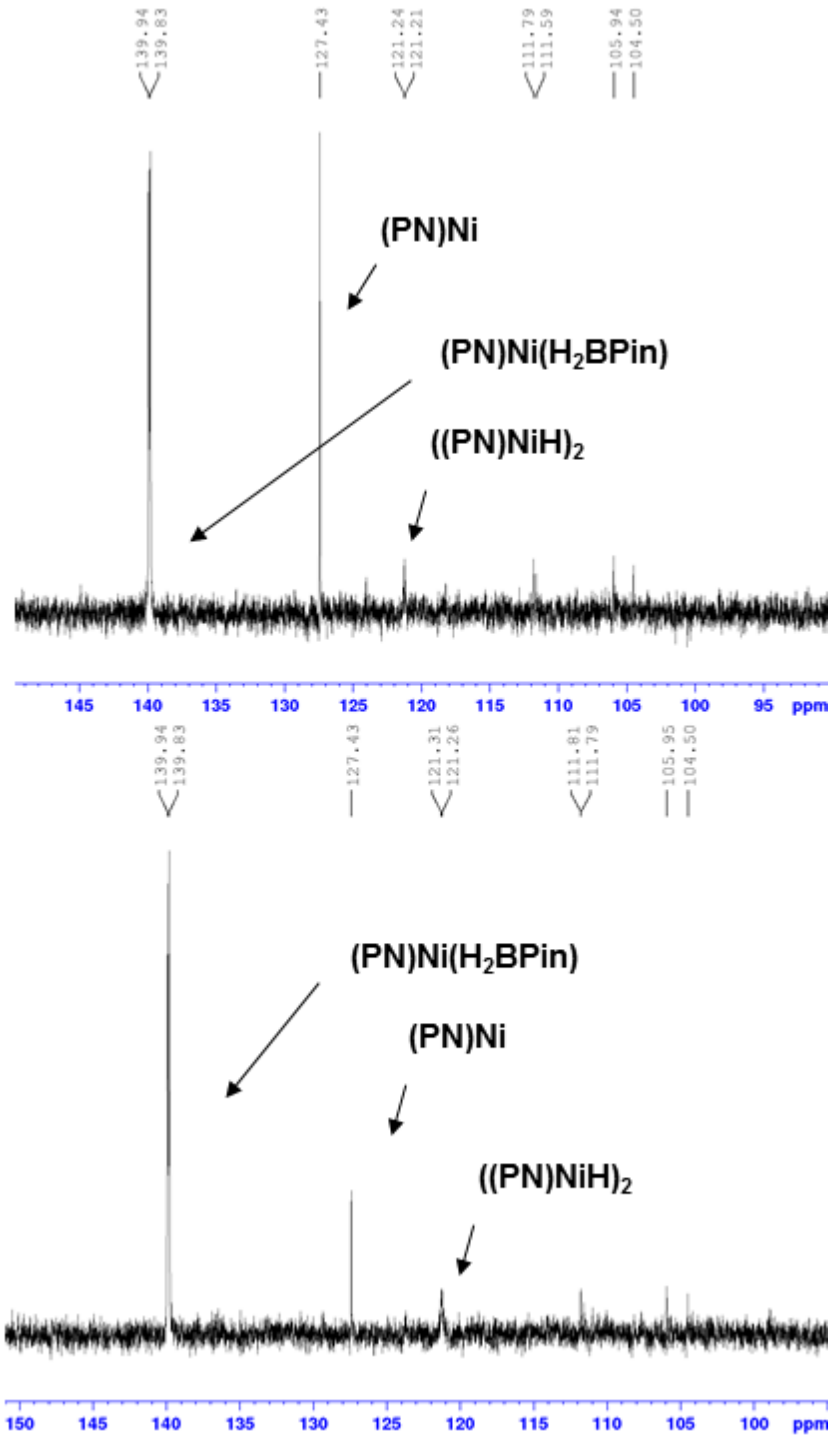

Figure S2-19. $^{31}P\{^{1}H\}$ NMR spectrum of the reaction mixture upon exposure of (PN)Ni to HBPin (33 equiv; 23 ˚C, C_6D_{12}, 121.5 MHz). Top: after 24 h. Bottom: after 43 h.

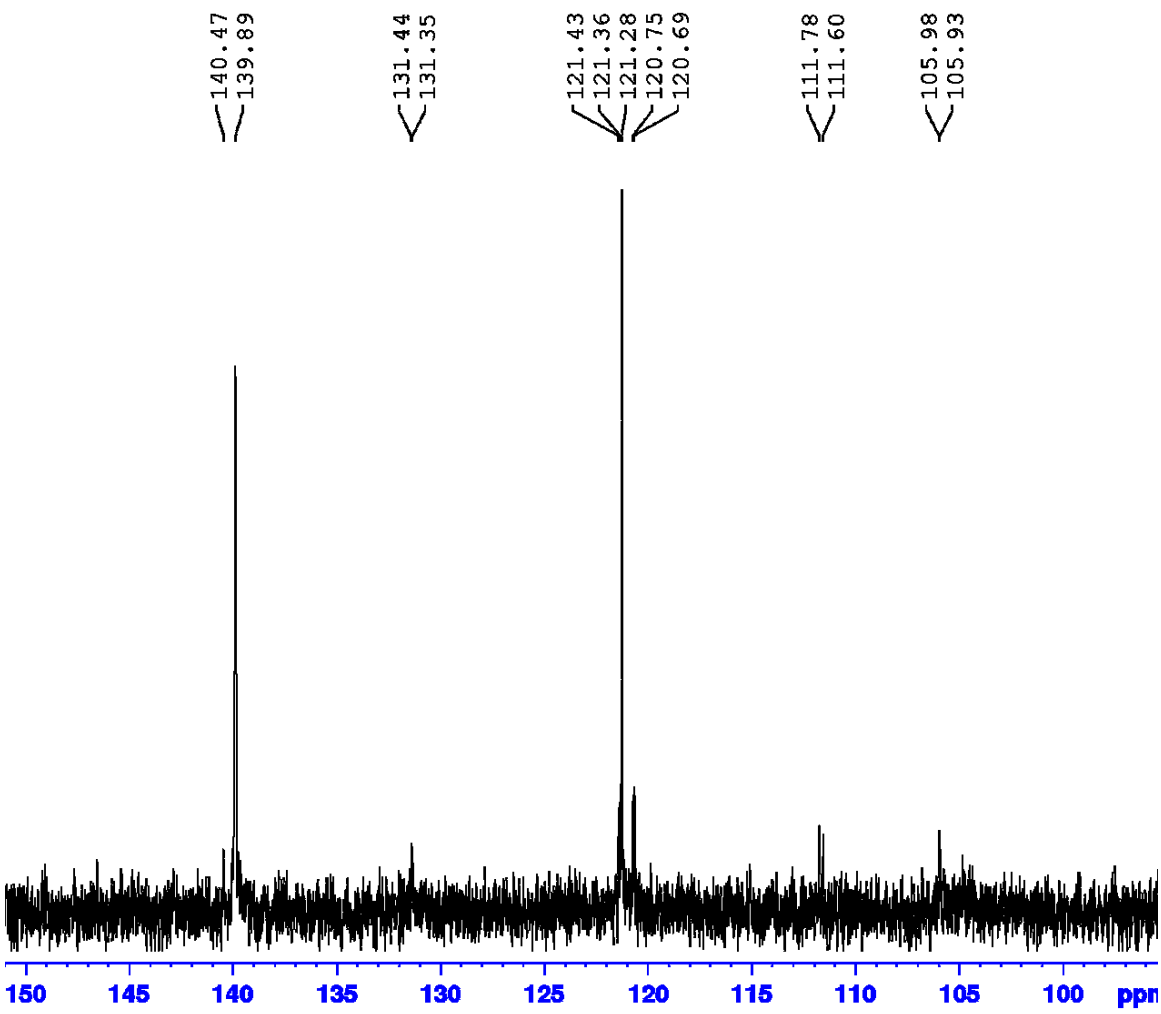

Figure S2-20. $^{31}P\{^{1}H\}$ NMR spectrum of the reaction mixture upon exposure of (PN)Ni to HBPin (33 equiv; 65 ˚C, 6 h, C_6D_{12}, 121.5 MHz).

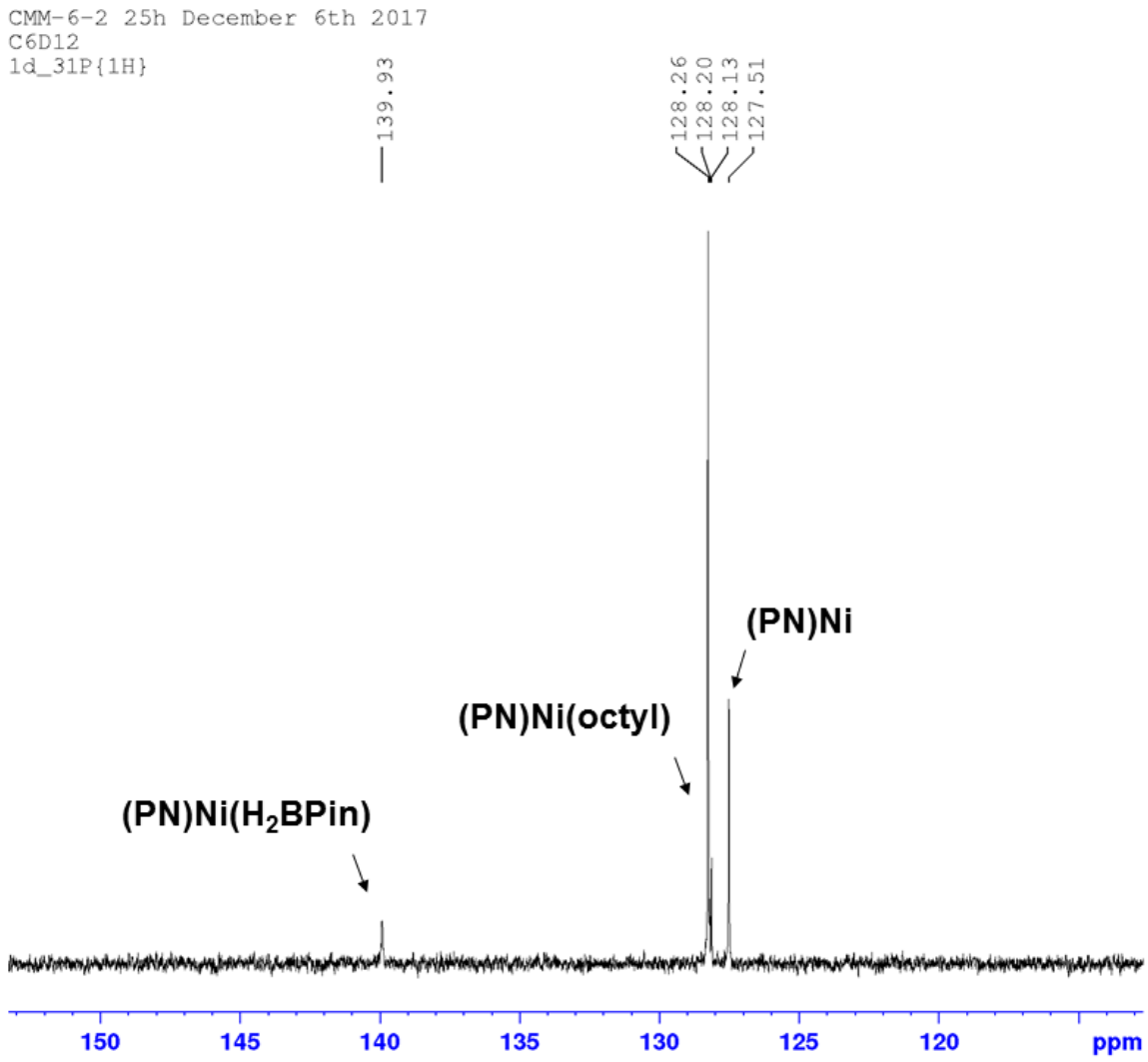

Figure S2-21. $^{31}P\{^{1}H\}$ NMR spectrum of the reaction mixture upon exposure of (PN)Ni to HBPin and 1a (33 equiv each; 25 ˚C, 25 h, C_6D_{12}, 121.5 MHz).

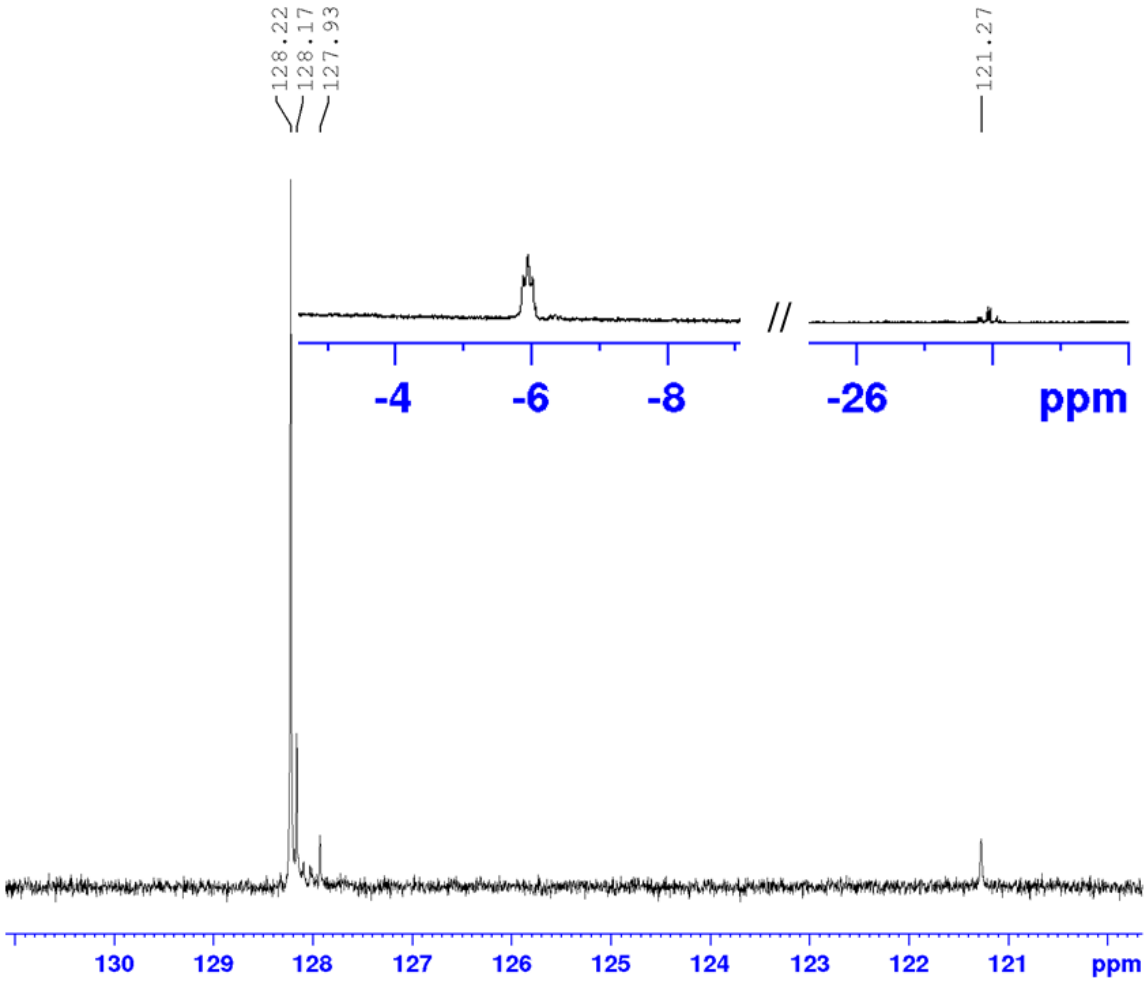

Figure S2-22. $^{31}P\{^{1}H\}$ NMR spectrum of the reaction mixture upon exposure of (PN)Ni to HBPin and 1a (33 equiv each; 65 ˚C, 21 h, C_6D_{12}, 121.5 MHz). Inset: signals observed in the hydride region of the ^{1}H NMR spectrum (C_6D_{12}, 300 MHz) obtained from the reaction mixture.

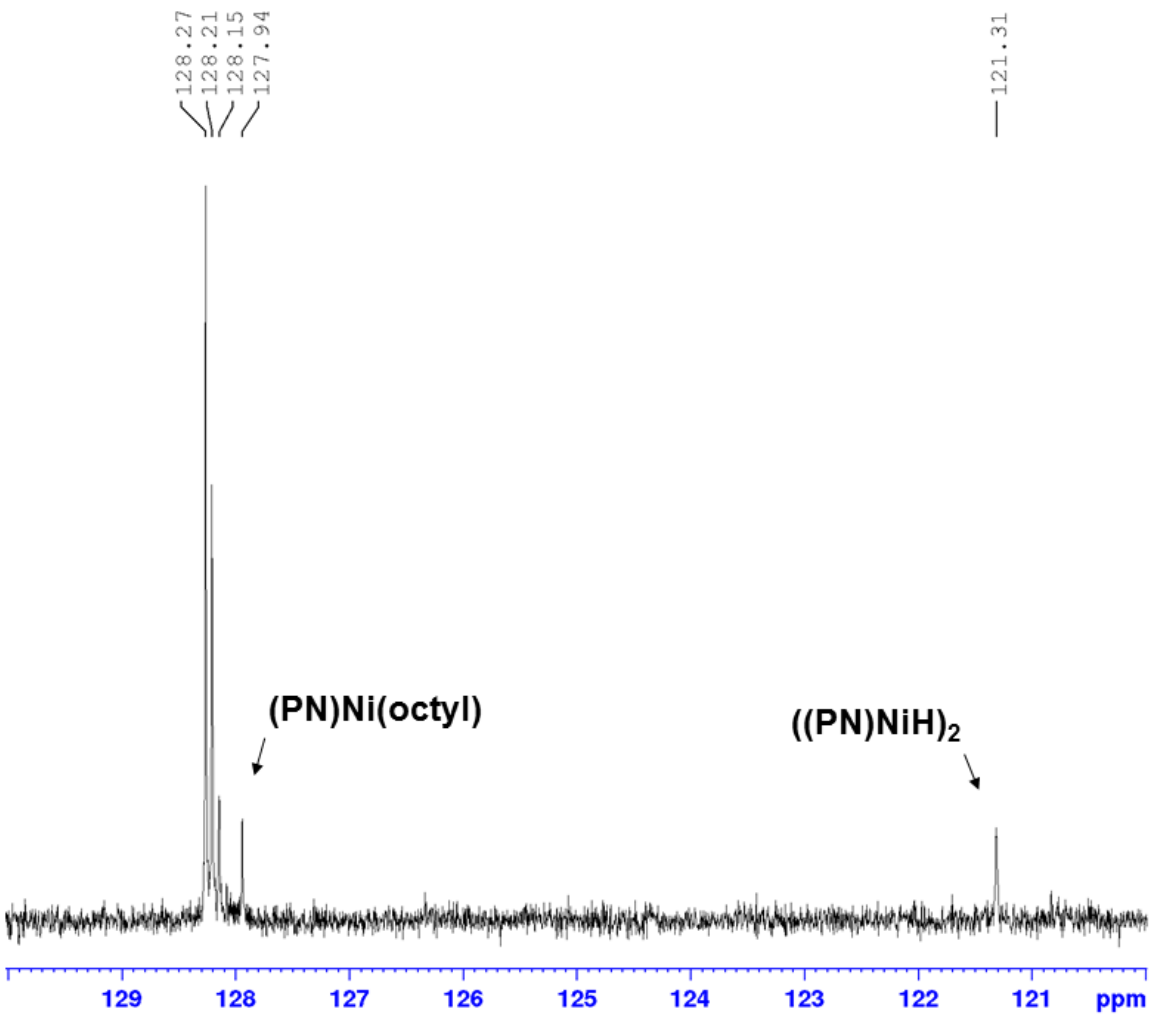

Figure S2-23. $^{31}P\{^{1}H\}$ NMR spectrum (C_6D_{12}, 121.5 MHz) of the reaction mixture upon: initial exposure of (PN)Ni to HBPin and 1a (33 equiv each; 65 ˚C, 21 h), subsequent addition of a fresh charge of HBPin and 1a, and further heating (33 equiv each; 65 ˚C, 24 h). Note that corresponding ^{1}H and ^{11}B NMR spectra indicate the generation of a similar distribution of products as after the initial exposure.

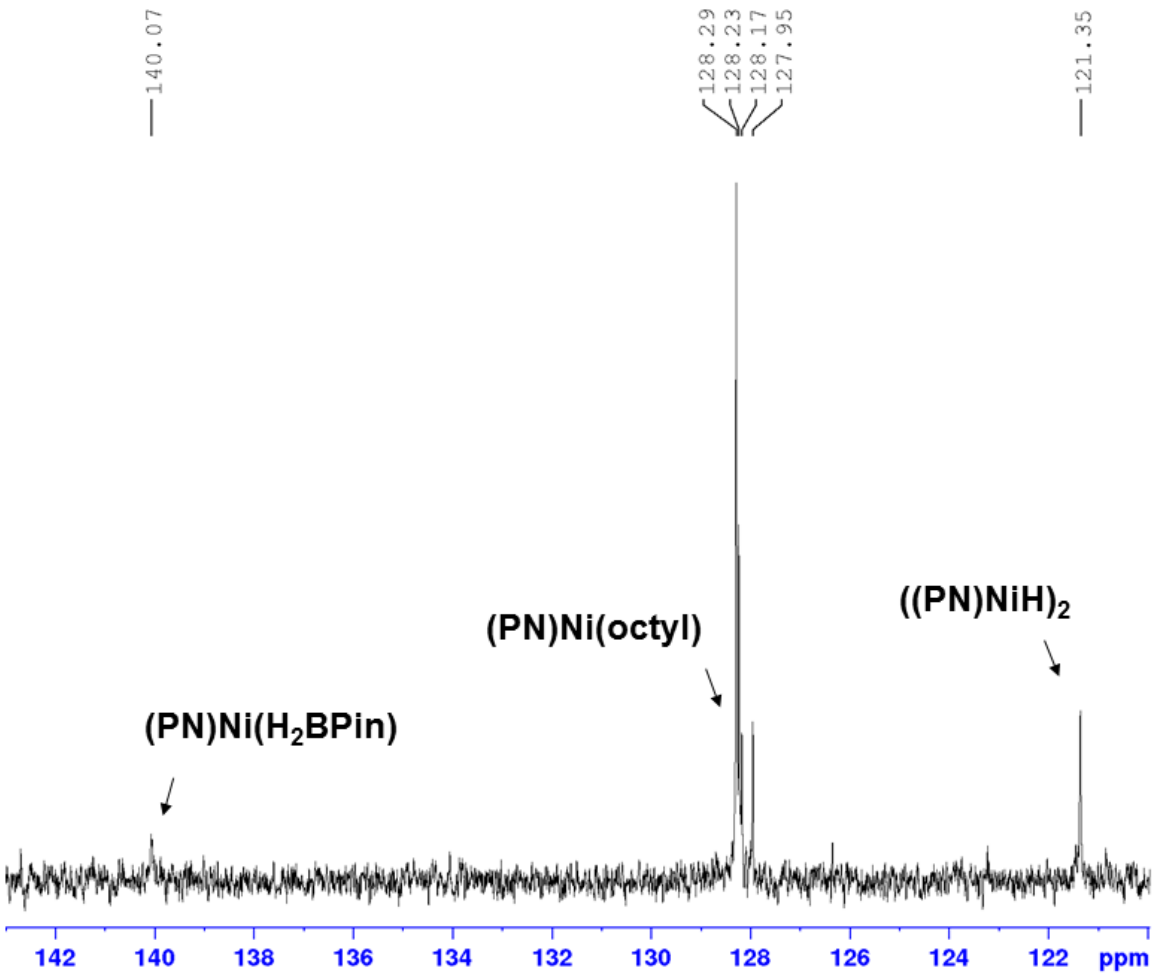

Figure S2-24. $^{31}P\{^{1}H\}$ NMR spectrum (C_6D_{12}, 121.5 MHz) of the reaction mixture upon: initial exposure of (PN)Ni to HBPin and 1a (33 equiv each; 65 ˚C, 21 h), subsequent addition of a fresh charge of HBPin and 1a, further heating (33 equiv each; 65 ˚C, 24 h), subsequent addition of a fresh charge of HBPin, and further heating (33 equiv; 65 ˚C, 1 h).

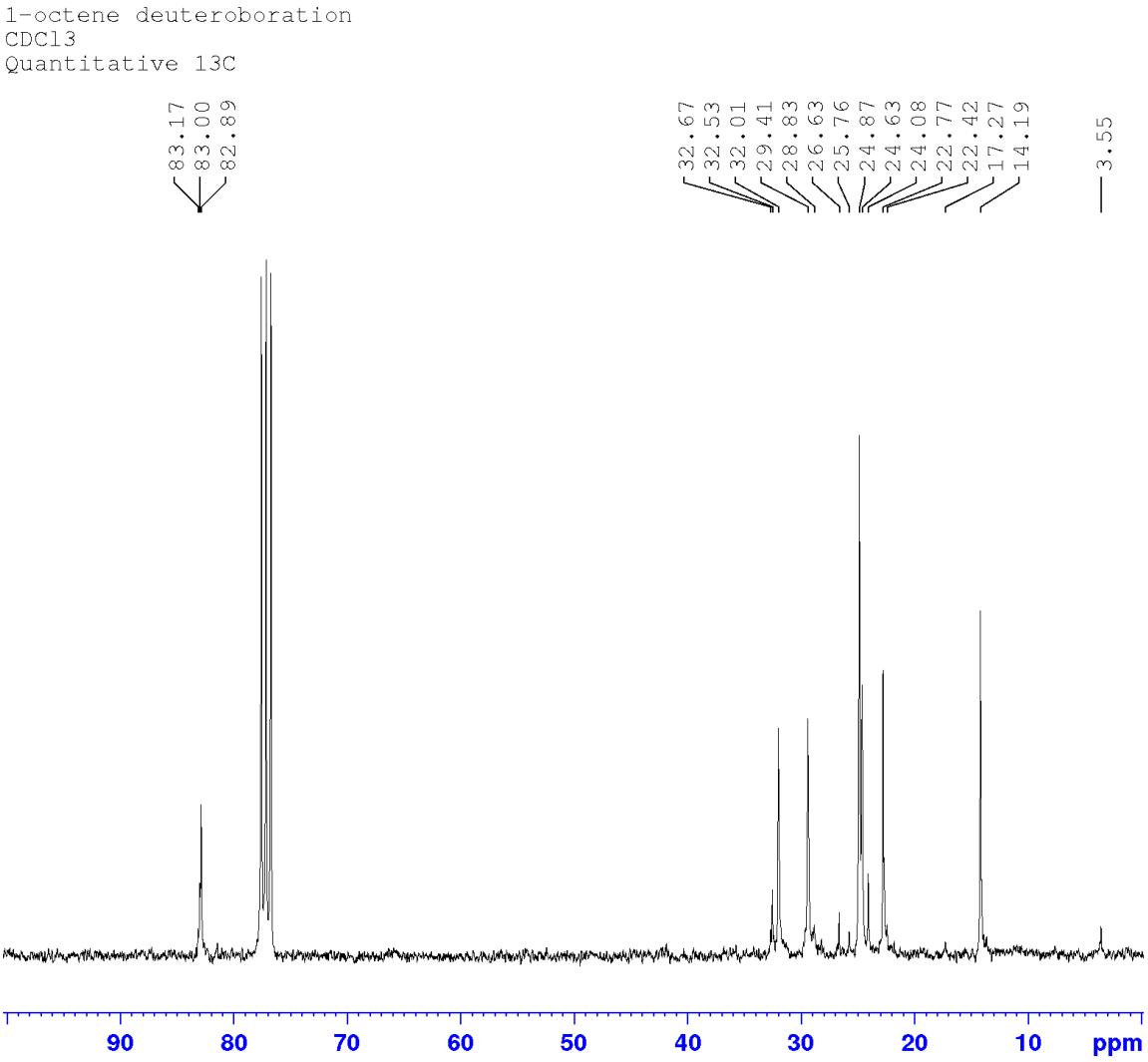

Figure S2-25. Quantitative $^{13}C\{^{1}H\}$ NMR spectrum of the $CDCl_3$ portion of the reaction mixture derived from the I-H of 1a with DBPin employing (PN)Ni (3 mol%) as a precatalyst.

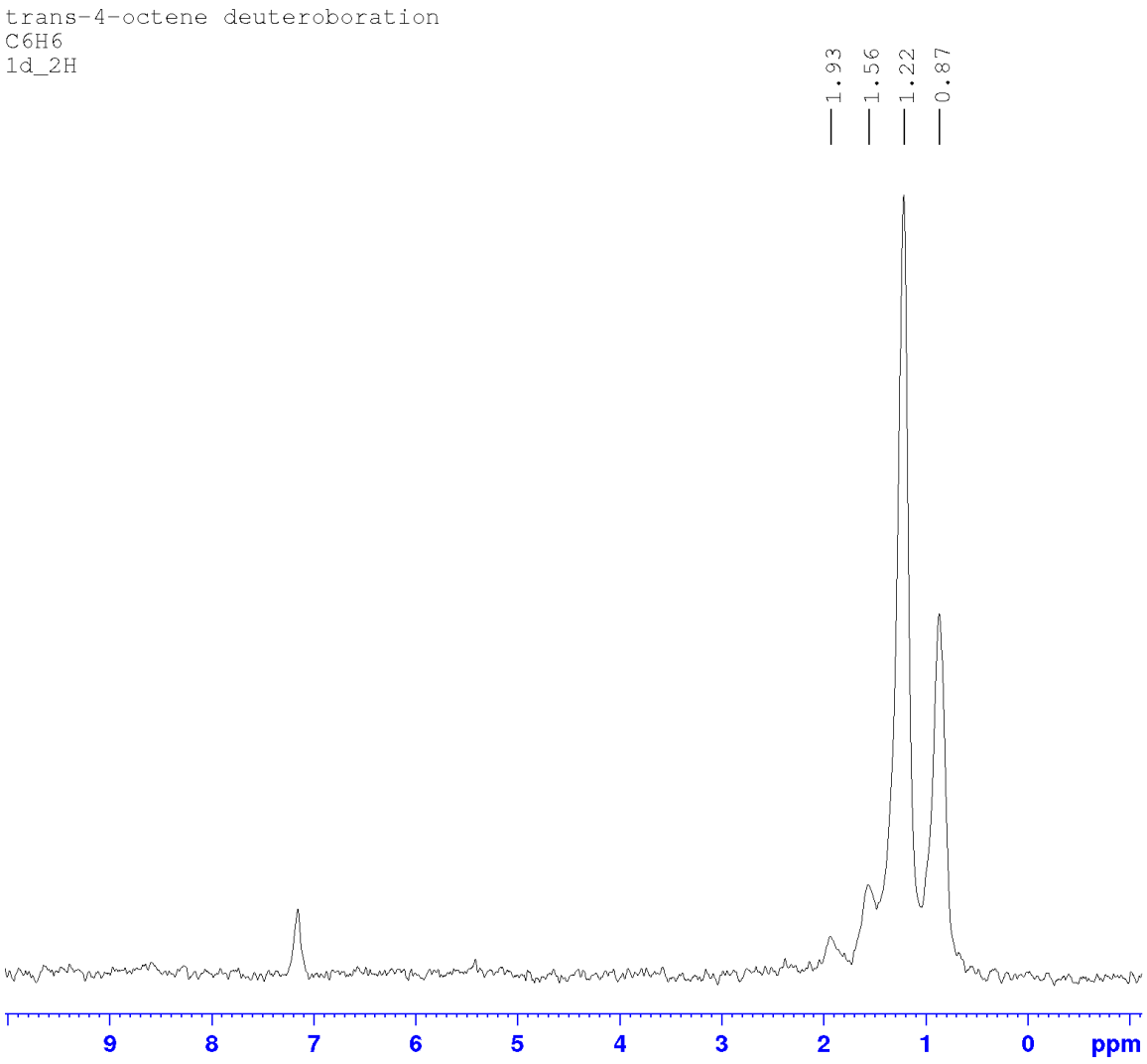

Figure S2-26. ^{2}H NMR spectrum of the C_6H_6 portion of the reaction mixture derived from the I-H of 1c) with DBPin employing (PN)Ni (3 mol%) as a precatalyst.

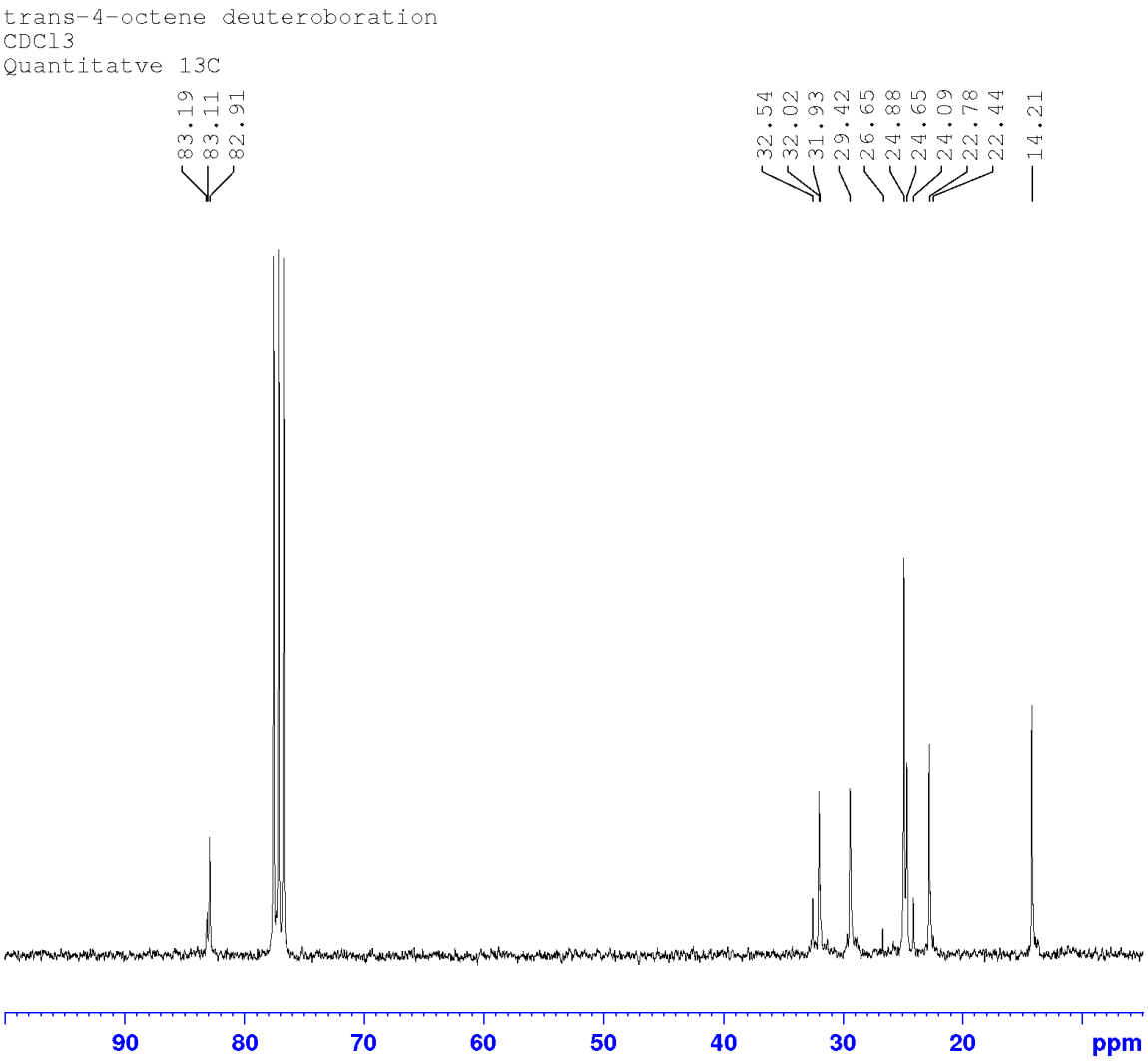

Figure S2-27. Quantitative $^{13}C\{^{1}H\}$ NMR spectrum of the $CDCl_3$ portion (see experimental protocol for details) of the reaction mixture derived from the I-H of 1c with DBPin employing (PN)Ni (3 mol%) as a precatalyst.

CHAPTER 3: A COMPARATIVE ANALYSIS OF HYDROSILATIVE AMIDE REDUCTION CATALYZED BY FIRST-ROW TRANSITION METAL (MN, FE, CO, AND NI) *N*-PHOSPHINOAMIDINATE COMPLEXES

3.1 Introduction

Amines derived from amide reduction[97] have been widely applied in pharmaceutical synthesis,[98] including in the initially reported synthesis of morphine;[99] however, these protocols typically require the use of harsh alkali metal hydrides (e.g., $LiAlH_4$) or related reductants. In this context, the use of more mild hydrosilane reducing agents[100] under the influence of transition metal[101] or other (e.g., boron[102] or zinc[103]) catalysis represents an attractive alternative to more conventional amide reduction protocols. The application of first row transition metal catalysts in the hydrosilative reduction of amides is appealing relative to the use of precious metal catalysts given the comparatively low cost and high natural abundance of the former; however, a relatively small number of such catalysts that are capable of effecting amide reductions of this type have been identified. In 2009, the groups of Beller[104] and Nagashima[105] independently reported the first successful hydrosilative reduction of amides employing first row transition metal catalysis, in which Fe carbonyl precatalysts were employed (6-30 mol% Fe, 100 ˚C, 24 h) in reductions of mostly tertiary amide substrates. This chemistry has been extended to less reactive amides including primary amides.[106] In the aforementioned report from the Beller group,[104] isotopic labeling studies provided evidence in support of the mechanism featured in Scheme 3-1, whereby metal-catalyzed hydrosilation of the amide carbonyl group affords the corresponding *O*-silylated

hemiaminal. Hydride transfer of the derived iminium ion in turn affords the corresponding amine, as well as a siloxane byproduct.

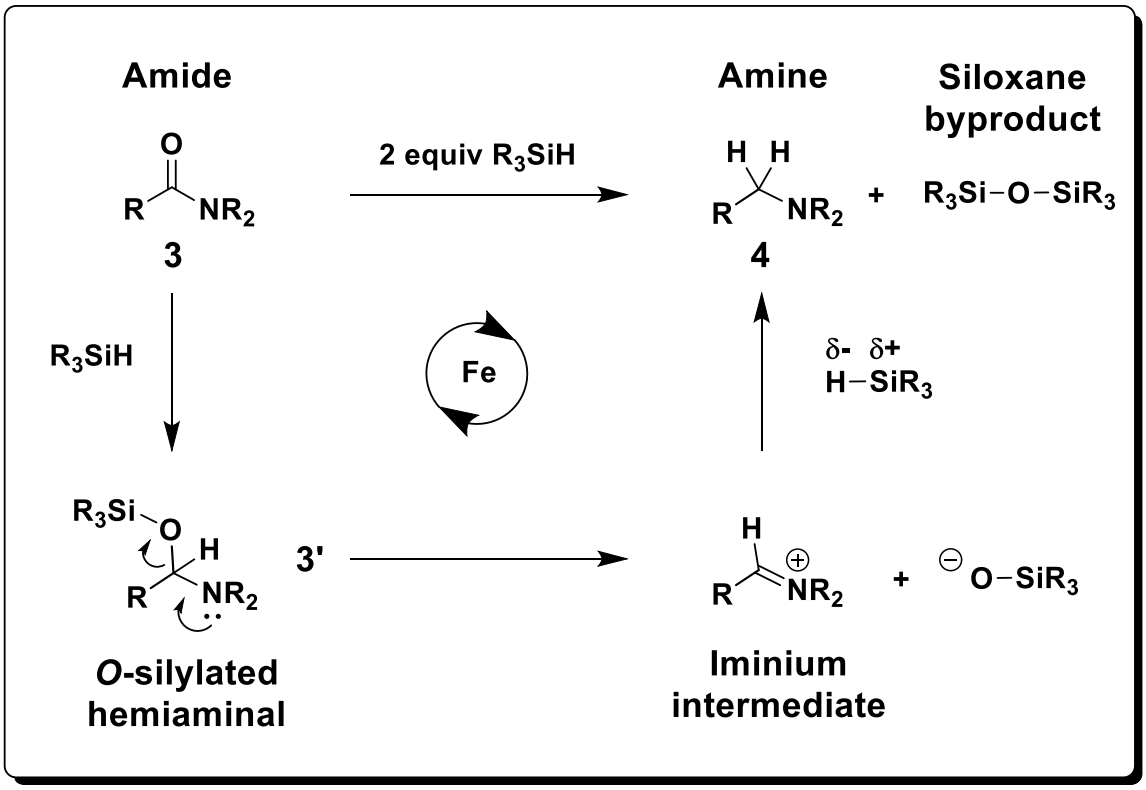

Scheme 3-1. Mechanism for the formation of amines via hydrosilative reduction of amides as proposed by Beller and co-workers.

Subsequent reports by the groups of Sortais and Darcel,[107] Buitrago and Adolfsson,[108] and Driess[109] document the use of NHC-ligated Fe species for such transformations. Prior work involving the Mn-, Co-, or Ni-catalyzed hydrosilative reduction of amides is much more limited. The use of $Co_2(CO)_8$ (1 mol% Co, 100 ˚C, 3-16 h) in such reductions of tertiary amides has been disclosed,[110] and the application of Ni catalysis in hydrosilative amide reductions is limited to a report by Mamillapalli and Sekar[111] regarding the reduction of α-keto amides (5 mol% $Ni(OAc)_2$, 10 mol% TMEDA, 10 mol% KO*t*Bu, 25-60 ˚C, 8-48 h), as well as a report by Garg and co-workers[112] regarding the hydrosilative reduction of amides employing $NiCl_2$dme (10

mol% Ni, 115 ˚C, 24 h). These Ni-based systems effected the hydrosilative reduction of a broad scope of both tertiary and secondary amides with synthetically useful substrate scope. Prior to 2017, only three isolated table entries documenting the Mn-catalyzed hydrosilative reduction of amides existed in the literature, involving the reduction of dimethylformamide or diethylformamide by use of $CpMn(CO)_3$ (5 mol% Mn, 120 ˚C, 24 h),[113] or featuring the use of $Mn_2(CO)_{10}$ for the reduction of *N*-acetylpiperidine (2 mol% Mn, 5 mol% Et_2NH co-catalyst, 100 ˚C, 16 h).[114] In targeting highly effective 3d transition metal catalysts supported by *N*-phosphinoamidinate ligation, the Dalhousie/CPChem team disclosed that three-coordinate **(PN)Mn** is an effective precatalyst for the hydrosilative reduction of various carbonyl compounds by use of $PhSiH_3$ (exclusively), including tertiary (but not primary or secondary) amides under reasonably mild conditions (5 mol% Mn, 75 ˚C, 1 h; 2 mol% Mn, 25 ˚C, 3-48 h).[88]

Encouraged by the useful catalytic profile exhibited by **(PN)Mn**,[88] my thesis research included a study focused on evaluating in a systematic manner the catalytic performance of **(PN)M** (M = Mn, Fe, Co, and Ni) and structurally related *N*-phosphinoamidinate precatalysts, in addition to $\mathbf{M(N(SiMe_3)_2)_n}$ (M = Li, Na, K, Mn, Fe, and Co) precatalysts,[90] in the hydrosilative reduction of selected amide test substrates (**3a** and **3b**). A summary of the research approach is provided in Scheme 3-2.

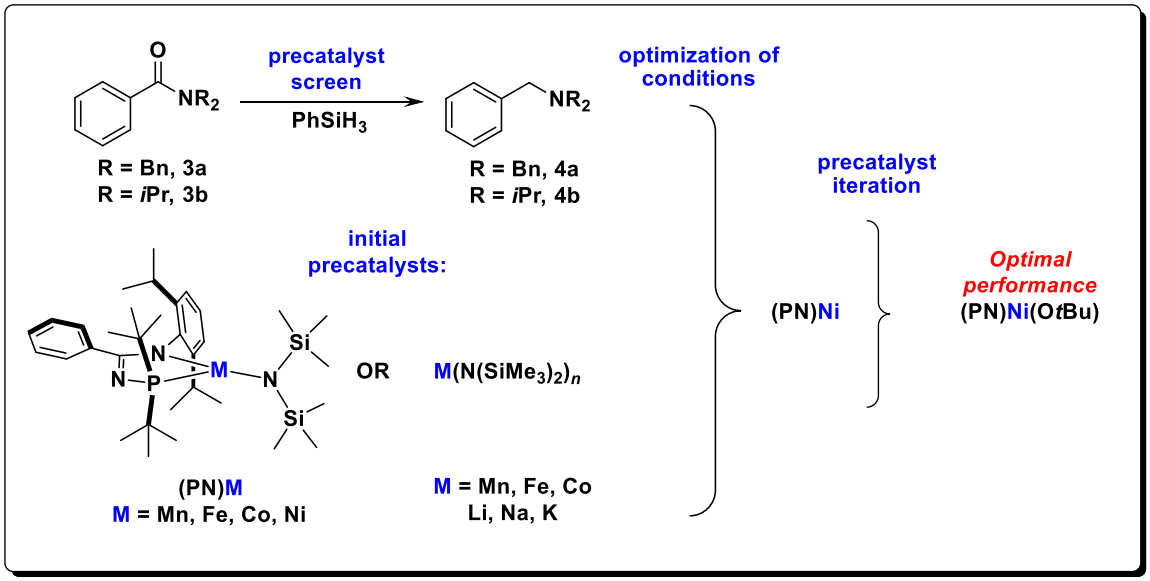

Scheme 3-2. Overview of efforts to develop catalysts for the hydrosilative reduction of amides as described in this chapter.

The results of this investigation are disclosed herein, which confirmed the superiority of 3d transition metals over simple alkali salts in this application, as well as the benefits of *N*-phosphinoamidinate ligation. Notably, the new mononuclear three-coordinate Ni precatalyst **(PN)Ni(O*t*Bu)** proved optimal, enabling both the room temperature reduction of *N*,*N*-diisopropylbenzamide (**3b**) in a manner that had not been achieved previously, and the reduction of selected secondary amide test substrates.

3.2 Results and Discussion

3.2.1 Contributions

Takahiko Ogawa was involved in the initial optimization of conditions for the reduction of compound **3b**. Crystallography was performed by Drs. Michael Ferguson and Robert McDonald at the University of Alberta. Otherwise all work presented in this chapter was carried out by the author.

3.2.2 Initial Catalytic Reactivity Survey

The catalytic reactivity survey was commenced by examination of the reduction of *N*,*N*-dibenzylbenzamide (**3a**) to dibenzylamine (**4a**) with $PhSiH_3$ employing the three-coordinate *N*-phosphinoamidinate precatalysts **(PN)M** (M = Mn, Fe, Co, and Ni) under reasonably mild reaction conditions (2 mol% M, 75 ˚C, 1 h, Table 3-1, Entries 1-4). In all cases, high conversion of the amide was achieved, with the Mn and Ni precatalysts offering optimal catalytic performance in terms of conversion to **4a** (>80%). The observation of $HNBn_2$ as a side-product in these reactions can be viewed as arising from hydrolysis of the putative *O*-silylated hemiaminal intermediate (**3a'**, Scheme 3-2) upon workup prior to calibrated GC analysis. The reduction of **3a** (Scheme 3-3) under conditions outlined in Entry 4 of Table 3-1 employing benzene in place of THF provided support for such a proposal. While complete consumption of **3a** was achieved in benzene after 1 h accompanied by the formation of **4a** (55%) and $HNBn_2$ (**4a'**, 37%), after a total reaction time of 18 h, high conversion to **4a** (88%) and negligible amounts of **4a'** (2%) were observed.

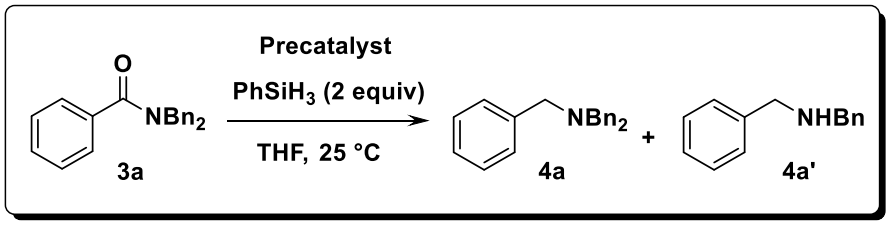

Scheme 3-3. Precatalyst screen for the reduction of 3a to 4a.

Entry	Precatalyst	Loading (%)	Conversion 3a (%)	Yield NBn_3 (4a, %)	Yield $HNBn_2$ (4a', %)
1	**(PN)Mn**	2	>95	84	<5
2	**(PN)Fe**	2	>95	73	10
3	**(PN)Co**	2	>95	61	<5
4	**(PN)Ni**	2	>95	85	<5
5	$Mn(N(SiMe_3)_2)_2$	2	67	63	<5
6	$Fe(N(SiMe_3)_2)_2$	2	39	33	<5
7	$Co(N(SiMe_3)_2)_2$	2	44	43	<5
8	$Li(N(SiMe_3)_2)$	30	84	27	27
9	$Na(N(SiMe_3)_2)$	30	>95	40	32
10	$K(N(SiMe_3)_2)$	30	>95	23	47

Table 3-1. Precatalyst screening for the hydrosilative reduction of 3a (0.2 mmol) with $PhSiH_3$ (0.4 mmol) in THF at 75 ˚C for 1 h. Conversion/yields given based on response-factor calibrated GC data using authentic samples versus dodecane as an internal standard, following workup of the crude reaction mixture.

Under analogous conditions, $M(N(SiMe_3)_2)_2$ precatalysts (M = Mn, Fe, and Co) proved inferior to their respective *N*-phosphinoamidinate counterparts (Table 3-1, Entries 5-7). Moreover, while high conversion of **3a** was achieved by use of alkali metal $M(N(SiMe_3)_2)$ precatalysts at rather high loadings (30 mol% Li, Na, or K, Table 1, Entries 8-10), poor selectivity for **4a** was achieved, due in part to the inefficient conversion of intermediate **3a'** as evidenced by the substantial amounts of **4a'** that were detected in the product mixture following workup. Although not conclusively

demonstrated, these results collectively suggest that transition metal catalysis may be involved in facilitating the conversion of **3a'** to **4a** (Scheme 3-1).

The hydrosilative reduction of *N*,*N*-diisopropylbenzamide (**3b**) to benzyldiisopropylamine (**4b**) was examined subsequently. A survey of the literature reveals **3b** to be a significantly more challenging substrate in this chemistry relative to **3a**, often requiring forcing reaction conditions to achieve suitable levels of conversion.[101] For example, in Beller's pioneering report on the use of $Fe_3(CO)_{12}$ as a precatalyst for the hydrosilative reduction of amides, only 59% yield of **4b** was achieved even after extended reaction times at elevated temperature (30 mol% Fe, 100 ˚C, 24 h).[104] In keeping with this trend, the reduction of **3b** proved difficult versus **3a** for our **(PN)M** precatalysts (2 mol% M, 75 ˚C, 1 h; Scheme 3-4, Table 3-2). Under these reaction conditions, **(PN)Co** and **(PN)Ni** each displayed a promising combination of **3b** consumption and conversion to **4b**. While all members of the $M(N(SiMe_3)_2)_2$ (M = Mn, Fe, and Co) precatalyst series performed poorly under similar conditions, the observed consumption of **3b** when using $M(N(SiMe_3)_2)$ (M = Li, Na, and K, 30 mol% M, 75 ˚C, 1 h), accompanied by the generation of significant amounts of **4b** (e.g., 37%, M = Na; 49%, M = K), further underscores the potential utility of such alkali metal salts in hydrosilative amide reduction chemistry (Table 3-2). Application of **(PN)M** precatalysts employing longer reaction times and higher catalyst loadings (5 mol% M, 18 h, Table 3-2) resulted uniformly in high conversion of **3b**, with Co and Ni each providing optimal (83%) formation of **4b**.

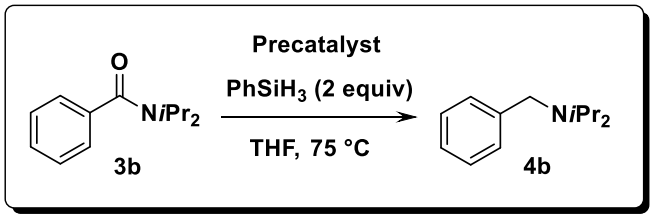

Scheme 3-4. Precatalyst screen for the reduction of 3b to 4b.

		(PN)M			
Time (h)	**Loading (mol% M)**	**Mn**	**Fe**	**Co**	**Ni**
		% Conversion of 3b (% yield 4b)			
1	2[a,b]	>95 (27)	32 (<5)	72 (47)	89 (67)
18	5	>95 (40)	92 (56)	>95 (83)	>95 (83)

Table 3-2. Screening for the hydrosilative reduction of 3b (0.2 mmol) with $PhSiH_3$ (0.4 mmol) in THF at 75 ˚C employing (PN)M precatalysts, yields reported based on calibrated GC data.[a] Use of alkali metal $M(N(SiMe_3)_2)$ precatalysts at higher loading (30 mol%), afforded high conversion of **3b**, but poor selectivity for **4b** (60 (15), M = Li); 83 (37), M = Na; 89 (49), M = K).[b] Using $M(N(SiMe_3)_2)$ precatalysts (M = Mn, Fe, or Co), < 10% conversion of 3b was observed.

3.2.3 Precatalyst Iteration

In evaluating the catalytic screening results featured in Table 3-1 and Table 3-2, only **(PN)Ni** proved capable of effecting the reduction of both **3a** and **3b** to the corresponding tertiary amine (**4a** and **4b**) in >80% yield under the test conditions employed. Building on this observation, I opted to examine alternative **(PN)NiX** precatalysts in such transformations.

I drew upon qualitative observations that **(PN)Ni(NHdipp)** reacted rapidly at ambient temperature with stoichiometric HBPin to form a nickel hydride **(**Scheme 2-9**)**, whereas **(PN)Ni** required large excesses of HBPin and longer reaction times (Scheme 2-10). In addition to comparing the performance of **(PN)Ni** versus **(PN)Ni(NHdipp)**,

related three-coordinate **(PN)Ni(OR)** (R = dmp or *t*Bu) complexes were identified as being potentially interesting targets of inquiry.[42,115] Exposure of **Ni_2Cl_2** to NaO*t*Bu (two equiv) in THF enabled the isolation of **(PN)Ni(O*t*Bu)** upon workup, and treatment of **(PN)Ni(NHdipp)** with 2,6-dimethylphenol (i.e., dmpOH, one equiv) in benzene upon workup afforded **(PN)Ni(Odmp)** (Scheme 3-5).

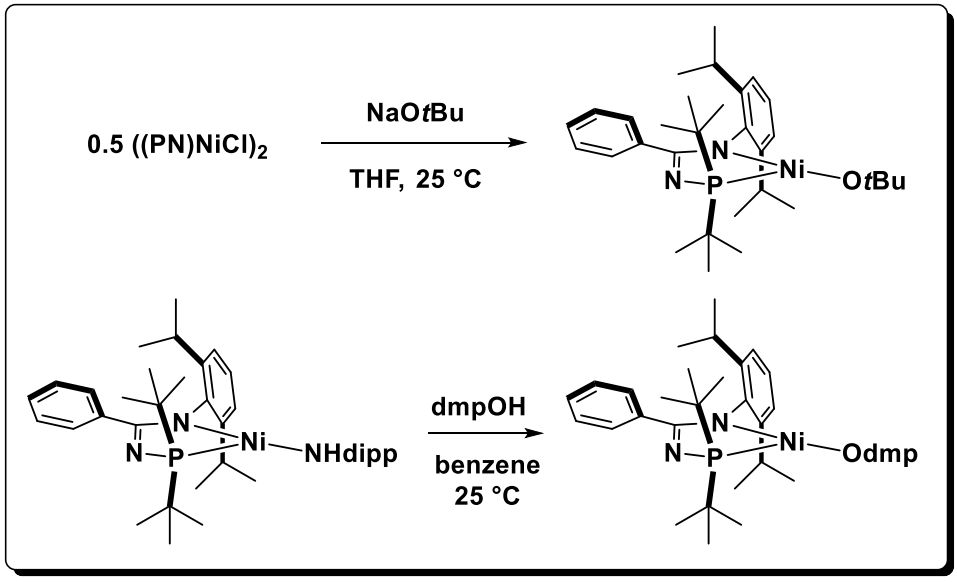

Scheme 3-5. Syntheses of (PN)Ni(O*t*Bu) and (PN)Ni(Odmp).

In each case the targeted **(PN)Ni(OR)** complex was obtained in analytically pure form and was characterized by use of both NMR spectroscopic and single-crystal X-ray crystallographic techniques. In keeping with **(PN)Ni** and **(PN)Ni(NHdipp)**, the newly prepared **(PN)Ni(OR)** species were found to be diamagnetic, exhibiting sharp resonances consistent with the proposed structural formulation (*i.e.*, Figure 3-1 and Figure 3-2).

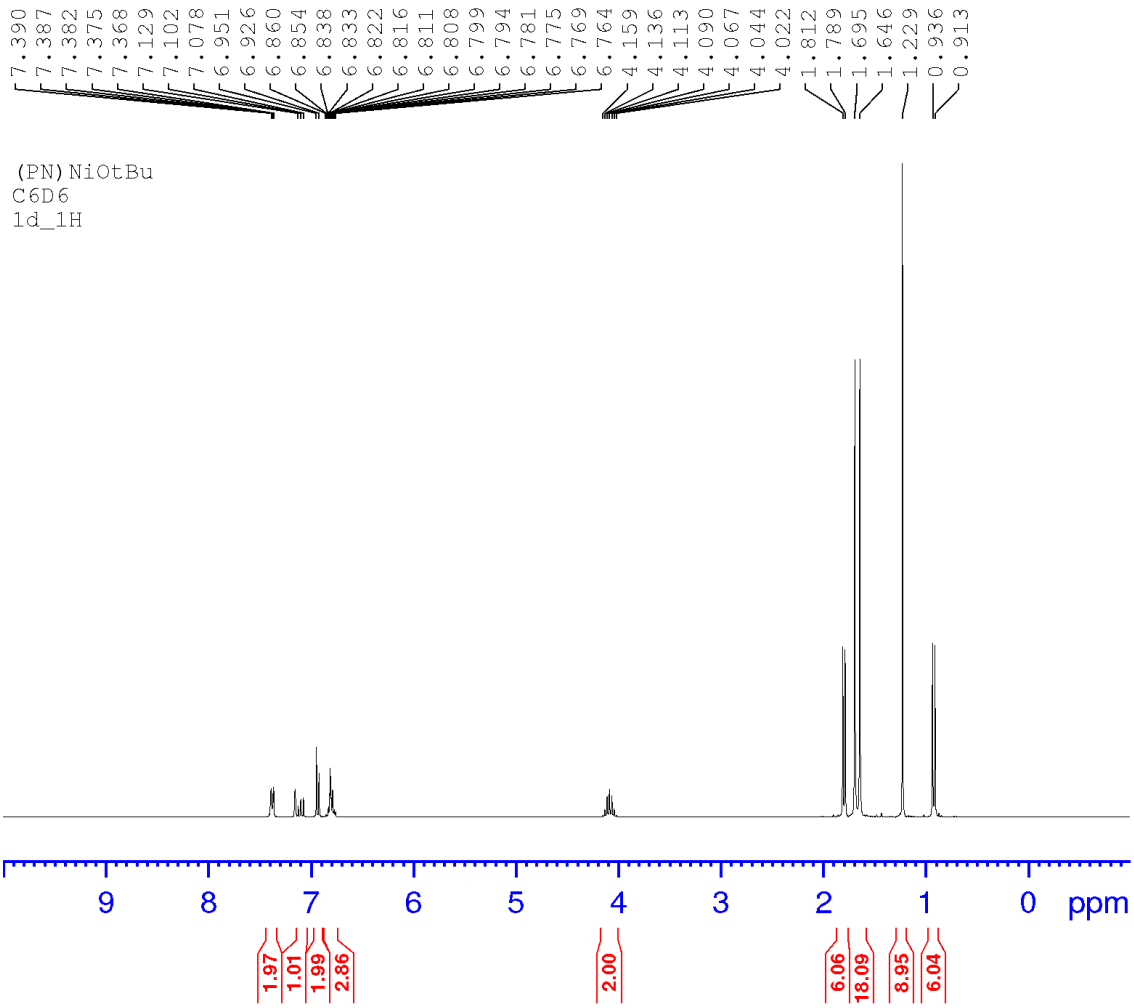

Figure 3-1. ^{1}H NMR Spectrum of (PN)Ni(O*t*Bu) (benzene-d_6, 500.1 MHz).

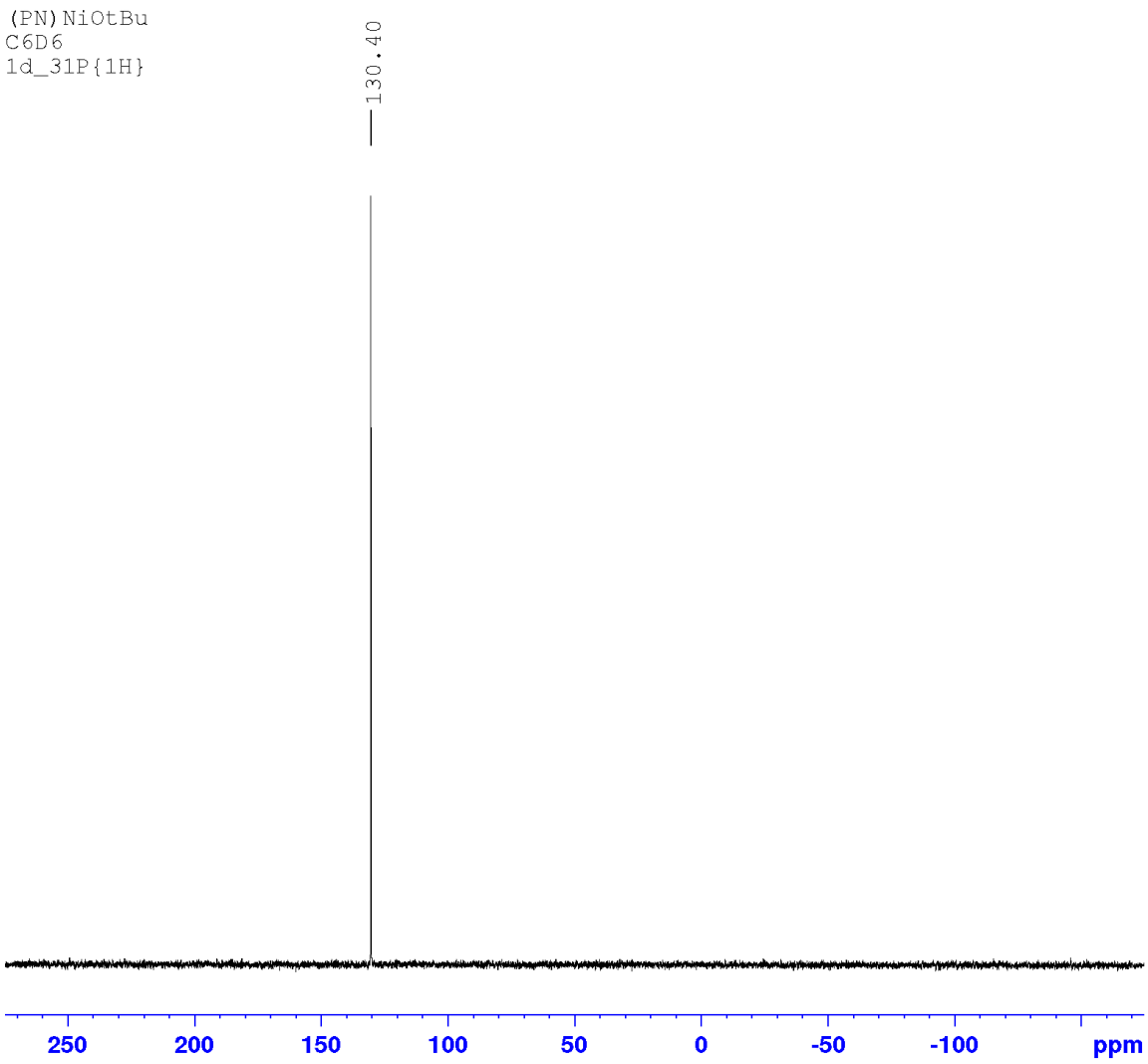

Figure 3-2. $^{31}P\{^{1}H\}$ NMR Spectrum of (PN)Ni(O*t*Bu) (benzene-d_6, 202.5 MHz).

The crystal structures of **(PN)Ni(O*t*Bu)** and **(PN)Ni(Odmp)** are presented in (Figure 3-3). Complex **(PN)Ni(O*t*Bu)** exhibits a highly distorted, three-coordinate T-shaped structure that is qualitatively similar to that of both **(PN)Ni** (Figure 2-4) and **(PN)Ni(NHdipp)** (Figure 2-12), with an empty coordination site located *trans* to phosphorus. Given that crystallographically characterized examples of mononuclear Ni alkoxo complexes (beyond methoxide) are limited to a small collection of four-coordinate (PCP)Ni(OR) species recently reported by Cámpora and co-workers (where R = Et, *n*Bu, *i*Pr, or CH_2CH_2OH),[116] the solid state structural characterization of three-

coordinate **(PN)Ni(O*t*Bu)** warrants discussion. The Ni-O distance in **(PN)Ni(O*t*Bu)** (1.7699(11) Å) is markedly shorter than the Ni-O contacts observed in the aforementioned (PCP)Ni(OR) series (1.84-1.89 Å). While it is tempting to invoke Ni-O π-bonding to account for this observation, the lack of observable hindered rotation phenomena in the ^{1}H NMR spectrum of **(PN)Ni(O*t*Bu)** at 300 K (Figure 3-1) would suggest that such interactions are not significant.

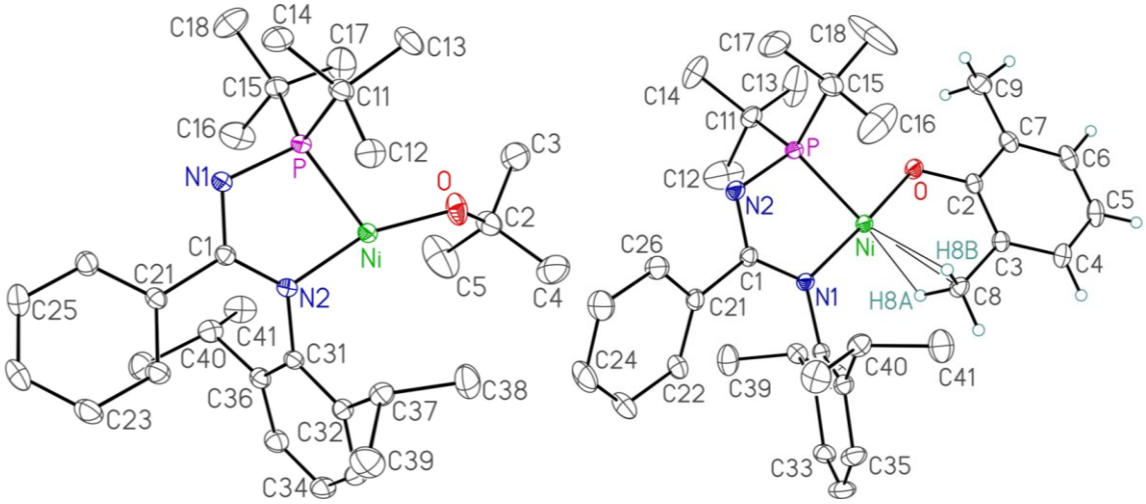

Figure 3-3. Crystallographically determined structures of (PN)Ni(O*t*Bu) and (PN)Ni(Odmp). Selected interatomic distances (Å) and angles (˚) for **(PN)Ni(O*t*Bu)**: Ni-P 2.1092(4), Ni-N 1.8589(11), Ni-O 1.7699(11), P-Ni-N 82.97(4), P-Ni-O 114.11(4), N-Ni-O 160.71(6). Selected interatomic distances (Å) and angles (˚) for **(PN)Ni(Odmp)**: Ni-P 2.1273(4), Ni-N 1.8859(12), Ni-O 1.8397(11), Ni···C8 2.3585(16), Ni···H8A 2.023(17), Ni···H8B 2.061(17), P-Ni-N 83.64(4), P-Ni-O 94.65(4), N-Ni-O 175.61(5), P-Ni-C8 162.00(5).

Whereas **(PN)Ni(O*t*Bu)** is apparently a *bona fide* three-coordinate complex that is devoid of additional coordinative interactions, **(PN)Ni(Odmp)** is best described as adopting a distorted square-planar geometry, whereby agostic interaction(s) involving a methyl group on the aryloxo ligand occur at the position *trans* to phosphorus. Such agostic interactions apparently do not result in a chemically significant difference in the Ni-P distance in **(PN)Ni(Odmp)** (2.1273(4) Å) versus **(PN)Ni(O*t*Bu)** (2.1092(4) Å). The

Ni-O distance observed in **(PN)Ni(Odmp)** (1.8397(11) Å), while significantly longer than that found in **(PN)Ni(O*t*Bu)** (1.7699(11) Å), is distinctly shorter than related Ni-O contacts found in some other crystallographically characterized square planar Ni(aryloxo) complexes (1.90-1.92 Å).[117]

3.2.4 Progress Towards Milder Catalytic Conditions

Given that all reported examples of the hydrosilative reduction of **3b** by use of 3d transition metal catalysis feature elevated reaction temperatures (≥ 100 ˚C), I sought to establish whether our **(PN)NiX** precatalysts could enable room temperature reactivity (5 mol% Ni, 25 ˚C, 18 h; Scheme 3-6, left). Except for **(PN)Ni**, each of the Ni precatalysts examined herein afforded ≥ 95% conversion of **3b**, with **(PN)Ni(O*t*Bu)** providing the highest conversion to **4b** (84%), followed closely by **(PN)Ni(Odmp)** (80%). In modifying our original conditions (Scheme 3-6, right) only such that the total volume of added liquids/solution was 250 µL rather than 500 µL, >95 % conversion of **3b** and 90% formation of **4b** was achieved.

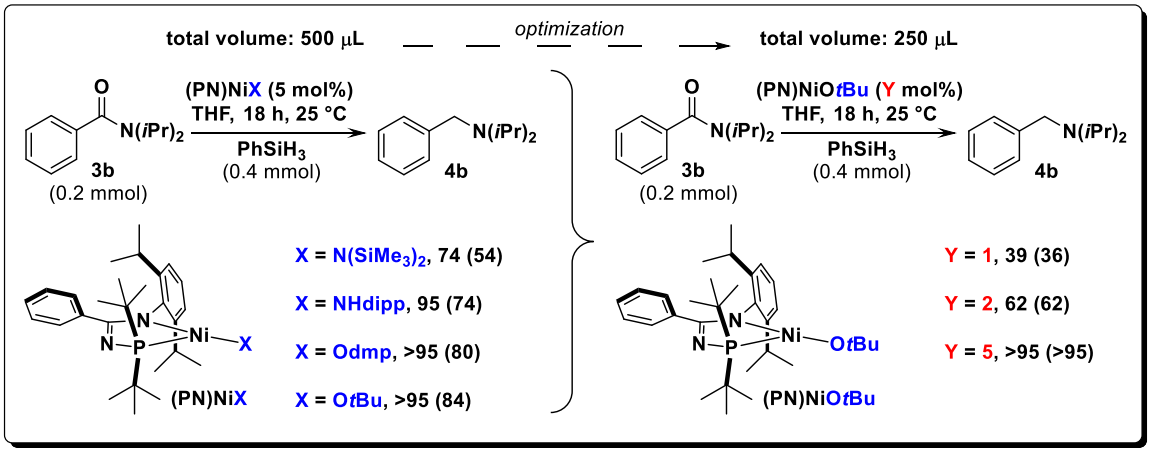

Scheme 3-6. Optimization of the room temperature reduction of *N*,*N*-diisopropylbenzamide (3b) employing (PN)NiX precatalysts, reported as % consumption 3b (% conversion to 4b) based on calibrated GC data.

In monitoring the progress of the reaction employing **(PN)Ni(O*t*Bu)**, 46% conversion of **3b** and 37% formation of **4b** was noted after only 30 mins, and 84% conversion of **3b** and 79% formation of **4b** was noted after 8 h, suggesting that an 18 h reaction time is not required in order to achieve high conversions with this particular precatalyst. By comparison, <10% and 31% conversion of **3b** was achieved after 2 h and 8 h, respectively, when using **(PN)Ni** as a precatalyst under similar conditions (outlined in experimental). Presuming that each of the **(PN)NiX** precatalysts afford a common catalytic intermediate such as **(PN)NiH** upon reaction with silane, the differing performance of **(PN)Ni(O*t*Bu)** and **(PN)Ni** can be attributed in part to the more efficient activation of the former. This assertion is qualitatively consistent with stoichiometric experiments involving treatment of these precatalysts with $PhSiH_3$ (40 equiv, benzene-d_6, 25 ˚C) in the absence of amide substrate. Under such conditions, **(PN)Ni(O*t*Bu)** was completely consumed upon mixing (^{1}H and ^{31}P NMR), and after 4 h afforded a mixture of **Ni_2H_2** and an unknown phosphorus-containing species (δ ^{31}P = 104 ppm) in *ca*. 2.7:1 ratio. By comparison, no reaction was observed between the silane and **(PN)Ni** under similar conditions after 20 minutes; after 4 h, a mixture of the aforementioned unknown phosphorus-containing species (δ ^{31}P = 104 ppm) and **Ni_2H_2**, along with detectable amounts of Ph_2SiH_2, were observed spectroscopically.

Having identified **(PN)Ni(O*t*Bu)** as an effective precatalyst for the hydrosilative reduction of the somewhat challenging tertiary amide **3b**, I attempted related test transformations involving selected secondary amides (Scheme 3-7). Each of *N*-benzylbenzamide and caprolactam were successfully reduced, under more mild conditions than those reported by Garg and co-workers[112] employing $NiCl_2$dme as a

precatalyst (10 mol% Ni, 115 ˚C, 24 h). Despite this success, **(PN)Ni(O*t*Bu)** did not prove to be a useful precatalyst for the reduction of either benzamide or pivalamide under a variety of reaction conditions; such reactions resulted in high conversion of the starting materials accompanied by the formation of complex mixtures.

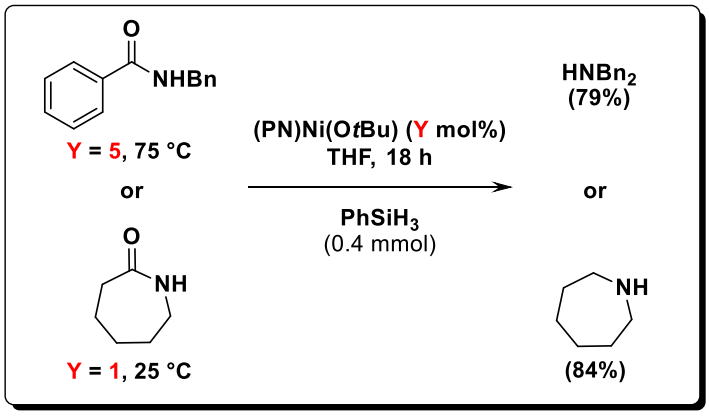

Scheme 3-7. Reduction of selected secondary amides employing precatalyst (PN)Ni(O*t*Bu) (0.2 mmol of amide; total volume of liquids = 250 µL).

3.3 Chapter Summary

In comparing the performance of **(PN)M** (M = Mn, Fe, Co, and Ni) precatalysts supported by *N*-phosphinoamidinate ligation, as well as $M(N(SiMe_3)_2)_n$ (M = Li, Na, K, Mn, Fe, and Co) precatalysts, in the hydrosilative reduction of selected tertiary amide test substrates using $PhSiH_3$, only **(PN)Ni** proved effective in the reduction of both *N*,*N*-dibenzylbenzamide (**3a**) and *N*,*N*-diisopropylbenzamide (**3b**). The utility of this Ni precatalyst in such reactions prompted iteration toward other **(PN)NiX** precatalysts, which included the new crystallographically characterized complexes **(PN)Ni(OR)** (R = 2,6-dimethylphenyl or *t*Bu). Whereas in the solid state **(PN)Ni(O*t*Bu)** exhibits a three-coordinate structure that is devoid of additional coordinative interactions, **(PN)Ni(Odmp)** was found to adopt a distorted square-planar geometry featuring agostic interaction(s) involving a methyl group on the aryloxo ligand. The three-coordinate **(PN)Ni(O*t*Bu)**

complex proved to be particularly effective in such amide reduction chemistry; further optimization allowed for unusually mild transformations, including those at room temperature involving *N*,*N*-diisopropylbenzamide and caprolactam. Directions for further inquiry based on these results are outlined in Chapter 5.

3.4 Experimental

3.4.1 General Experimental Considerations

Unless otherwise indicated, all experimental procedures were conducted in a nitrogen-filled, inert-atmosphere glovebox using oven-dried glassware and purified solvents. The following solvent purification methods were used: benzene, toluene, and pentane were deoxygenated by sparging with nitrogen gas followed by passage through a double column solvent purification system packed with alumina and copper-Q5 reactant and storage over activated 4 Å molecular sieves; tetrahydrofuran was dried over Na/benzophenone followed by distillation under an atmosphere of nitrogen gas. Solvents were stored over activated 4 Å molecular sieves. Phenylsilane and benzene-d_6 were degassed via three freeze-pump-thaw cycles and stored over 4 Å molecular sieves. *N,N*-dibenzylbenzamide and *N,N*-diisopropylbenzamide were prepared as described previously,[88] and the latter was further purified by recrystallization from THF at -35 °C. **(PN)M** (M = Mn,[88] Fe,[69] Co,[69] and Ni[89]), **((PN)NiCl)$_2$**,[89] **(PN)Ni(NHdipp)**,[89] and **M(N(SiMe$_3$)$_2$)$_2$** (M = Mn, Fe, and Co)[118] were prepared according to literature procedures. All other reagents were purchased from commercial suppliers and were used without further purification. Unless otherwise stated, ^{1}H, ^{13}C, and ^{31}P NMR characterization data were collected at 300 K on a Bruker AV-500 spectrometer operating at 500.1, 125.7, and 202.5 MHz (respectively) with chemical shifts reported in parts per

million downfield of $SiMe_4$ for ^1H and ^{13}C, and 85% H_3PO_4 in D_2O for ^{31}P. ^1H and ^{13}C NMR chemical shift assignments are based on data obtained from ^{13}C-DEPTQ135, ^1H-^1H COSY, ^1H- ^{13}C HSQC, and ^1H- ^{13}C HMBC NMR experiments. Gas chromatography (GC) data were obtained on a Shimadzu instrument equipped with an SGE BP-5 column (30 m, 0.25 mm i.d.), whereby response-factor calibration was carried out using authentic samples relative to an internal standard. HPLC-MS data were collected on an Agilent LC-MSD system. The column used was Agilent Poroshell 120 EC-C-18 (3 X 150 mm, 2.7 μm) and the flow rate was 2 mL/min. For the gradient, solvent A was H_2O with 0.1% formic acid, solvent B was acetonitrile with 0.1% formic acid. Gradient started with 90% solvent A (10% solvent B) and in 15 minutes finished with 100% solvent B. The mass spectrometer scanned from 100 – 1000 m/z in positive ESI mode. Crystallographic data were obtained at or below 193(2) K on a Bruker PLATFORM/APEX II diffractometer equipped with a CCD area detector, employing samples that were mounted in inert oil and transferred to a cold gas stream on the diffractometer. Unit cell parameters were determined and refined on all reflections. Data reduction, correction for Lorentz polarization, and absorption correction were each performed. Structure solution and least-squares refinement on F^2 were used throughout. All non-hydrogen atoms were refined with anisotropic displacement parameters. Full crystallographic solution and refinement details are provided in the deposited CIFs (CCDC 1856638 and 1856639).

3.4.2 Specific Experimental Considerations

Synthesis of (PN)Ni(Odmp). A glass vial equipped with a magnetic stir bar was charged with a solution of **(PN)Ni(NHdipp)** (0.200 g, 0.30 mmol) in benzene (*ca.* 5 mL). Stirring was initiated, and a solution of 2,6-dimethylphenol (0.037 g, 0.30 mmol) in

benzene (*ca.* 2 mL) was added to the stirring solution, which was stirred at room temperature for 18 h. The volatile components of the reaction mixture were then removed *in vacuo*. The remaining residue was first triturated with pentane (3 × *ca.* 1 mL), then washed with cold pentane (3 × *ca.* 0.5 mL, -35 °C) to remove residual 2,6-diisopropylaniline. The remaining residue was dissolved in Et_2O (*ca.* 8 mL) and filtered through Celite to remove any insoluble side-products. Solvent removal *in vacuo* from the collected eluent, followed by fractional recrystallization in two crops of the crude material from a concentrated Et_2O/pentane (1:1) solution at -35 °C afforded **(PN)Ni(Odmp)** (0.082 g, 45%) as dark orange crystals. Anal. Calcd. For $C_{35}H_{49}N_2NiOP$: C, 69.66; H, 8.18; N, 4.64. Found: C, 69.71; H, 7.92; N, 4.73. ^{1}H NMR (500.1 MHz, benzene-d_6): δ 7.34 (m, 2 H, H_{arom}), 7.08 (m, 1 H, H_{arom}), 6.91 – 6.88 (4 H, H_{arom}), 6.83 – 6.75 (3 H, H_{arom}), 6.57 (apparent t, 1 H, $^3J_{HH}$ = 7 Hz, H_{arom}), 4.11 (apparent septet, 2 H, $^3J_{HH}$ = 7 Hz, C*H*Me$_2$), 2.30 (s, 3 H, OCC*Me*), 2.29 (s, 3 H, OCC*Me*), 1.69 (d, 18 H, $^3J_{PH}$ = 15 Hz, P*tBu*$_2$), 1.49 (d, 6 H, $^3J_{HH}$ = 7 Hz, CH*Me*$_2$), 0.82 (d, 6 H, $^3J_{HH}$ = 7 Hz, CH*Me*$_2$). ^{13}C{^{1}H} NMR (125.7 MHz, benzene-d_6): δ 175.7 (N*C*N), 165.6 (C_{arom}), 145.1 (C_{arom}), 134.4 (C_{arom}), 130.8 (*C*H$_{arom}$), 129.3 (*C*H$_{arom}$), 127.9 (*C*H$_{arom}$), 127.5 (*C*H$_{arom}$), 126.9 (*C*H$_{arom}$), 124.8 (*C*H$_{arom}$), 124.0 (C_{arom}), 115.1 (*C*H$_{arom}$), 39.8 (d, $^1J_{CP}$ = 23 Hz, P*C*Me$_3$), 29.0 (*C*HMe$_2$), 28.1 (d, $^3J_{CP}$ = 2 Hz, PC*Me*$_3$), 24.8 (CH*Me*$_2$), 23.7 (CH*Me*$_2$), 18.7 (OCC*Me*$_2$), 18.6 (OCC*Me*$_2$). ^{31}P{^{1}H} NMR (202.5 MHz, benzene-d_6): δ 121.2. Crystals of **(PN)Ni(Odmp)** suitable for X-ray diffraction were grown from a concentrated pentane solution at -35 °C.

Synthesis of (PN)Ni(O*t*Bu). A glass vial equipped with a magnetic stir bar was charged with NaO*t*Bu (0.059 g, 0.61 mmol). **Ni$_2$Cl$_2$** (0.300 g, 0.29 mmol) was added to the vial as

a solution in THF (*ca*. 5 mL). The reaction mixture was stirred at room temperature for 18 h, after which a color change from dark red-purple to dark green/brown was observed. Following removal of solvent *in vacuo*, the remaining dark green residue was extracted into pentane (*ca.* 10 mL) and filtered through a Celite pad in a glass-fritted filter funnel. Solvent was removed *in vacuo* from the collected eluent, to obtain a dark green powder (0.288 g, 89% crude yield). This material was recrystallized from a concentrated solution of pentane at -35 °C to obtain dark green crystals (0.160 g, 50%). Anal. Calcd. for $C_{31}H_{49}N_2NiOP$: C, 67.04; H, 8:89; N, 5.04. Found: C, 66.89; H, 8.71; N, 4.86. ^{1}H NMR (500.1 MHz, benzene-d_6): δ 7.40 – 7.37 (m, 2 H, H_{arom}), 7.13 – 7.08 (m, 1 H, H_{arom}), 6.95 – 6.93 (m, 2 H, H_{arom}), 6.86 – 6.76 (overlapping resonances, 3 H, H_{arom}), 4.16 – 4.02 (app septet, 2 H, $^3J_{HH}$ = 7 Hz, C*H*Me$_2$), 1.80 (d, 6 H, $^3J_{HH}$ = 7 Hz, CH*Me*$_2$), 1.67 (d, 18 H, $^3J_{PH}$ = 15 Hz, P*tBu*$_2$), 1.23 (s, 9 H, O*tBu*), 0.92 (d, 6 H, $^3J_{HH}$ = 7 Hz, CH*Me*$_2$). ^{13}C{^{1}H} NMR (125.7 MHz, benzene-d_6): δ 175.2 (N*C*N), 146.2 (C_{arom}), 140.7 (C_{arom}), 134.1 (C_{arom}), 130.5 (CH$_{arom}$), 129.2 (CH$_{arom}$), 127.5 (CH$_{arom}$), 126.9 (CH$_{arom}$), 124.6 (CH$_{arom}$), 70.1 (O*C*Me$_3$), 38.1 (d, $^1J_{PC}$ = 27 Hz, P*C*Me$_3$), 35.1 (OC*Me*$_3$), 29.0 (*C*HMe$_2$), 28.1 (d, $^2J_{PC}$ = 2 Hz, PC*Me*$_3$), 25.2 (CH*Me*$_2$), 23.1 (CH*Me*$_2$). ^{31}P{^{1}H} NMR (202.5 MHz, benzene-d_6): δ 130.4. Crystals suitable for X-ray diffraction were grown from a concentrated solution of pentane at -35 °C.

General catalytic procedure. A glass vial was charged with reaction components in the following order: amide (**3a** or **3b**, 0.2 mmol), solvent (as needed such that the total volume of added liquids/solutions was 500 μL, unless otherwise stated), precatalyst (as a stock solution), and phenylsilane (0.4 mmol). For the reduction of *N*-benzylbenzamide or caprolactam, the reaction components were added in the following order: amide, solvent,

phenylsilane, then precatalyst, with a total volume of 250 μL. Liquids/solutions were dispensed by micropipette. The vial was then sealed with a cap featuring a PTFE septum. For reactions requiring temperatures above 25 °C, the cap/vial contact was further sealed externally by wrapping with PTFE tape and electrical tape, and then taken out of the glovebox and heated in an aluminum heating block set to the desired temperature. In some cases, vigorous bubbling of the reaction mixture was observed. Upon completion, the reaction vial was opened in air, dodecane was added as an internal standard for GC analysis, and benchtop Et_2O or THF (*ca*. 1 mL in either case) was added. The mixture was then filtered through a short plug of silica. The filtrate was then sampled (*ca.* 100 μL), transferred to a vial suited for use on a GC autosampler (GC vial), diluted further (*ca*. 1 mL), and analyzed by GC. Conversions of amide starting material and yield of products were determined via response-factor calibration employing authentic samples versus a dodecane internal standard. For the reduction of **3a**, reaction product identification, following workup, was confirmed independently by use of HPLC-MS techniques.

Procedure for time trial of (PN)Ni(O*t*Bu) and (PN)Ni precatalysts.

In the glovebox, a glass vial was charged with a magnetic stir bar, **3b** (1.0 mmol), precatalyst (0.05 mmol), dodecane, and THF (total reaction volume: 2500 μL). Stirring was initiated, and phenylsilane (2.0 mmol) was added to the stirring solution as a single aliquot, and the vial was sealed with a Teflon screw cap. In the case of **(PN)Ni(O*t*Bu)**, the reaction mixture immediately turned orange and bubbled vigorously, whereas for **(PN)Ni**, no such initial color change or bubbling was observed. At given time intervals, 50 μL of the reaction mixture was sampled via micropipette and diluted with THF (*ca.* 1

mL). This solution was taken out of the glovebox, filtered through silica into a GC vial, and analyzed by GC.

3.5 Supporting Figures

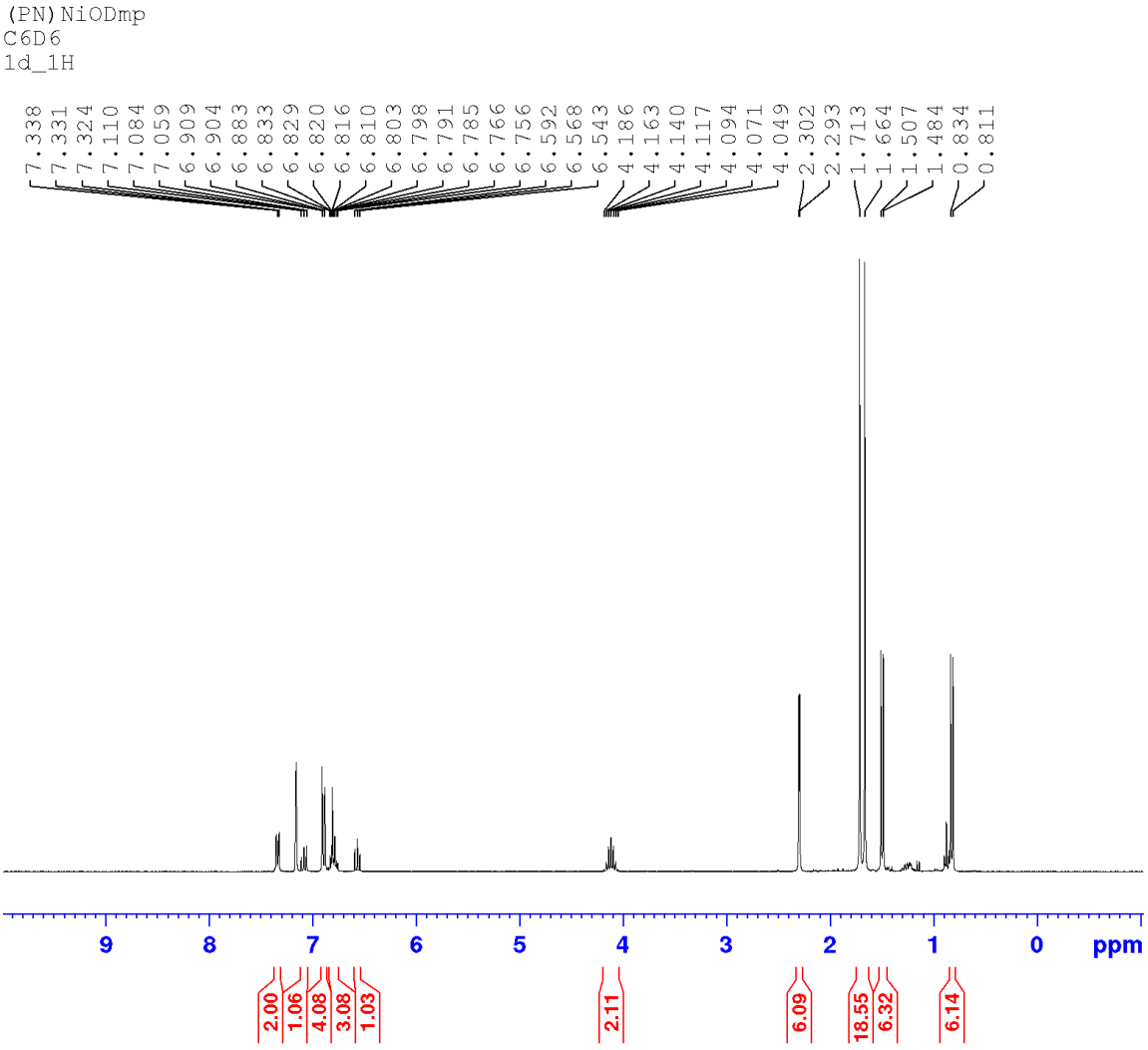

Figure S3-1. ^{1}H NMR Spectrum of (PN)Ni(Odmp) (benzene-d_6, 500.1 MHz).

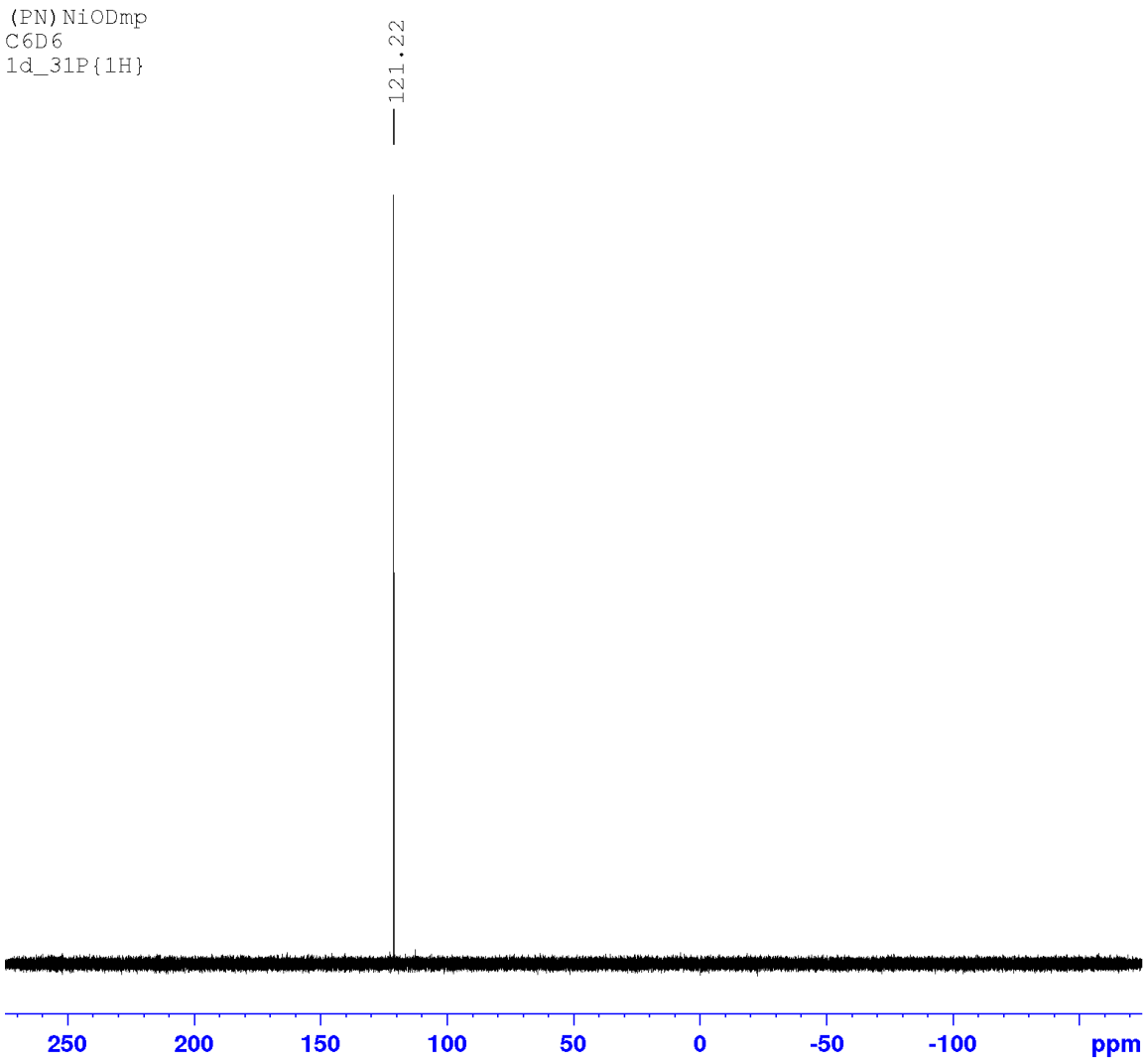

Figure S3-2. $^{31}P\{^{1}H\}$ NMR Spectrum of (PN)Ni(Odmp) (benzene-d_6, 202.5 MHz).

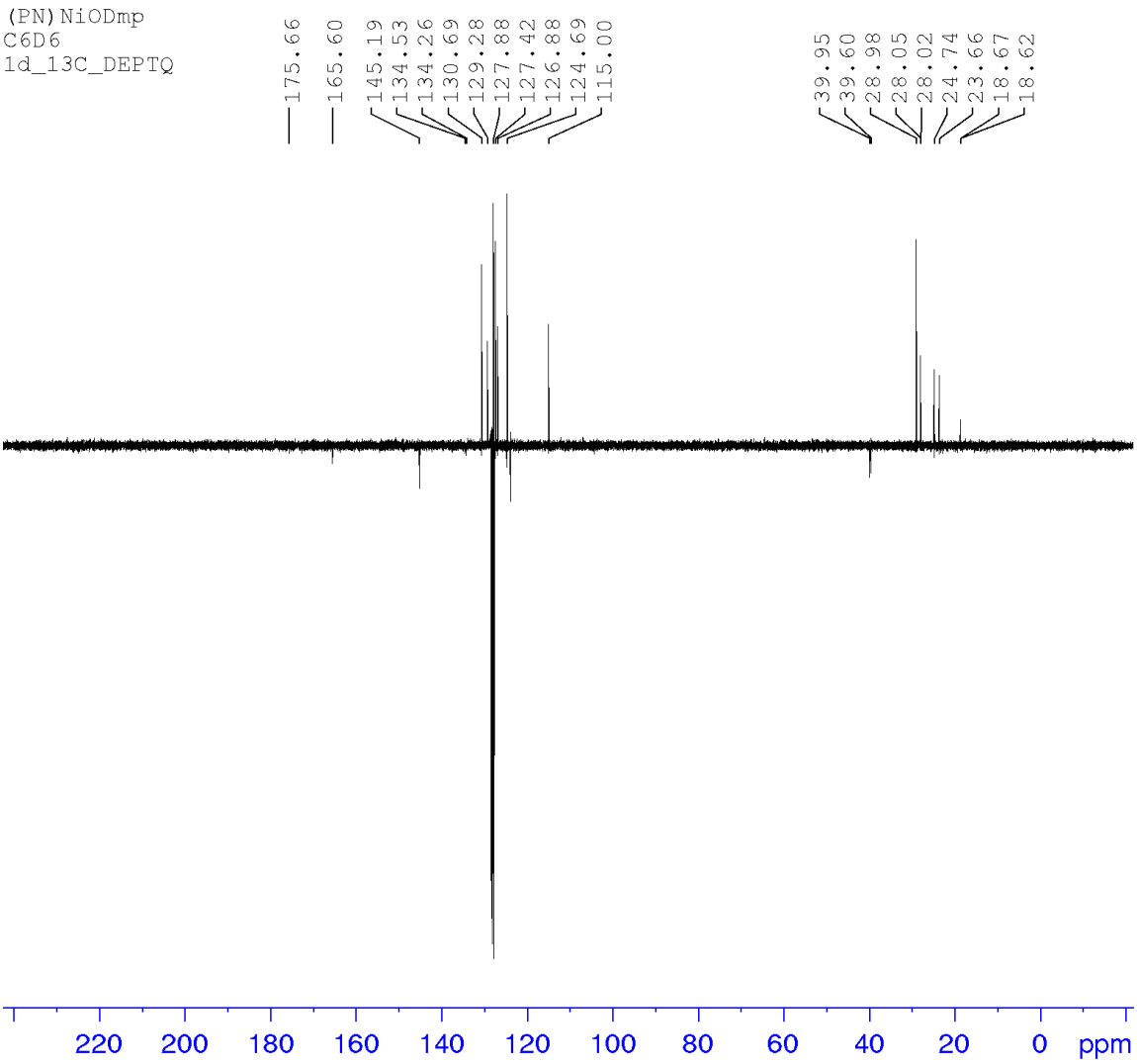

Figure S3-3. ^{13}C DEPTQ NMR Spectrum of (PN)Ni(Odmp) (benzene-d_6, 125.7 MHz).

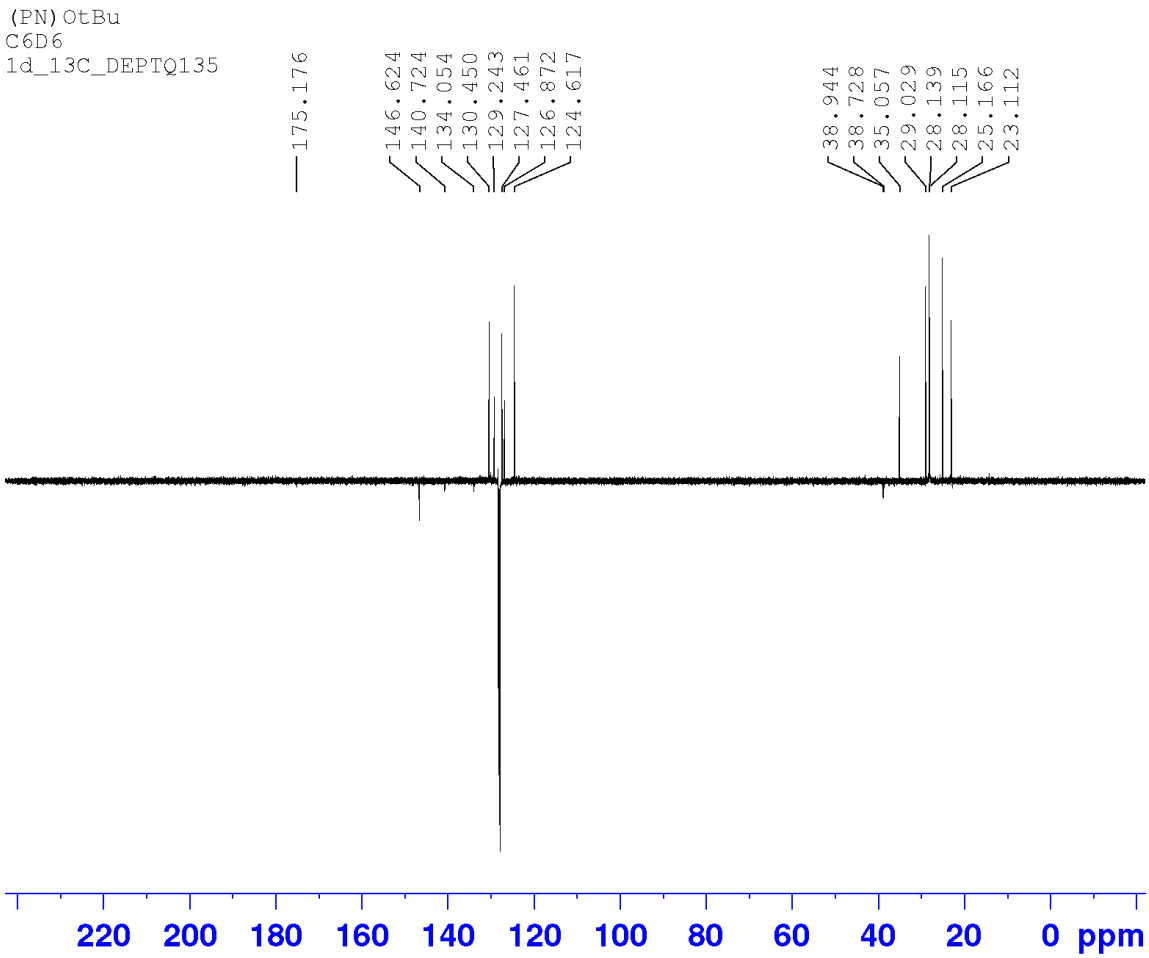

Figure S3-4. ^{13}C DEPTQ NMR Spectrum of (PN)Ni(O*t*Bu) (benzene-d_6, 125.7 MHz).

CHAPTER 4: CHEMISTRY AND CHARACTERIZATION OF UNSATURATED NICKEL HYDRIDES AND AGOSTIC NICKEL ALKYLS, FEATURING BENZENE INSERTION INTO A NICKEL HYDRIDE BOND

4.1 Introduction

Low-coordinate nickel hydride complexes are commonly invoked as key intermediates in a diversity of catalytic applications involving transformations of unsaturated multiple bonds, including alkene hydrogenation, hydrosilation, isomerization, hydroboration, and beyond.[52,119] In this regard, there is ongoing motivation to identify efficient means of preparing such complexes, and/or to exploit their formation in developing new stoichiometric and catalytic reactivity. Clearly, these motivations drove several research projects included in this thesis. Chapter 2 describes the challenges our collaborative research team faced in applying *in situ*-generated three-coordinate **(PN)NiH** in catalytic alkene I-H,[89] whereas in Chapter 3, challenging hydrosilative amide reactions were facilitated by putative **(PN)NiH**.[120] As outlined in (Scheme 4-1), access to **(PN)NiH** in these chapters was made possible via exposure of crystallographically characterized low-coordinate **(PN)NiX** precursors (X =N(SiMe$_3$)$_2$, NHdipp, O*t*Bu, and/or Odmp) to HBPin (neat or in alkane solvent) or PhSiH$_3$ (with superior results in THF versus benzene), respectively, with concomitant loss of E-X (E = B or Si). Although **(PN)NiH** could not be detected unequivocally in these studies, dimerization to form the diamagnetic and crystallographically characterized **Ni$_2$H$_2$**[89] proved favorable under a range of experimental conditions. Moreover, a comparison of various **(PN)NiX** species in hydrosilative amide reduction revealed precatalysts featuring X =N(SiMe$_3$)$_2$ to be inferior

to those where X = NHDipp or O*t*Bu,[120] presumably arising from more efficient activation of the latter complexes to afford **(PN)NiH**.

Building on these observations, I sought to identify conditions under which the efficient formation of **(PN)NiH** could be exploited as a means of accessing new chemistry, whereby formation of **Ni_2H_2** might be circumvented. Related explorations targeted the preparation of analogous low-coordinate **(PN)Ni(alkyl)** complexes, and if isolable alkyl variants might provide alternative access to **(PN)NiH** by way of BHE. This chapter details the generation of putative **(PN)NiH** under appropriate conditions in benzene (neat, or as a solution in C_6H_{12}) to afford a dinuclear product, **{(PN)Ni}$_2$(μ^2-η^3:η^3-C_6H_8)** (i.e., **5**) that formally arises from net double **(PN)***Ni-H* addition to C=C units within a single benzene molecule. Also described are synthetic investigations of three-coordinate **(PN)Ni(alkyl)** complexes stabilized by β-agostic (alkyl = Et, *n*-Bu, *n*-hexyl) or γ-agostic (alkyl = Np) interactions (Scheme 4-1).

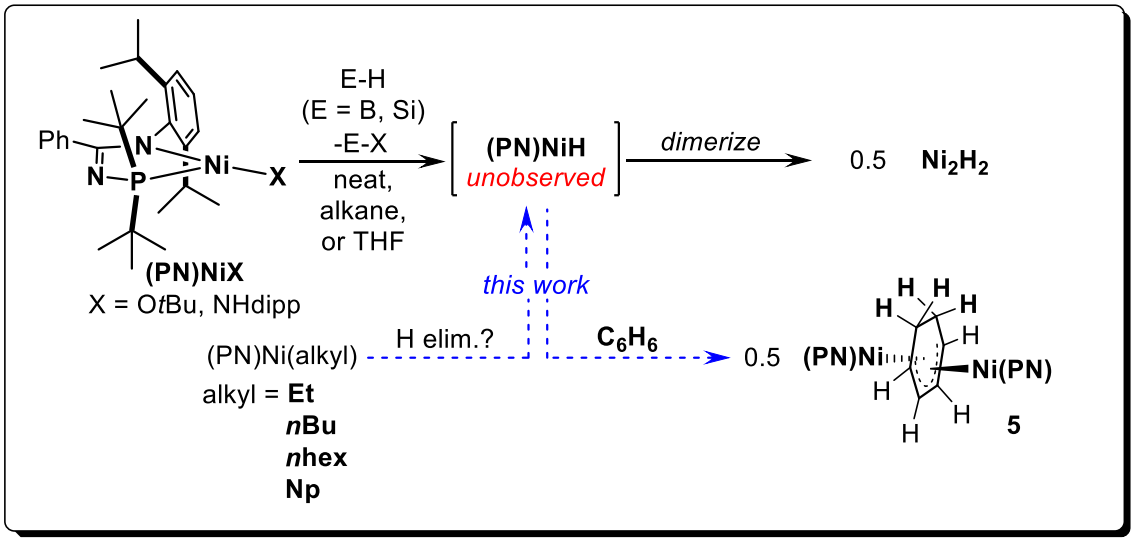

Scheme 4-1. Generation, dimerization, and reactivity derived from the unobserved intermediate (PN)NiH.

4.2 Results and Discussion

4.2.1 Contributions

The team at Brigham Young University (Madhu Samolia, and Daniel H. Ess) was responsible for the computational work. Crystallography was performed by Drs. Michael Ferguson and Robert McDonald at the University of Alberta. All other reported work was performed by the author.

4.2.2 Observation and Investigation of Benzene Insertion into (PN)NiH

In seeking to evaluate the reactivity properties of putative **(PN)NiH** generated *in situ* in benzene solvent, precursor complexes **(PN)NiX** (X = NHdipp or O*t*Bu) were chosen given their established clean and rapid reaction with E-H bonds (E = B or Si) in alternative solvents (Scheme 4-1). Upon exposure of these **(PN)NiX** precursors to HBPin in benzene at room temperature (Scheme 4-2), $^{31}P\{^{1}H\}$ NMR spectroscopic analysis of the crude reaction mixture revealed the presence of **(PN)Ni(H$_2$BPin)**[89] and **Ni$_2$H$_2$**, along with other signals including at 114.1, 111.9, and 110.3 ppm (relative ratio of *ca.* 0.06 : 1 : 0.06). Mixtures comprising **Ni$_2$H$_2$** and the set of signals at 114.1, 111.9, and 110.3 ppm (similar relative ratio) were also observed in related reactions employing H_2 or $PhSiH_3$. However, when using Me_2PhSiH, the production of **Ni$_2$H$_2$** was suppressed such that the set of resonances at 114.1, 111.9, and 110.3 ppm (Figure 4-1) represented the dominant signals in the $^{31}P\{^{1}H\}$ NMR spectrum of the crude reaction mixture.

Workup of the reaction mixture allowed for the isolation of this material, which in turn was identified on the basis of NMR, single-crystal X-ray, and elemental analysis data as the dinuclear species **5**, ostensibly the net product of double **(PN)***Ni-H* addition to C=C units within a single benzene molecule (Scheme 4-2).

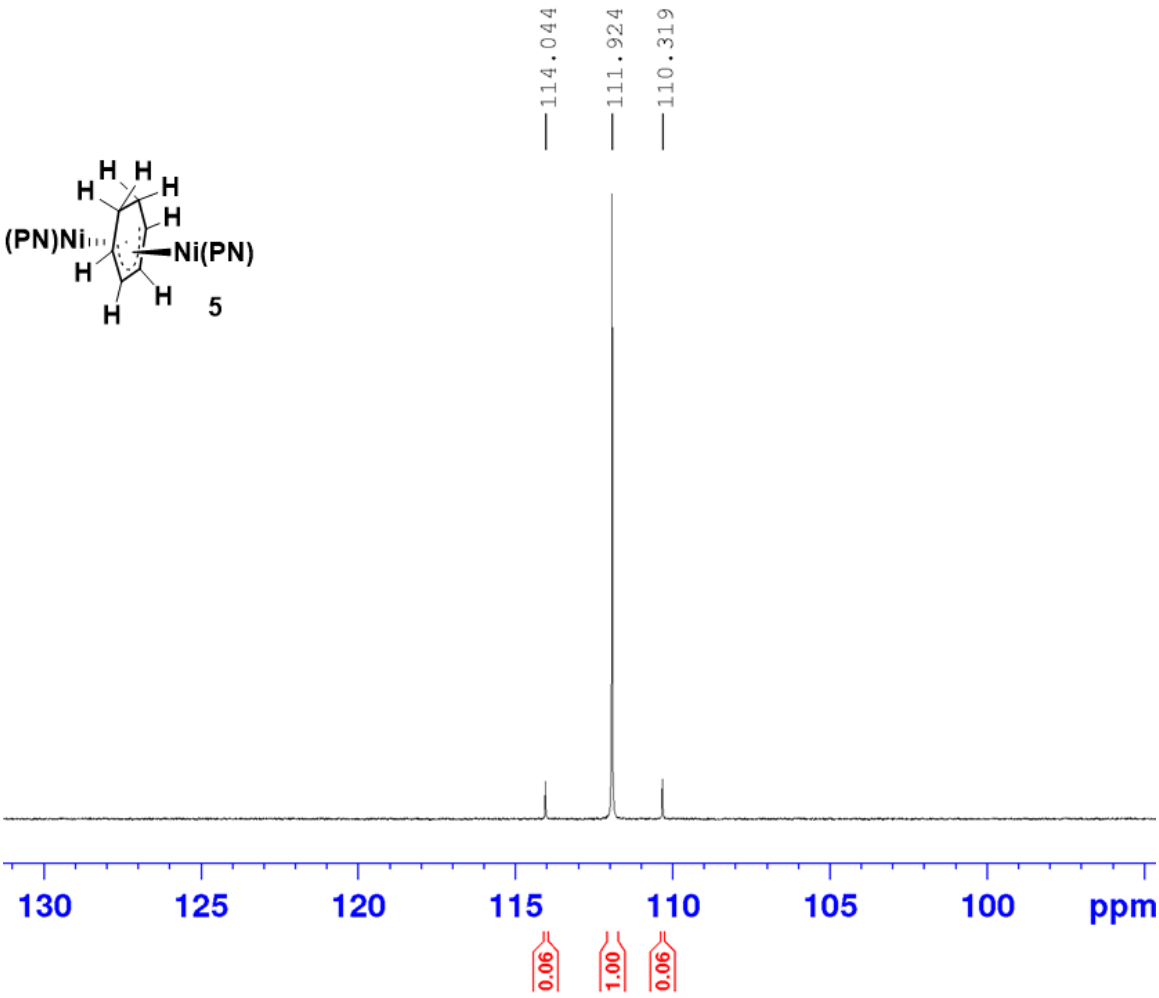

Figure 4-1. $^{31}P\{^{1}H\}$ NMR spectrum of 5 (202.5 MHz, benzene-d_6).

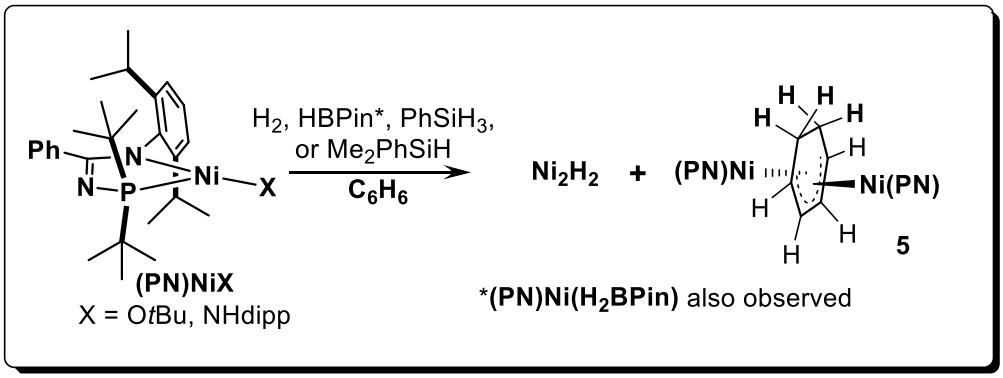

Scheme 4-2. Select conditions that generate 5.

The crystal structure of **5** presented in Figure 4-2 supports the formulation of this compound as the C_2-symmetric, antifacial-coordinated dinuclear species depicted in

Scheme 4-2. The comparatively long C3-C4 (1.510(2) Å) and C4-C4' (1.528(4) Å) distances relative to C2-C2' (1.444(3) Å) and C2-C3 (1.443(3) Å) are consistent with the saturation the formerly C4=C4' fragment arising from two Ni-H additions. Moreover, the similarity of the C2-C2' and C2-C3 distances, as well as the observed Ni-C2, Ni-C2', and Ni-C3 contacts (2.19-1.98 Å), imply a delocalized bonding motif involving the μ^2-η^3:η^3-$C_6H_8^{-2}$ group. While an in-depth theoretical analysis of the bonding in **5** was beyond the scope of this thesis, a preliminary DFT computational analysis (Prof. Dan Ess, BYU) employing the crystallographically determined coordinates of **5** support the view of this structure as involving the coordination of two $(PN)Ni^+$ fragments to a substituted butadiene dianion.[121]

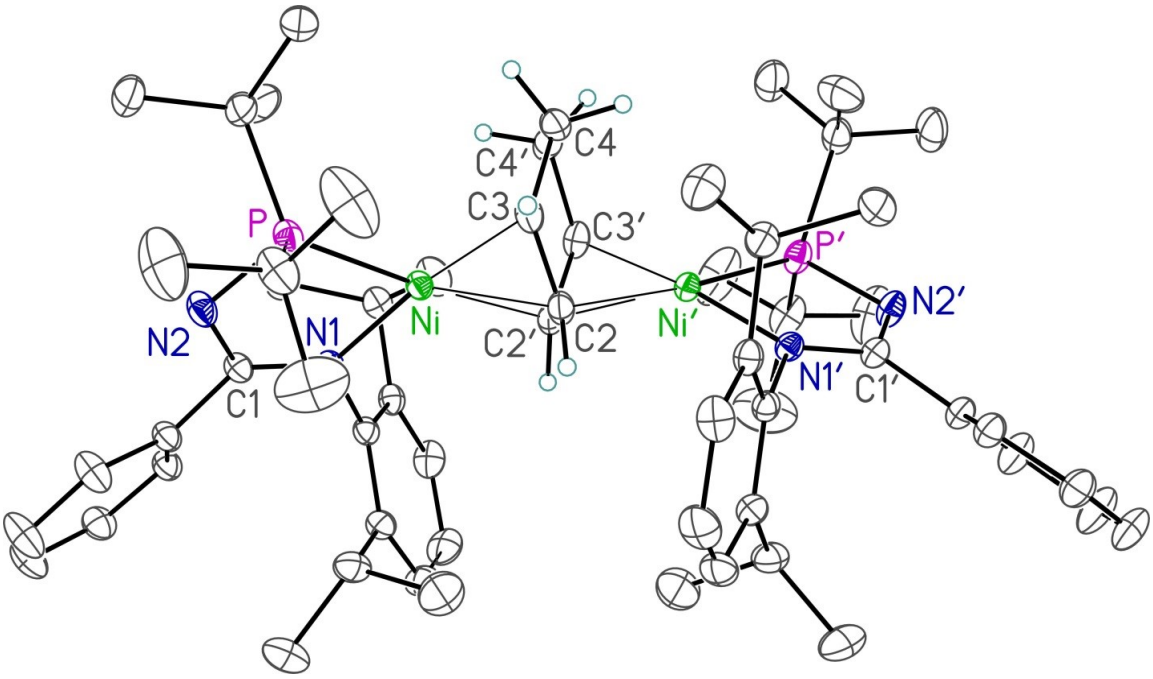

Figure 4-2. Crystallographically determined structure of 5, shown with 30% probability ellipsoids and with selected hydrogen atoms omitted for clarity. Selected interatomic distances (Å) and angles (°): Ni-P, 2.1730(4), Ni-N1 1.9407(11), Ni-C2 2.0070(14), Ni-C2' 2.1918(15), Ni-C3 1.9799(14), C2-C2' 1.444(3), C2-C3 1.443(2), C3-C4 1.510(2), C4-C4' 1.528(4), P-Ni-N1 83.81(4), C2'-C2-C3 115.35(10), Ni-C3-C2 69.79(8), Ni-C3-C4 112.05(11), C2-C3-C4 118.55(13), C3-C4-C4' 113.02(10).

The crystallographically characterized C_2-symmetric product **5** may be viewed as the major product observed in solution (δ ^{31}P = 111.9 ppm, Figure 4-1), as evidenced by NMR spectroscopic analysis, whereby resonances associated with the chelating ligand, as well as for the bridging $C_6H_8^{2-}$ moiety, were identified (Figure 4-3 and Figure S4-1).

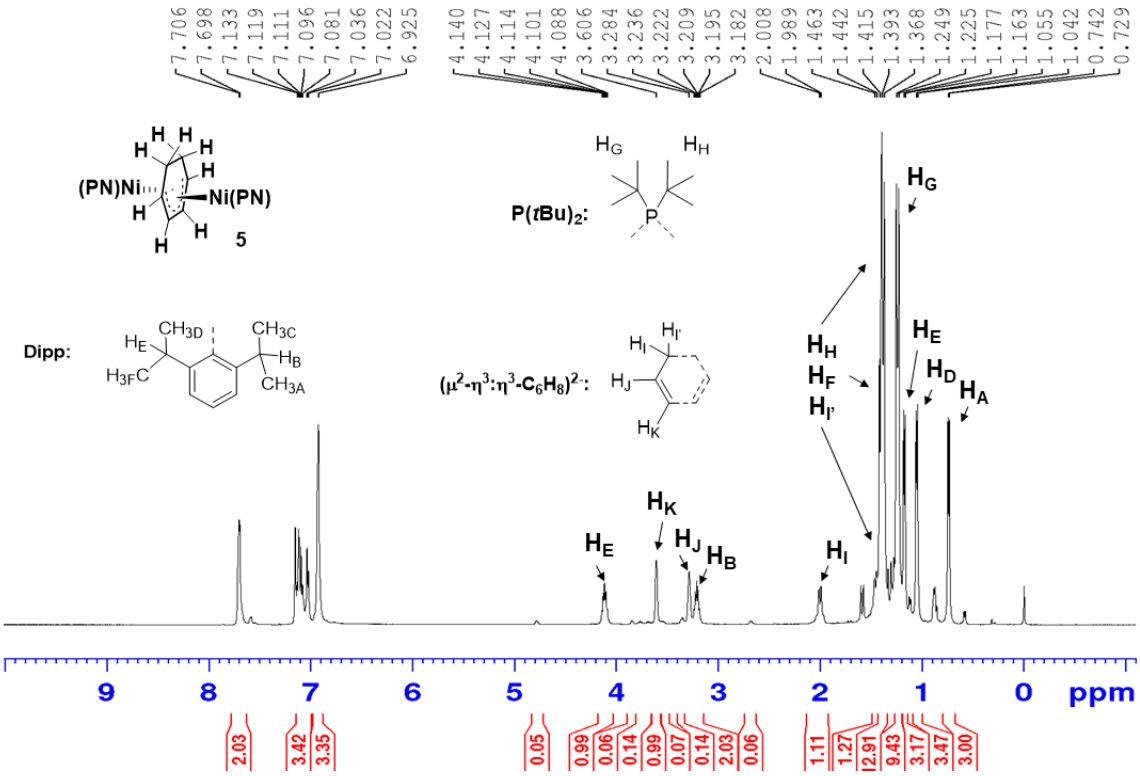

Figure 4-3. ^{1}H NMR spectrum of 5, including selected assignments (500.1 MHz, benzene-d_6). Integrations correspond to the asymmetric unit of **5**.

While one of the two ^{1}H NMR resonances arising from the diastereotopic protons within the methylene units is obscured (H_I'), a ^{1}H-^{1}H COSY NMR experiment revealed coupling between the obscured (H_I') and the well-resolved (H_I) methylene resonances, and a ^{1}H-^{13}C HSQC NMR experiment confirmed that these protons are attached to the same carbon atom (i.e., C4/C4' in Figure 4-2). These methylene protons also exhibit coupling to the adjacent CH unit (i.e., C3-H/C3'-H in Figure 4-2) in the ^{1}H-^{1}H COSY

NMR spectrum. As noted above, the generation of **5** is invariably accompanied by the observation of low-intensity ^{31}P NMR signals at 114.1 and 110.3 ppm, with each being approximately 6% the intensity of the major product (**5**; $\delta\ ^{31}P$ = 111.9 ppm).

These low-intensity signals plausibly arise from **5'**, where **5'** is a dinuclear isomer of **5** featuring inequivalent phosphorus environments, or alternatively two isomers of **5**, each having equivalent phosphorus environments. Elemental analysis data obtained on so-formed **5**/**5'** mixtures indirectly support **5'** as being an isomeric form of **5**. Moreover, variable temperature NMR analysis (^{1}H and $^{31}P\{^{1}H\}$, toluene-d_8, -80 to +80 °C) employing so-formed **5**/**5'** mixtures showed no significant change in relative proportions of **5** and **5'** over the temperature range; as the temperature was increased from 60 - 80 °C (*ca.* 1 h), both **5** and **5'** decompose to give **Ni$_2$*n*H$_2$**, with only modest deuterium incorporation noted at the Ni-H site.

Notably, **5**/**5'** mixtures appear to undergo deuterium incorporation more extensively, as well as decomposition concurrently, upon heating at 65 °C in benzene-d_6. In monitoring such processes by use of $^{31}P\{^{1}H\}$ NMR methods (Figure 4-4), the **5**/**5'** resonances observed initially at 114.1, 111.9, and 110.3 ppm disappear over the course of 17 h, and new signals at 114.2, 112.0, and 110.4 ppm (relative ratio of *ca.* 0.06 : 1 : 0.06; collectively, **5$_d$** and **5$_d$'**) clearly emerge. Loss of ^{1}H NMR signals associated with the $C_6H_8^{2-}$ moiety occurs over this time period, along with the appearance of what are assigned as $C_6H_nD_{6-n}$ resonances, although I am unable to comment specifically on the composition of these benzene isotopologues. Continued heating under these conditions results in the formation of **Ni$_2$*n*H$_2$**.[89]

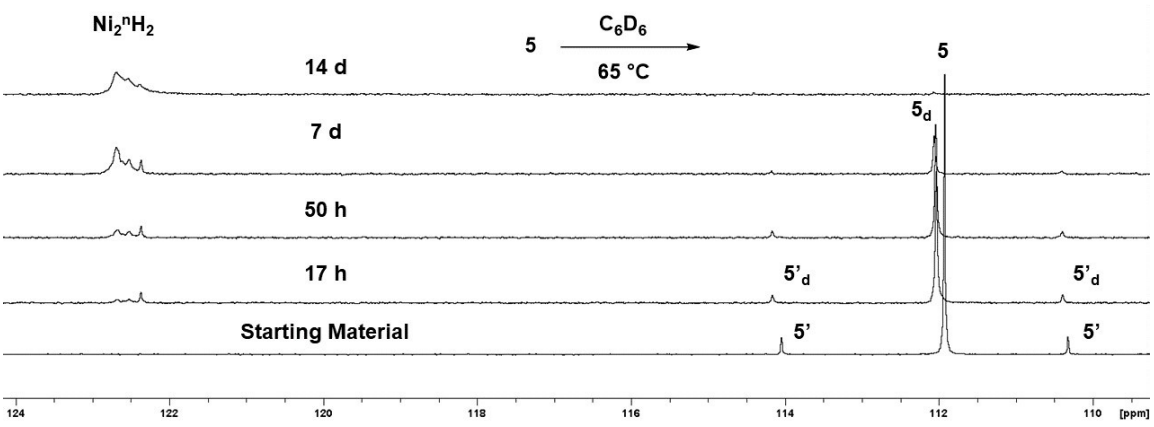

Figure 4-4. $^{31}P\{^{1}H\}$ spectra illustrating the conversion of 5 to 5' and $Ni_2{}^nH_2$ upon heating (benzene-d_6, 121.5 MHz).

When putative **(PN)NiH** is generated *in situ* by use of Me_2PhSiH as described above, but in benzene-d_6 solvent, the set of signals at 114.2, 112.0, and 110.4 ppm (similar relative ratio as assigned for **5d**/**5d'**) is similarly observed in the $^{31}P\{^{1}H\}$ NMR spectrum. Although one might expect that the generation of a coordinated $C_6D_6H_2^{2-}$ moiety, rather than a fully deuterated $C_6D_8^{2-}$ group, should occur under these conditions, no ^{1}H NMR signals attributable to this fragment were detected at any point in the reaction. While definitive mechanistic data are lacking, it is plausible that the initially generated **(PN)NiH** is efficiently transformed into **(PN)NiD** via reversible C=C insertion/β-hydride elimination involving benzene-d_6 thereby resulting in the generation of **5**/**5'** featuring a fully deuterated $C_6D_8^{2-}$ bridging fragment.

To the best of our knowledge, the structure of **5** represents the first documented example of benzene insertion into a Ni-H bond. Notably, such transformations have been invoked as key steps in the context of the reductive cleavage of inert C-O bonds with silanes involving substituted anisoles.[122] The formation of **5** complements observations by Agapie and co-workers[123] who documented intramolecular insertions of Ni-H

fragments within a synfacial-coordinated (rather than the antifacial-coordination in **5**) and geometrically pre-disposed bisphosphine-arene pincer ligand, to give a tethered $C_6H_6R_2^{2-}$ bridging unit featuring similar geometrical parameters to the $C_6H_8^{2-}$ group in **5**. In contrast to the formation of the dinuclear **(PN)** complex **5**, both NacNac[94] and α-diimine-ligated[124] Ni^{II}-H species have been shown to undergo reduction in the presence of arenes such as toluene, to form bridging dinuclear tolyl dianion complexes, with loss of dihydrogen.

To determine the importance of benzene concentration relative to the formation of **5**, **(PN)Ni(O*t*Bu)** (18 mM) with was treated with Me_2PhSiH (1 equiv) in varying mixtures of benzene in cyclohexane. Quantitative ^{31}P NMR analysis (qNMR[125]) of the reaction mixtures thereafter indicated that even in 25% benzene/cyclohexane, **5** was formed preferentially to **Ni_2H_2** in a 1.6 : 1 ratio. Of the converted **(PN)Ni(O*t*Bu)** (65%) under these conditions, these two products collectively accounted for 85% of the phosphorus-containing product mixture. Unfortunately, our efforts to extend this reaction chemistry to other aromatic solvents (e.g., toluene, thiophene, C_6H_5F, and C_6F_6) failed to yield analogues of **5** or other products that could be isolated and/or definitively characterized. Efforts to reduce further the coordinated $C_6H_8^{2-}$ fragment in **5** via exposure to H_2 in benzene-d_6 under various conditions were unsuccessful, resulting in the formation of complex reaction mixtures that contained **$Ni_2{}''H_2$** and HD. At ambient temperature, **5** was observed not to react with excesses of MeOH, NH_2dipp, pyridine, DMAP, COD, PMe_3, Me_2PhSiH, or $PhSiH_3$.

4.2.3 Synthesis and Reactivity of β-Agostic (PN)Ni(alkyl) Complexes

Intrigued by our ability to identify conditions for the selective formation of the benzene insertion product **5**, I became interested in exploring alternative routes for the formation of **(PN)NiH** from **(PN)Ni(alkyl)** precursor complexes via BHE, thus circumventing the need for exogenous activation. The viability of reversible alkene insertion/BHE steps involving **(PN)NiH** and isomeric **(PN)Ni(octyl)** species was established in the course of our recent mechanistic investigation of alkene I-H chemistry, although no pure **(PN)Ni(alkyl)** complexes were isolated.[89] Moreover, there is ongoing interest in the study of low-coordinate Ni-alkyl complexes supported by homobidentate or heterobidentate ligation, given their relevance to alkene oligomerization and polymerization processes.[126]

Consequently, neutral (i.e. P_2,[127] α-diimine[128]) or anionic (NacNac [129]) homobidentate ligands have been employed to stabilize a limited set of cationic or neutral (respectively) three-coordinate L_2Ni^{II}(alkyl) complexes that exhibit additional agostic[130] stabilizing interactions. Conversely, while four-coordinate (LX)Ni^{II}(alkyl)(L') complexes supported by anionic P,N ligation and an additional co-ligand (e.g. L' = PMe_3) are known,[41] to the best of our knowledge, related neutral three-coordinate **(PN)Ni(alkyl)** complexes have yet to be reported. Treatment of **Ni_2Cl_2** (0.5 equiv) with EtLi or *n*-BuLi (Scheme 4-3) afforded the corresponding alkyl complexes **(PN)NiEt** and **(PN)Ni*n*Bu** as the major products, which in turn were isolated and characterized on the basis of elemental analysis and NMR spectroscopic data (Figure S4-2 to Figure S4-4 and Figure S4-9 to Figure S4-11, respectively).

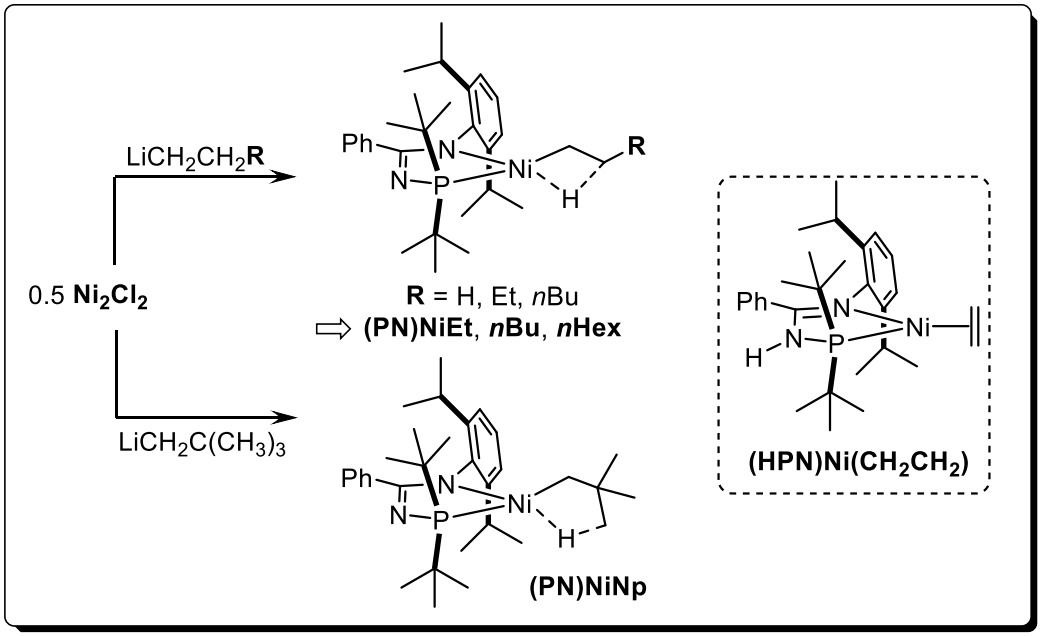

Scheme 4-3. Synthesis of the agostic (PN)Ni(alkyl) complexes, and the proposed rearrangement product, (HPN)Ni(CH_2CH_2).

The existence of β-agostic interactions in these complexes is evident in their room temperature ^{1}H NMR resonances, with associated diagnostic resonances appearing at -1.93 and -2.50 ppm (respectively) that display reduced average $^1J_{CH}$ coupling constants relative to the corresponding Ni-CH_2-R (non-agostic) fragments[130] (summarized in Table S4-1). While **(PN)Ni*n*Bu** appears to exist upon dissolution in benzene-d_6 as an isomeric mixture featuring a major *n*-alkyl isomer, **(PN)NiEt** undergoes gradual decomposition to a new diamagnetic product that I tentatively assign as **(HPN)Ni(CH_2CH_2)** (Scheme 4-3, right), which lacks agostic or hydridic ^{1}H NMR resonances and exhibits a ^{31}P{^{1}H} NMR resonance at 110 ppm (Figure S4-6 to Figure S4-8). Our assignment of **(HPN)Ni(CH_2CH_2)** was based initially on the observation of a ^{1}H NMR resonance 5.26 ppm, suggesting the presence of protonated HPN ligand, in keeping with other *N*-phosphinoamidine pro-ligands and related complexes. [68,71,91] Accordingly, an ^{1}H-^{15}N HMQC experiment showed a single correlation between this

resonance and an ^{15}N NMR resonance at -278 ppm. ^{1}H NMR resonances attributable to an L_2Ni(ethylene) species were also observed.[127a] Upon treatment of a mixture of **(PN)NiEt** and **(HPN)Ni(CH_2CH_2)** with excess cyclooctene, complete consumption of **(HPN)Ni(CH_2CH_2)** was noted along with the formation of **(PN)Ni*n*Bu**, plausibly via displacement of ethylene from **(HPN)Ni(CH_2CH_2)** and subsequent insertion of this liberated ethylene into the Ni-Et bond of **(PN)NiEt**. Support for the viability of this proposed reaction scenario comes from the fact that upon exposure of **(PN)NiEt** to ethylene (~ 1 atm, Figure 4-5), both **(PN)Ni*n*Bu**, and **(PN)Ni*n*Hex** (generated independently from *n*-hexyllithium; Figure S4-12 to Figure S4-14) are generated in significant quantities as evidenced by NMR spectroscopic analysis. Similarly, upon exposure to ethylene (~ 1 atm, Figure S4-17), complex **(PN)Ni*n*Bu** was completely consumed, resulting in the formation of **(PN)Ni*n*Hex** as the major product prior to further apparent insertions of ethylene. By comparison, no reaction was observed between ethylene and **Ni_2H_2** under similar conditions.

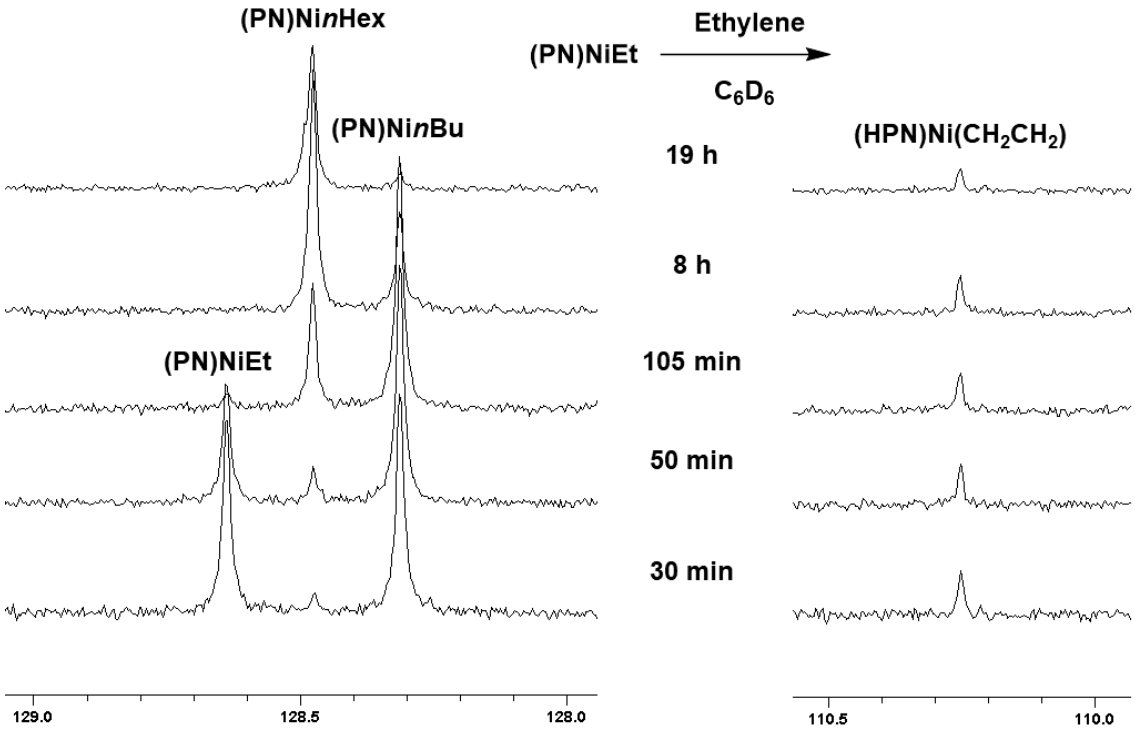

Figure 4-5. Stacked $^{31}P\{^1H\}$ NMR spectra of the reaction of (PN)NiEt with ethylene (121.5 MHz, benzene-*d*$_6$; shifts in ppm).

With the *n*-alkyl complexes **(PN)NiEt** and **(PN)Ni*n*Bu** in hand, I examined their ability to serve as a reactive source of **(PN)NiH** via BHE, *en route* to the benzene insertion product **5**. Unfortunately, such reactions were not useful in forming **5**. While benzene solutions of **(PN)NiEt** slowly generate **(HPN)Ni(CH_2CH_2)** at room temperature as outlined above, upon heating at 65 °C, a complex mixture of phosphorus-containing products was generated over the course of 2-96 h, on the basis of the features observed in the $^{31}P\{^1H\}$ NMR spectrum of the reaction mixture. While **Ni_2H_2** was not observed as a product in such reactions involving **(PN)NiEt,** under similar conditions employing **(PN)Ni*n*Bu** (40 °C, 2-96 h), **Ni_2H_2** was detected as the major product in solution, in the absence of **5**.

4.2.4 Synthesis and Structure of the γ-Agostic Complex (PN)NiNp

While the formally 14-electron **(PN)Ni(alkyl)** complexes **(PN)NiEt** and (**PN)Ni*n*Bu** stabilized by secondary β-agostic interactions did not prove useful in the synthesis of **5**, the rarity of such species and the lack of crystallographic data for **(PN)NiEt** and (**PN)Ni*n*Bu** provided motivation for the synthesis of alternative complexes of this type. Accordingly, I targeted the β-saturated **(PN)NiNp**, which might exhibit γ-agostic interactions, as is found in related (P_2)Rh species reported by Hofmann and co-workers,[131] as well as (P_2)Ni complexes described by Hillhouse.[127b]

Exposure of **Ni_2Cl_2** (0.5 equiv) to NpLi (Scheme 4-3) afforded upon workup the desired complex **(PN)NiNp** as an analytically pure solid in 93% isolated yield; a representative $^{31}P\{^1H\}$ spectrum is shown in Figure 4-6. Single-crystal X-ray diffraction analysis of **(PN)NiNp (**Figure 4-7) revealed some disorder in the neopentyl group, with the major orientation being consistent with a γ-agostic interaction as depicted in Scheme 4-3. The room temperature ^1H and $^{13}C\{^1H\}$ NMR spectra of **(PN)NiNp** exhibit averaged Ni-$CH_2C(CH_3)_3$ signals, which is in keeping with a relatively small difference in the average $^1J_{CH}$ coupling constants measured for the Ni-$CH_2C(CH_3)_3$ (128 Hz, non-agostic) and $NiCH_2C(CH_3)_3$ (123 Hz, γ-agostic) fragments (Figure S4-15, Figure S4-16, and Table S4-1). Notably, **(PN)NiNp** represents the first crystallographically characterized three-coordinate Ni-alkyl complex featuring a heterobidentate ligand, and the first neutral γ-agostic Ni^{II}-alkyl complex.[129a,132]

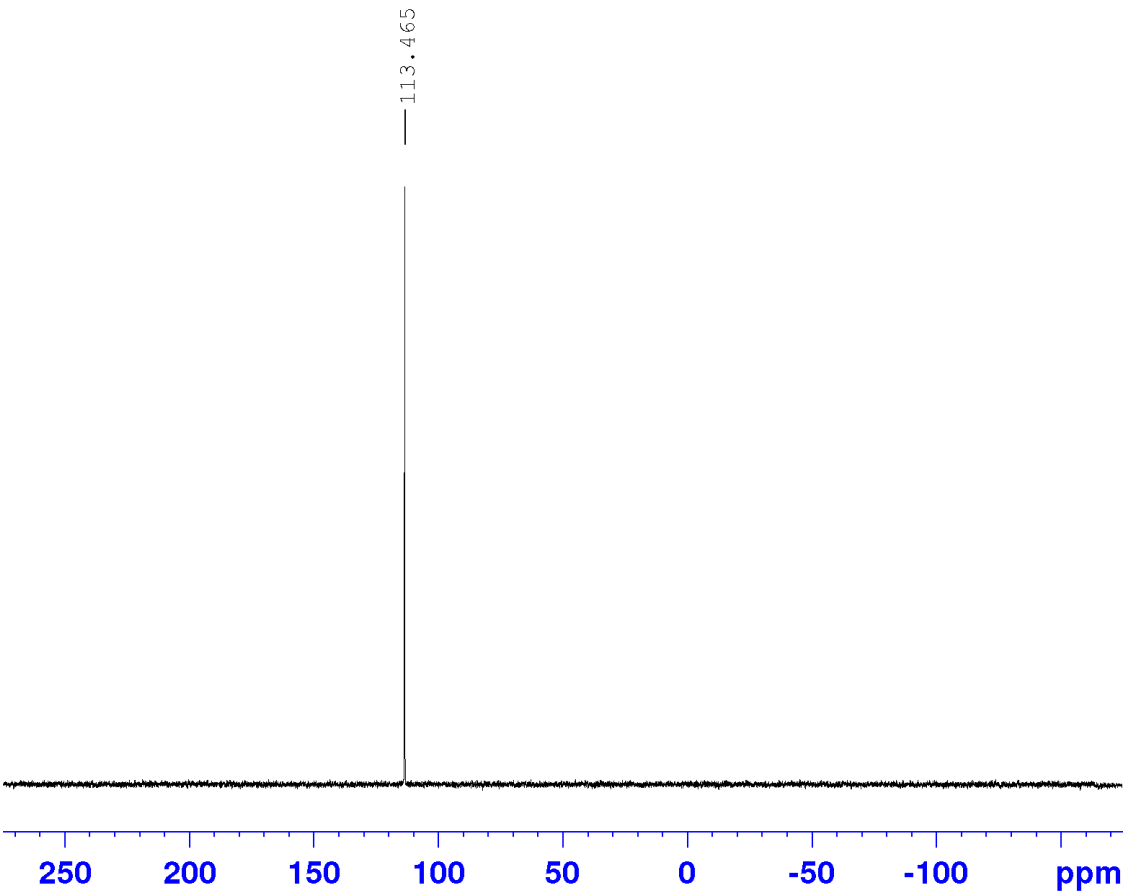

Figure 4-6. $^{31}P\{^{1}H\}$ NMR spectrum of (PN)NiNp (121.5 MHz, benzene-d_6).

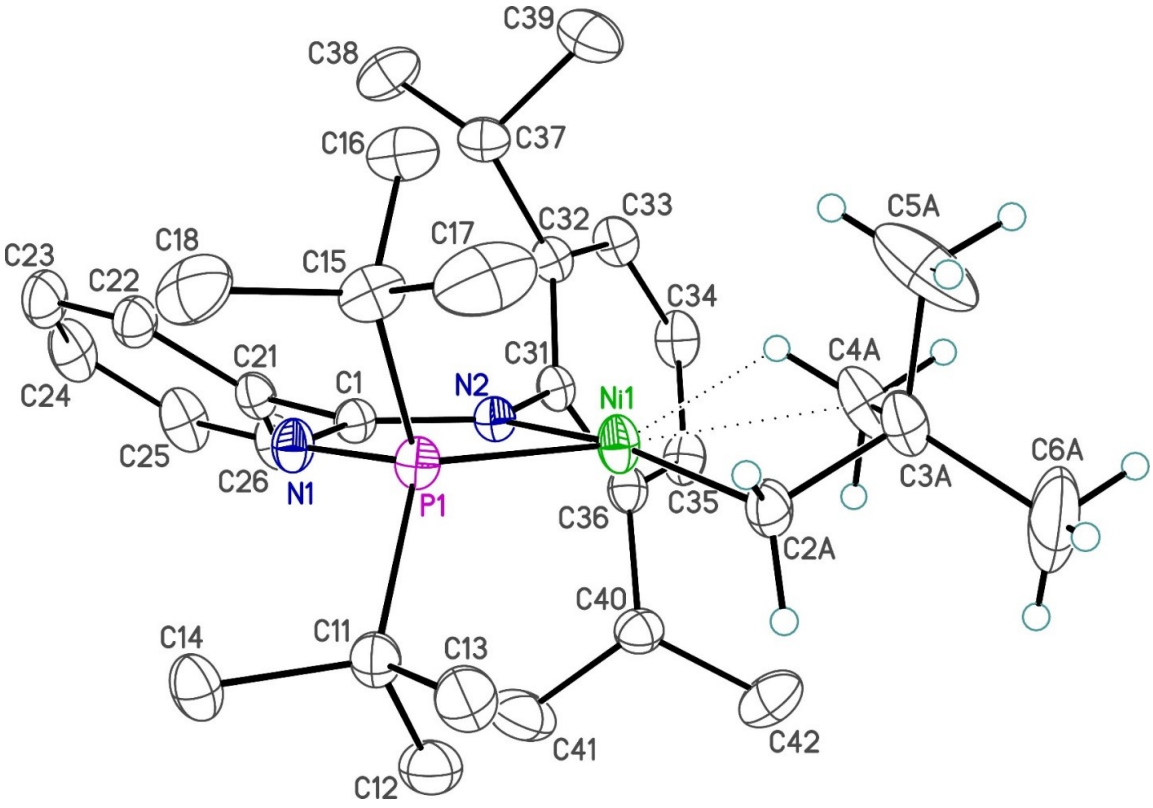

Figure 4-7. Crystallographically determined structure of (PN)NiNp (major disorder contributor shown), shown with 30% probability ellipsoids and with selected hydrogen atoms omitted for clarity. Selected interatomic distances (Å) and angles (°): Ni1-C2A 1.920(3), Ni1-C4A, 2.452(15), Ni1-P1 2.0934(4), Ni1-N2 1.9310(12), P1-Ni1-N2 84.97(4), C2A-Ni1-C4A 67.1(3), C2A-C3A-C4A 106.1(7), Ni1-C2A-C3A 100.2(4).

For context, γ-agostic interactions are observed in the structure of the complex cation $(dtbpe)Ni^{II}(CH_2SiMe_3)^+$, which features disordered $CH_{2\alpha}$ and $CH_{3\gamma}$ groups and is reported with average Ni-$C_{\alpha,\gamma}$ distances of 2.150(8) and 2.300(8) Å, respectively. The related $(dtbpe)Ni^{I}(CH_2C(CH_3)_3)$ complex features a Ni-CH_2 distance of 1.982(3) Å and no apparent[127b] agostic bonding interactions. Whereas the Ni-CH_2 distance in **(PN)NiNp** (1.920(3) Å) is shorter than both of the related distances in these (dtbpe)Ni comparator compounds, the γ-agostic Ni-C contact in **(PN)NiNp** (Ni1-C4A, 2.452(15) Å) is significantly longer than that observed in $(dtbpe)Ni^{II}(CH_2SiMe_3)^+$. The small Rh-$C_\alpha$-$C_\beta$ angle featured in the neutral, d^8 γ-agostic complex (dtbpm)Rh(neopentyl) (101.0(2)°) has

been invoked as possibly being representative of an "attractive relationship" between Rh and the C_α-C_β bond, as a precursor to β-carbon elimination.[131] A similar angle is found in **(PN)NiNp** (Ni1-C2A-C3A, 100.2(4)°). There was insufficient evidence to support of β-carbon elimination involving **(PN)NiNp**; rather, complex thermal decomposition pathways are observed for this complex in benzene whereby neither **5** nor **Ni_2H_2** are generated. Compound **(PN)NiNp** inserts ethylene to form complex product mixtures that display β-agostic resonances like those noted for **(PN)Ni*n*Bu** and **(PN)Ni*n*Hex**, suggesting replacement of γ- for β-agostic stabilization of the resultant Ni-alkyl complexes.

4.3 Chapter Summary

In conclusion, the utilization of *N*-phosphinoamidinate ligation enabled the synthesis and characterization of the first isolated product arising from insertion of benzene into a Ni-H bond (**5**), as well as the first examples of isolable, three-coordinate, heterobidentate nickel-alkyl complexes stabilized by secondary β- or γ-agostic interactions (**(PN)NiEt**, **(PN)Ni*n*Bu** and **(PN)NiNp**). Both NMR spectroscopic and X-ray crystallographic (for **5** and **(PN)NiNp**) data allowed for the unequivocal characterization of these new complexes. Computational analysis provided support for the bonding in **5** as involving the coordination of two $(PN)Ni^+$ fragments to a substituted butadiene dianion μ^2-η^3:η^3-$C_6H_8^{-2}$ moiety. Future efforts will be directed toward exploiting such low-coordinate (*N*-phosphinoamidinate)Ni complexes in the development of new and synthetically useful chemistry.

4.4 Experimental

4.4.1 General Experimental Considerations

Unless stated, all experiments were conducted at ambient temperature under nitrogen in an inert-atmosphere glovebox or by using standard Schlenk techniques using oven-dried glassware. Dry, oxygen-free solvents were used unless otherwise indicated. Benzene, toluene, and pentane were deoxygenated and dried by sparging with nitrogen and subsequent passage through a double-column solvent purification system packed with alumina and copper-Q5 reactant. Tetrahydrofuran and diethyl ether were purified by distillation under nitrogen from Na/benzophenone. Deuterated solvents, cyclooctene, $SiMe_4$ and Me_2PhSiH were degassed via three freeze–pump–thaw cycles. All purified/degassed chemicals were stored over 4 Å molecular sieves. **Ni_2Cl_2**,[89] **Ni_2H_2**,[89] **(PN)Ni(NHdipp)**,[89] and **(PN)Ni(O*t*Bu)**[120] were synthesized according to literature procedures. All other reagents were purchased from commercial suppliers and used without further purification. Unless otherwise stated, ^{1}H, ^{13}C, and ^{31}P NMR characterization data were collected at 300 K on a Bruker AV-500 spectrometer operating at 500.1, 125.7, and 202.5 MHz (respectively) with chemical shifts reported in parts per million downfield of $SiMe_4$ for ^{1}H and ^{13}C, and 85% H_3PO_4 in D_2O for ^{31}P. ^{1}H and ^{13}C NMR chemical shift assignments are based on data obtained from ^{13}C-UDEFT, ^{1}H–^{1}H COSY, ^{1}H–^{13}C HSQC, ^{1}H–^{13}C HMBC, and ^{1}H–^{15}N HMQC NMR experiments. In some cases, fewer than expected unique ^{13}C NMR resonances were observed, despite prolonged acquisition times. Splitting patterns are abbreviated as follows: br, broad; app, apparent; s, singlet; d, doublet; t, triplet; m, multiplet, with all coupling constants (*J*) reported in Hertz (Hz). Crystallographic data were obtained at or below 193(2) K on a

Bruker D8/APEX II CCD diffractometer equipped with a CCD area detector, employing samples that were mounted in inert oil and transferred to a cold gas stream on the diffractometer. Unit cell parameters were determined and refined on all reflections. Data reduction, correction for Lorentz polarization, and absorption correction were each performed. Structure solution and least-squares refinement on F^2 were used throughout. All non-hydrogen atoms were refined with anisotropic displacement parameters. Full crystallographic solution and refinement details are provided in the deposited CIFs (CCDC 1950518-1950519).

4.4.2 Specific Experimental Considerations

Synthesis of 5. In the glovebox, **(PN)Ni(NHdipp)** (0.079 g, 0.012 mmol) was dissolved in benzene (*ca.* 10 mL) in a glass vial containing a magnetic stirring bar to form a dark brown solution. Stirring was initiated, and Me_2PhSiH (18.4 μL, 0.012 mmol) was added by micropipette. After 48 h, the solution had turned red-brown. Removal of benzene *in vacuo* left a sticky solid. This material was triturated with pentane (*ca.* 1 mL), then extracted with pentane (*ca.* 8 mL), concentrated *in vacuo*, and cooled to -35 °C overnight, whereupon an amorphous solid precipitated. The supernatant was decanted, and the solid was dried *in vacuo*. This solid was washed with cold (-35 °C) $SiMe_4$ (3 x *ca.* 250 μL) and pentane (*ca.* 500 μL). The resultant powder was suspended in cold $SiMe_4$ (*ca.* 4 mL), and the suspension was filtered through Celite. The filter cake was flushed with benzene (*ca.* 4 mL) through the filter into a separate glass vial, then dried *in vacuo*. Finally, this material was washed with cold $SiMe_4$ (3 x *ca.* 500 μL), then dried *in vacuo*, leaving **5** as an analytically pure red powder. Yield: 0.030 g, 48%. Single crystals of **5** suitable for X-ray diffraction were grown from a concentrated solution of pentane at -35

°C. Anal. Calcd for $C_{60}H_{88}N_4Ni_2P_2$: C, 68.98; H, 8.49; N, 5.36. Found: C, 68.57; H, 8.22; N, 5.41. ^{1}H NMR (500.1 MHz, benzene-d_6): δ 7.71 – 7.70 (m, 4H, H_{arom}) 7.13 – 7.02 (overlapping resonances, 6H, H_{arom}), 6.93 (overlapping resonances, 6H, H_{arom}), 4.11 (m, 2H, CH_EMe$_2$), 3.61 (m, 2H, CH_K) 3.28 (m, 2H, CH_J), 3.21 (m, 2H, CH_BMe$_2$) 2.01 – 1.99 (m, 2H, CHCHCH_IH), 1.46 – 1.37 (overlapping resonances, 26 H, CHCHCH$H_{I'}$, CHMe_FMe$_D$, PCMe_{H3}), 1.24 (d, 6 H $^3J_{PH}$ = 13 Hz, PCMe_{G3}), 1.17 (d, 6 H, $^3J_{HH}$ = 7 Hz, CHMe_CMe$_A$), 1.05 (d, 6 H, $^3J_{HH}$ = 7 Hz, CHMe$_F$$Me_D$), 0.74 (d, 6 H, $^3J_{HH}$ = 7 Hz, CHMe$_C$$Me_A$). ^{13}C{^{1}H} NMR (125.8 MHz, benzene-d_6): δ 176.1 (NCN), 151.1 (C$_{arom}$), 142.9 (C_{arom}), 141.9 (C_{arom}), 137.4 (m, C_{arom}), 131.8 (CH$_{arom}$), 128.7 (CH$_{arom}$), 127.0 (CH$_{arom}$) 124.5 (CH$_{arom}$), 123.8 (CH$_{arom}$), 123.4 (CH$_{arom}$), 74.2 (C_KHCHCH$_2$) 46.4 (CHC_JHCH$_2$), 38.4 (m, PCMe$_{H3}$) 37.3 (m, PCMe$_{G3}$) 29.1 (C_EHMe$_2$) 28.7 (PCMe_{H3}), 28.4 (overlapping resonances, PCMe_{G3} and C_BHMe$_2$), 25.7(CHC_IH$_2$), 25.2 (CHMe_FMe$_D$), 24.8 (CHMe_CMe$_A$), 23.8 (CHMe$_F$$Me_D$), 23.2 (CHMe$_C$$Me_A$). ^{31}P{^{1}H} (202.5 MHz, benzene-d_6): δ 111.9 (accompanying minor signals at 114.1 and 110.3 ppm, with each being *ca* 6% of the major signal at 111.9 ppm).

Synthesis of (PN)NiEt. In the glovebox, a glass vial was charged with **Ni$_2$Cl$_2$** (0.66 mg, 0.064 mmol) and then benzene (*ca*. 8 mL), forming a dark purple-red solution. To this solution, EtLi (0.5 M in cyclohexane/benzene, 255 μL, 0.128 mmol) was added as a single aliquot. The dark orange reaction mixture was sealed with a Teflon screw-cap, shaken vigorously, and then immediately filtered through Celite, leaving a dark filter cake and a dark red-orange filtrate. The filtrate was concentrated *in vacuo* to a brown powder, which was extracted with pentane (*ca*. 5 mL) and filtered through Celite, leaving a brown filter cake and a purple filtrate. Removal of pentane *in vacuo* gave a dull purple

powder consisting of **(PN)NiEt** alongside a <10% impurity consisting of the isomeric compound **(HPN)Ni(CH$_2$CH$_2$)** and trace **(PN)Ni*n*Bu**. 42 mg, 60%. Anal. Calcd for $C_{29}H_{45}N_2NiP$: C, 68.12; H, 8.87; N, 5.48. Found: C, 67.88; H, 8.59; N, 5.37. ^{1}H NMR (500.1 MHz, benzene-d_6): δ 7.60 – 7.58 (m, 2 H, H_{arom}), 7.16 (overlapping with benzene-d_6, 1 H, H_{arom}) 7.02 (m, 2 H, H_{arom}), 6.95– 6.90 (overlapping resonances, 3 H, H_{arom}), 3.79 (app septet, 2 H, $^3J_{HH}$ = 7 Hz, C*H*Me$_2$), 1.43 (d, 18 H, $^3J_{HP}$ = 14 Hz, P(C*Me*$_3$)$_2$), 1.32 (d, 6 H, $^3J_{HH}$ = 7 Hz, CH*Me*$_2$) 1.07 (d, 6 H, $^3J_{HH}$ = 7 Hz, CH*Me*$_2$), 0.50 (m, 2 H, NiC*H*$_2$CH$_3$), -1.93 (m, 3H, NiCH$_2$C*H*$_3$). ^{13}C{^{1}H} NMR (125.8 MHz, benzene-d_6): δ 175.8 (C_{arom}), 150.4 (C_{arom}), 142.6 (C_{arom}), 137.8 (d, $^3J_{CP}$ = 19 Hz), 130.1 (*C*H$_{arom}$), 128.3 (overlapping with solvent, *C*H$_{arom}$), 127.1 (*C*H$_{arom}$), 125.0 (*C*H$_{arom}$), 123.5 (*C*H$_{arom}$), 36.9 (d, $^1J_{PC}$ = 30 Hz, P(*C*Me$_3$)$_2$), 28.6 (overlapping resonances, P(C*Me*$_3$)$_2$ and *C*HMe$_2$), 25.2 (CH*Me*$_2$), 22.8 (CH*Me*$_2$), 2.7 (d, $^2J_{CP}$ = 12 Hz, NiCH$_2$CH$_3$), -6.5 (d, $^3J_{CP}$ = 3 Hz, NiCH$_2$CH$_3$). ^{31}P{^{1}H} (202.5 MHz, benzene-d_6): δ 128.7.

Synthesis of (PN)Ni*n*Bu. In the glovebox, a glass vial was charged with a magnetic stirring bar, **Ni$_2$Cl$_2$** (0.058 g, 0.056 mmol), and pentane (*ca*. 4 mL). Magnetic stirring was initiated to afford a dark red-purple slurry, which was then was cooled to -35 °C. In a separate glass vial, *n*-BuLi (1.6 M in hexanes, 70 µL, 0.112 mmol) was diluted with pentane (*ca*. 2 mL) and cooled to -35 °C in the glovebox freezer. Each vial was removed from the freezer, magnetic stirring was re-initiated, and the solution containing *n*-BuLi was immediately added dropwise (*ca*. 3 drops /sec) to the slurry containing **Ni$_2$Cl$_2$**. Immediately afterwards, the vial was cooled to -35 °C. After *ca*. 60 min, the vial contained a red-orange supernatant and dark precipitate, and the contents were filtered through Celite, giving a cloudy yellow filtrate and a dark filter cake (soluble in benzene;

consisting of **Ni_2Cl_2**, **(PN)Ni*n*Bu**, and multiple unidentified phosphorus- and/or hydride-containing products). This filtrate was cooled to -35 °C. After *ca*. 4 h, additional precipitate had formed, so the filtrate was filtered again, yielding a clear orange eluent, and a yellow-orange filter cake. This filtrate was cooled at -35 °C overnight, then filtered once more. $^{31}P\{^1H\}$ NMR analysis of this pentane filtrate indicated confirmed the presence of **(PN)Ni*n*Bu** in acceptably high purity. Removal of pentane *in vacuo* yielded **(PN)Ni*n*Bu** as an orange solid. Yield: 0.02 g, 30%. Anal. Calcd for $C_{31}H_{49}N_2NiP$: C, 69.03; H, 9.16; N, 5.19. Found: C, 69.32; H, 8.87; N, 5.12. ^1H NMR (300 MHz, benzene-d_6): δ 7.66 – 7.63 (m, 2 H, H_{arom}), δ 7.02 (overlapping resonances, 3 H, H_{arom}), 6.96 – 6.90 (overlapping resonances, 3 H, H_{arom}), 3.80 (apparent septet, 2 H, $^3J_{HH}$ = 7 Hz, C*H*Me$_2$), 1.46 (d, 18 H, $^3J_{HP}$ = 14 Hz, P(C*Me*$_3$)$_2$, 1.35 (d, 6 H, $^3J_{HH}$ = 7 Hz, CH*Me*$_2$), 1.11 – 1.03 (overlapping resonances, 8 H, CH*Me*$_2$ and NiCH$_2$CH$_2$C*H*$_2$CH$_3$), 0.58 – 0.49 (overlapping resonances, 5 H, NiC*H*$_2$CH$_2$CH$_2$CH$_3$ and NiCH$_2$CH$_2$CH$_2$C*H*$_3$), -2.50 (m, 2H, NiCH$_2$C*H*$_2$CH$_2$CH$_3$). $^{13}C\{^1H\}$ NMR (75.5 MHz, benzene-d_6): δ 175.4 (N*C*N), 151.4 (C_{arom}), 142.4 (C_{arom}), 137.6 (d, $^3J_{CP}$ = 19 Hz), 130.3 (CH_{arom}), 128.3 (overlapping with solvent, CH_{arom}), 127.1 (CH_{arom}), 124.7 (CH_{arom}), 123.5 (CH_{arom}), 36.9 (d, 1 J_{PC} = 30 Hz, P(*C*Me$_3$)$_2$), 28.6 (overlapping resonances, P(C*Me*$_3$)$_2$ and *C*HMe$_2$), 25.1 (CH*Me*$_2$), 24.8 ($CH_{2\gamma}$), 14.8 ($CH_{3\delta}$), 14.6 (d, $^3J_{CP}$ = 2 Hz, $CH_{2\beta}$), 9.8 (d, $^2J_{CP}$ = 12 Hz, $CH_{2\alpha}$). $^{31}P\{^1H\}$ (121.5 MHz, benzene-d_6): δ 128.3.

Generation of (PN)Ni*n*Hex. In the glovebox, a glass vial was charged with a magnetic stirring bar, **Ni_2Cl_2** (0.054 g, 0.052 mmol), and pentane (*ca*. 6 mL). Magnetic stirring was initiated, and the resultant slurry was cooled to -35 °C. In a separate glass vial, *n*-hexyllithium (2.3 M in hexanes, 46.5 μL, 0.107 mmol, 2.05 equiv) was added to cold (-35

°C) pentane (*ca*. 4 mL), and re-cooled to -35 °C in the glovebox freezer. These vials were removed from the freezer, magnetic stirring was re-initiated, and the solution containing *n*-hexyllithium was immediately added dropwise (*ca*. 3 drops /sec) to the slurry containing **Ni$_2$Cl$_2$**. The color of the slurry turned from dark red-purple to orange over the course of the addition, and immediately afterwards, the vial was cooled to -35 °C. After 90 min, the vial was cloudy orange, and the contents were filtered through Celite, giving a cloudy orange filtrate and a dark filter cake. This filtrate was cooled to -35 °C. After *ca*. 12 h, the filtrate was filtered again, yielding a clear orange filtrate, and a dark and yellow filter cake. The filtrate was sampled for NMR, indicating presence of retained **Ni$_2$Cl$_2$**. Solvent was removed in vacuo, and resultant orange solid was brought up in cold $SiMe_4$ (*ca.* 2 mL), then filtered through Celite. Removal of solvent *in vacuo* yielded an oily dark solid which was characterized as a mixture of **(PN)Ni*n*Hex**, possible internal isomers, and **Ni$_2$Cl$_2$** in a *ca*. 7 : 1 : 1 ratio. While **(PN)Ni*n*Hex** is not claimed herein as an isolated analytically pure compound, the formation of **(PN)Ni*n*Hex** from *n*-hexyllithium in this manner provides independent support for the identity of this complex in reactions that involve **(PN)NiEt** and **(PN)Ni*n*Bu** as described in the text. ^{1}H NMR (300 MHz, benzene-d_6): δ 7.67 – 7.64 (m, 2 H, H_{arom}), 7.07 – 6.92 (overlapping resonances, 6 H, H_{arom}), 3.80 (apparent septet, 2 H, $^3J_{HH}$ = 7 Hz, C*H*Me$_2$), 1.47 (d, 18 H, $^3J_{HP}$ = 14 Hz, P(C*Me*$_3$)$_2$), 1.35 (d, 6 H, $^3J_{HH}$ = 7 Hz, CH*Me*$_2$), 1.16 – 0.57 (overlapping resonances, 17 H, CH*Me*$_2$, Ni*n*Hex), -2.45 (m, 2H, Ni*n*Hex$_\beta$). ^{13}C{^{1}H} NMR (75.5 MHz, benzene-d_6): δ 175.4 (N*C*N), 151.1 (d, $^3J_{CP}$ = 3 Hz, C_{arom}), 142.3 (C_{arom}), 137.6 (d, $^3J_{CP}$ = 19 Hz C_{arom}), 130.3 (*C*H$_{arom}$), 128.3 (overlapping with solvent, *C*H$_{arom}$), 127.1 (*C*H$_{arom}$), 124.7 (*C*H$_{arom}$), 123.6 (*C*H$_{arom}$), 36.9 (d, $^1J_{PC}$ = 30 Hz, P(*C*Me$_3$)$_2$), 32.8 (*C*H$_{2\delta}$), 31.4 (*C*H$_{2\gamma}$), 28.7 – 28.6

(overlapping resonances, P(C*Me*$_3$)$_2$ and *C*HMe$_2$), 25.1 (CH*Me*$_2$), 23.0 (CH*Me*$_2$), 22.4, (*C*H$_{2\varepsilon}$), 14.1 (CH$_{3\zeta}$), 12.8, (d, $^3J_{CP}$ = 2 Hz, *C*H$_{2\beta}$), 10.2 (d, $^2J_{CP}$ = 12 Hz, *C*H$_{2\alpha}$). ^{31}P{^{1}H} (121.5 MHz, benzene-d_6): 128.5.

Synthesis of (PN)NiNp. In the glovebox, a glass vial was charged with **Ni$_2$Cl$_2$** (100 mg, 0.097 mmol) and benzene (*ca*. 6 mL). This purple-red solution was frozen at -35 °C. In a separate vial, NpLi (0.017 mg, 0.19 mmol) was dissolved in benzene (*ca*. 2.5 mL), and frozen at -35 °C. These vials were removed from the freezer, and immediately upon the thawing of each, the solution containing NpLi was added dropwise (*ca*. 2 drops / sec) to the solution containing **Ni$_2$Cl$_2$**. The solution was allowed to stand at ambient temperature for 17 h, at which point the reaction mixture had turned brown. Following removal of benzene *in vacuo*, the resultant solid was triturated with pentane (4 x *ca.* 1 mL), extracted into pentane (*ca*. 8 mL) and filtered through Celite, leaving a dark filter cake and a red-brown filtrate. Removal of pentane *in vacuo* yielded a red-brown semicrystalline solid. Yield: 0.098 g, 93%. Crystals of **(PN)NiNp** suitable for single-crystal X-ray diffraction were grown from a concentrated solution of pentane at -35 °C. Anal. Calcd for $C_{32}H_{51}N_2NiP$ C, 69.43; H, 9.29; N, 5.06. Found: C, 69.56; H, 9.15; N, 4.70. ^{1}H NMR (500.1 MHz, benzene-d_6): δ 7.57 – 7.53 (m, 2 H, *H*$_{arom}$), 7.07 – 6.98 (overlapping resonances, 3 H, *H*$_{arom}$), 6.91 – 6.87 (overlapping resonances, 3 H, *H*$_{arom}$), 4.06 (apparent sept, 2 H, C*H*Me$_2$), 1.58 – 1.53 (overlapping resonances, 24 H, CH*Me*$_2$ and P*tBu*), 0.98 (d, 6 H, $^3J_{HH}$ = 7 Hz, CH*Me*$_2$), 0.76 (d, J = 2 Hz, 9 H, CH$_2$C*Me*$_3$), 0.12 (d, 2 H, $^3J_{HP}$ = 3 Hz, C*H*$_2$CMe$_3$). ^{13}C{^{1}H} NMR (75.47 MHz, benzene-d_6): δ 171.1 (N*C*N), 145.6 (*C*$_{arom}$), 143.5 (*C*$_{arom}$), 137.0 (d, $^3J_{CP}$ = 20 Hz, *C*$_{arom}$), 130.6 (*C*H$_{arom}$), 128.5 (*C*H$_{arom}$), 127.2 (*C*H$_{arom}$), 125.2 (*C*H$_{arom}$), 123.8 (*C*H$_{arom}$), 38.3 (d, $^1J_{CP}$ = 30 Hz,

P(*C*Me$_3$)$_2$), 32.1 (d, $^3J_{CP}$ = 2 Hz, CH$_2$*C*Me$_3$), 29.2 (CH$_2$C*Me$_3$*), 28.8 – 28.7 (overlapping resonances, P(C*Me$_3$*)$_2$ + *C*HMe$_2$), 24.9 (CH*Me$_2$*), 23.3 (CH*Me$_2$*), 9.9 (d, $^2J_{CP}$ = 26 Hz, *C*H$_2$CMe$_3$). ^{31}P{^{1}H} (202.5 MHz, benzene-d_6): 113.4.

Procedure for determining concentration effects of benzene in the formation of 5. (PN)Ni(O*t*Bu) (0.030 g, 0.054 mmol) was dissolved in benzene (750 μL). This dark green solution was split into three 250 μL portions (A, B, C) in three glass vials. Portion A was diluted with benzene (500 μL), B with benzene and cyclohexane (250 μL each), and C with cyclohexane (500 μL). Then 250 μL of a solution of Me$_2$PhSiH in cyclohexane (composed of 15 μL and 1359 μL, respectively; 0.018 mmol) was added to each, and samples A – C were transferred to NMR tubes. Conversion of **(PN)Ni(O*t*Bu)** and yields of **5** and **Ni$_2$H$_2$** were determined by use of ^{31}P qNMR methods.

General procedure for reactions involving ethylene or H$_2$. In the glovebox, a J-Young tube was charged with solvent (500 – 750 μL), metal complex (0.005 – 0.010 g), and sealed. The tube was cycled onto an evacuated Schlenk line equipped with a mercury bubbler, which was then pressurized with the desired gas (~ 1 atm). After the headspace of the tube was exposed to vacuum (*ca*. 5 sec), the contents of the tube were exposed to the gas, and the reaction was monitored by use of NMR methods. In some cases, where a higher concentration of dissolved gas was desired, the contents of the tube were degassed via three freeze-pump-thaw cycles.

4.5 Supporting Figures and Table

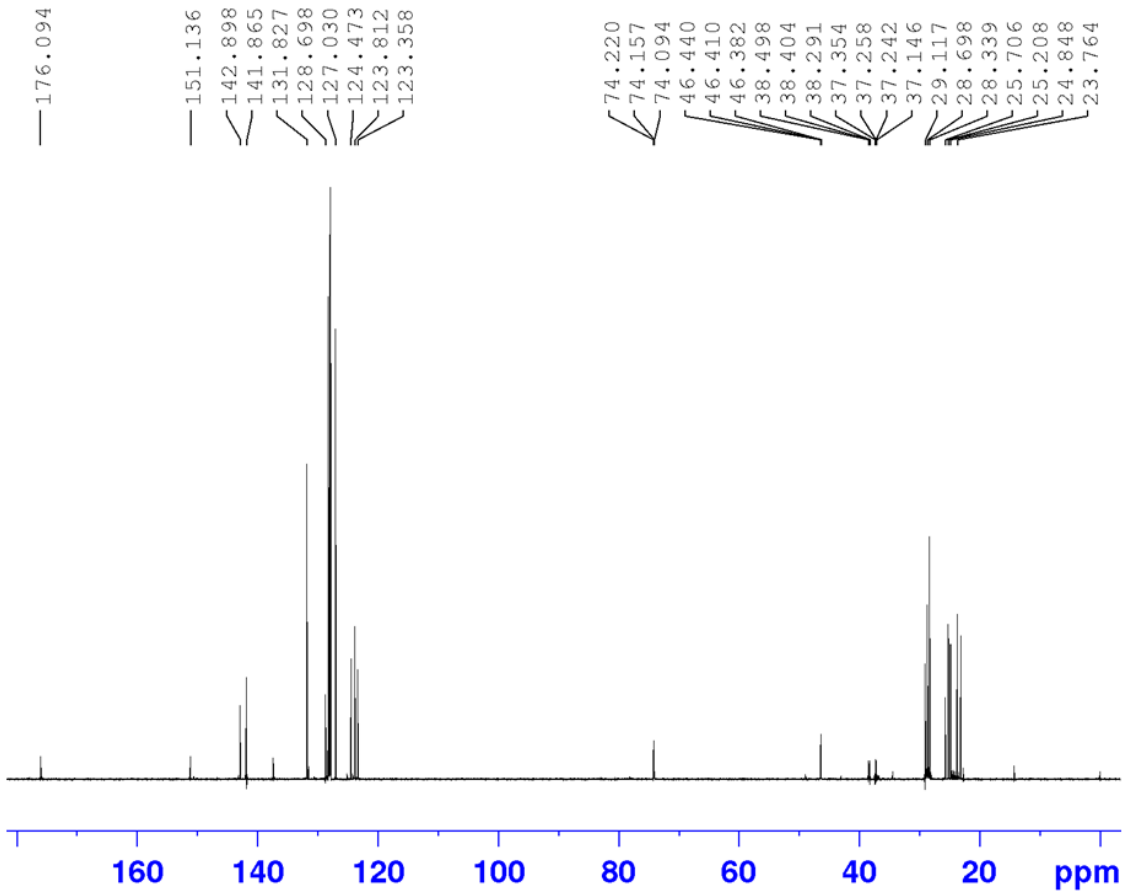

Figure S4-1. $^{13}C\{^{1}H\}$ UDEFT spectrum of 5 (125.7 MHz, benzene-d_6).

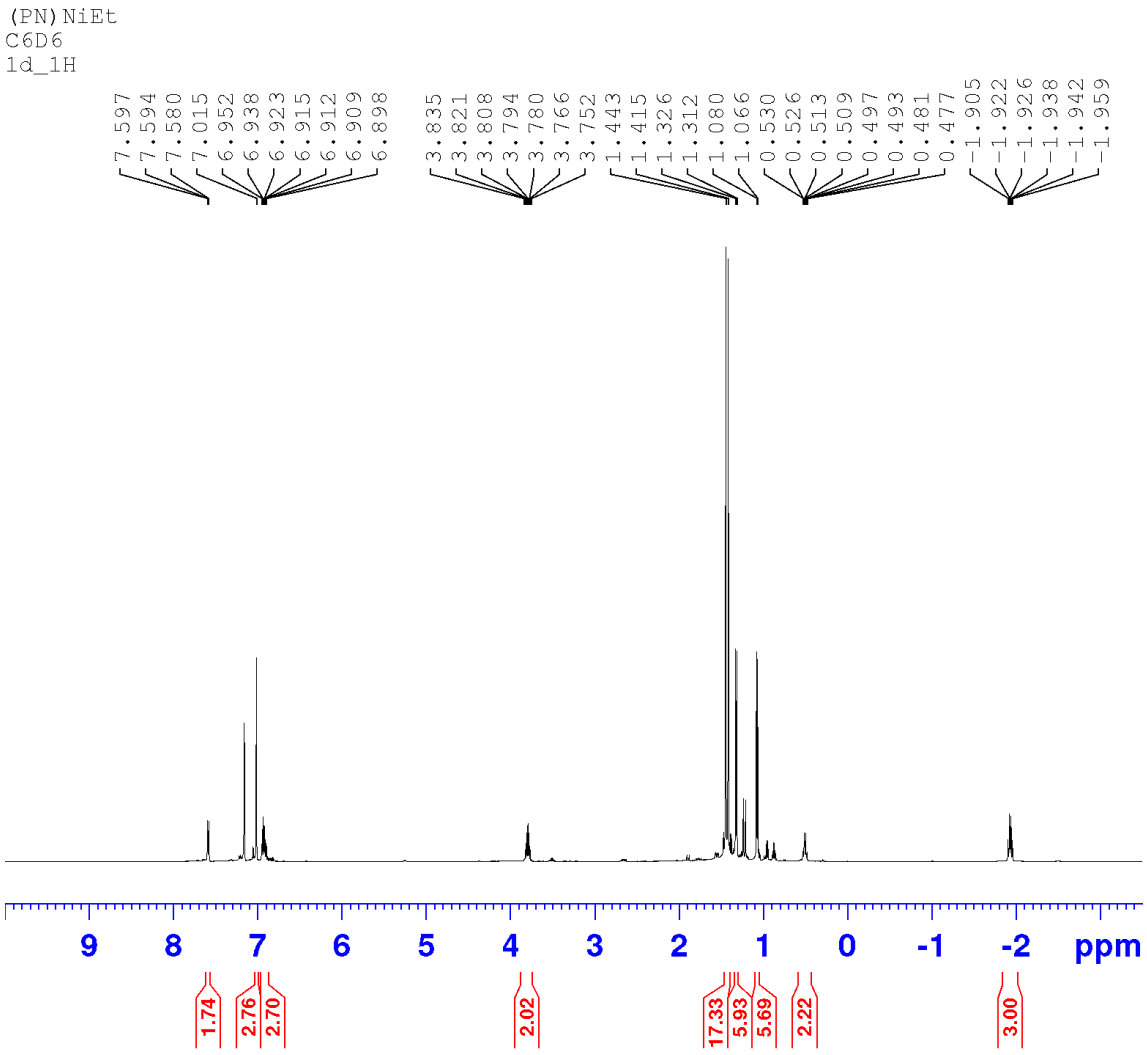

Figure S4-2. ^{1}H NMR spectrum of (PN)NiEt (500.1 MHz, benzene-d_6).

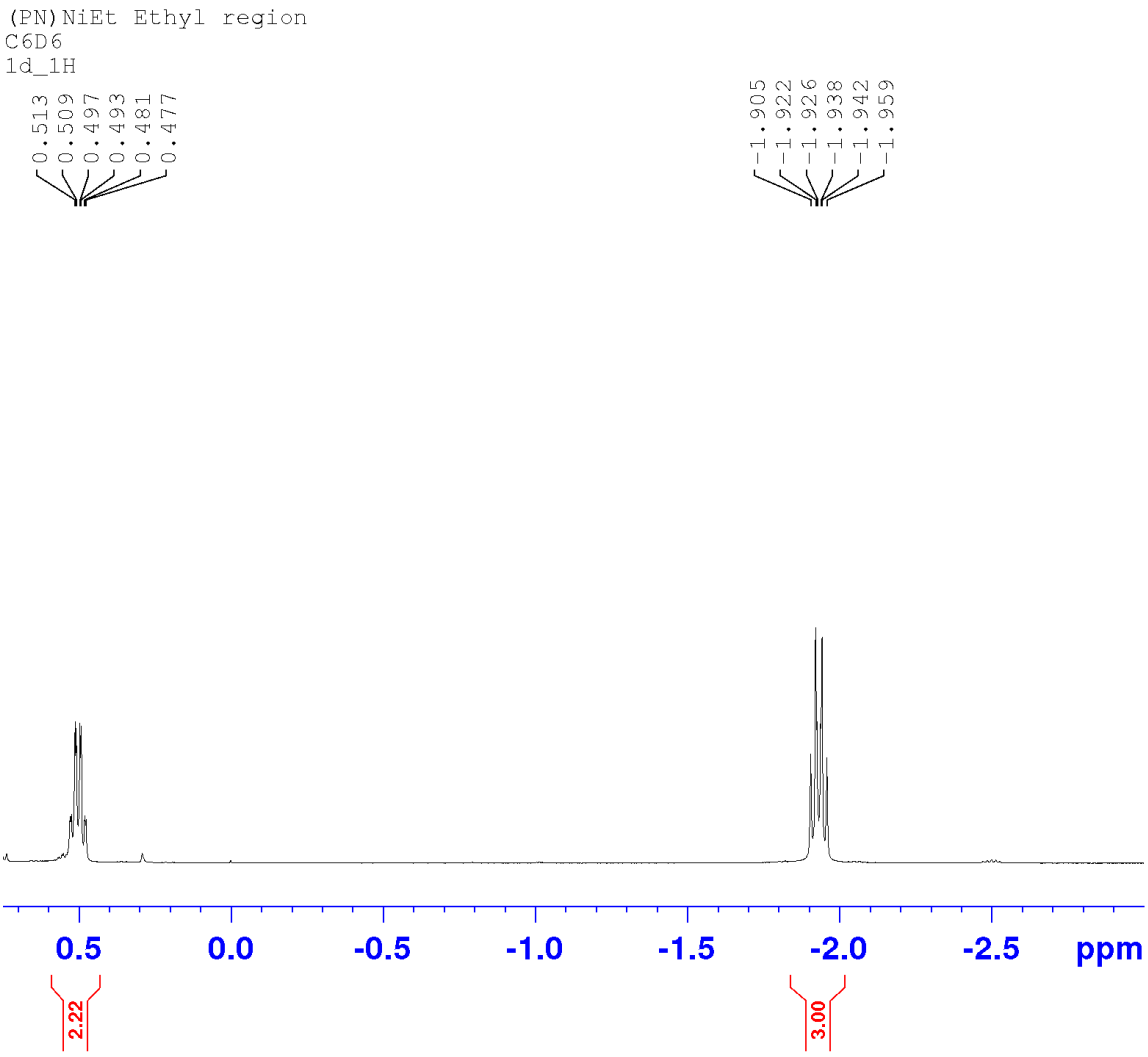

Figure S4-3. Low-frequency region of the ^{1}H NMR spectrum of (PN)NiEt (500.1 MHz, benzene-d_6).

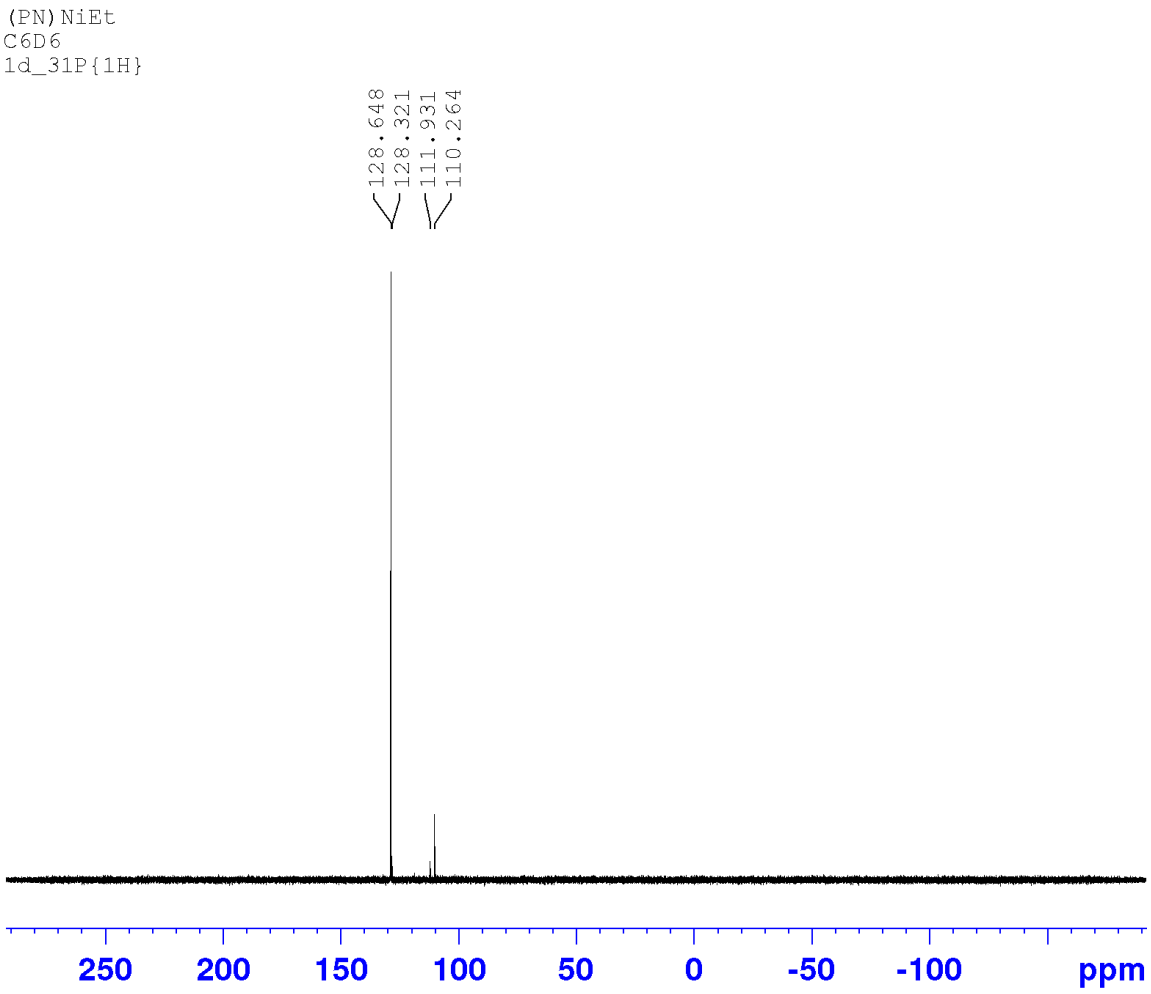

Figure S4-4. $^{31}P\{^{1}H\}$ NMR spectrum of (PN)NiEt (202.5 MHz, benzene-d_6).

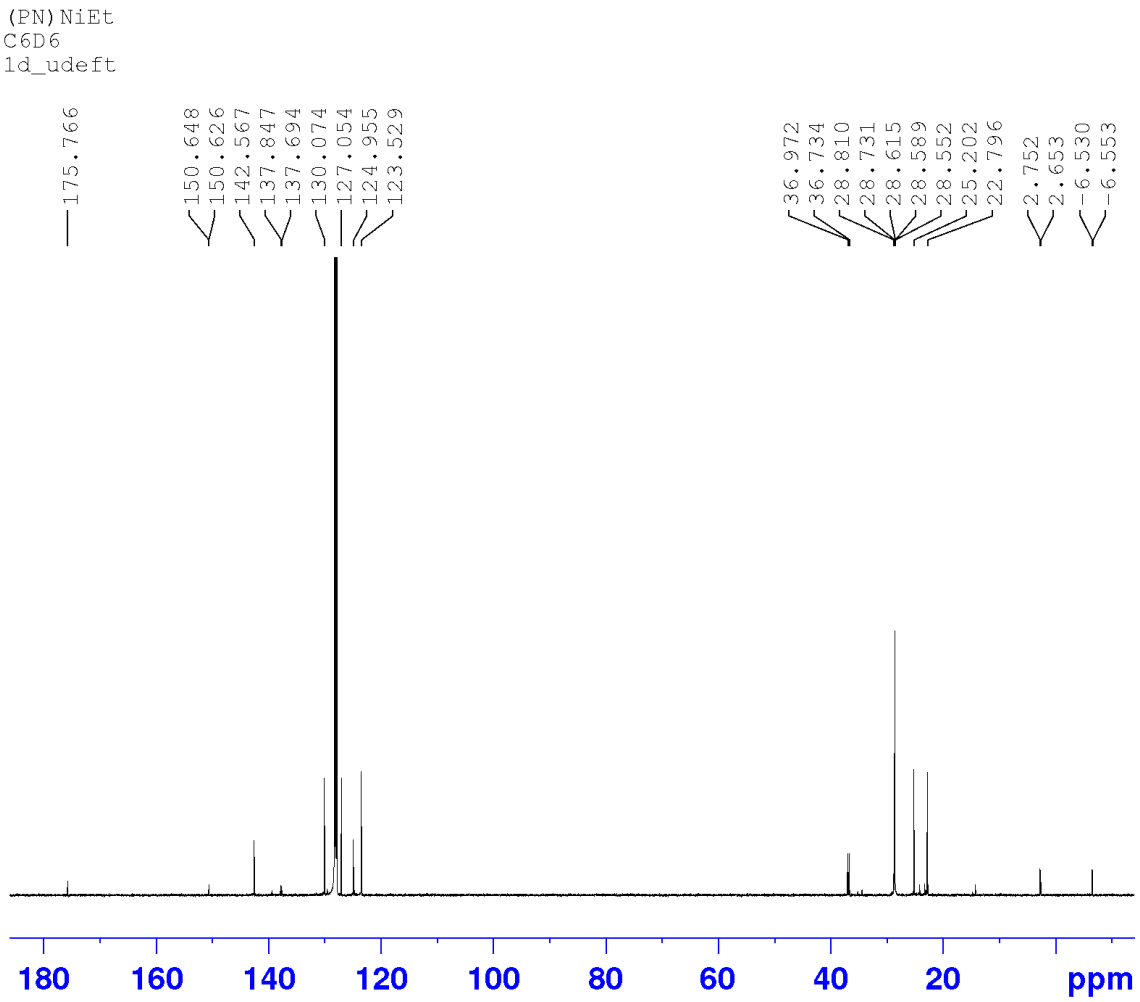

Figure S4-5. $^{13}C\{^{1}H\}$ UDEFT NMR spectrum of (PN)NiEt (75.5 MHz, benzene-d_6).

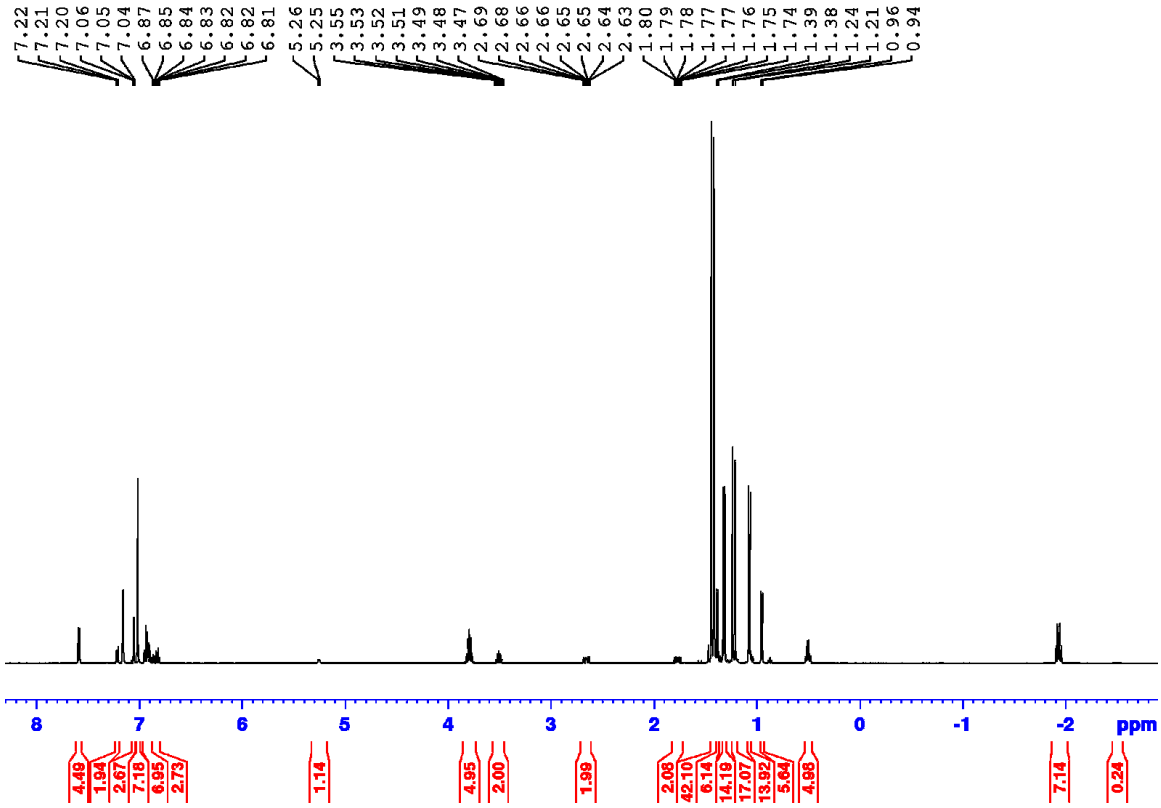

Figure S4-6. ^{1}H NMR spectrum of a mixture of (PN)NiEt, (HPN)Ni(CH_2CH_2), and (PN)Ni*n*Bu, including assigned chemical shifts for (HPN)Ni(CH_2CH_2) (500.1 MHz, benzene-d_6).

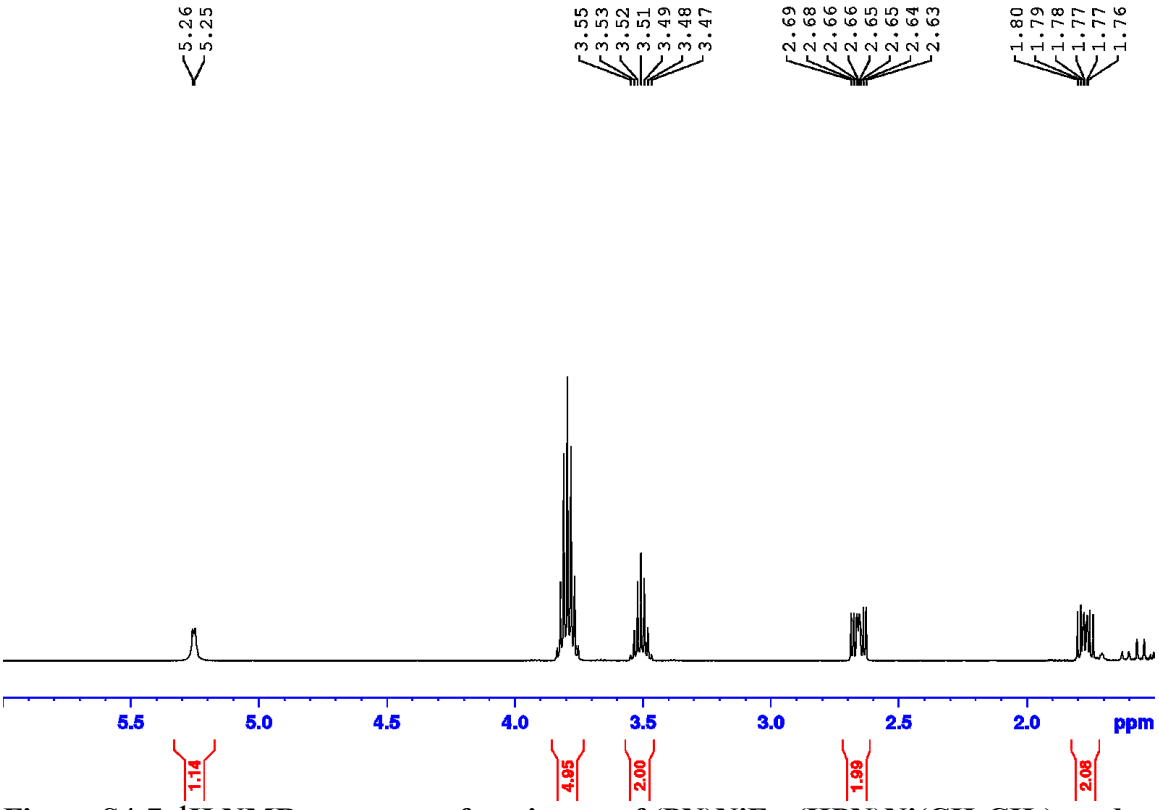

Figure S4-7. ^{1}H NMR spectrum of a mixture of (PN)NiEt, (HPN)Ni(CH_2CH_2), and (PN)Ni*n*Bu, featuring the tentatively assigned NH, methine, and ethylene resonances of (HPN)Ni(CH_2CH_2) (500.1 MHz, benzene-d_6).

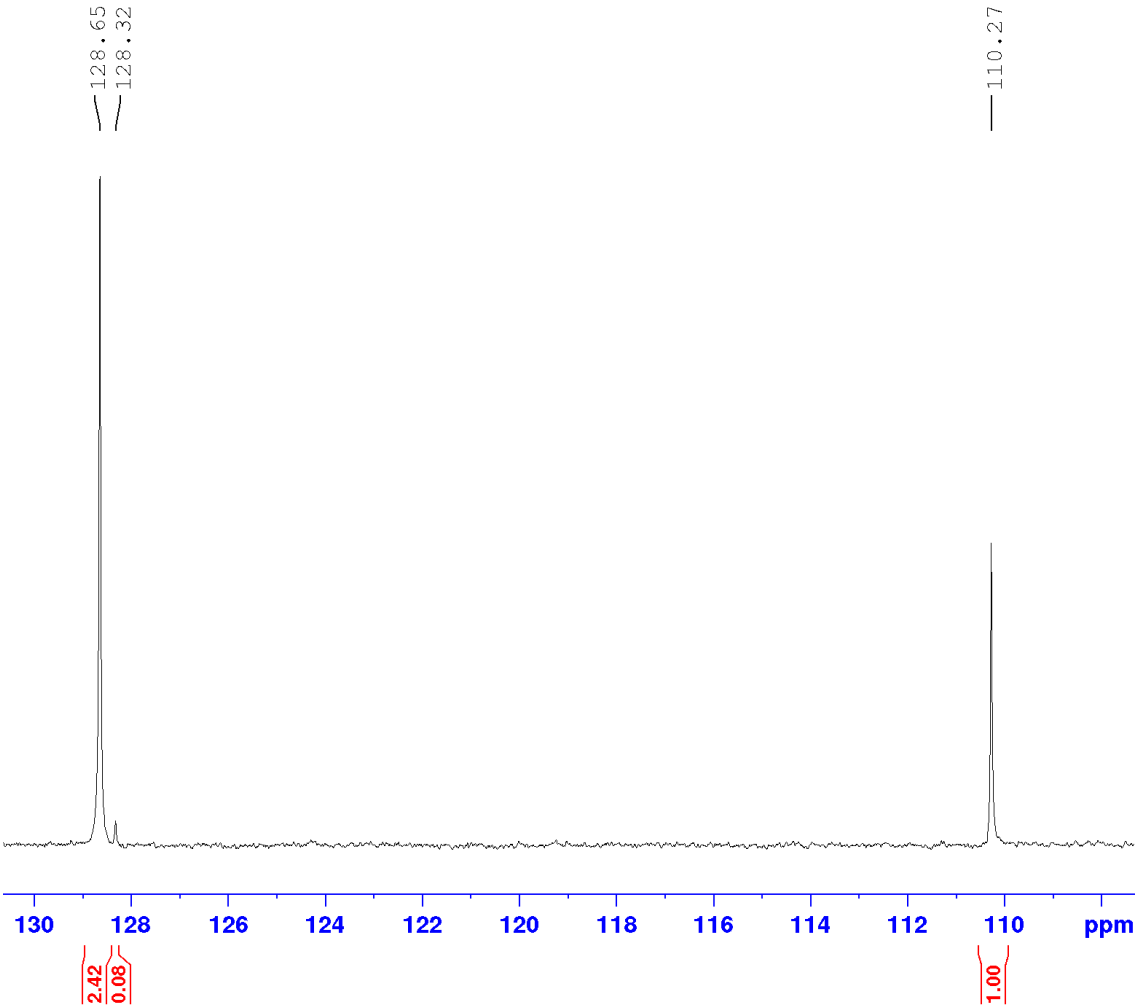

Figure S4-8. $^{31}P\{^{1}H\}$ NMR spectrum of a mixture of (PN)NiEt, (HPN)Ni(CH_2CH_2), and (PN)Ni*n*Bu (202.5 MHz, benzene-d_6).

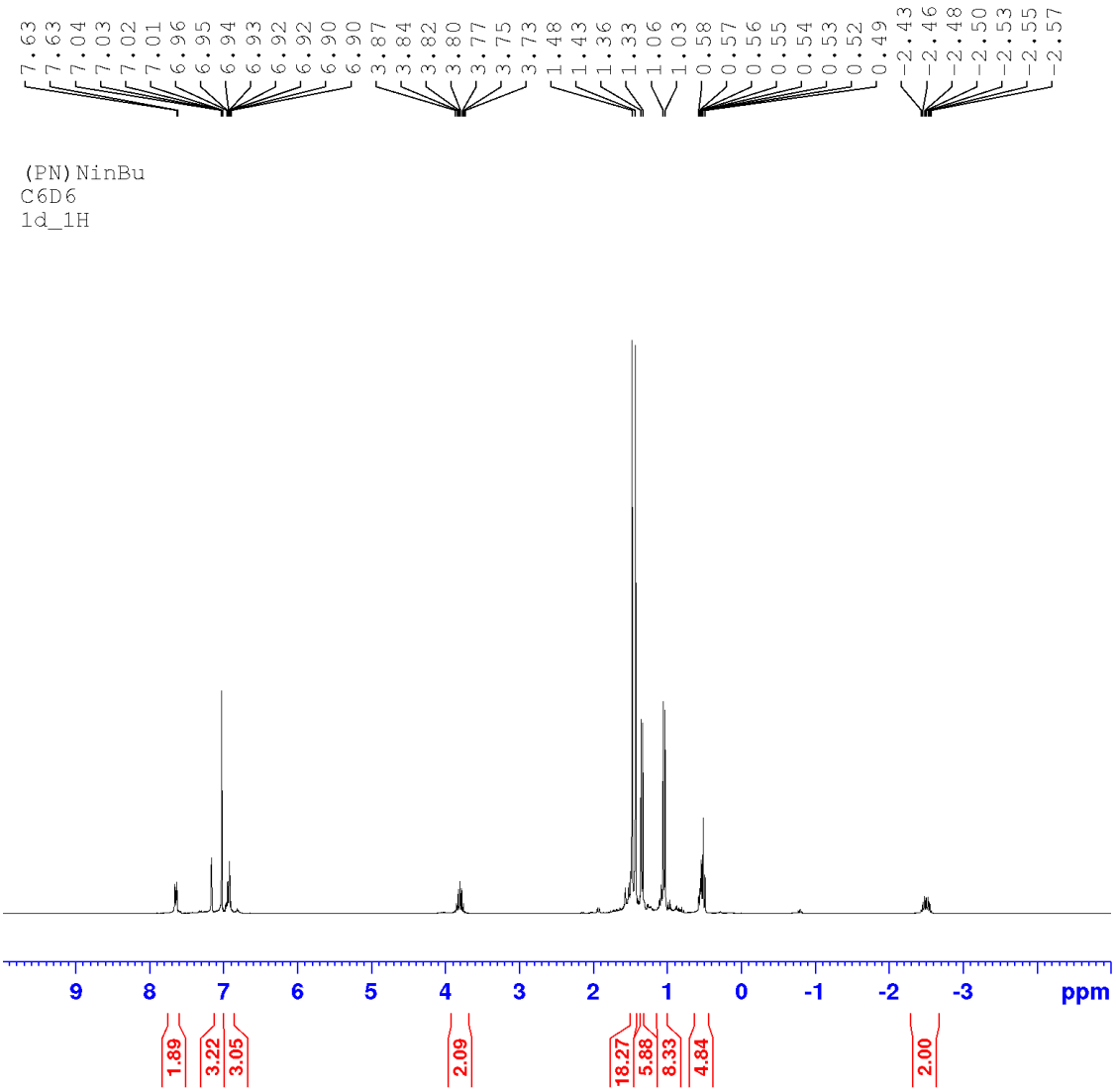

Figure S4-9. ^{1}H NMR spectrum of (PN)Ni*n*Bu (300 MHz, benzene-d_6).

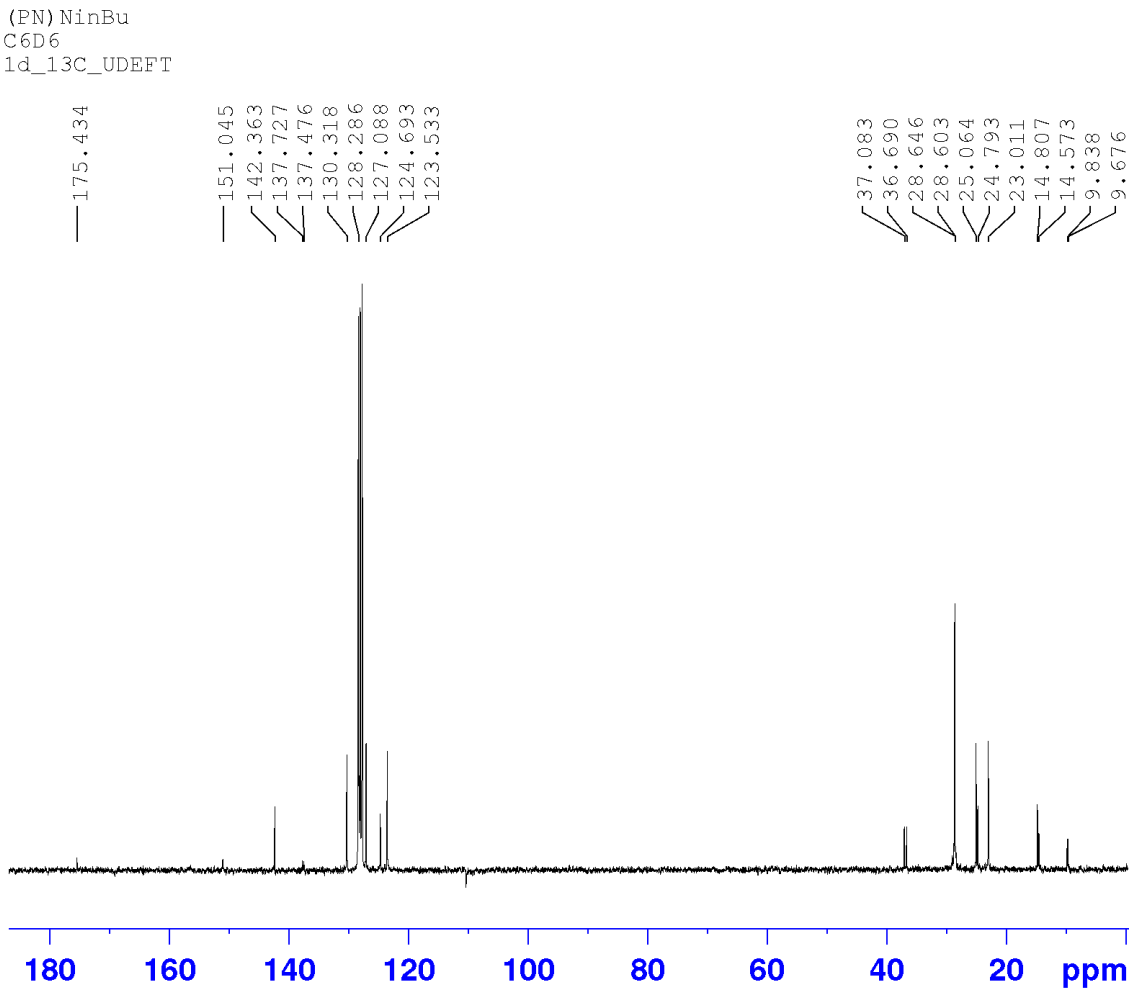

Figure S4-10. $^{13}C\{^{1}H\}$ UDEFT spectrum of (PN)Ni*n*Bu (75.5 MHz, benzene-d_6).

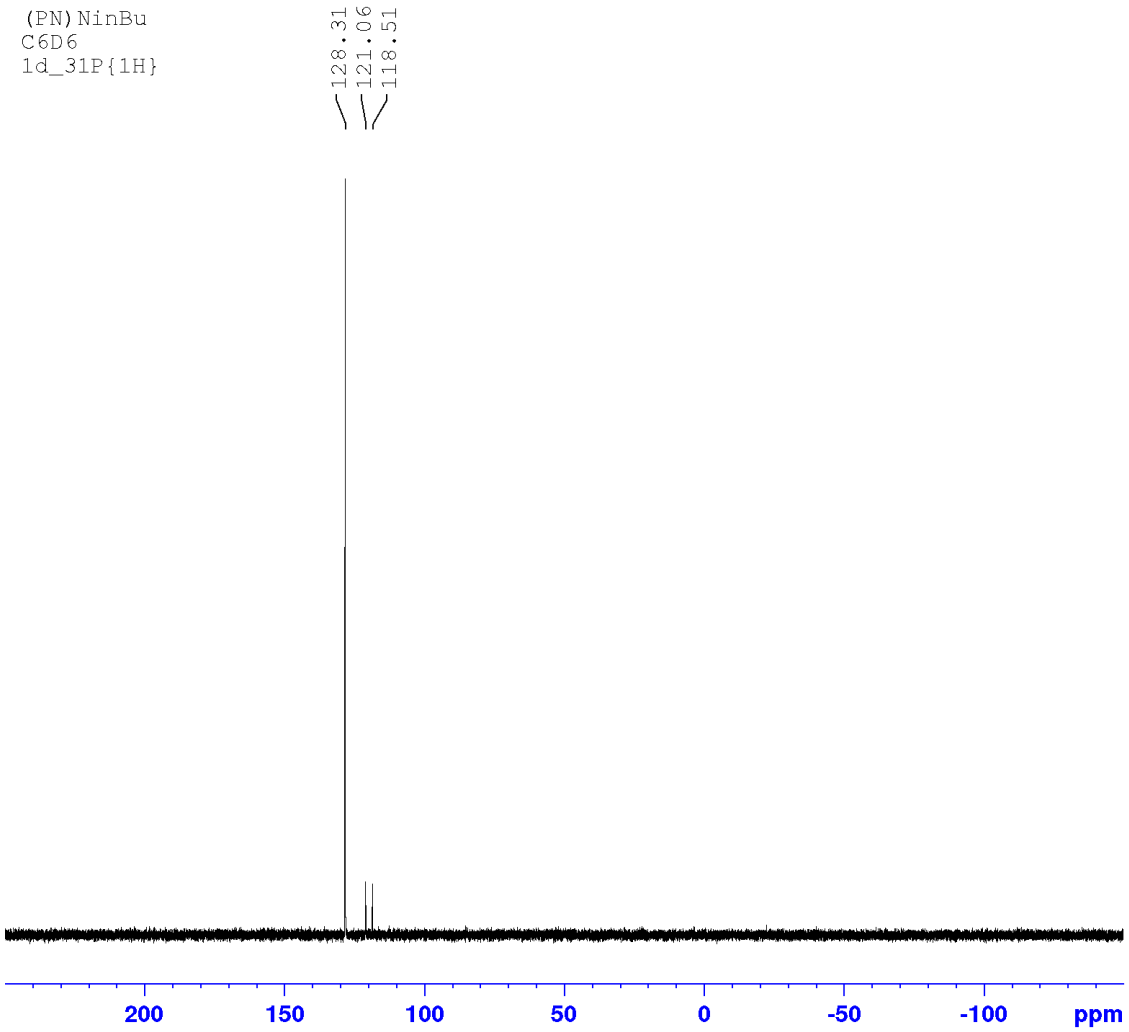

Figure S4-11. $^{31}P\{^{1}H\}$ NMR spectrum of (PN)Ni*n*Bu (121.5 MHz, benzene-d_6).

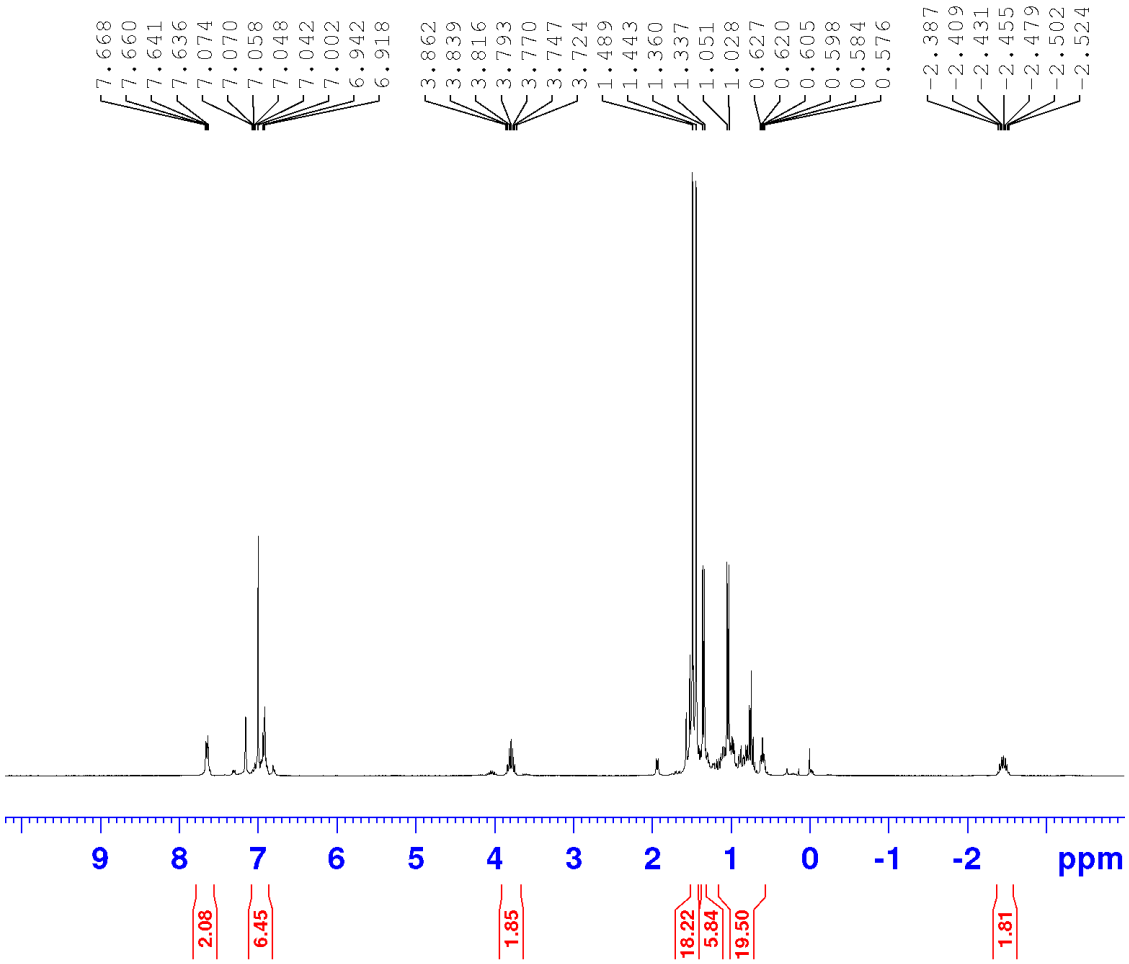

Figure S4-12. ^{1}H NMR spectrum of (PN)Ni*n*Hex (300 MHz, benzene-d_6).

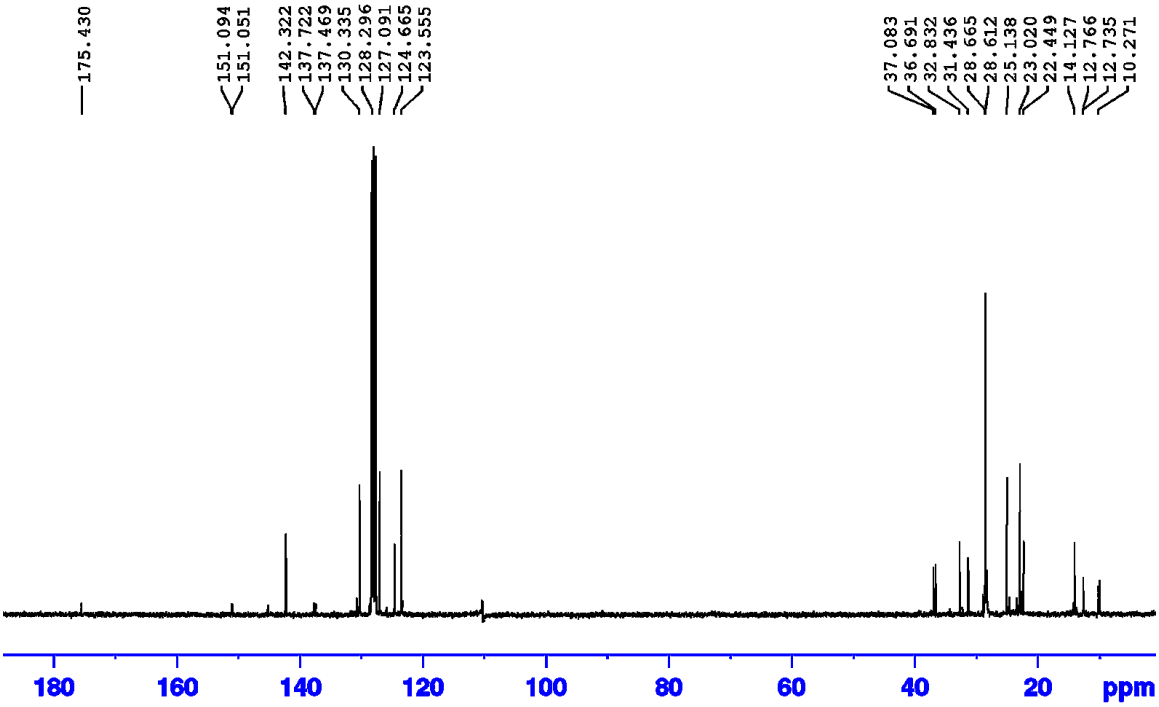

Figure S4-13. $^{13}C\{^{1}H\}$ UDEFT NMR spectrum of (PN)Ni*n*Hex (75.5 MHz, benzene-d_6).

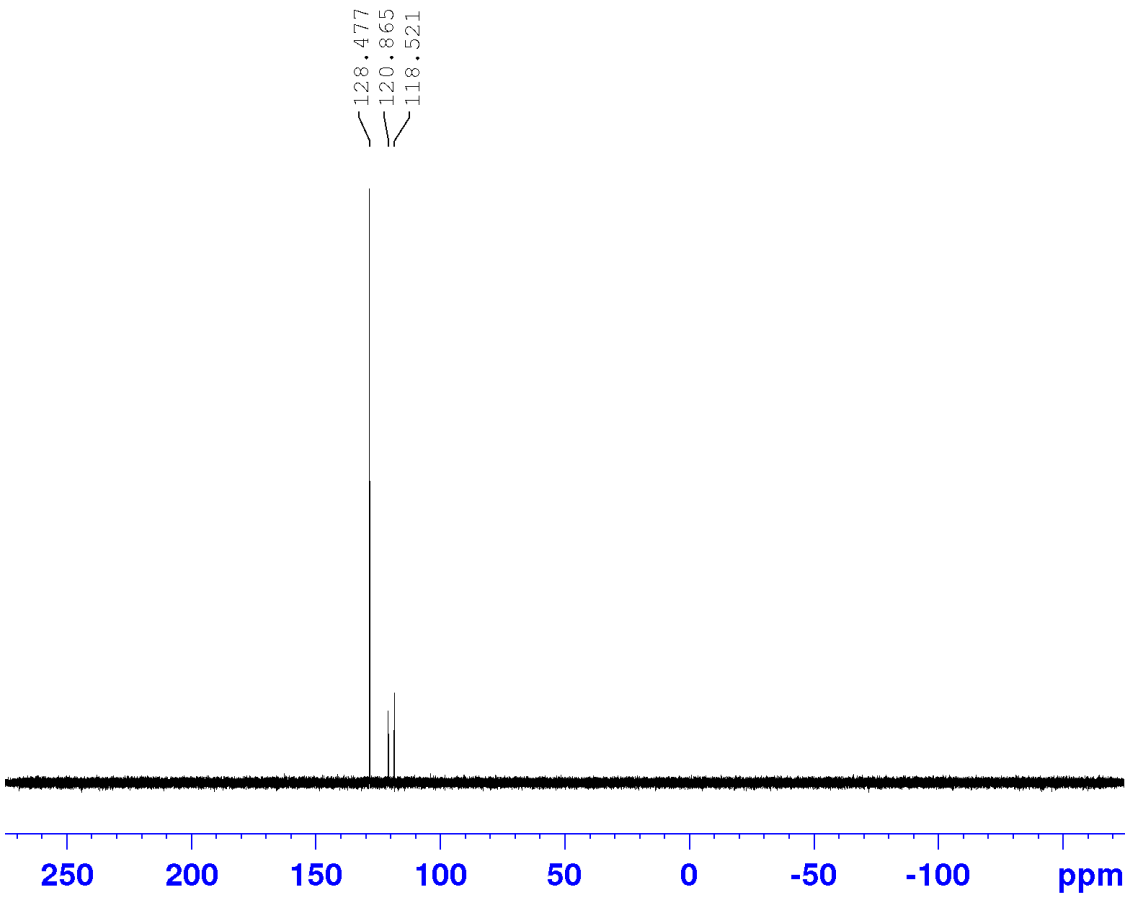

Figure S4-14. $^{31}P\{^{1}H\}$ NMR spectrum of (PN)Ni*n*Hex (121.5 MHz, benzene-d_6).

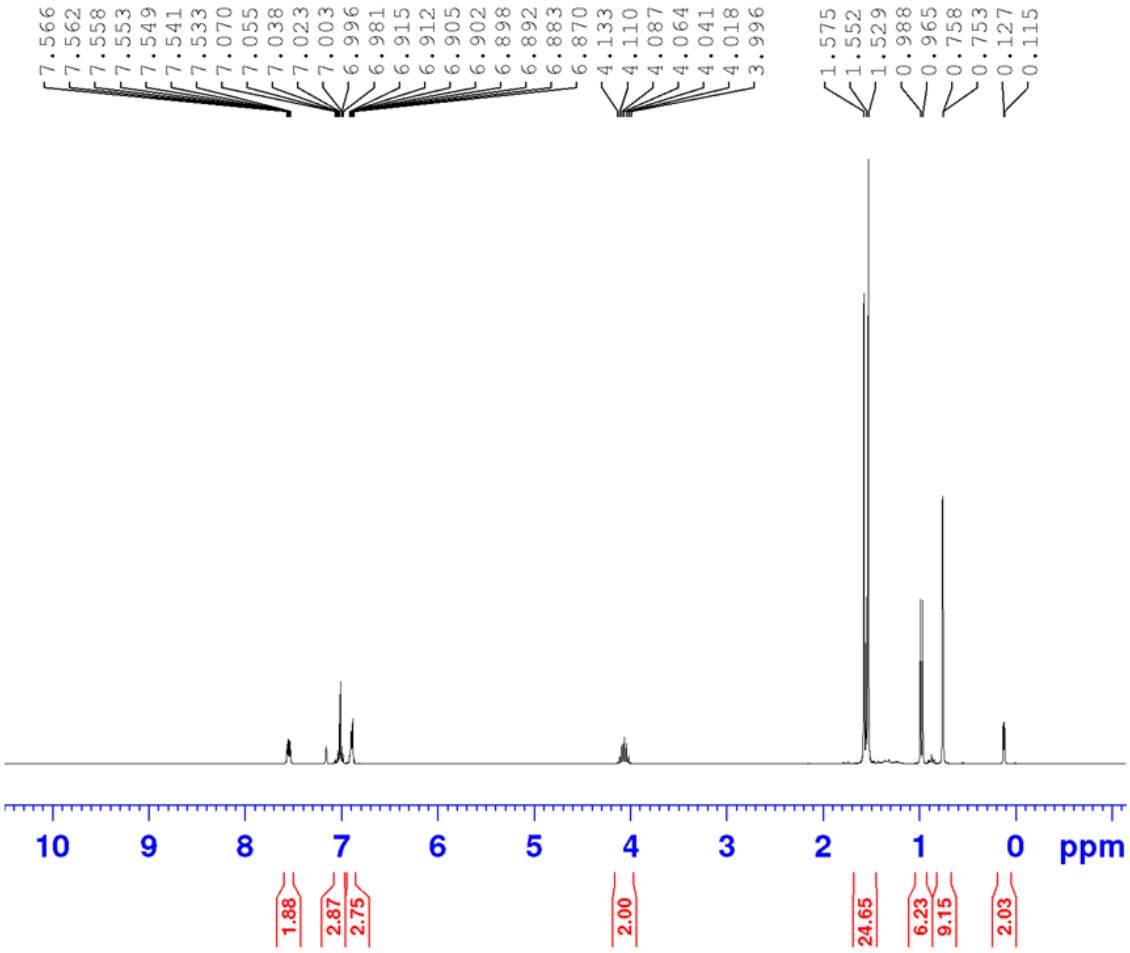

Figure S4-15. ^{1}H NMR spectrum of (PN)NiNp (300 MHz, benzene-d_6).

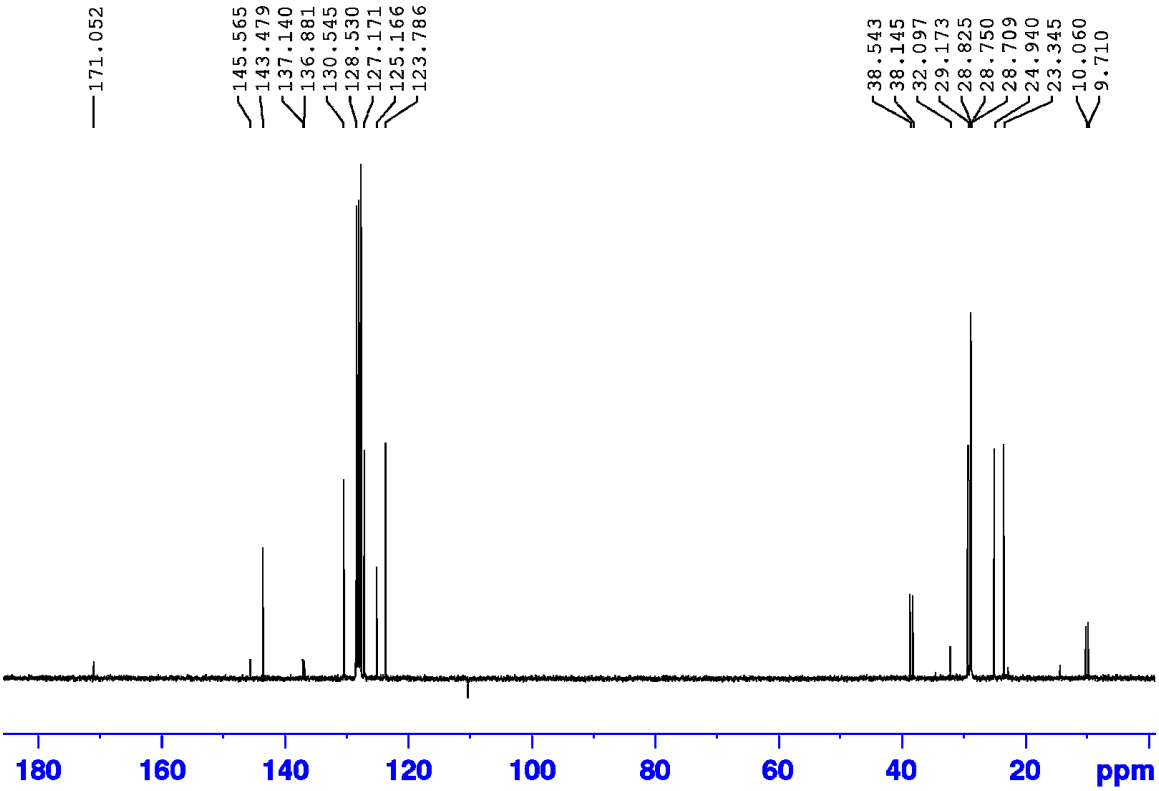

Figure S4-16. $^{13}C\{^{1}H\}$ UDEFT NMR spectrum of (PN)NiNp (75.5 MHz, benzene-d_6).

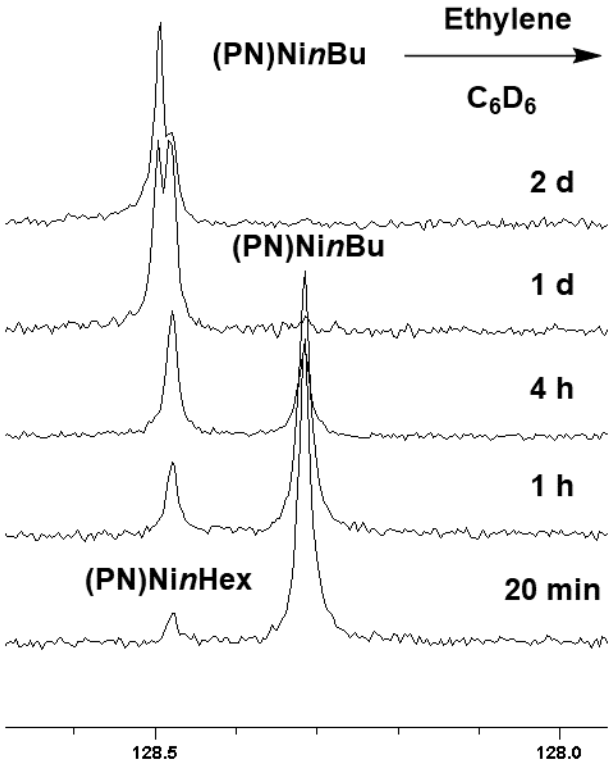

Figure S4-17. Stacked $^{31}P\{^{1}H\}$ NMR spectra of the reaction of (PN)Ni*n*Bu with ethylene (121.5 MHz, benzene-d_6; shifts in ppm).

	(PN)NiEt	(PN)Ni*n*Bu	(PN)Ni*n*Hex	(PN)NiNp
$^{1}J_{CH}$ α-CH_2 (Hz)	151	150	147	128
$^{1}J_{CH}$ β- or γ-agostic (Hz)	123 (β)	117 (β)	116 (β)	123(γ)

Table S4-1. Summary of average $^{1}J_{CH}$ coupling constants for agostic complexes (300 K).

CHAPTER 5: CONCLUSION

5.1 Chapter 2 Conclusions and Future Work

As summarized in section 2.4.3, **(PN)M** precatalysts for alkene I-H were compared experimentally and theoretically, with divergent results. While **(PN)Co** and **(PN)Fe** facilitated high activity and selectivity, **(PN)Mn** showed no activity, and **(PN)Ni** showed high activity and poor selectivity. Future work is required to fully understand these differences.

As suggested in Section 2.2.3.4, metathesis of the $N(SiMe_3)_2$ group is qualitatively slow compared to alkene I-H catalyzed by the products of this metathesis. Future work could involve incubating **(PN)M**/HBPin mixtures prior to substrate addition and comparing these reactions to where **(PN)M** is added last or involve quantifying rates of precatalyst activation. Perhaps **(PN)MX** precatalysts with smaller X groups might allow for faster activation (Scheme 5-1, bottom) analogous to the findings in Section 3.2.3. Attempts at synthesizing isolable **(PN)MH** (M = Mn, Fe, Co) derivatives for use as (pre)catalysts could help confirm their role in the proposed catalytic cycle, although these materials may require X-ray diffraction experiments to confirm connectivity, due to their likely paramagnetism. The reported Ni analogues, **Ni_2H_2**, **(PN)NiH(pyr)**, and **(PN)NiH(DMAP)** showed poor performance, so one might attempt using more labile L-donors, or a bulkier ancillary ligand, to maximize the amount of **(PN)MH** available in solution. Ideally, the L-donors would feature solubilizing groups, as these Ni analogues showed poor solubility in neat reaction mixtures or C_6H_{12} (Scheme 5-1, top). Accordingly, a more comprehensive solvent screen could plausibly find better conditions for Ni catalysis; perhaps a higher polarity, weakly coordinating solvent such as THF

would improve performance. Further analysis of decomposition products of the proposed Ni intermediates could confirm whether or not heterogeneous products are formed, such as nickel boride[133], which could be responsible for the catalytic hydrogenation observed.

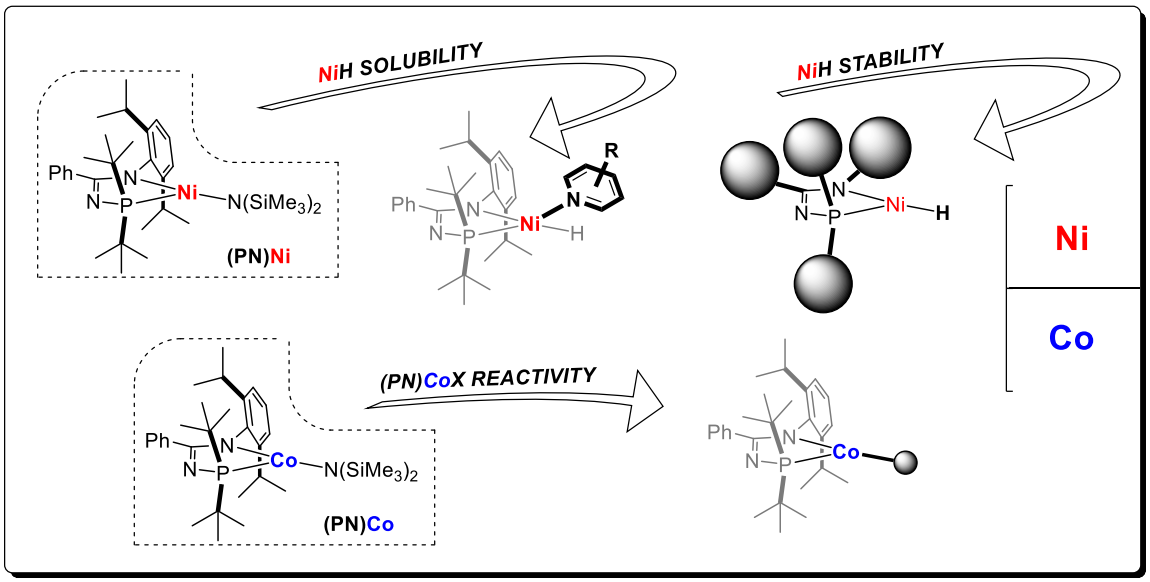

Scheme 5-1. Designs toward improved I-H (pre)catalysts.

5.2 Chapter 3 Conclusions and Future Work

As summarized in Section 3.3, iteration of **(PN)MX** precatalysts for hydrosilative amide reduction allowed for mild reduction of select tertiary and secondary amides. Future work could involve broadening the scope of amide substrates to determine the utility of this methodology. More detailed analysis, perhaps via chromatography coupled with mass spectrometry, of the products of primary amide reduction could add clarity.

Given the utility **(PN)M** precatalysts in hydrosilative amide reduction, investigations towards analogous amide hydrogenation[134] are warranted, as such processes avoid stoichiometric Si-containing waste, although they may require high pressures of H_2. Compound **5** could be applied as a **(PN)NiH** source for such catalysis without generating potentially troublesome metathesis byproducts, as it appears to

liberate **(PN)NiH** and benzene upon heating instead of otherwise reacting with a variety of substrates. Conversely, hydrogenation of a **(PN)Ni(O*t*Bu)** precatalyst would release *tert*-butanol, which contains both a relatively acidic alcohol and oxygenic lone pairs. Additionally, given the orthogonal reactivity of **5** and excess MeOH, this method may be the most practical way of preparing **(PN)NiH** in the presence of secondary or primary amides; **(PN)NiX** precatalysts might be deprotonated by the amide to form NO chelates.

Whereas **(PN)NiX** precatalysts were found to be lead candidates in hydrosilative amide reduction chemistry, Mn, Fe, and Co derivatives performed comparably in many instances. Perhaps complete derivatization and optimization of these analogues would develop complementary or superior precatalysts (Scheme 5-2, right). Based on the finding that smaller X groups helped hasten precatalyst activation with $PhSiH_3$, perhaps alterations to the PN ligand to reduce its steric bulk could further improve reaction rates or allow for use of more readily available silane substrates. While **(PN)Ni(O*t*Bu)** performed well as a precatalyst, addition of **(HPN)**, $NiCl_2$dme, and NaO*t*Bu to a mixture of amide and silane could plausibly facilitate similar chemistry and avoid several synthetic steps; this may also be an approach congruent with the synthesis and screening of a series of HPN ligand derivatives without requiring full characterization of each complex (Scheme 5-2, left). Synthesis, isolation, and application of **(PN)M(SiR_3)** complexes could help understand if such complexes are implicated in the reaction mechanism.

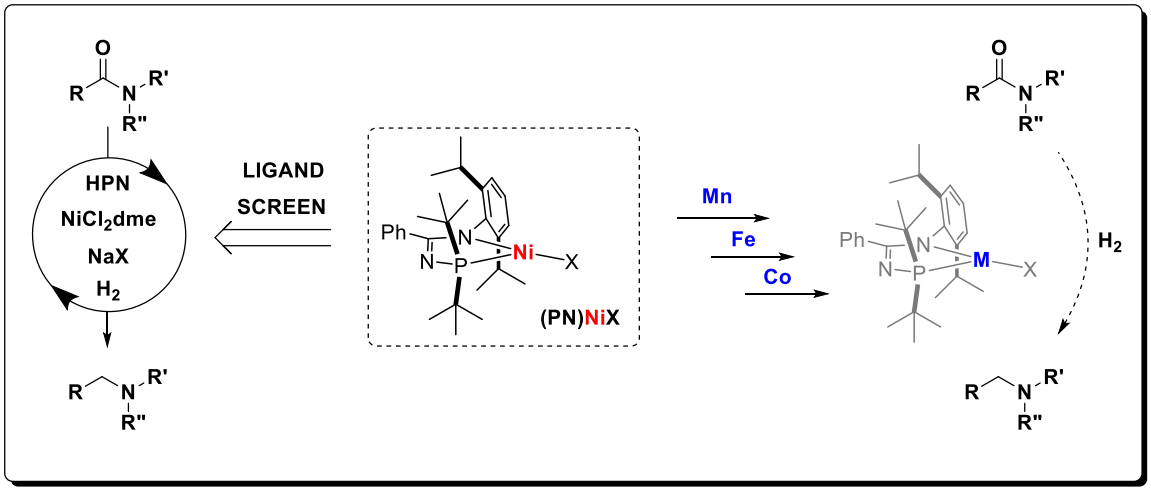

Scheme 5-2. Designs toward hydrogenative amide reduction precatalyst screening.

5.3 Chapter 4 Conclusions and Future Work

As summarized in Section 4.X, reactive screening of **(PN)NiX** complexes with hydride sources led to the isolation of **5**, a product ostensibly the result of insertions of benzene into nickel hydride bonds. Attempts to generate **(PN)NiH** *in situ* via treatment of **Ni_2Cl_2** with alkyllithium reagents instead generated the β- or γ-agostic **(PN)Ni(alkyl)** complexes. These findings lay the groundwork for future study.

A study of ligand effects on this reaction is warranted, given the possible competing reaction modes of transient **(PN)NiH**. Increased ligand sterics would plausibly inhibit both dimerization and benzene coordination; decreased ligand sterics would instead promote those reactions. Such a screen of ligand effects would help elucidate which factor is dominant for facilitating benzene insertion into the nickel hydride bond, guiding optimization of the insertion (Scheme 5-3, right). However, changes to ligand parameters may also influence BHE, the reverse reaction. Another possible pitfall for these approaches may be slight changes to electronic parameters of the derivative ligands resulting in complexes that are sensitive to reductive loss of H_2, as has been observed

with (NacNac)NiH analogues. Modifying the ligand parameters may also allow access to insertions and possibly reductions of more diverse unsaturated groups. Ligand-influenced selective insertions or reductions of polycyclic aromatic hydrocarbons[135] could be attractive targets, as these molecules represent abundant pollutants (Scheme 5-3, left).

While **5** did not appear to react with H_2 to eliminate dearomatized species, exposure of **5**, or **(PN)NiX** precursors, to higher pressures of H_2 using a Parr reactor could plausibly facilitate this reaction (Scheme 5-3, bottom).

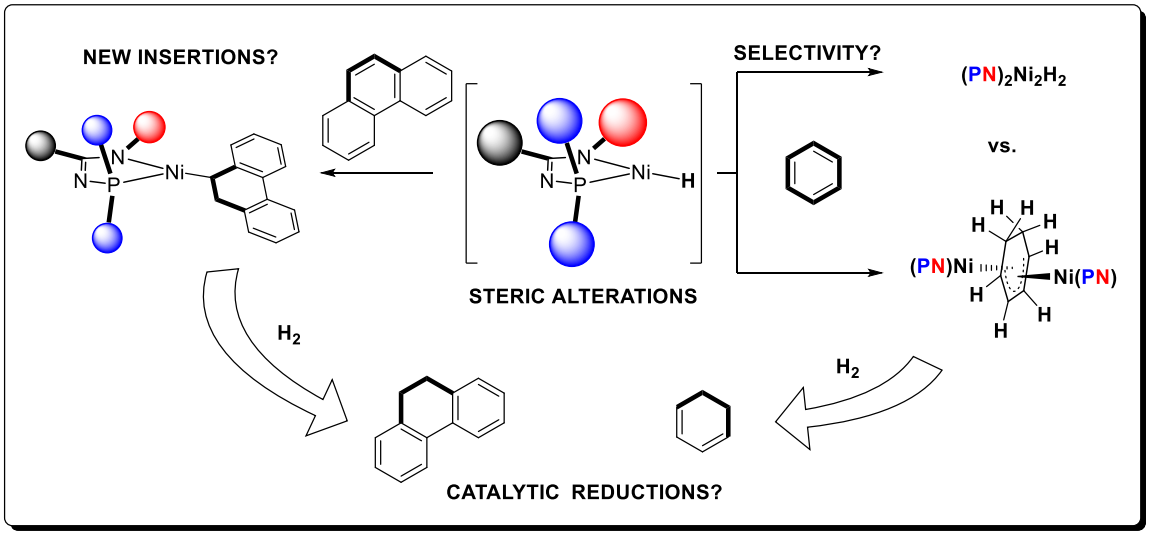

Scheme 5-3. Possible influences of steric alterations on arene insertions into Ni-H.

The apparent formation of the Ni(0) complex **(HPN)Ni(CH_2CH_2)** via decomposition of **(PN)NiEt** also raises intriguing questions (Scheme 5-4). Synthesis of deuterium-labelled **(PN)NiEt** isotopologues via salt metathesis using isotopically-labelled Grignard reagents (e.g., CD_3CD_2MgI[129a]) could lead to the formation of **(DPN)Ni(CD_2CD_2)**, and answer questions about the mechanism of this decomposition. Independent synthesis of **(HPN)Ni(CH_2CH_2)** via treatment of **(HPN)** with $Ni(COD)_2$ followed by exposure to ethylene could independently verify the connectivity of this compound and allow for experiments to determine if perhaps **(HPN)Ni(CH_2CH_2)** and

(PN)NiEt interconvert via acid/base catalysis. Additionally, treatment of **(HPN)Ni(CH_2CH_2)** with H_2 could offer access to **(HPN)Ni($H)_2$** via OA (Scheme 5-4). Mononuclear Ni(H_2) complexes, despite their implication in H_2O/H_2 electrocatalysis,[136] remain sparsely explored,[137] especially those featuring a bidentate ligand. Attempts toward related (P_2)Ni and (NacNac)Ni complexes involve elimination of H_2 to form dimeric species; perhaps the HPN ligand framework could offer stability to a mononuclear nickel dihydride.

Given the unanticipated cooperative behavior of the (PN) – (HPN) ligand system involving the *P*R_2-N position, one could envision targeted ligand modifications to reduce possible metal-ligand cooperativity. Treatment of **(PN)MX** complexes with hard, sterically available Lewis acids could generate *P*R_2-N-inhibited complexes. It may be challenging to find acids that would bind to the *P*R_2-N position selectively versus the phosphine or the metal without use of early transition metals. Introducing these acids could complicate coordination chemistry and derivation of structure-property ligand parameters. Alternatively, replacement of the (HPN) N-H group with non-protic N-R groups (e.g., R = F, CH_3) should help preserve the amidine character of the ligand even in the presence of basic substrates, potentially allowing for formation of **(XPN)NiH_2** complexes via treatment of **(XPN)NiCl_2** complexes with hydride sources (Scheme 5-4, bottom), whereas analogous treatment of **(HPN)NiCl_2** would result instead dehydrohalogenation to first generate **Ni_2Cl_2** and then **Ni_2H_2**. Finally, steric modifications to the ligand, perhaps via introduction of *ortho*-substitutions of the phenyl group or bulkier phosphine substituents, would block access to the *P*R_2-N position.

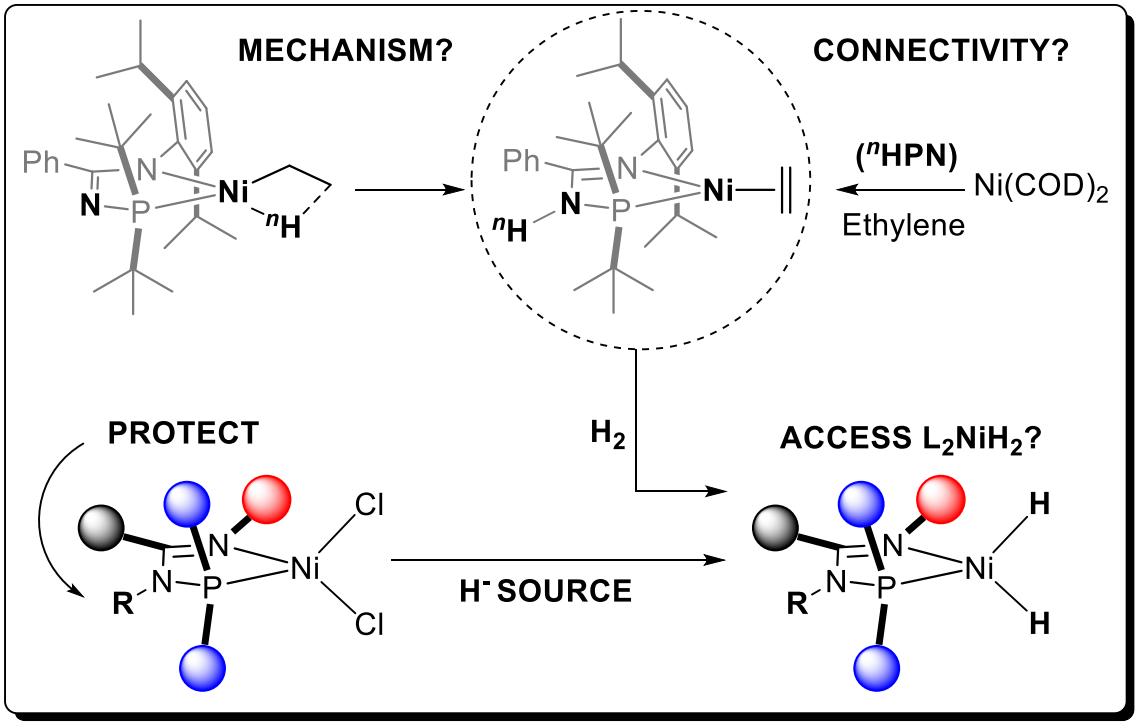

Scheme 5-4. Future work towards understanding origin of (HPN)Ni(CH_2CH_2), and possible routes towards L_2NiH_2 complexes via OA or ligand alterations.

REFERENCES

(1) Knowles, W. S. *Angew. Chem. Int. Ed.* **2002**, *41*, 1998-2007.

(2) (a) Schrock, R. R. *Angew. Chem. Int. Ed.* **2006**, *45*, 3748-3759; (b) Grubbs, R. H. *Angew. Chem. Int. Ed.* **2006**, *45*, 3760-3765; (c) Chauvin, Y. *Angew. Chem. Int. Ed.* **2006**, *45*, 3740-3747.

(3) (a) Negishi, E.-i. *Angew. Chem. Int. Ed.* **2011**, *50*, 6738-6764; (b) Wu, X.-F.; Anbarasan, P.; Neumann, H.; Beller, M. *Angew. Chem. Int. Ed.* **2010**, *49*, 9047-9050.

(4) (a) Fuerstner, A.; Leitner, A.; Mendez, M.; Krause, H. *J. Am. Chem. Soc.* **2002**, *124*, 13856-13863; (b) Bolm, C.; Legros, J.; Le Paih, J.; Zani, L. *Chem. Rev.* **2004**, *104*, 6217-6254; (c) Jana, R.; Pathak, T. P.; Sigman, M. S. *Chem. Rev.* **2011**, *111*, 1417-1492; (d) Tasker, S. Z.; Standley, E. A.; Jamison, T. F. *Nature* **2014**, *509*, 299-309.

(5) Negishi, E.-i.; Baba, S. *J. Chem. Soc. D* **1976**, 596-597.

(6) Magano, J.; Dunetz, J. R. *Chem. Rev.* **2011**, *111*, 2177-2250.

(7) (a) Lavoie, C. M.; McDonald, R.; Johnson, E. R.; Stradiotto, M. *Adv. Synth. Catal.* **2017**, *359*, 2972-2980; (b) Chong, E.; Kampf, J. W.; Ariafard, A.; Canty, A. J.; Sanford, M. S. *J. Am. Chem. Soc.* **2017**, *139*, 6058-6061; (c) Matthew, C.; Daniela, B.; Y.-C., C. J.; P., R. A.; J., T. N.; Colin, N.; Michael, S. *Angew. Chem. Int. Ed.* **2009**, *48*, 290-294; (d) Vladimir, D.; Anthony, L. *Angew. Chem. Int. Ed.* **2003**, *42*, 2631-2633; (e) Klein, H.-F.; Bickelhaupt, A.; Jung, T.; Cordier, G. *Organometallics* **1994**, *13*, 2557-2559; (f) Martinez, G. E.; Ocampo, C.; Park, Y. J.; Fout, A. R. *J. Am. Chem. Soc.* **2016**, *138*, 4290-4293; (g) Camasso, N. M.; Sanford, M. S. *Science* **2015**, *347*, 1218-1220.

(8) Neese, F. *Coord. Chem. Rev.* **2009**, *253*, 526-563.

(9) Bruin, B. d.; Gualco, P.; Paul, N. D. In *Ligand Design in Metal Chemistry*; John Wiley & Sons, Inc.: 2016.

(10) (a) Lagaditis, P. O.; Lough, A. J.; Morris, R. H. *Inorg. Chem.* **2010**, *49*, 10057-10066; (b) Lagaditis, P. O.; Lough, A. J.; Morris, R. H. *J. Am. Chem. Soc.* **2011**, *133*, 9662-9665; (c) Mikhailine, A.; Lough, A. J.; Morris, R. H. *J. Am. Chem. Soc.* **2009**, *131*, 1394-1395; (d) Zuo, W.; Lough, A. J.; Li, Y. F.; Morris, R. H. *Science* **2013**, *342*, 1080-1083.

(11) Page, M. I.; Jencks, W. P. *Proc. Natl. Acad. Sci. U.S.A.* **1971**, *68*, 1678-1683.

(12) Orpen, A. G.; Connelly, N. G. *Organometallics* **1990**, *9*, 1206-1210.

(13) Tolman, C. A. *Chem. Rev.* **1977**, *77*, 313-348.

(14) Osborn, J. A.; Jardine, F. H.; Young, J. F.; Wilkinson, G. *J. Chem. Soc. A* **1966**, 1711-1732.

(15) Milstein, D.; Stille, J. K. *J. Am. Chem. Soc.* **1979**, *101*, 4992-4998.

(16) Miyaura, N.; Suzuki, A. *Chem. Rev.* **1995**, *95*, 2457-2483.

(17) Heck, R. F. In *Organic Reactions*; John Wiley & Sons, Inc.: 2004.

(18) Arduengo, A. J.; Harlow, R. L.; Kline, M. *J. Am. Chem. Soc.* **1991**, *113*, 361-363.

(19) Jacobsen, H.; Correa, A.; Poater, A.; Costabile, C.; Cavallo, L. *Coord. Chem. Rev.* **2009**, *253*, 687-703.

(20) Trnka, T. M.; Grubbs, R. H. *Acc. Chem. Res.* **2001**, *34*, 18-29.

(21) Higman, C. S.; Lummiss, J. A. M.; Fogg, D. E. *Angew. Chem. Int. Ed.* **2016**, *55*, 3552-3565.

(22) (a) Ayme, J.-F.; Beves, J. E.; Campbell, C. J.; Leigh, D. A. *Chem. Soc. Rev.* **2013**, *42*, 1700-1712; (b) Ayme, J.-F.; Gil-Ramírez, G.; Leigh, D. A.; Lemonnier, J.-F.; Markevicius, A.; Muryn, C. A.; Zhang, G. *J. Am. Chem. Soc.* **2014**, *136*, 13142-13145.

(23) Liu, Y.; Wang, L.; Deng, L. *Organometallics* **2015**, *34*, 4401-4407.

(24) Knowles, W. S. *Acc. Chem. Res.* **1983**, *16*, 106-112.

(25) Dang, T. P.; Kagan, H. B. *J. Chem. Soc. D* **1971**, 481-481.

(26) Noyori, R.; Takaya, H. *Acc. Chem. Res.* **1990**, *23*, 345-350.

(27) Wolfe, J. P.; Wagaw, S.; Buchwald, S. L. *J. Am. Chem. Soc.* **1996**, *118*, 7215-7216.

(28) (a) Burk, M. J.; Casy, G.; Johnson, N. B. *J. Org. Chem.* **1998**, *63*, 6084-6085; (b) Burk, M. J.; Feaster, J. E. *J. Am. Chem. Soc.* **1992**, *114*, 6266-6267; (c) Burk, M. J.; Feaster, J. E.; Nugent, W. A.; Harlow, R. L. *J. Am. Chem. Soc.* **1993**, *115*, 10125-10138.

(29) (a) Fox, J. M.; Huang, X.; Chieffi, A.; Buchwald, S. L. *J. Am. Chem. Soc.* **2000**, *122*, 1360-1370; (b) Kranenburg, M.; van der Burgt, Y. E. M.; Kamer, P. C. J.; van

Leeuwen, P. W. N. M.; Goubitz, K.; Fraanje, J. *Organometallics* **1995**, *14*, 3081-3089; (c) Yin, J.; Buchwald, S. L. *J. Am. Chem. Soc.* **2002**, *124*, 6043-6048.

(30) (a) Lavoie, C. M.; MacQueen, P. M.; Rotta-Loria, N. L.; Sawatzky, R. S.; Borzenko, A.; Chisholm, A. J.; Hargreaves, B. K. V.; McDonald, R.; Ferguson, M. J.; Stradiotto, M. *Nat. Commun.* **2016**, *7*; (b) Lavoie, C. M.; Stradiotto, M. *ACS Catal.* **2018**, *8*, 7228-7250.

(31) (a) Parks, J. E.; Holm, R. H. *Inorg. Chem.* **1968**, *7*, 1408-1416; (b) McGeachin, S. G. *Can. J. Chem.* **1968**, *46*, 1903-1912.

(32) Bourget-Merle, L.; Lappert, M. F.; Severn, J. R. *Chem. Rev.* **2002**, *102*, 3031-3066.

(33) Pearson, R. G. *J. Chem. Ed.* **1987**, *64*, 561.

(34) Braunstein, P.; Naud, F. *Angew. Chem. Int. Ed.* **2001**, *40*, 680-699.

(35) Carroll, M. P.; Guiry, P. J. *Chem. Soc. Rev.* **2014**, *43*, 819-833.

(36) Braunstein, P.; Naud, F.; Rettig, S. J. *New J. Chem.* **2001**, *25*, 32-39.

(37) Keim, W. *Angew. Chem. Int. Ed.* **2013**, *52*, 12492-12496.

(38) Heyndrickx, W.; Occhipinti, G.; Minenkov, Y.; Jensen, V. R. *Chem. Eur. J.* **2011**, *17*, 14628-14642.

(39) (a) Younkin, T. R.; Connor, E. F.; Henderson, J. I.; Friedrich, S. K.; Grubbs, R. H.; Bansleben, D. A. *Science* **2000**, *287*, 460-462; (b) Xi, Z.; Bazzi, H. S.; Gladysz, J. A. *J. Am. Chem. Soc.* **2015**, *137*, 10930-10933.

(40) Ansell, C. W. G.; McPartlin, M.; Tasker, P. A.; Cooper, M. K.; Duckworth, P. A. *Inorganica Chim. Acta* **1983**, *76*, L135.

(41) Chen, M.-T.; Lee, W.-Y.; Tsai, T.-L.; Liang, L.-C. *Organometallics* **2014**, *33*, 5852-5862.

(42) Tran, B. L.; Pink, M.; Mindiola, D. J. *Organometallics* **2009**, *28*, 2234-2243.

(43) (a) Schmid, B.; Ribbe, M. W.; Einsle, O.; Yoshida, M.; Thomas, L. M.; Dean, D. R.; Rees, D. C.; Burgess, B. K. *Science* **2002**, *296*, 352-356; (b) Holland, P. L. *Can. J. Chem.* **2005**, *83*, 296-301.

(44) (a) Andres, H.; Bominaar, E. L.; Smith, J. M.; Eckert, N. A.; Holland, P. L.; Münck, E. *J. Am. Chem. Soc.* **2002**, *124*, 3012-3025; (b) Holland, P. L.; Cundari, T. R.; Perez, L. L.; Eckert, N. A.; Lachicotte, R. J. *J. Am. Chem. Soc.* **2002**, *124*, 14416-14424.

(45) Pfirrmann, S.; Limberg, C.; Herwig, C.; Stößer, R.; Ziemer, B. *Angew. Chem. Int. Ed.* **2009**, *48*, 3357-3361.

(46) Shannon, R. *Acta Cryst. A* **1976**, *32*, 751-767.

(47) Eckert, N. A.; Bones, E. M.; Lachicotte, R. J.; Holland, P. L. *Inorg. Chem.* **2003**, *42*, 1720-1725.

(48) Crabtree, R. In *The Organometallic Chemistry of the Transition Metals* 2005.

(49) Ding, K.; Brennessel, W. W.; Holland, P. L. *J. Am. Chem. Soc.* **2009**, *131*, 10804-10805.

(50) Léonard, N. G.; Chirik, P. J. *ACS Catal.* **2018**, *8*, 342-348.

(51) Keim, W.; Kowaldt, F. H.; Goddard, R.; Krüger, C. *Angew. Chem. Int. Ed.* **1978**, *17*, 466-467.

(52) Eberhardt, N. A.; Guan, H. *Chem. Rev.* **2016**, *116*, 8373-8426.

(53) MacInnis, M. C.; McDonald, R.; Ferguson, M. J.; Tobisch, S.; Turculet, L. *J. Am. Chem. Soc.* **2011**, *133*, 13622-13633.

(54) Murphy, L. J.; Hollenhorst, H.; McDonald, R.; Ferguson, M.; Lumsden, M. D.; Turculet, L. *Organometallics* **2017**, *36*, 3709-3720.

(55) Mitton, S. J.; McDonald, R.; Turculet, L. *Angew. Chem. Int. Ed.* **2009**, *48*, 8568-8571.

(56) Morgan, E.; MacLean, D. F.; McDonald, R.; Turculet, L. *J. Am. Chem. Soc.* **2009**, *131*, 14234-14236.

(57) Zhang, J.; Leitus, G.; Ben-David, Y.; Milstein, D. *Angew. Chem. Int. Ed.* **2006**, *45*, 1113-1115.

(58) Chakraborty, S.; Zhang, J.; Krause, J. A.; Guan, H. *J. Am. Chem. Soc.* **2010**, *132*, 8872-8873.

(59) (a) Zhang, G.; Scott, B. L.; Hanson, S. K. *Angew. Chem. Int. Ed.* **2012**, *51*, 12102-12106; (b) Zhang, G.; Vasudevan, K. V.; Scott, B. L.; Hanson, S. K. *J. Am. Chem. Soc.* **2013**, *135*, 8668-8681.

(60) Friedfeld, M. R.; Shevlin, M.; Hoyt, J. M.; Krska, S. W.; Tudge, M. T.; Chirik, P. J. *Science* **2013**, *342*, 1076-1080.

(61) Church, T. L.; Andersson, P. G. *Coord. Chem. Rev.* **2008**, *252*, 513-531.

(62) Friedfeld, M. R.; Zhong, H.; Ruck, R. T.; Shevlin, M.; Chirik, P. J. *Science* **2018**, *360*, 888-893.

(63) Gao, J.-X.; Ikariya, T.; Noyori, R. *Organometallics* **1996**, *15*, 1087-1089.

(64) Sui-Seng, C.; Freutel, F.; Lough, A. J.; Morris, R. H. *Angew. Chem. Int. Ed.* **2008**, *47*, 940-943.

(65) Borzenko, A.; Rotta-Loria, N. L.; MacQueen, P. M.; Lavoie, C. M.; McDonald, R.; Stradiotto, M. *Angew. Chem. Int. Ed.* **2015**, *54*, 3773-3777.

(66) Green, R. A.; Hartwig, J. F. *Angew. Chem. Int. Ed.* **2015**, *54*, 3768-3772.

(67) Collins, S. *Coord. Chem. Rev.* **2011**, *255*, 118-138.

(68) Sydora, O. L.; Jones, T. C.; Small, B. L.; Nett, A. J.; Fischer, A. A.; Carney, M. J. *ACS Catal.* **2012**, *2*, 2452-2455.

(69) Ruddy, A. J.; Kelly, C. M.; Crawford, S. M.; Wheaton, C. A.; Sydora, O. L.; Small, B. L.; Stradiotto, M.; Turculet, L. *Organometallics* **2013**, *32*, 5581-5588.

(70) Ruddy, A. J.; Sydora, O. L.; Small, B. L.; Stradiotto, M.; Turculet, L. *Chem. Eur. J.* **2014**, *20*, 13918-13922.

(71) Kelly, C. M.; Ruddy, A. J.; Wheaton, C. A.; Sydora, O. L.; Small, B. L.; Stradiotto, M.; Turculet, L. *Can. J. Chem.* **2014**, *92*, 194-200.

(72) Kelly, C. M.; Kwon, D.-H.; Ferguson, M. J.; Bischof, S. M.; Sydora, O. L.; Ess, D. H.; Stradiotto, M.; Turculet, L. *Angew. Chem. Int. Ed.* **2015**, *54*, 14498-14502.

(73) Saito, B.; Fu, G. C. *J. Am. Chem. Soc.* **2007**, *129*, 9602-9603.

(74) Geist, E.; Kirschning, A.; Schmidt, T. *Nat. Prod. Rep.* **2014**, *31*, 441-448.

(75) Buslov, I.; Becouse, J.; Mazza, S.; Montandon-Clerc, M.; Hu, X. *Angew. Chem. Int. Ed.* **2015**, *54*, 14523-14526.

(76) Chakraborty, S.; Bhattacharya, P.; Dai, H.; Guan, H. *Acc. Chem. Res.* **2015**, *48*, 1995-2003.

(77) (a) *Contemporary Boron Chemistry*; Davidson, M.; Hughes, A. K.; Marder, T. B.; Wade, K., Eds.; Royal Society of Chemistry: Cambridge, UK, 2000; (b) *Boranes in Organic Chemistry*; Brown, H. C., Ed.; Cornell University Press: Ithaca, New York, 1972.

(78) (a) Jana, R.; Pathak, T. P.; Sigman, M. S. *Chem. Rev.* **2011**, *111*, 1417-1492; (b) Suzuki, A. *Angew. Chem. Int. Ed.* **2011**, *50*, 6722-6737; (c) Guram, A. S. *Org. Process Res. Dev.* **2016**, *20*, 1754-1764; (d) Lennox, A. J. J.; Lloyd-Jones, G. C. *Chem. Soc. Rev.* **2014**, *43*, 412-443; (e) Slagt, V. F.; de Vries, A. H. M.; de Vries, J. G.; Kellogg, R. M. *Org. Process Res. Dev.* **2010**, *14*, 30-47; (f) Slagt, V. F.; de Vries, A. H. M.; de Vries, J. G.; Kellogg, R. M. *Org. Process Res. Dev.* **2010**, *14*, 30-47.

(79) (a) Beletskaya, I.; Pelter, A. *Tetrahedron* **1997**, *53*, 4957-5026; (b) Crudden, C. M.; Edwards, D. *Eur. J. Org. Chem.* **2003**, 4695-4712; (c) Vogels, C.; Westcott, S. *Curr. Org. Chem.* **2005**, *9*, 687-699.

(80) Larionov, E.; Li, H. H.; Mazet, C. *Chem. Commun.* **2014**, *50*, 9816-9826.

(81) Vasseur, A.; Bruffaerts, J.; Marek, I. *Nat. Chem.* **2016**, *8*, 209-219.

(82) Julia-Hernandez, F.; Moragas, T.; Cornella, J.; Martin, R. *Nature* **2017**, *545*, 84-88.

(83) (a) Pereira, S.; Srebnik, M. *J. Am. Chem. Soc.* **1996**, *118*, 909-910; (b) Yamamoto, Y.; Fujikawa, R.; Umemoto, T.; Miyaura, N. *Tetrahedron* **2004**, *60*, 10695-10700; (c) Edwards, D. R.; Crudden, C. M.; Yam, K. *Adv. Synth. Catal.* **2005**, *347*, 50-54; (d) Hadebe, S. W.; Robinson, R. S. *Tetrahedron Lett.* **2006**, *47*, 1299-1302; (e) Lata, C. J.; Crudden, C. M. *J. Am. Chem. Soc.* **2010**, *132*, 131-137.

(84) Obligacion, J. V.; Chirik, P. J. *J. Am. Chem. Soc.* **2013**, *135*, 19107-19110.

(85) Ruddy, A. J.; Sydora, O. L.; Small, B. L.; Stradiotto, M.; Turculet, L. *Chem. Eur. J.* **2016**, *22*, 12589.

(86) Ogawa, T.; Ruddy, A. J.; Sydora, O. L.; Stradiotto, M.; Turculet, L. *Organometallics* **2017**, *36*, 417-423.

(87) (a) Palmer, W. N.; Diao, T. N.; Pappas, I.; Chirik, P. J. *ACS Catal.* **2015**, *5*, 622-626; (b) Scheuermann, M. L.; Johnson, E. J.; Chirik, P. J. *Org. Lett.* **2015**, *17*, 2716-2719; (c) Obligacion, J. V.; Chirik, P. J. *Org. Lett.* **2013**, *15*, 2680-2683; (d) Zheng, J.; Sortais, J.-B.; Darcel, C. *ChemCatChem* **2014**, *6*, 763-766; (e) Tseng, K. N. T.; Kampf, J. W.; Szymczak, N. K. *ACS Catal.* **2015**, *5*, 411-415.

(88) Kelly, C. M.; McDonald, R.; Sydora, O. L.; Stradiotto, M.; Turculet, L. *Angew. Chem. Int. Ed.* **2017**, *56*, 15901-15904.

(89) Macaulay, C. M.; Gustafson, S. J.; Fuller, J. T.; Kwon, D. H.; Ogawa, T.; Ferguson, M. J.; McDonald, R.; Lumsden, M. D.; Bischof, S. M.; Sydora, O. L.; Ess, D. H.; Stradiotto, M.; Turculet, L. *ACS Catal.* **2018**, *8*, 9907-9925.

(90) Faust, M.; Bryan, A. M.; Mansikkamäki, A.; Vasko, P.; Olmstead, M. M.; Tuononen, H. M.; Grandjean, F.; Long, G. J.; Power, P. P. *Angew. Chem. Int. Ed.* **2015**, *54*, 12914-12917.

(91) Kelly, C. M.; Fuller, J. T.; Macaulay, C. M.; McDonald, R.; Ferguson, M. J.; Bischof, S. M.; Sydora, O. L.; Ess, D. H.; Stradiotto, M.; Turculet, L. *Angew. Chem. Int. Ed.* **2017**, *56*, 6312-6316.

(92) Geier, S. J.; Westcott, S. A. *Rev. Inorg. Chem.* **2015**, *35*, 69-79.

(93) Xi, Y.; Hartwig, J. F. *J. Am. Chem. Soc.* **2017**, *139*, 12758-12772.

(94) Pfirrmann, S.; Limberg, C.; Ziemer, B. *Dalton Trans.* **2008**, 6689-6691.

(95) (a) Liptrot, D. J.; Arrowsmith, M.; Colebatch, A. L.; Hadlington, T. J.; Hill, M. S.; Kociok-Köhn, G.; Mahon, M. F. *Angew. Chem. Int. Ed.* **2015**, *54*, 15280-15283; (b) Liptrot, D. J.; Hill, M. S.; Mahon, M. F.; Wilson, A. S. S. *Angew. Chem. Int. Ed.* **2015**, *54*, 13362-13365.

(96) Wei, C. S.; Jiménez-Hoyos, C. A.; Videa, M. F.; Hartwig, J. F.; Hall, M. B. *J. Am. Chem. Soc.* **2010**, *132*, 3078-3091.

(97) (a) Magano, J.; Dunetz, J. R. *Org. Process Res. Dev.* **2012**, *16*, 1156-1184; (b) Blanchet, J.; Chardon, A.; Morisset, E.; Rouden, J. *Synthesis* **2018**, *50*, 984-997.

(98) Lawrence, S. A. *Amines: Synthesis, Properties and Applications*; Cambridge University Press: Cambridge, 2006.

(99) Gates, M.; Tschudi, G. *J. Am. Chem. Soc.* **1956**, *78*, 1380-1393.

(100) Pesti, J.; Larson, G. L. *Org. Process Res. Dev.* **2016**, *20*, 1164-1181.

(101) Li, B.; Sortais, J. B.; Darcel, C. *RSC Adv.* **2016**, *6*, 57603-57625.

(102) (a) Li, Y. H.; de la Torre, J. A. M.; Grabow, K.; Bentrup, U.; Junge, K.; Zhou, S. L.; Bruckner, A.; Beller, M. *Angew. Chem. Int. Ed.* **2013**, *52*, 11577-11580; (b) Blondiaux, E.; Cantat, T. *Chem. Commun.* **2014**, *50*, 9349-9352; (c) Oestreich, M.; Hermeke, J.; Mohr, J. *Chem. Soc. Rev.* **2015**, *44*, 2202-2220; (d) Chardon, A.; El Dine, T. M.; Legay, R.; De Paolis, M.; Rouden, J.; Blanchet, J. *Chem. Eur. J.* **2017**, *23*, 2005-2009; (e) Peruzzi, M. T.; Mei, Q. Q.; Lee, S. J.; Gagne, M. R. *Chem. Commun.* **2018**, *54*, 5855-5858.

(103) (a) Das, S.; Addis, D.; Zhou, S.; Junge, K.; Beller, M. *J. Am. Chem. Soc.* **2010**, *132*, 4971-4971; (b) Das, S.; Zhou, S. L.; Addis, D.; Enthaler, S.; Junge, K.; Beller, M. *Top. Catal.* **2010**, *53*, 979-984; (c) Das, S.; Addis, D.; Junge, K.; Beller, M. *Chem. Eur. J.* **2011**, *17*, 12186-12192; (d) Kovalenko, O. O.; Volkov, A.; Adolfsson, H. *Org. Lett.* **2015**, *17*, 446-449.

(104) Zhou, S.; Junge, K.; Addis, D.; Das, S.; Beller, M. *Angew. Chem. Int. Ed.* **2009**, *48*, 9507-9510.

(105) Sunada, Y.; Kawakami, H.; Imaoka, T.; Motoyama, Y.; Nagashima, H. *Angew. Chem. Int. Ed.* **2009**, *48*, 9511-9514.

(106) Das, S.; Wendt, B.; Moeller, K.; Junge, K.; Beller, M. *Angew. Chem. Int. Ed.* **2012**, *51*, 1662-1666.

(107) Bezier, D.; Venkanna, G. T.; Sortais, J.-B.; Darcel, C. *ChemCatChem* **2011**, *3*, 1747-1750.

(108) Volkov, A.; Buitrago, E.; Adolfsson, H. *Eur. J. Org. Chem.* **2013**, 2066-2070.

(109) Blom, B.; Tan, G. W.; Enthaler, S.; Inoue, S.; Epping, J. D.; Driess, M. *J. Am. Chem. Soc.* **2013**, *135*, 18108-18120.

(110) Dombray, T.; Helleu, C.; Darcel, C.; Sortais, J. B. *Adv. Synth. Catal.* **2013**, *355*, 3358-3362.

(111) Mamillapalli, N. C.; Sekar, G. *Chem. Commun.* **2014**, *50*, 7881-7884.

(112) Simmons, B. J.; Hoffmann, M.; Hwang, J.; Jackl, M. K.; Garg, N. K. *Org. Lett.* **2017**, *19*, 1910-1913.

(113) Arias-Ugarte, R.; Sharma, H. K.; Morris, A. L. C.; Pannell, K. H. *J. Am. Chem. Soc.* **2012**, *134*, 848-851.

(114) Igarashi, M.; Fuchikami, T. *Tetrahedron Lett.* **2001**, *42*, 1945-1947.

(115) Postigo, L.; Royo, B. *Adv. Synth. Catal.* **2012**, *354*, 2613-2618.

(116) Martinez-Prieto, L. M.; Palma, P.; Alvarez, E.; Campora, J. *Inorg. Chem.* **2017**, *56*, 13086-13099.

(117) (a) Campora, J.; Lopez, J. A.; Maya, C.; Palma, P.; Carmona, E.; Valerga, P. *J. Organomet. Chem.* **2002**, *643*, 331-341; (b) Kruckenberg, A.; Wadepohl, H.; Gade, L. H. *Organometallics* **2013**, *32*, 5153-5170.

(118) Andersen, R. A.; Faegri, K.; Green, J. C.; Haaland, A.; Lappert, M. F.; Leung, W. P.; Rypdal, K. *Inorg. Chem.* **1988**, *27*, 1782-1786.

(119) (a) Obligacion, J. V.; Chirik, P. J. *Nat. Rev. Chem.* **2018**, *2*, 15-34; (b) Sommer, H.; Julia-Hernandez, F.; Martin, R.; Marek, I. *ACS Central Sci.* **2018**, *4*, 153-165.

(120) Macaulay, C. M.; Ogawa, T.; McDonald, R.; Sydora, O. L.; Stradiotto, M.; Turculet, L. *Dalton Trans.* **2019**, *48*, 9581-9587.

(121) Fraenkel, G.; Chen, X.; Chow, A.; Gallucci, J. *J. Org. Chem.* **2013**, *78*, 1149-1156.

(122) Cornella, J.; Gómez-Bengoa, E.; Martin, R. *J. Am. Chem. Soc.* **2013**, *135*, 1997-2009.

(123) Lin, S. B.; Day, M. W.; Agapie, T. *J. Am. Chem. Soc.* **2011**, *133*, 3828-3831.

(124) Dong, Q. S.; Zhao, Y. X.; Su, Y. T.; Su, J. H.; Wu, B. A.; Yang, X. J. *Inorg. Chem.* **2012**, *51*, 13162-13170.

(125) Weber, M.; Hellriegel, C.; Rueck, A.; Wuethrich, J.; Jenks, P.; Obkircher, M. *Anal. Bioanal. Chem.* **2015**, *407*, 3115-3123.

(126) (a) Ittel, S. D.; Johnson, L. K.; Brookhart, M. *Chem. Rev.* **2000**, *100*, 1169-1203; (b) Gibson, V. C.; Spitzmesser, S. K. *Chem. Rev.* **2003**, *103*, 283-315; (c) Speiser, F.; Braunstein, P.; Saussine, W. *Acc. Chem. Res.* **2005**, *38*, 784-793; (d) Matsugi, T.; Fujita, T. *Chem. Soc. Rev.* **2008**, *37*, 1264-1277; (e) Mu, H. L.; Pan, L.; Song, D. P.; Li, Y. S. *Chem. Rev.* **2015**, *115*, 12091-12137.

(127) (a) Conroylewis, F. M.; Mole, L.; Redhouse, A. D.; Litster, S. A.; Spencer, J. L. *J. Chem. Soc. D* **1991**, 1601-1603; (b) Kitiachvili, K. D.; Mindiola, D. J.; Hillhouse, G. L. *J. Am. Chem. Soc.* **2004**, *126*, 10554-10555; (c) Scherer, W.; Herz, V.; Bruck, A.; Hauf, C.; Reiner, F.; Altmannshofer, S.; Leusser, D.; Stalke, D. *Angew. Chem. Int. Ed.* **2011**, *50*, 2845-2849.

(128) (a) Leatherman, M. D.; Svejda, S. A.; Johnson, L. K.; Brookhart, M. *J. Am. Chem. Soc.* **2003**, *125*, 3068-3081; (b) Xu, H. W.; White, P. B.; Hu, C. H.; Diao, T. N. *Angew. Chem. Int. Ed.* **2017**, *56*, 1535-1538.

(129) (a) Kogut, E.; Zeller, A.; Warren, T. H.; Strassner, T. *J. Am. Chem. Soc.* **2004**, *126*, 11984-11994; (b) Wiencko, H. L.; Kogut, E.; Warren, T. H. *Inorganica Chim. Acta* **2003**, *345*, 199-208.

(130) Brookhart, M.; Green, M. L. H.; Parkin, G. *Proc. Natl. Acad. Sci. U.S.A.* **2007**, *104*, 6908-6914.

(131) Urtel, H.; Meier, C.; Eisenträger, F.; Rominger, F.; Joschek, J. P.; Hofmann, P. *Angew. Chem. Int. Ed.* **2001**, *40*, 781-784.

(132) Laskowski, C. A.; Bungum, D. J.; Baldwin, S. M.; Del Ciello, S. A.; Iluc, V. M.; Hillhouse, G. L. *J. Am. Chem. Soc.* **2013**, *135*, 18272-18275.

(133) Brown, C. A. *J. Org. Chem.* **1970**, *35*, 1900-1904.

(134) Zou, Y.-Q.; Chakraborty, S.; Nerush, A.; Oren, D.; Diskin-Posner, Y.; Ben-David, Y.; Milstein, D. *ACS Catal.* **2018**, *8*, 8014-8019.

(135) Han, B.; Ma, P.; Cong, X.; Chen, H.; Zeng, X. *J. Am. Chem. Soc.* **2019**, *141*, 9018-9026.

(136) Luca, O. R.; Blakemore, J. D.; Konezny, S. J.; Praetorius, J. M.; Schmeier, T. J.; Hunsinger, G. B.; Batista, V. S.; Brudvig, G. W.; Hazari, N.; Crabtree, R. H. *Inorg. Chem.* **2012**, *51*, 8704-8709.

(137) (a) Connelly, S. J.; Zimmerman, A. C.; Kaminsky, W.; Heinekey, D. M. *Chem. Eur. J.* **2012**, *18*, 15932-15934; (b) Yang, J. Y.; Bullock, R. M.; Shaw, W. J.; Twamley, B.; Fraze, K.; DuBois, M. R.; DuBois, D. L. *J. Am. Chem. Soc.* **2009**, *131*, 5935-5945; (c) Tsay, C.; Peters, J. C. *Chem. Sci.* **2012**, *3*, 1313-1318.

APPENDIX: COPYRIGHT

Chapter 2: Reproduced in part with permission from: Macaulay, C. M.; Gustafson, S. J.; Fuller, J. T.; Kwon, D. H.; Ogawa, T.; Ferguson, M. J.; McDonald, R.; Lumsden, M. D.; Bischof, S. M.; Sydora, O. L.; Ess, D. H.; Stradiotto, M.; Turculet, L. *ACS Catal.* **2018**, *8*, 9907-9925. Copyright 2019 American Chemical Society.

Also reproduced in part under the following agreement:

This Agreement between Dr. Casper M. Macaulay -- Casper Macaulay ("You") and John Wiley and Sons ("John Wiley and Sons") consists of your license details and the terms and conditions provided by John Wiley and Sons and Copyright Clearance Center.

License Number	4722050069480
License date	Dec 04, 2019
Licensed Content Publisher	John Wiley and Sons
Licensed Content Publication	Angewandte Chemie International Edition
Licensed Content Title	Dehydrogenative B−H/C(sp3)−H Benzylic Borylation within the Coordination Sphere of Platinum(II)
Licensed Content Author	Laura Turculet, Mark Stradiotto, Daniel H. Ess, et al
Licensed Content Date	Mar 30, 2017
Licensed Content Volume	56
Licensed Content Issue	22
Licensed Content Pages	5
Type of Use	Dissertation/Thesis
Requestor type	Author of this Wiley article
Format	Electronic
Portion	Text extract
Number of Pages	2
Will you be translating?	No
Title of your thesis / dissertation	N-Phosphinoamidinate Nickel Complexes
Expected completion date	Dec 2019
Expected size (number of pages)	200

Chapter 3: Reproduced from Ref. 120 with permission from the Royal Society of Chemistry.